THE UNIVERSITY OF CALGARY

An Experimental and Modeling Study of Homogeneous Gas Phase Reactions Occurring in the Modified Claus Process

by

Kunal Karan

A DISSERTATION

SUBMITTED TO THE FACULTY OF GRADUATE STUDIES

IN PARTIAL FULFILLMENT OF THE REQUIREMENTS FOR THE

DEGREE OF DOCTOR OF PHILOSOPHY

DEPARTMENT OF CHEMICAL AND PETROLEUM ENGINEERING

CALGARY, ALBERTA

DECEMBER, 1998

National Library of Canada
Acquisitions and Bibliographic Services
395 Wellington Street
Ottawa ON K1A 0N4
Canada

Bibliothèque nationale du Canada
Acquisitions et services bibliographiques
395, rue Wellington
Ottawa ON K1A 0N4
Canada

Your file Votre référence

Our file Notre référence

0-612-38481-0

Canada

ABSTRACT

This thesis reports a thermodynamic feasibility study, experimental data and modeling results for key side reactions occurring in the front-end units, i.e. the reaction furnace (RF) and the waste heat boiler (WHB), of Claus plants for sulfur recovery.

A detailed chemical reaction equilibrium study was initially performed to select thermodynamically important reactions that lead to the formation and the consumption of CO, H_2, COS and CS_2 under the conditions encountered in the front-end of a Claus plant. An extensive experimental and modeling study was conducted to obtain kinetic data for the selected key side reactions. All experiments were conducted in a novel high-temperature flow-reactor system. From the modeling of the experimental data for key reactions, intrinsic kinetic rate expressions were determined.

Next, experiments on the partial oxidation of acid gas mixtures were conducted. The experimental data provided useful information on the formation of key species under oxidation conditions. Simulation and modeling studies, using detailed reaction kinetic schemes involving elementary reactions, were also conducted. A comparison of experimental data with simulation results showed that the kinetic scheme for H_2S oxidation could adequately predict gas compositions at higher temperatures (> 1100 °C) but not at lower temperatures. These simulation studies also highlighted the need for the kinetics of many reactions involving sulfur containing species and carbon containing species.

Finally, modeling studies of the front-end units, the RF and the WHB of a Claus plant was conducted. The formation of COS in the tubes of an industrial WHB was simulated using new kinetics and compared with plant data. The simulation showed that up to a fifty percent reduction in COS production in the

WHB may be achieved by operational and design changes. This represents a significant reduction in COS formation and has major implications on Claus plant sulfur emissions and recovery. Further, an attempt was also made to predict the gas composition from the RF using a true kinetic model. The kinetic model performed well in predicting the compositions of chemical species of interest, CO and H_2.

ACKNOWLEDGEMENTS

First and foremost, I wish to acknowledge Dr. Leo Behie's tremendous and unconditional support. I do not have enough words to express my gratitude to Dr. Behie for his patience, guidance, assistance, and understanding. The vicissitudes of life were certainly very apparent during the extremely trying situations over the four years of my doctoral research and I must admit that without Dr. Behie's exceptional support, this thesis would not have been possible. Thank you Dr. Behie for everything. I will always cherish my days here at University of Calgary.

I would like to acknowledge Dr. Anil K. Mehrotra's support, guidance and understanding. I am grateful to you, Dr. Mehrotra, for all that you have done for me. I thoroughly enjoyed working with you Dr. Mehrotra.

I wish to thank Dr. R.A. Heidemann for the many discussions we had and for his helpful suggestions and acknowledge his support.

I wish to express my thanks to all the staff of the Department of Chemical and Petroleum Engineering for their friendliness and their help.

I would like to thank Mr. Mark Toonen, the glassblower, for fixing more than the broken pieces of the equipment and, more importantly, for providing useful insight in designing some equipment.

I wish to acknowledge the financial support for my project from Gas Research Institute (GRI), Chicago, Shell Canada Limited and Alberta Department of Energy. I would like to acknowledge the financial support provided by The Department of Chemical and Petroleum Engineering, Alberta Research Council, Izaak Walton Killam Memorial Scholarship, University of Calgary Silver Anniversary Graduate Fellowship.

I wish to acknowledge the supportive and friendly work environment provided by my peers at the department. Special thanks to my close friends (names withheld) whose tremendous support helped me realize my objective.

I want to express my thanks and gratitude to my family for their patience and support.

Finally, I would like to thank my wife, Tulika, for her patience and for helping me complete my thesis.

DEDICATION

Dedicated to the one who dwells up above in the sky.

TABLE OF CONTENTS

LIST OF TABLES

LIST OF FIGURES

NOMENCLATURE

A	Arrhenius parameters (in s, kmol, m^3 units) Also, cross sectional area of tubes, m^2
a	element abundant matrix
a_{ij}	number of element of type *j* in species *i*
a_1	coefficient in free energy correlation
a_2	coefficient in free energy correlation
b_1	coefficient in free energy correlation
b_2	coefficient in free energy correlation
b_j	number of elements j in feed mixture
c	number of chemical species
c_1	coefficient in free energy correlation
c_2	coefficient in free energy correlation
d_1	coefficient in free energy correlation
d_2	coefficient in free energy correlation
D	tube diameter (mm, cm or m)
e_1	coefficient in free energy correlation
e_2	coefficient in free energy correlation
f	free energy function
F_j	Molar flow rate of component *j* (mol/s)
G	Total molar Gibbs energy of a system (kJ)
g_i°	Gibbs energy of formataion of *i*th species (kJ/mol)

k_i	reaction rate constant for reaction i (kmol, m^3, s units)
m′	rank of element abundant matrix
P	Pressure (kPa)
r_j	rate of formation of component I (kmol/m^3.s)
R	Universal Gas Constant
T	Temperature (K)

Greek symbols

X^2	Chi square function
Σ	summation symbol
σ	weight factor
λ_j	Langrangian multiplier

Chapter 1

Introduction

1.1 Background

The emissions of sulfur dioxide to the atmosphere pose serious environmental threat in form of acid rains. The seriousness of this problem is reflected in the increasing stringency of governmental regulations on sulfur emissions. In Canada, industrial sulfur emissions are being curbed in the seven eastern most provinces to meet the commitment of Helsinki Protocol. Additionally, Canada plans to cap its annual SO_2 emissions to 3.2×10^6 t in accordance with the Green plan (EPS Report, 1993). A reduction in sulfur emissions from the three western provinces of British Columbia, Alberta and Saskatchewan will help to reach this goal rapidly. The natural gas and tar sands industry contributes to 80% of licensed, non-power plant sulfur dioxide emissions in these three provinces. Alberta has the largest number of natural gas plants operating in Canada; 622 out of 675 plants (True, 1995). The sulfur emissions from 176 sour gas processing plants and two tar sands plants in Alberta represent more than 90% of the total licensed SO_2 emissions from the three western provinces (EPS Report, 1993).

The major source of sulfur emissions in the sour gas processing plants can be traced to the Claus plants, where sulfur is recovered from the acid gases. Clearly, any improvement in sulfur recovery from Claus plants results in a direct reduction in emissions of sulfur dioxide to the atmosphere. The sulfur recovery from Claus plants can be improved by optimizing the plant operations, which requires a detailed and clearer understanding of the process chemistry and reaction kinetics of the numerous reactions occurring in the front-end units, i.e. reaction furnace and waste heat boiler, of a Claus plant. As much as 65 percent of the total plant sulfur recovery can be achieved in the front-end units of a straight-through plant. Therefore, to

suggest means of reducing SO_2 emissions from these Claus plants, one needs to develop a thorough understanding of the process chemistry, especially in the front-end of the Claus plants. Twenty years ago, Paskall (1979) published an excellent overview on the capabilities of the modified Claus process. The report is also a comprehensive compilation of numerous literature published prior to 1976. Recently, Hyne and Goar (1996 a, b, c and 1997) published a series of papers in which they tried to address issues related to and novel ideas for improving sulfur recovery from the modified Claus plants.

1.2 Description of the modified Claus process

The modified Claus process for the recovery of sulfur from hydrogen sulfide can be described by the deceptively simple overall reaction (Claus Reaction):

$$H_2S + 1/2\ O_2 \leftrightharpoons 1/x\ S_x + H_2O \qquad (1.1)$$

where, S_x represents the sulfur allotrope (x=1,2...8) and depends on temperature. The conversion to sulfur is attained in two reaction steps in the modified Claus process. The first step is a thermal step in which one-third of feed hydrogen sulfide is partially oxidized to produce sulfur dioxide at very high temperatures. In the second step, the unreacted H_2S is reacted over catalysts with the SO_2 produced in the thermal step at cooler temperatures. The relevant reactions can be represented as follows:

$$3H_2S + 3/2\ O_2 \leftrightharpoons SO_2 + 2H_2S + H_2O \qquad (1.2)$$

$$2H_2S + SO_2 \leftrightharpoons 3/x\ S_x + 2H_2O \qquad (1.3)$$

The schematic flow sheet of a modified Claus process with two catalytic converter stages is shown in Figure 1.1 The thermal step in Claus plants is carried out in the refractory lined cylindrical vessel called the reaction furnace (RF). The gas streams are fed to the RF at pressures of 130- 180 kPa. The RF operates at temperature ranging from 975 to 1300 °C and is designed to provide a gas residence between 0.5 and 2.0 seconds. The contaminants such as CO_2, hydrocarbons, ammonia etc. in the RF feed interact via numerous complex side reactions resulting in a product

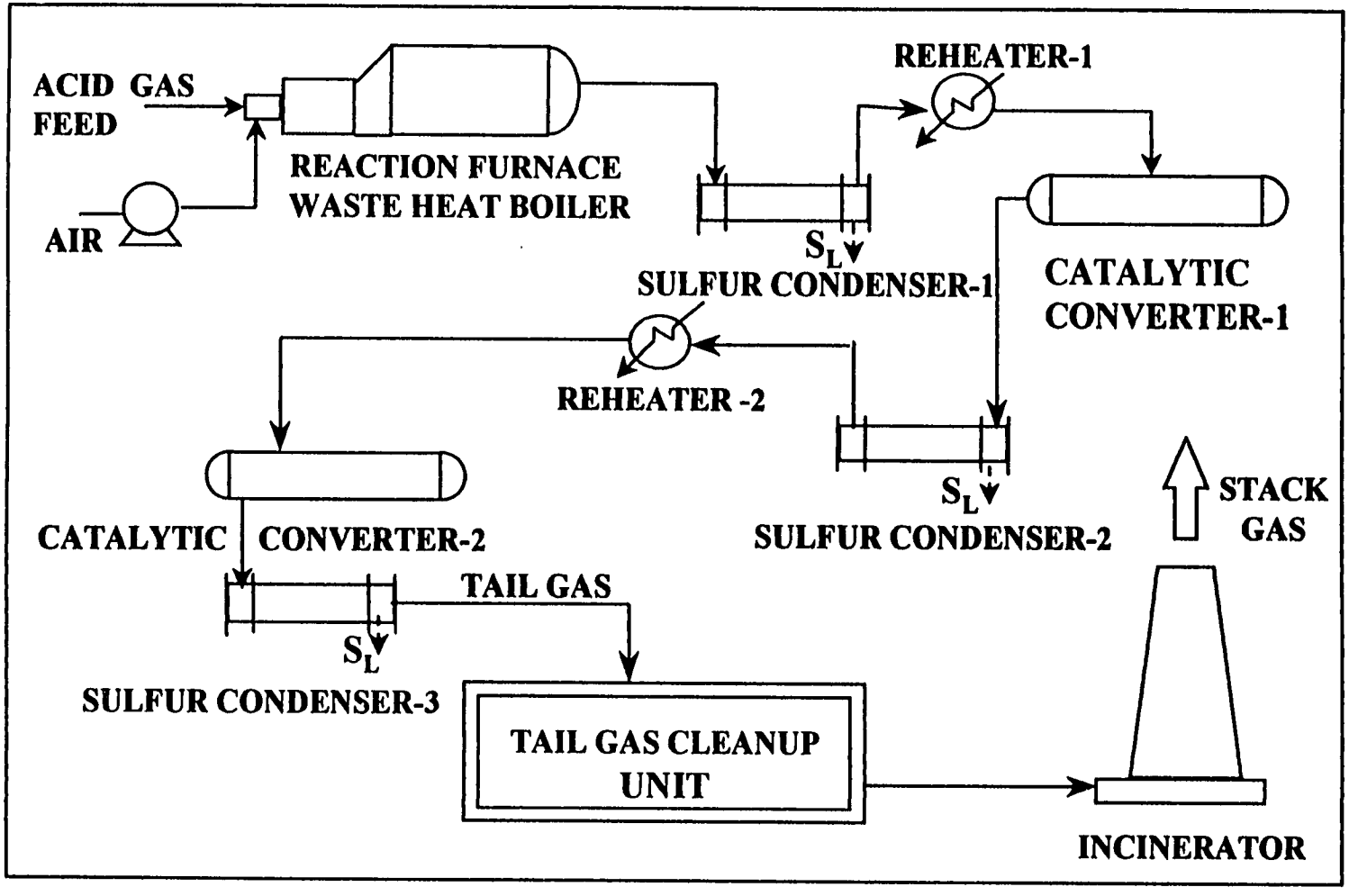

Figure 1.1 A schematic diagram of a two-catalytic stage modified Claus process.

stream that contains CO, H_2, COS and CS_2 among the other expected chemical species such as SO_2, H_2S, H_2O, N_2 and sulfur. The RF is followed by a shell and tube type heat exchanger with one or two tube passes and is commonly referred to as the waste heat boiler (WHB). The heat from the furnace product gases is recovered by cooling the gas to a temperature less than 250 °C in the tubes of the WHB. The RF and WHB usually form a single unit as shown in Figure 1. Elemental sulfur is produced in the RF from thermal decomposition of hydrogen sulfide to hydrogen and sulfur and also from reaction (1.3). In a *straight through* furnace, as much as 65 percent sulfur can be produced in the RF. The sulfur produced in RF is recovered in a sulfur condenser placed downstream of the RF/WHB. The gas stream leaving the condenser is at the dew point of sulfur, however, some liquid sulfur does get entrained in the gas stream. The liquid sulfur can plug the catalyst pores in the downstream converters and effectively deactivate the catalyst. To avoid this, the gas stream from condenser is heated prior to being fed to the fixed bed reactors called the catalytic converters. The most popular catalysts used in the converters are the alumina catalysts, although, the trend these days is to use the high efficiency, but expensive, titania catalysts. The sulfur produced in the converters is recovered in the condenser following the converter. Typically, two to three catalytic stages are employed in Claus plants, which achieve an overall sulfur recovery in the range of 95-98 percent. The gas stream resulting from the sulfur condenser downstream of the last catalytic converter is called the tail gas and comprises of unreacted H_2S and SO_2, COS, CS_2, N_2, CO, H_2, H_2O and entrained sulfur.

Typically, overall sulfur recovery for a Claus plant is in the range of 96 to 98.5 percent which can be achieved with three to four staged catalytic converter (Kwong and Meissner, 1995). Depending on the processing capacity of the plant, additional recovery of sulfur from the tail gas may be required to comply with the present sulfur emission regulations. For example, in Alberta (Canada), the sulfur recovery requirement of sour gas plants processing less than 50 tons/day of inlet

sulfur is up to 96.2 percent. However, the percent recovery requirement increases to 99.8 for plants processing greater than 2000 tons/day of inlet sulfur. To attain more than 98.5 % of overall sulfur recovery, tail gas cleanup (TGCU) processes have to be employed. The TGCU processes can be broadly classified as either dry bed or wet scrubbing processes. Some examples of proprietary dry processes are: Shell Flue Gas Desulfurization (SFGD), Sulfreen, Amoco's CBA, MCRC; while those of wet processes are: SCOT, LoCat, Alberta Sulfur Research's Sulfoxide, Union Carbide's UCAP (GPSA Data Book, 1987). The problem with a TGCU is that it may cost as much as the whole Claus plant even though it adds only about 2% in the total plant sulfur recovery.

1.3 Importance of the Claus plant front-end units: RF and WHB

The reaction furnace, by virtue of being located at the front-end of the plant, plays a critically important role in determining the product distribution from the downstream units and, ultimately, the recovery and the emissions from the plant. It is ironic, however, that even after half a century of being in operation, a clear picture of the reactions occurring in the reaction furnace and their kinetic behavior has not emerged.

An improvement in the plant sulfur recovery may be achieved by optimizing the operation of the front-end units of a Claus plant, i.e., the reaction furnace and the waste heat boiler. This may eliminate the need of a tail gas cleanup unit, at least in plants that require marginal increment in sulfur recovery. It must be restated here that up to 65 percent of the total plant sulfur recovery may be attained in the front-end of the Claus plant. Moreover, the RF and WHB are the only Claus plant units where formation of CO and H_2 and the two problematic sulfur species COS and CS_2 takes place. Of these four compounds, only hydrogen may be a potentially useful species. COS and CS_2 tie up sulfur and therefore their loss from plant represents a sulfur loss from the plant. Although, CO is normally considered to be an inert species for sulfur recovery purposes, it is now known that CO is a precursor to COS, and therefore is a problem species from sulfur recovery perspective.

1.4 Importance of CO, H_2, COS and CS_2

The four chemical compounds, CO, H_2, COS and CS_2 are problematic from the modeling perspective because their formation in a Claus reaction furnace is limited by kinetics (Fisher, 1974; Grancher, 1978; Paskall, 1979; Chou et al., 1991).

1.4.1 COS and CS_2: Contribution to the plant sulfur emissions

Carbonyl sulfide and carbon disulfide are formed in the RF and WHB (Sames and Paskall, 1984). Moreover, the concentrations of COS and CS_2 in the furnace/ waste heat boiler exit gas have been measured at a number of plants and found to lie typically between 100 ppm and 2.0 mol % (Sames and Paskall, 1984). However, these seemingly low concentrations of the two components in the furnace product stream can represent a large percentage (i.e. up to 50 percent) of sulfur emissions from the tail gas cleanup unit (Luinstra and d'Haene, 1989), and hence the plant. These two sulfur compounds could possibly be hydrolyzed back to hydrogen sulfide in the catalytic converters by the following reactions:

$$COS + H_2O \xleftrightarrow{catalyst} CO_2 + H_2S \qquad (1.4)$$

$$CS_2 + 2H_2O \xleftrightarrow{catalyst} CO_2 + 2H_2S \qquad (1.5)$$

Tong et al. (1992, 1993) from the University of Alberta have recently reported intrinsic kinetic rate expressions for these two reactions in the presence of both titania and alumina catalysts.

In order to maximize the conversion from the main Claus reaction (1.3), the catalytic converters should be operated at as low a temperature as possible, such that the exit temperature is slightly above the sulfur dew point. This is true because this reaction is reversible and exothermic. Hence, the equilibrium conversion increases with decreasing temperature. On the other hand, the hydrolysis reactions are relatively slow and higher temperatures (> 315 ^{0}C) are required to obtain substantial conversions. Under the operating conditions (low residence time and low temperature) of the catalytic converters, the hydrolysis reactions do not achieve complete conversions. Another factor that contributes further to a lower conversion

for hydrolysis reaction is the catalyst deactivation. The net result is that COS and CS_2 once formed at the front-end of the Claus plant can pass through the downstream units without being consumed completely and ultimately end up contributing substantially to the sulfur emissions.

1.4.2 H_2 and CO: Formation in RF and their importance

Both H_2 and CO have been found to be present at significant concentrations in the gas stream from the reaction furnace (Sames et al., 1990). The measured quantities of these two components were lower than those predicted from thermodynamic considerations. Moreover, hydrogen is considered to be an inert component from the operational point of view for Claus process. However, production of hydrogen from hydrogen sulfide in the RF results in a few benefits; (i) reduced hydrogen requirement for treating tail gas in TGCU's that employ a reduction method (i.e. like the SCOT TGCU); (ii) lower oxygen requirement in RF. Also, carbon monoxide production in the RF leads to a lower demand for oxygen and lowers the furnace temperature (Paskall, 1979; Sames et al., 1990).

Apart from the lowered oxygen requirement in the RF, the production of CO and H_2 in the RF has far reaching implications; namely, that on the sulfur emissions from the plant. The field measurement study of Sames et al. (1990) conclusively showed that most of the COS coming from the front end of a Claus plant is formed in the waste heat boiler contrary to the prior belief that it is all produced in the reaction furnace. They measured the gas compositions at the furnace exit or the WHB entrance and again at the exit of WHB and found an increase in the amount of hydrogen sulfide and carbonyl sulfide plus a decrease in the amounts of hydrogen, carbon monoxide and sulfur across the waste heat boiler. Based on these results, the occurrence of the reassociation reaction of hydrogen and sulfur to form hydrogen sulfide and the reaction between carbon monoxide and sulfur to produce carbonyl sulfide were proposed for the WHB. These reactions can be represented as follows:

$$H_2 + \tfrac{1}{2} S_2 \quad \rightleftharpoons \quad H_2S \qquad (1.6)$$

$$CO + \tfrac{1}{2} S_2 \quad \leftrightharpoons \quad COS \qquad (1.7)$$

The rapid quenching of both of these reactions in the WHB could result in recovery of a larger amount of sulfur at the RF/WHB exit. A benefit that might occur from the quenching of the reaction between CO and S_2 is the reduction in the amount of COS produced, and hence, a reduction in sulfur emissions from the plant.

In addition, both CO and H_2 are not present in the feed to the RF, and are likely formed via some reactions in the RF. Additionally, the formation of CO is directly linked with the formation of COS. It may be speculated that a significant amount of CO produced in RF could be via the reaction between H_2 and CO_2. The formations of H_2 and CO are, hence, an important step towards the formation of COS in the Claus furnace.

1.5 Claus process modeling and simulation

Numerous studies on the simulation of the front-end reaction furnace (Boas and Andrade, 1972; Dalla Lana and Truong, 1979; Wen et al., 1987; Chou et al., 1991; Monnery et al., 1993; and Moore, 1993) and modeling of hydrolysis reactions in the catalytic reactors (Kerr et al., 1976; Kerr and Paskall, 1976; Kerr et al., 1976; Wen et al., 1987) have been reported. A majority of these studies have focussed on the simulation of the reaction furnace and have employed a thermodynamic equilibrium approach, while the modeling of reactions in the catalytic converters have included chemical reaction intrinsic kinetics.

1.5.1 Claus furnace modeling

As mentioned earlier, the most widely employed method to model the product composition from the Claus reaction furnace has been to assume that thermodynamic equilibrium prevails for all the reactions. To improve upon the kinetic limitations, especially for CO, H_2, COS and CS_2; empirical correlations are included in the model (Wen et al., 1987 and Chou et al., 1991).

Two similar studies from the University of Calgary (Monnery et al., 1993; Moore, 1993) have compared the various methods that are currently being

employed to predict the composition of the gas mixture exiting the furnace. Two empirical models (Western Research correlation and Fisher Nomograph) and a thermodynamic reaction equilibrium model were considered. Most important, the results from the three models were compared with published plant data. Both Monnery et al. (1993) and Moore (1993) demonstrated that the equilibrium model consistently underpredicted the COS and CS_2 concentrations while it overpredicted the CO composition at the waste heat boiler exit. The H_2 concentration was underpredicted at lower temperatures and overpredicted at higher temperatures. The important point here is that the inability to correctly predict the composition of H_2, CO, COS and CS_2 in the reaction furnace effluent clearly indicates the deficiency of the empirical models resulting from the kinetic limitations of the reactions in the RF.

Monnery et al. (1993) have emphasized the need for extensive kinetic data of the many homogeneous reactions occurring in the reaction furnace.

1.5.2 Modeling waste heat boiler

For many years, the waste heat boiler had been treated simply as a heat recovery unit operation. Heat is recovered from the hot furnace product gases by quenching the gases in the tubes from 1500 to 500 K. Any gas phase reactions occurring in the reaction furnace that could possibly continue in the WHB were considered to quench instantaneously upon entering the WHB. In simple words, the gas compositions at the inlet and the outlet of WHB were considered to be same for design calculations. As pointed out earlier, it is now well known that at least two reactions do occur, and hence, the WHB is indeed a reactor. Neglecting the occurrence of the two reactions in the WHB leads to incorrect boiler duty. More importantly, the effect of quenching these two reactions is completely overlooked.

In a study at the University of Calgary, Nasato et al. (1994) proposed a detailed model of waste heat boiler in which, both the effects, i.e., heat transfer and reactions were included. The proposed model was then improved upon to include the radiative heat transfer effects (Karan et al., 1994, Mehrotra et al., 1995). It was

concluded that heat transfer due to radiation from gas to tubes accounted for 20 % of the total heat transferred. In both of these works approximate kinetics of the reactions were employed to study the effect of quenching these two reactions in the WHB. These two studies demonstrated that the configuration of the tubes in the WHB could quite significantly affect sulfur emissions from a Claus plant. Overall, the results were in limited agreement with the limited field data available, reasserting the need for reliable intrinsic kinetics of the reactions.

1.6 Scope of the research

The brief discussions in the previous sections have highlighted the need for further reductions in sulfur emissions from the Canadian hydrocarbon processing industry. This requires a better understanding of the kinetics and chemistry of the process, especially of the reactions occurring the front-end of the Claus plants, i.e. the reaction furnace and waste heat boiler. The inadequacy of the existing models to predict product gas composition at the front-end of the plant, specifically for the chemical species CO, H_2, COS and CS_2 was also identified. For improved sulfur recovery and for optimizing process operation with a view of reducing sulfur emissions, kinetic models for the reaction furnace and waste boiler are required. All of the above issues point towards a pressing need, i.e. the requirement of reliable kinetic data for various homogeneous reactions occurring in the reaction furnace and waste heat boiler of the Claus plants.

Therefore, the objectives of this research were as follows:

- To identify the important CO, H_2, COS and CS_2 forming reactions.
- To obtain kinetic data for important CO, H_2, COS and CS_2 forming reactions.
- To analyze the kinetic data, develop intrinsic kinetic rate expressions and attempt kinetic modeling for reactions occurring in acid gas mixtures.

Chapter 2

Chemical Reaction Equilibrium Study

2.1 Thermodynamics and reaction kinetics issues

The second law of thermodynamics provides us with the information that a closed and isolated system approaches an *equilibrium* state in which its properties are independent of time (Benson, 1968). While thermodynamics dictates the ultimate state of a chemical system it cannot predict the rate at which the final state can be attained, which is governed by the kinetics of the process.

In general, the thermodynamic data are more readily available compared to kinetic data. For chemically reacting systems, equilibrium composition can be readily calculated using thermodynamic data. Therefore, in the absence of *a priori* knowledge of the reaction itself and the associated kinetics, these calculations can provide useful information pertaining to the chemical process, at least from a driving force point of view.

2.2 Objective of the equilibrium study

The objective of the reaction equilibrium study presented in this thesis was to determine the thermodynamic feasibility or favorability for the formation or the consumption of important molecular chemical species, such as H_2, CO, COS and CS_2, under Claus reaction furnace and waste heat boiler conditions (High T and low P) via a given reaction or from a reacting mixture. The thermodynamically favorable reactions and reacting mixtures were then selected for experimental studies to obtain the necessary intrinsic reaction kinetic information.

It must be borne in mind, however, that the chemical reaction equilibrium study was used only as a tool for selecting the important reactions

from a large number of reactions. It must be restated that the thermodynamic feasibility of a reaction may or may not have any direct bearing on the actual formation/consumption of the chemical species of interest under plant operation conditions, which is dictated by the reaction kinetics. However, this procedure (based on thermodynamic favorability) of selecting the key reactions is better than a random selection method or selection procedure based solely on beliefs of previous researchers.

2.3 Free energy minimization (FEM) method for calculating chemical reaction equilibrium.

The condition that the Gibbs free energy of a system at fixed T and P be minimum at equilibrium is widely employed to calculate the distribution of various species at equilibrium condition (Walas, 1985). The only input parameters needed for calculating the equilibrium composition via the free-energy minimization method are specifying the chemical species expected to be present at equilibrium and their free energy of formation data. The temperature and pressure of the system and the mole numbers of various species define the total Gibbs free energy of the system. The challenge is to find the set of mole numbers, at a fixed temperature and a pressure, that give a minimum Gibbs free energy.

In this thesis, a FORTRAN program was written to calculate the composition of the reacting mixture at chemical equilibrium. The calculation method outlined by Walas (1985) was mainly used, however, the book by Smith and Missen (1991) was frequently used for further directions.

Mathematical formulation of FEM of a reacting system

This section deals with the mathematical equations relevant to free energy minimization for an ideal gas system. At high temperatures (800-1500 K) and low pressures (120-160 kPa) encountered in the reaction furnace and the waste heat

boiler of Claus plants, the chemical species and the chemical system can be well approximated as an ideal gas.

Governing Equations

In an ideal gas system comprising of "c" compounds and "m" elements, the Gibbs free energy is given by:

$$g = nG/RT = \sum_{i=1}^{c} n_i [g_i^{\circ} + \ln(n_i P/n)] \qquad (2.1)$$

where, g represents the Gibbs energy function, G is total molar Gibbs free energy, n represents number of moles, P is the total pressure, T is the temperature and R is the universal gas constant.

The chemical elements are conserved in a reaction, which introduces the closed-system constraint. Therefore, the following set of equality constraints has to be satisfied:

$$b_j - \sum_{i=1}^{c} a_{ij} n_i = 0 \quad ; j=1,2,3...m \qquad (2.2)$$

where, b_j is the total number of element j in the feed and a_{ij} is the number of element j in a chemical species i. This terminology has been referred to by both Walas (1985) and Smith and Missen (1991).

Introducing the Lagrange Multipliers to incorporate the constraints in the body of the problem (Walas, 1985), the function to be minimized can be represented as:

$$f = g + \sum_{i=1}^{m'} \lambda_j \left(b_j - \sum_{i=1}^{c} a_{ij} n_i\right) \qquad (2.3)$$

where, λ's are the langrangian multipliers. It should be noted that the number of equality constraints used are m' instead of m, where m' is given by the following expression:

$$m' = \text{rank}(\mathbf{a}) \qquad (2.4)$$

In equation (2.4), **a** is the element abundance matrix comprised of elements a_{ij}. For some systems the number of linearly independent constraint equations (m') are less than the number of chemical elements (m). For a detailed discussion of this topic, the reader is referred to Smith and Missen (1991).

Energy of Formation Data

For computations, the free energy of formation data were obtained from the JANAF thermochemical tables (Chase et al., 1985) and TRC tables (Marsh et al., 1985). The data were fitted with an expression of following form:

$$g^{\circ}(i) = a_1(i) + b_1(i)T + c_1(i)T^{1.5} + d_1(i)T^2 + e_1(i)T^3 \quad \text{for } 0 < T < 900 \text{ K}$$

$$= a_2(i) + b_2(i)T + c_2(i)T^{1.5} + d_2(i)T^2 + e_2(i)T^3 \quad \text{for } 900 < T < 6000 \text{ K} \qquad (2.5)$$

The coefficients a's, b's, c's, d's and e's for the various chemical species have been presented in Table 2.1

2.4 Verification of the FEM program

As mentioned earlier, in this thesis a FORTRAN program program was written to compute the equilbria of a reacting mixture. To verify whether the equilibria being computed from the computer program provide the right solution, the predictions were compared to published results. The equilibrium constants for the main Claus reaction were compared with those reported in GPSA handbook (1986). The agreement between the two were within 2 percent. Towler and Lynn (1993) presented the results of their calculation for C-O-S-H system for an initial

Table 2.1 Parameters *a, b, c, d, e* of correlation for energy of formation.

Component	Temp.	a	b	c	d	e
H_2S	0-3000	-17.575	-5.858×10^{-02}	-7.194×10^{-04}	6.469×10^{-05}	-1.189×10^{-08}
CO_2	0-3000	-393.255	-5.507×10^{-03}	1.054×10^{-04}	-4.757×10^{-07}	4.778×10^{-11}
CO	0-3000	-110.332	-9.081×10^{-02}	-6.924×10^{-05}	3.289×10^{-06}	-1.255×10^{-10}
H_2O	0-3000	-240.257	2.407×10^{-02}	1.062×10^{-03}	-1.033×10^{-05}	3.466×10^{-10}
COS	< 900 > 900	-138.513 -202.336	-6.935×10^{-02} -8.914×10^{-03}	-2.674×10^{-03} -8.346×10^{-05}	8.630×10^{-05} 1.367×10^{-06}	-1.156×10^{-08} -1.717×10^{-11}
CS_2	<900 >900	116.104 -10.418	-9.194×10^{-02} -4.079×10^{-03}	-9.292×10^{-03} -1.563×10^{-04}	3.133×10^{-04} 2.178×10^{-06}	-7.540×10^{-08} 4.600×10^{-11}
SO_2	< 900 > 900	-294.308 -347.047	-2.223×10^{-02} 2.789×10^{-02}	-1.017×10^{-03} 1.441×10^{-03}	7.336×10^{-05} -1.447×10^{-05}	-1.941×10^{-08} 5.018×10^{-10}
SO_3	0-3000	-380.701	-9.562×10^{-02}	8.601×10^{-03}	-8.833×10^{-05}	3.028×10^{-09}
S_1	< 900 > 900	291.430 269.371	-3.056×10^{-01} 5.639×10^{-02}	7.963×10^{-03} -1.621×10^{-02}-	-7.991×10^{-05} 3.969×10^{-04}	2.628×10^{-09} -5.315×10^{-08}
S_2	< 882 > 882	125.739 0	-7.449×10^{-03} 0	-1.752×10^{-02} 0	5.637×10^{-04} 0	-1.447×10^{-07} 0
S_3	< 900 > 900	249.887 -47.185	-2.024 5.975×10^{-02}	1.393×10^{-01} 3.986×10^{-04}	-3.272×10^{-03} -4.041×10^{-06}	6.511×10^{-07} 5.224×10^{-11}
S_4	< 900 > 900	275.447 -111.310	-2.397 1.556×10^{-01}	1.667×10^{-01} -5.138×10^{-04}	-3.917×10^{-03} 3.422×10^{-06}	7.838×10^{-07} -1.089×10^{-10}
S_5	< 900 > 900	287.933 -212.195	-3.213 2.893×10^{-01}	2.315×10^{-01} -1.122×10^{-03}	-5.457×10^{-03} 8.329×10^{-06}	1.088×10^{-16} -1.833×10^{-07}
S_6	< 900 > 900	314.340 -283.054	-3.812 3.580×10^{-01}	2.759×10^{-01} -1.536×10^{-03}	-6.512×10^{-03} 1.108×10^{-05}	1.299×10^{-06} -2.247×10^{-10}
S_7	< 900 > 900	360.949 -336.223	-4.4359 0.42716	0.3216 -0.00019	-0.00759 1.3175e-5	1.5165×10^{-5} -2.966×10^{-10}
S_8	< 900 > 900	104.183 -414.36	-0.06891 0.5311	-0.0184 -0.00258	-0.000715 1.8315×10^{-05}	1.7039×10^{-07} -3.7014×10^{-10}
CH_4	0-6000	-71.901	0.0337	0.00269	-2.856×10^{-05}	1.0463×10^{-9}
C_2H_6	0-1500	-68.216	-0.0351	1.231×10^{-02}	-1.925×10^{-04}	1.722×10^{-8}
C_3H_8	0-1500	-81.707	-0.0327	1.815×10^{-02}	-2.97×10^{-04}	2.873×10^{-8}

reacting mixture of CO_2 and H_2S. A comparison between the prediction from their calculations and the prediction from the program developed in this study is presented in Table 2.2 The results compare well, which validates the correctness of the basic algorithm and the calculations from the computer program. The maximum deviation is of the order of seven percent. The deviation may be due either to the difference in convergence criterion or to the difference in fitting of the free energy data.

2.5 Literature review of equilibrium calculations related to Claus process

Several studies on equilibria calculations pertaining to Claus process have been reported in the literature [Gamson and Elkins (1953); Eriksson and Rosen (1968); Bennett and Meisen (1973); Meisen and Bennett (1978); Dalla Lana and Truong (1979); Monnery et al. (1993), Moore (1993) and Khudenko et al. (1993)].

The study by Gamson and Elkins (1953) can be considered to be the first detailed study on the equilibria in a H_2S-Air system. Although, they recognized that the presence of CO_2 in the initial reacting mixture would affect the equilibrium, they included only S_2, S_6, S_8, SO_2, H_2S, H_2O and N_2 in their calculations. They solved the mass balance equations iteratively. Meisen and Bennett (1973), in perhaps the first paper among the many of Claus equilbria studies, reported calculation results in H_2S-Air system up to a temperature of 2000 K. They included up to 36 chemical species that included many nitrogen compounds and radicals. In another of their studies (Meisen and Bennett, 1974), extended the number of chemical species by including carbon, carbon-nitrogen and carbon-sulfur species in calculating equilibria for H_2S-CO_2-Air mixtures. Dalla Lana and Truong (1979), in the wake of the controversy surrounding thermochemical properties of the sulfur allotropes, were of the opinion that equilibrium calculations should be based on the experimentally obtained results

Table 2.2 Comparison of fractional distribution of sulfur-containing species for an equimolar feed of H_2S and CO_2 at 900 °C and 1.0 atm. 17

Species	Towler and Lynn (1993)	This study	% Difference
S_2	0.324	0.3199	1.282
H_2S	0.614	0.616	0.647
SO_2	0.000811	0.000738	9.89
COS	0.0607	0.0634	4.17
CS_2	0.0000087	0.0000079	9.14

for conversion of H_2S to sulfur. They reported the use of free energy minimization program for calculation of equilibria. In recent years, Monnery et al. (1993) and Khudenko et al. (1995) have reported equilibria calculations for Claus furnace reactions employing the energy minimization method. The primary objective of both Moore (1993) and Monnery et al. (1993) studies were to highlight the inadequacy of the various methods (Equilbrium method, Fisher Nomograph and Western Research correlation) in correctly predicting the product composition from the reaction furnace. Khudenko et al. (1993) employed the commercially available software (STANJAN) capable of computing three phase multi-component reaction equilibrium studies. The objective of their study was to predict the equilibria for Claus process under oxygen-enrichment conditions.

In all of the above-mentioned studies, the primary objective was to predict the performance of the Claus process. There was no attempt made to elucidate the chemistry of the various reactions taking place in the reaction furnace. The results of the present study, presented and discussed in the following section, are distinguished from earlier studies because the focus here is on finding the thermodynamic favorability of the formation of certain chemical species.

2.6 Results and discussions

Prior to the presentation and discussion of the equilibrium results, a clarification needs to be made regarding the selection of important reactions depending on the thermodynamic favorability of formation (or consumption) of a component of interest. For a reacting system, where only a single reaction is allowed to occur, one can conclude from the computed equilibrium composition whether the reaction is favored to occur thermodynamically or not. However, for a reacting system where multiple reactions are allowed to occur, it is not possible to conclude if a particular reaction is favoring the formation (or consumption) of a

certain chemical species. In such a case, the reacting feed can be assigned to be a favorable reacting mixture for formation (or consumption) of the species.

2.7 H_2 and CO formation and consumption reactions

The CO and H_2 related reactions that could possibly occur in the reaction furnace are given in Table 2.3 It is important to note that only molecular reactions have been included. Under Claus furnace conditions, the actual reactions may proceed via many elementary reactions involving atoms and radicals. However, only the molecular species are typically measured and they are usually present at relatively higher concentrations than the atoms and radicals. Therefore, it is meaningful to compute equilibrium for systems composed of molecular species only.

Equilibrium predictions for the H_2S dissociation reaction. The equilibrium distribution of various species resulting from a pure H_2S feed at 101.3 kPa and over temperatures of 400 to 2000 K is shown in Figure 2.1.The molecular species included for the calculations were H_2, H_2S, and S_i, where i=1 to 8. Above 800 K, where the dissociation is significant, the dominant sulfur species is S_2. Below 800 K, the H_2S dissociation is negligible.

Effect of pressure on H_2 yields from H_2S decomposition reaction.

To demonstrate the effect of pressure on the equilibria of a chemically reacting system, the results for H_2 yield (i.e. number of moles of hydrogen divided the total number of moles of hydrogen containing species) from H_2S decomposition reaction is presented in Figure 2.2. The decomposition of H_2S to H_2 and S_2 takes places with an increase in number of moles during the reaction. Therefore, as expected from Le Chatelier's principle a decrease in pressure promotes the H_2S decomposition reaction.

Table 2.3 Possible CO/H_2 Reactions Occurring in RF/WHB (based on Paskall, 1979)

H_2S	$\leftrightharpoons$	$H_2 + ½ S_2$	(2.6)
CO_2	$\leftrightharpoons$	$CO + ½ O_2$	(2.7)
$CO_2 + H_2S$	$\leftrightharpoons$	$CO + H_2O + ½ S_2$	(2.8)
$2CO_2 + H_2S$	$\leftrightharpoons$	$2CO + H_2 + SO_2$	(2.9)
$CO_2 + H_2$	$\leftrightharpoons$	$CO + H_2O$	(2.10)
$CH_4 + 3/2\ O_2$	$\leftrightharpoons$	$CO + 2H_2O$	(2.11)
$CH_4 + O_2$	$\leftrightharpoons$	$CO + H_2O + H_2$	(2.12)
$CH_4 + 2H_2O$	$\leftrightharpoons$	$CO_2 + 4H_2$	(2.13)
$H_2 + ½ O_2$	$\leftrightharpoons$	H_2O	(2.14)

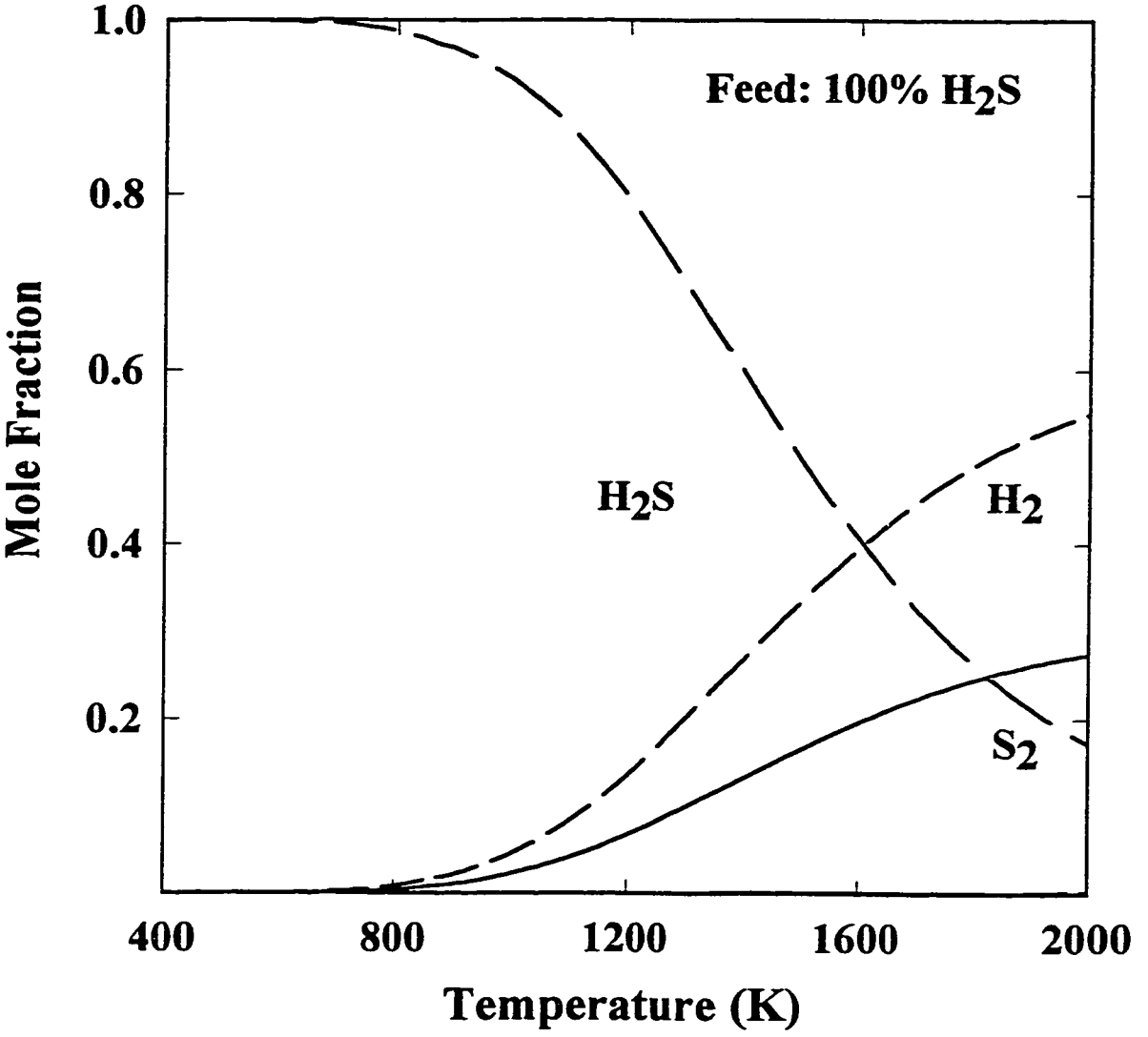

Figure 2.1 Equilibrium gas composition in a H_2S-H_2-S_i (i=1,2...8) system. (Feed: 100% H_2S; P=101.3 kPa)

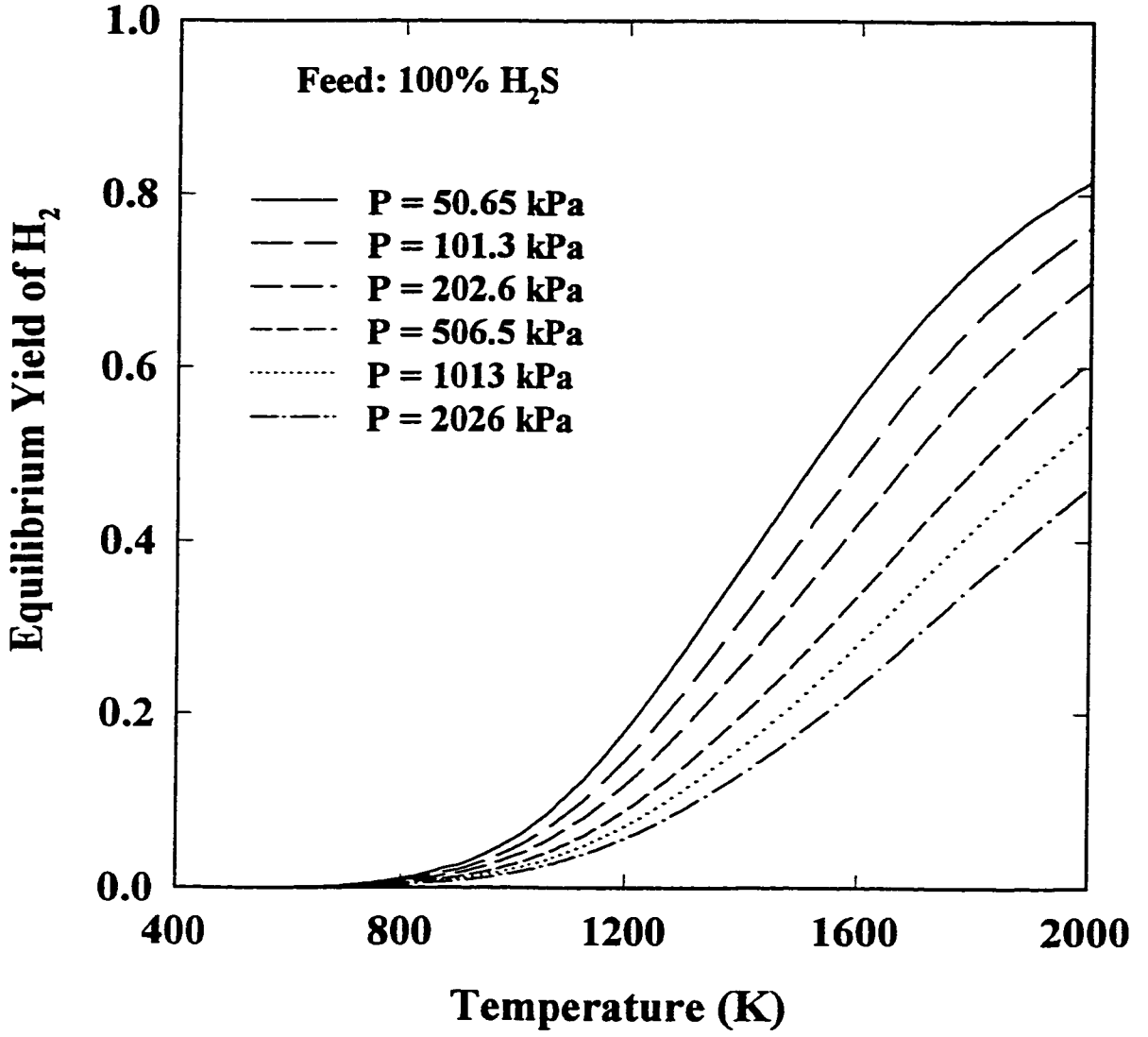

Figure 2.2 Effect of pressure on equilibrium H_2 yields for a pure H_2S feed.

Equilibrium predictions for the CO_2 dissociation reaction. Equilibrium calculations were performed to obtain the ultimate yield of CO produced via reaction (2.7) from a pure CO_2 feed, by including only three molecular species: CO_2, CO and O_2. The total system pressure was fixed at 101.3 kPa. The results presented in Figure 2.3 show that CO_2 dissociation reaction is not favored up to a temperature of 1400 K. Even at 2000 K, the equilibrium CO yield is less than one percent. Thus, this reaction is not an important CO formation reaction.

Equilibrium predictions for a reacting system with a CO_2+H_2S feed. Figure 2.4 gives the equilibrium distribution of various species in a C-O-S-H system from an equimolar feed of CO_2 and H_2S. The species included for the calculations were limited to those associated with reactions (2.8) and (2.9) and were CO_2, H_2S, CO, H_2, H_2O, SO_2 and S_i where i=1 to 8. On the assumption that CO is produced only via these two reactions, it can be seen from Figure 2.4 that reaction (2.9) is favored only above a temperature of 1200 K. This can be inferred from the fact that SO_2, one of the products of reaction (2.9), only appears in the equilibrium mixture above 1200 K. In the temperature range of 800-1200 K, the equilibrium mole fractions of CO and H_2O are identical, following the stoichiometry of reaction (2.9). Above 1200 K, the mole fraction of CO is always greater than that of H_2O suggesting that CO is produced via a reaction other than reaction (2.8).

Equilibrium prediction for the reverse of water gas shift reaction. Another important reaction that may cause the production of CO is the reverse of the water gas shift reaction (2.10). The equilibrium distributions of CO, CO_2, H_2, H_2O at 101.3 kPa from an equimolar feed of CO_2 and H_2 were computed. The results are presented in Figure 2.5. The CO_2 conversion to CO increased from less than

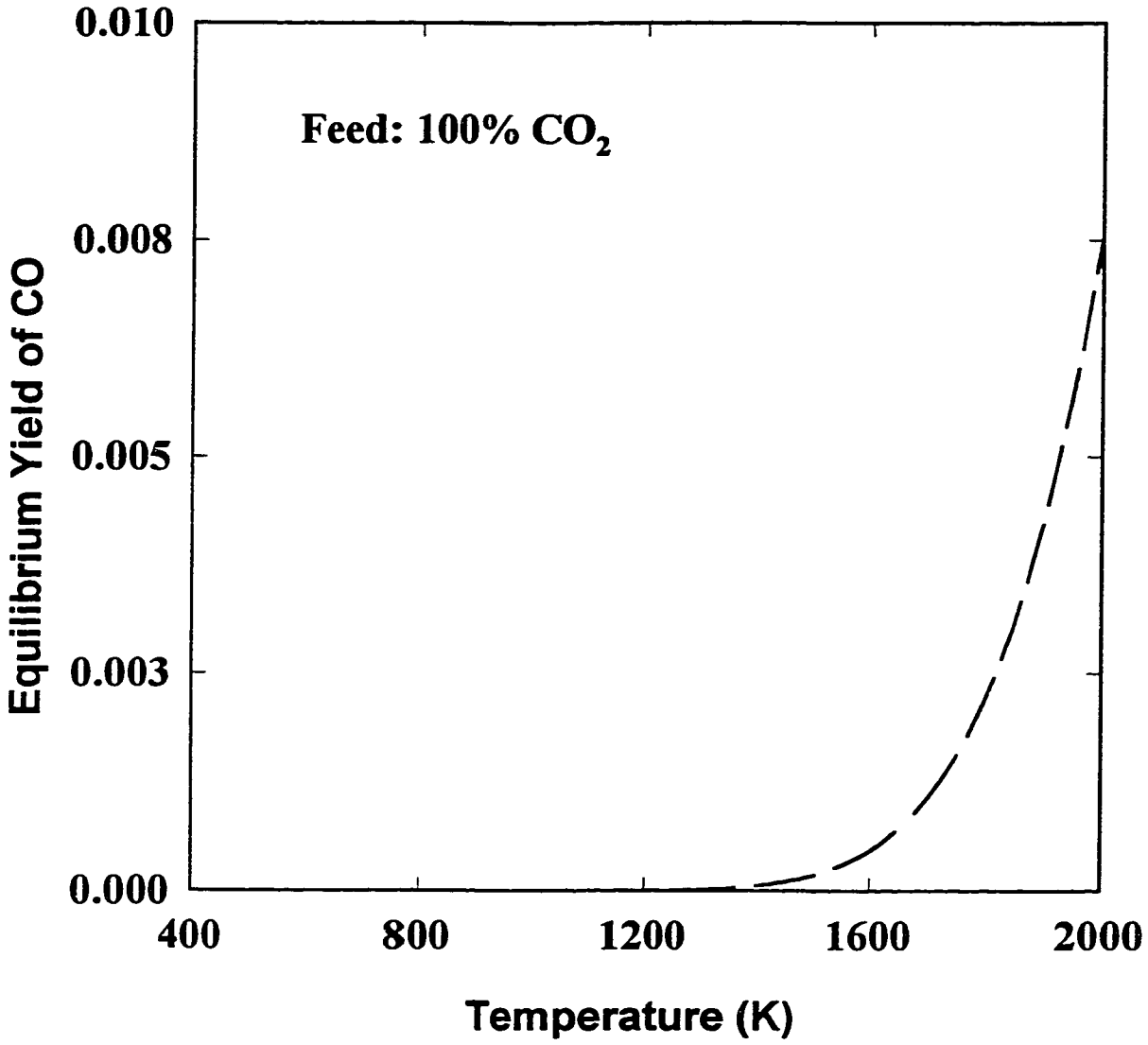

Figure 2.3 Equilibrium CO yield from an equimolar feed of CO_2 and N_2 (P=101.3 kPa).

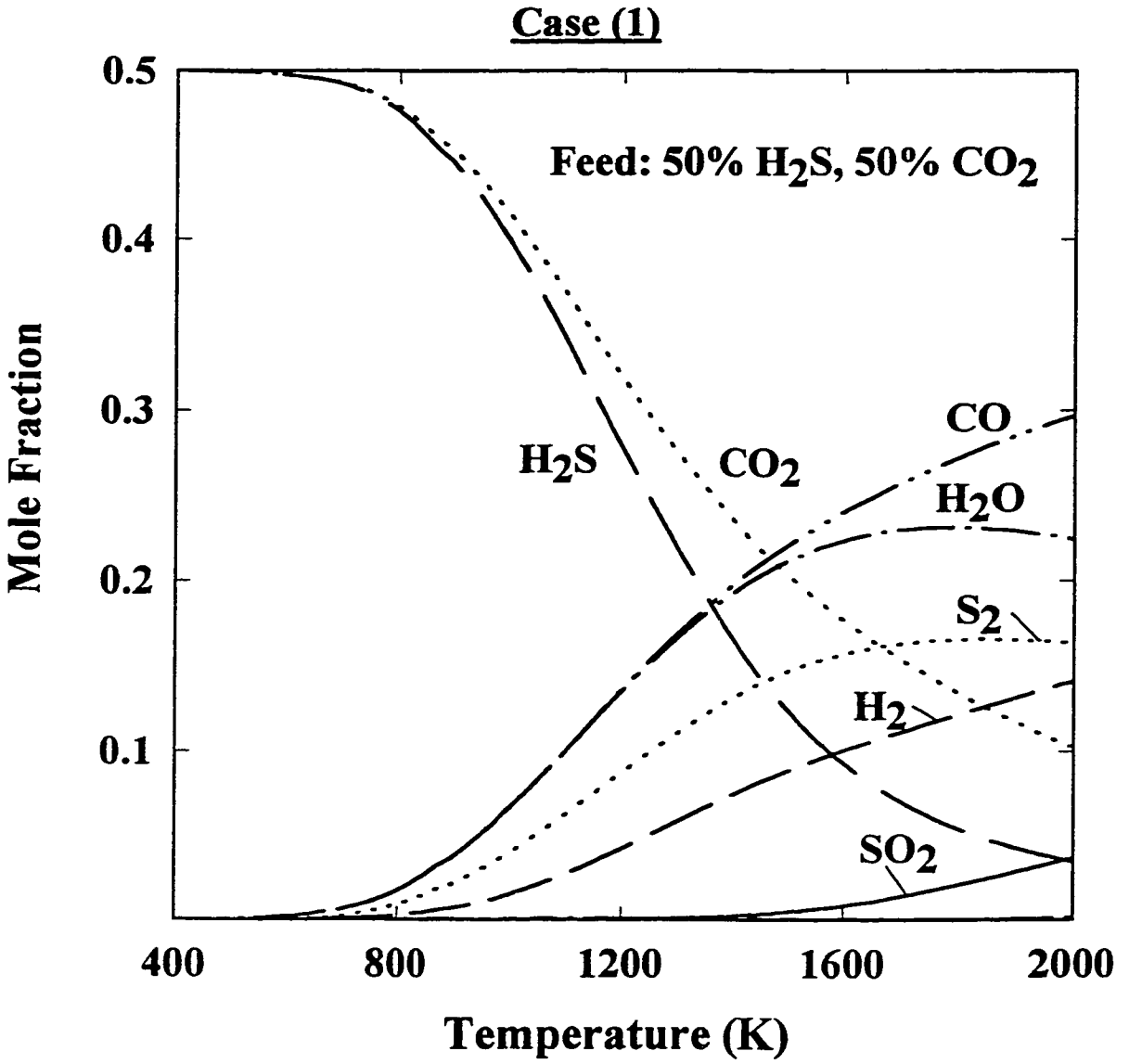

Figure 2.4 Equilibrium gas composition for an equimolar feed of H_2S and CO_2. (P=101.3 kPa).

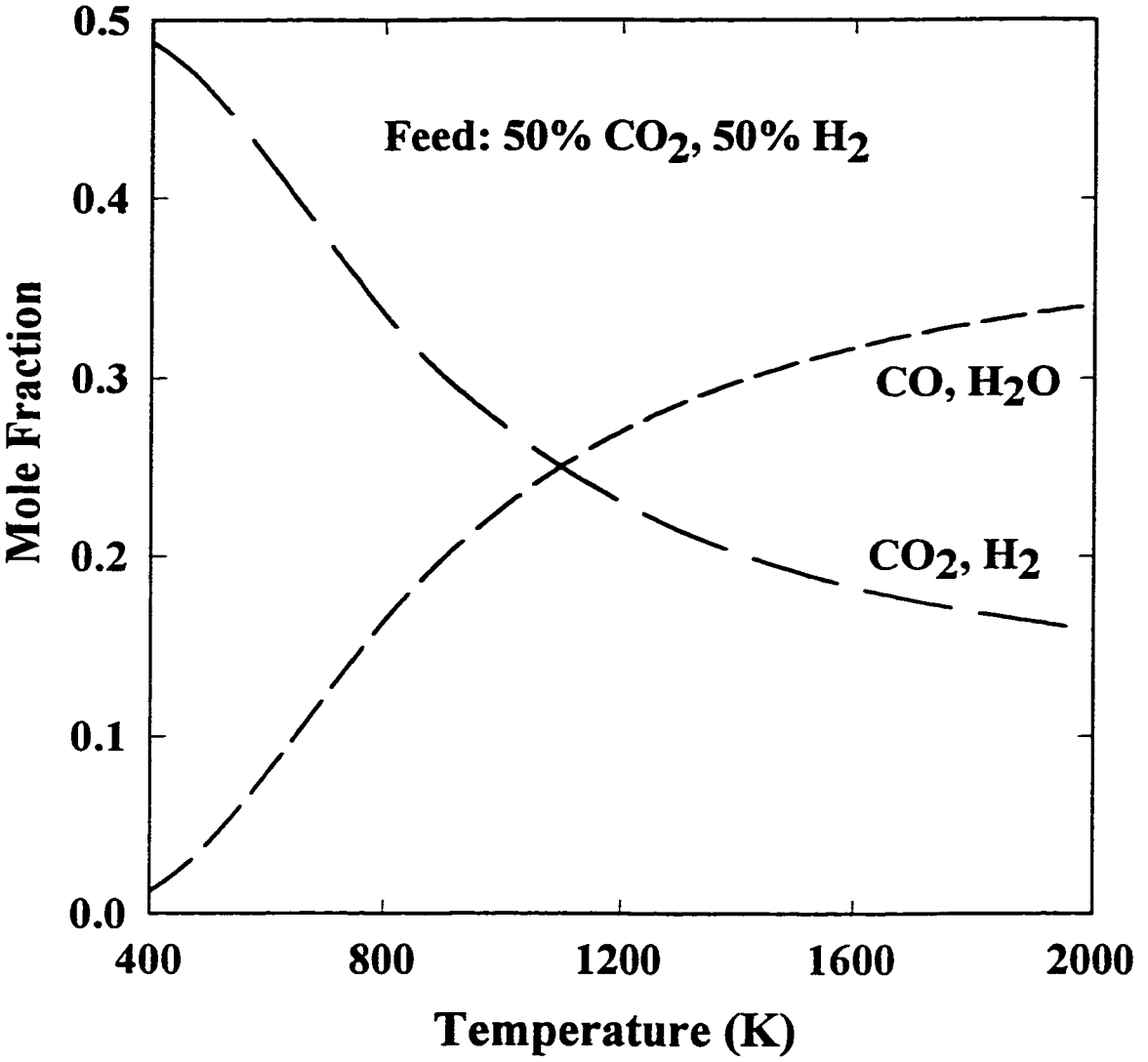

Figure 2.5 Equilibrium distribution of CO_2-CO-H_2O-H_2 for an equimolar feed of CO_2 and H_2. (P=101.3 kPa).

5% at 400 K to more than 65% at 2000 K. At temperatures of our interest (800-1600 K), CO_2 conversion to CO varies from over 30% to about 60%.

CO from a reacting feed of CO_2 and H_2S From the detailed study of possible reactions, the reaction (2.8) between CO_2 and H_2S can be proposed to be comprised of a two step mechanism. The first step is the production of H_2 from H_2S dissociation and the second step is the reaction of H_2 with CO_2 to produce CO and H_2O. This can be represented by the following set of reactions:

$$H_2S \rightleftharpoons H_2 + \tfrac{1}{2} S_2 \qquad (2.7)$$

$$CO_2 + H_2 \rightleftharpoons CO + H_2O \qquad (2.10)$$

$$CO_2 + H_2S \rightleftharpoons CO + H_2O + \tfrac{1}{2} S_2 \qquad (2.8)$$

To support the proposed mechanism, the equilibrium yields of CO and H_2 for systems with equimolar H_2S+N_2, H_2S+CO_2 and CO_2 +H_2 feeds have been plotted in Figure 2.6. The equilibrium yields of CO and H_2 were calculated as $YIELD_{CO} = y_{CO}/\Sigma y_{Ci}$ and $YIELD_{H2} = y_{H2}/\Sigma y_{Hi}$, where y_{co} and y_{H2} are equilibrium mole fractions of CO and H_2 respectively, and y_{Ci} and y_{Hi} are the equilibrium mole fraction of *i* th carbon and *i* th hydrogen containing species. The equilibrium H_2 yields from H_2S cracking reaction were obtained for an equimolar H_2S and N_2 feed. Nitrogen was added to eliminate the effect of H_2S partial pressure in the feed on H_2 yield. From Figure 2.6, it can be noted that the appearance of H_2 at 800 K in the system with H_2S–CO_2 feed coincides with that for the system with H_2S-N_2 feed. This indicates that even in a reacting system with H_2S–CO_2 feed, H_2 is produced via thermal decomposition of H_2S. Additionally, the appearance of CO in a system with H_2S–CO_2 feed also occurs approximately at the same temperature at which H_2 appears. However, in a system with CO_2–H_2 feed, CO is present at significant levels even at lower temperatures which suggests that if H_2 had been produced by some reaction at a temperature lower than 800 K, it would be favored to react with CO_2 to produce CO. Thus, the limiting step for CO

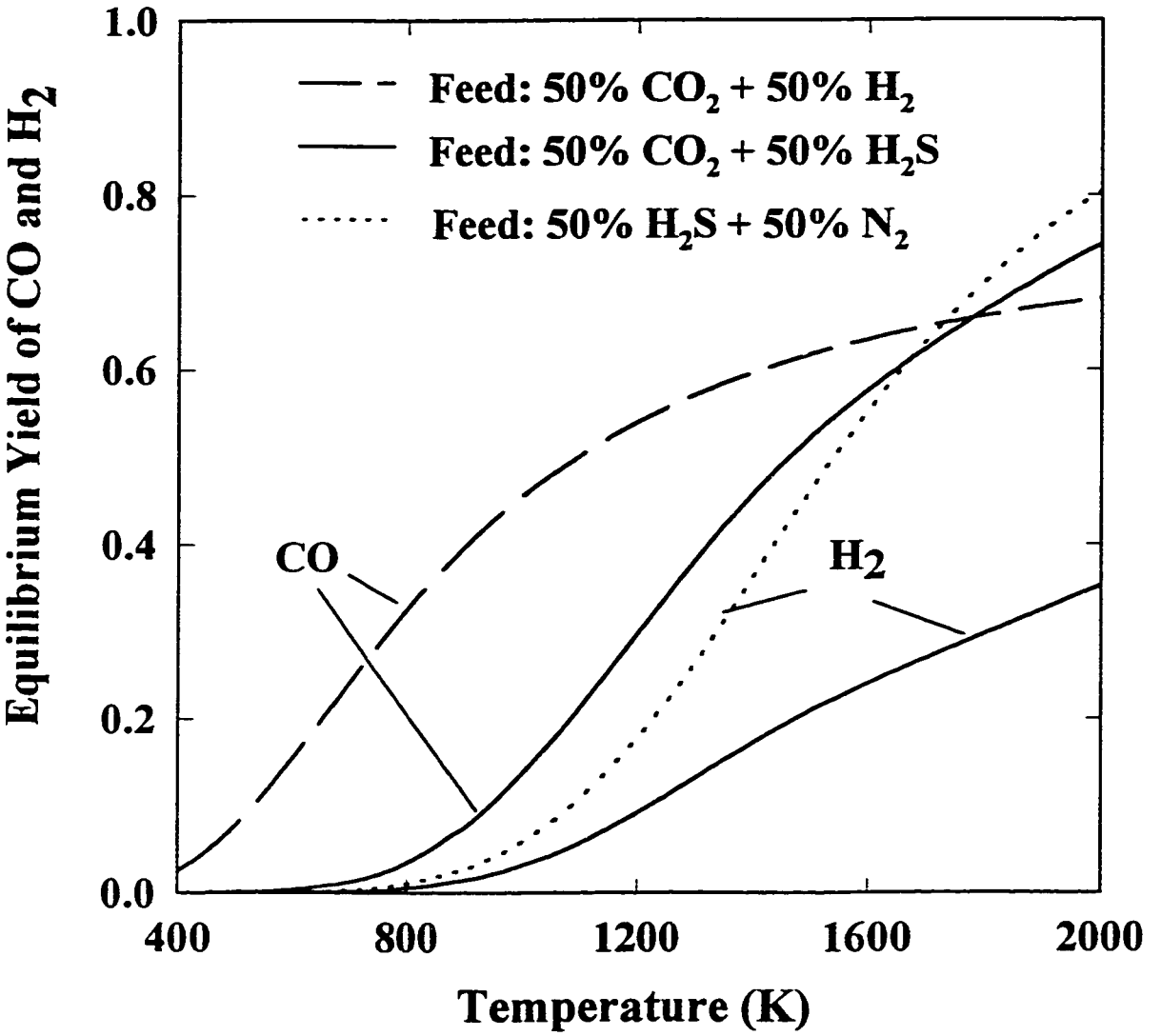

Figure 2.6 Equilibrium yields of H_2 and CO from equimolar feeds of H_2S and N_2, H_2S and CO_2, H_2 and CO_2. (P=101.3 kPa).

production in the reaction furnace can be proposed to be the dissociation of hydrogen sulfide to produce hydrogen.

2.8 COS formation and consumption reactions

The important COS reactions that can possibly occur in the furnace are listed in Table 2.4 Of the nine reactions, four have either CH_4 or CS_2 as one of the reactants. Typically, CH_4 is present only at low concentrations (< 2 mol%) in the RF feed. For CH_4 to react with SO_2 to form COS, SO_2 is to be produced first from H_2S oxidation reaction. During the process of H_2S oxidation, a majority of CH_4 may get oxidized too. Hence, significant COS formation from CH_4-SO_2 reaction may not occur. CS_2 formation is known to be kinetically limited, thus, COS production from CS_2 will be kinetically limited too. Moreover, low CS_2 concentrations will result in a lower COS production.

Equilibrium prediction for reaction between CO_2 and S_2. Calculations were performed for the C-O-S system with an equimolar feed of CO_2 and S_2 and by including the molecular species CO_2, CO, COS, SO_2 and S_1-S_8. The equilibrium gas composition for this system is presented in Figure 2.7. From the Figure, it can be seen that the COS mole fraction increases up to a temperature of 1000 K above which it decreases. This is due to the decomposition of COS into CO and S_i, which is favored at higher temperatures. A peak value of 4% COS yield is reached at 1000 K which then reduces to 1.5% at 1600 K. Overall, from these results, we can infer that this reaction will not contribute significantly to the production of COS either in the RF or in the WHB.

Equilibrium prediction for reaction between CO and S_i. Calculations were also performed for an equimolar feed of CO and S_2 and by including the molecular species COS, CO and S_1-S_8. The equilibrium composition of the mixture at

Table 2.4 **Possible COS Reactions Occurring RF/WHB (based on Paskall, 1979)**

$2CO_2 + 1.5\ S_2$	$\leftrightharpoons$	$2COS + SO_2$	(2.15)
$2CO_2 + S_2$	$\leftrightharpoons$	$COS + CO + SO_2$	(2.16)
$CO + ½\ S_2$	$\leftrightharpoons$	COS	(2.17)
$COS + H_2O$	$\leftrightharpoons$	$H_2S + CO_2$	(2.18)
$CO + H_2S$	$\leftrightharpoons$	$COS + H_2$	(2.19)
$CH_4 + SO_2$	$\leftrightharpoons$	$COS + H_2O + H_2$	(2.20)
$2CH_4 + 3SO_2$	$\leftrightharpoons$	$2COS + ½\ S_2 + 4H_2O$	(2.21)
$CS_2 + H_2O$	$\leftrightharpoons$	$COS + H_2S$	(2.22)
$CS_2 + CO_2$	$\leftrightharpoons$	$2COS$	(2.23)

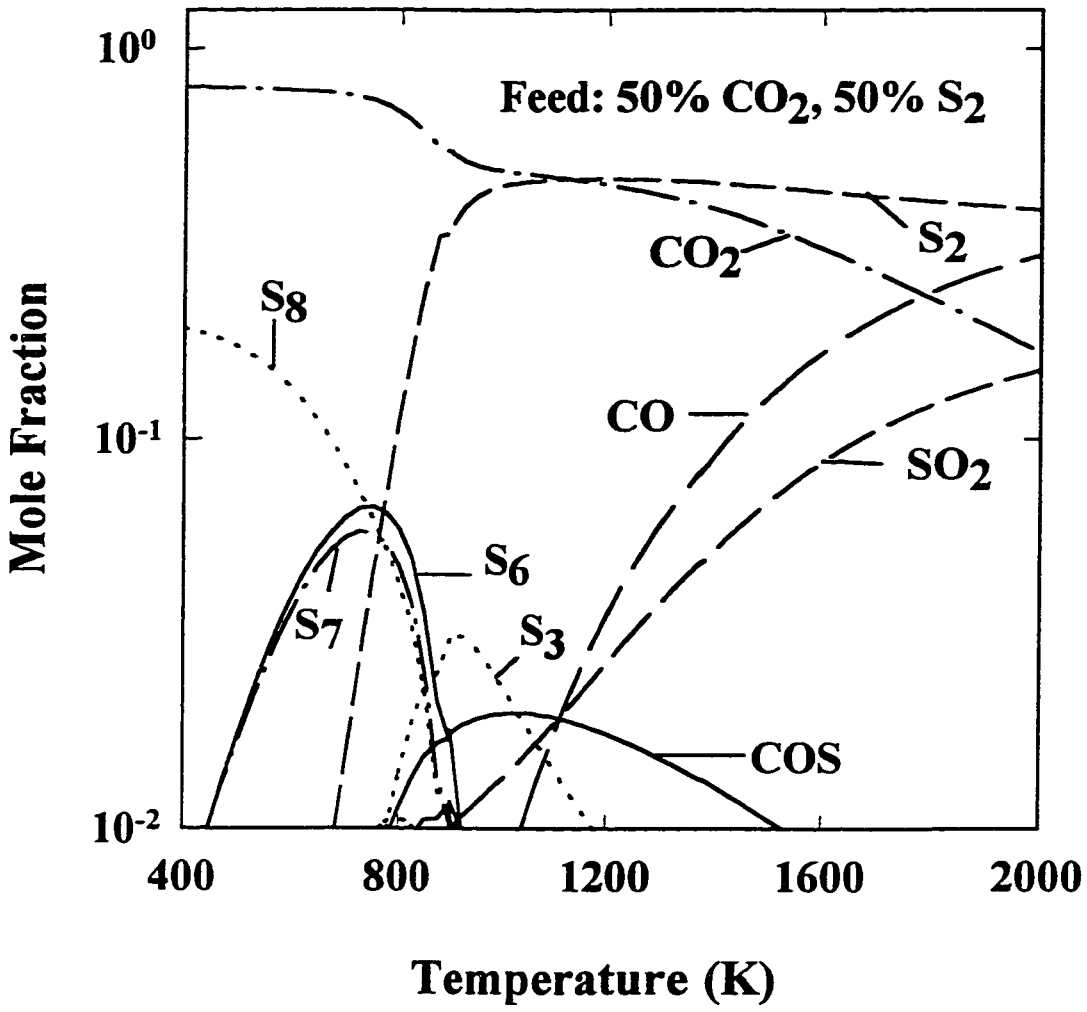

Figure 2.7 Equilibrium gas composition for an equimolar feed of CO_2 and S_2. (P=101.3 kPa)

101.3 kPa has been illustrated in Figure 2.8. Below 800 K, the COS mole fraction in the mixture is higher than that of any other species by an order of magnitude. Thus, we conclude that COS formation is heavily favored at lower temperatures (<800 K) such as those encountered in the WHB. This result also supports the findings of Sames et al. (1990) that CO and S_i recombine to produce COS in the WHB. It is also known that COS cracking is favored at higher temperatures (>1000 K) such as those encountered in the RF.

Equilibrium predictions for the reverse of COS hydrolysis reaction. Calculations were performed for an equimolar feed of H_2S and CO_2 to predict the equilibrium of the reverse of the COS hydrolysis reaction (2.18). The results shown in Figure 2.9 indicated that, thermodynamically, COS formation via this reaction is favored at higher temperatures, whereas we know that the COS hydrolysis is the favored reaction at lower temperatures such as those encountered in the catalytic converters. The equilibrium conversion to COS increased from less than 2% at 400 K to about 30% at 2000 K. The conversion here is calculated as moles of COS produced per mole of C containing species in the feed, which is CO_2.

The C-O-S-H system. Calculations were also performed for the C-O-S-H system by including the following chemical species: CO_2, H_2S, CO, H_2, O_2, H_2O, SO_2, S_i, COS, CS_2 and SO_3. The equilibrium composition for this system at 101.3 kPa for an equimolar feed of H_2S and CO_2 is presented in Figure 2.10 (case 2). It should be noted that results for the same feed at the same system pressure were illustrated in Figure 2.4 (case 1); however, the molecular species COS, CS_2 and SO_3 had not been included for that calculation. On comparing the two figures, we can see that all of the components except for COS and H_2O follow similar trends. H_2O in an appreciable concentration is present at 600 K for case 2 but not for case 1. For case 2, a maximum in COS mole fraction is

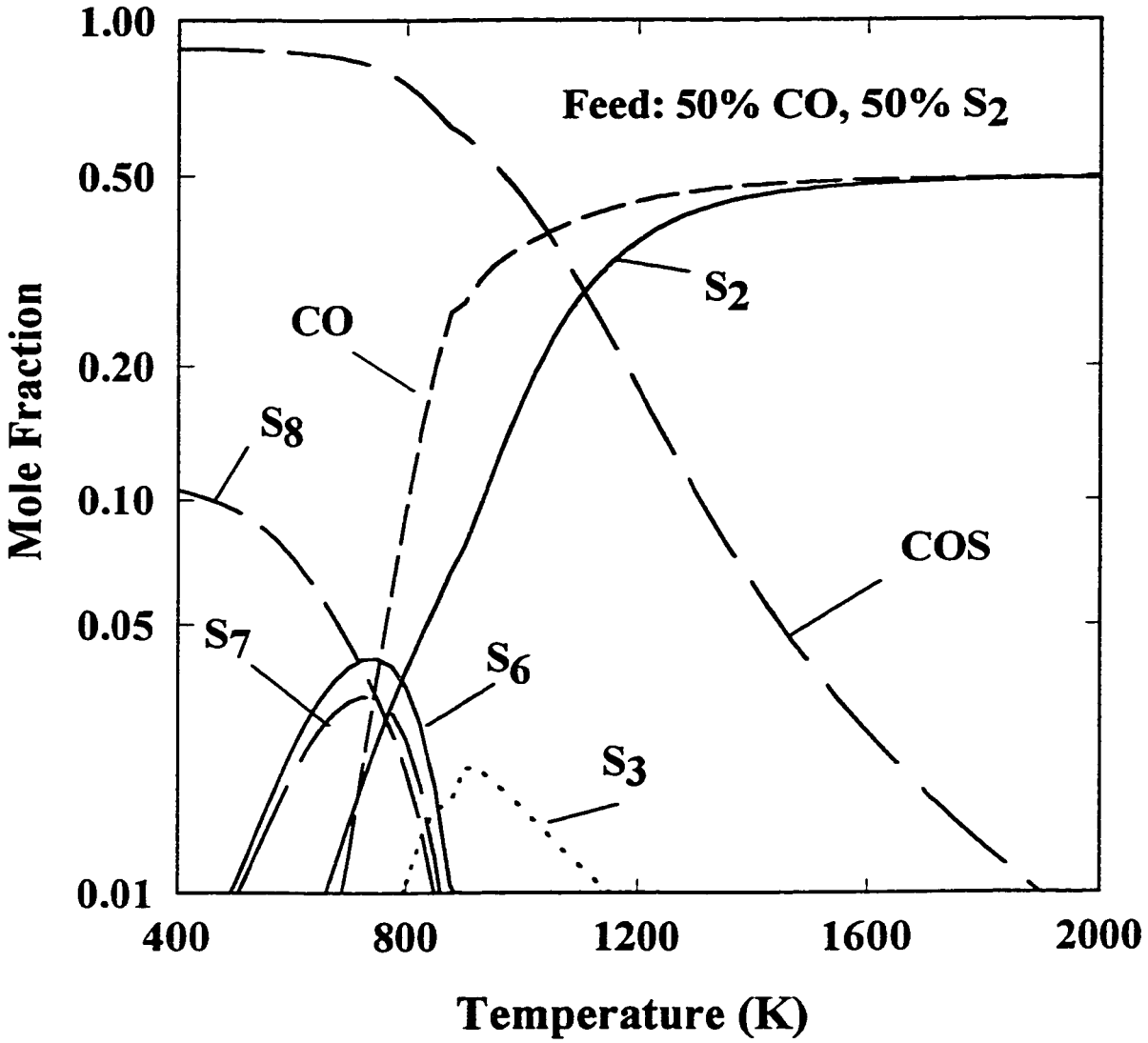

Figure 2.8 Equilibrium gas composition for an equilmolar feed of CO and S_2. (P=101.3 kPa).

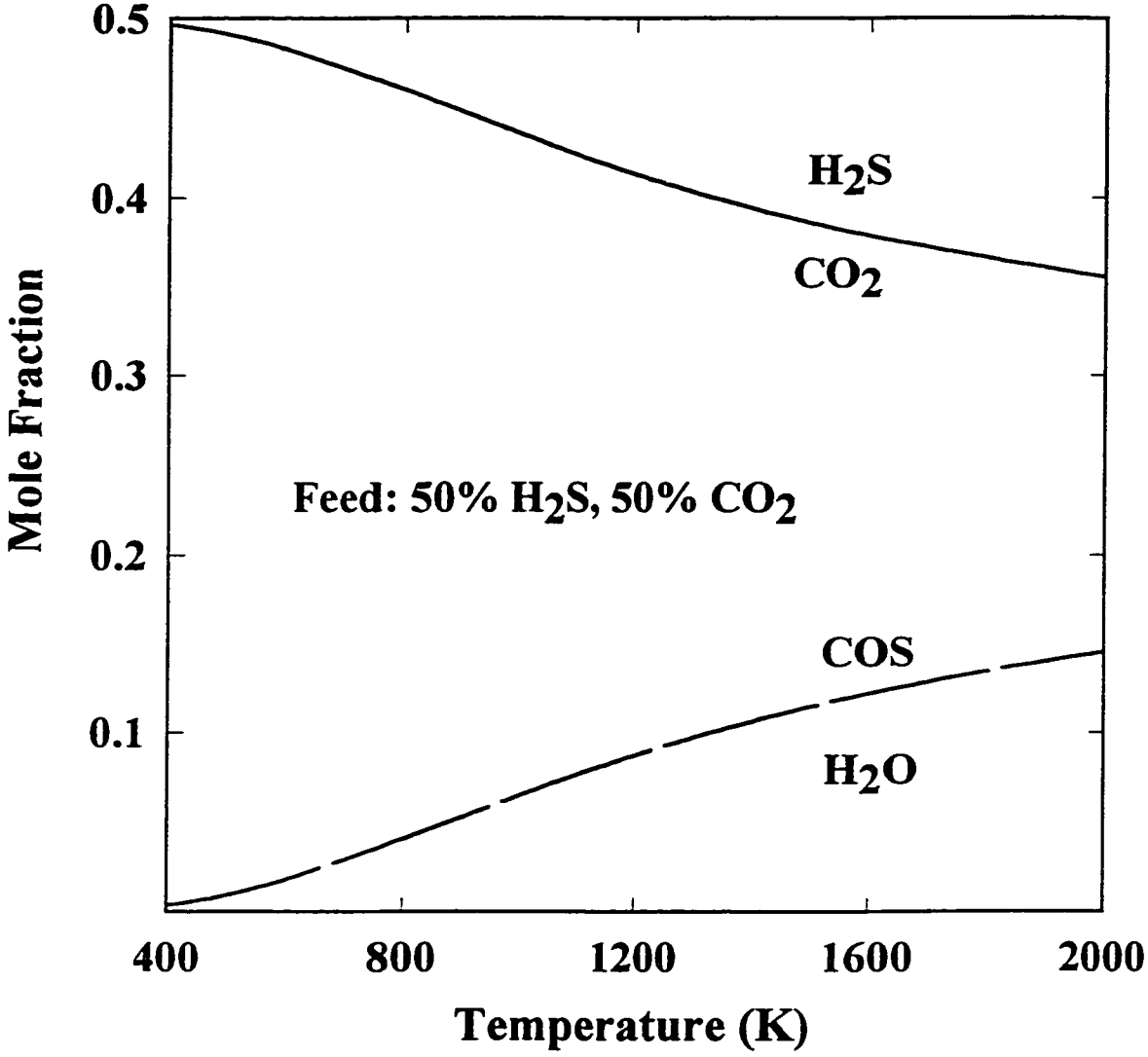

Figure 2.9 Equilibrium distribution of COS, H_2O, CO_2 and H_2S for an equimolar feed of H_2S and CO_2. (P=101.3 kPa)

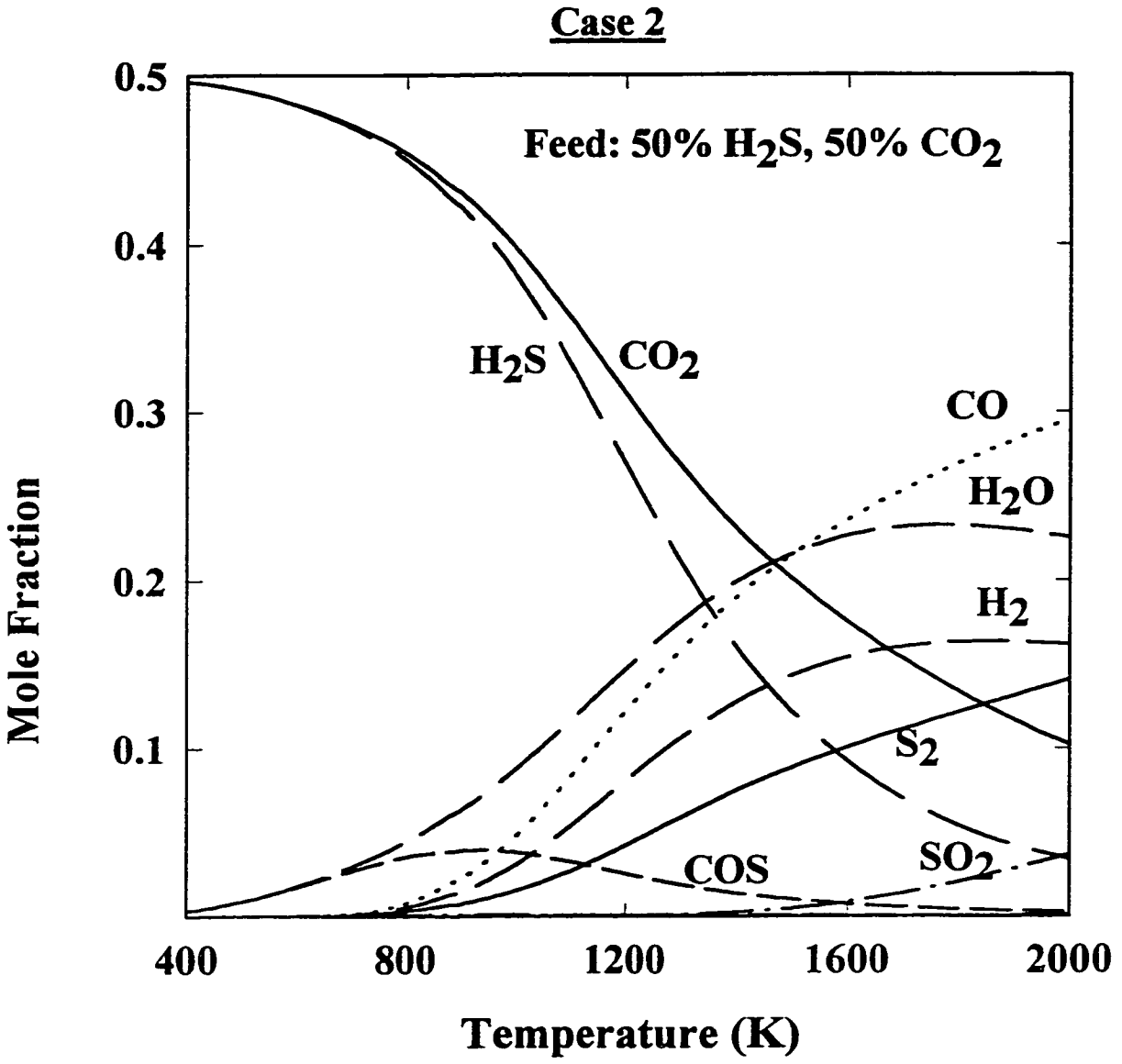

Figure 2.10 Equilibrium gas composition for an equimolar feed of CO_2 and H_2S. (P=101.3 kPa)

observed at a temperature of 950 K, this coincides with the temperature of COS maximum in an equimolar CO_2-S_2 feed. The COS mole fraction decreases at temperatures above 950 K due to the COS decomposition reaction which is favored at higher temperatures.

Equilibrium predictions for a reacting feed of CO and H_2S. Two sets of calculations were performed for an equimolar feed of H_2S and CO, the results of which are presented in Figures 2.11 (a) and 2.11 (b). For the first set, the chemical species included were CO, H_2S, COS and H_2 while for the second set, to allow for hydrogen sulfide dissociation, additional species included were elemental sulfur or S_i, where i=1 to 8. It can seen from Figure 2.11 (a) that COS formation via reaction (2.19) is practically unaffected by the temperatures and the equilibrium conversions can be calculated to be about 20 percent. Comparing the Figures 2.11 (a) and 2.11 (b), it can be observed that at temperatures below 1000 K the COS and H_2 formation is via reaction (2.19), however, at higher temperatures the dissociation of COS and H_2S is highly favored resulting in increased equilibrium production of H_2 but a low equilibrium yield of COS.

Equilibrium prediction for reaction between CH_4 and SO_2.

The equilibrium distribution of various species from an equimolar feed of CH_4 and SO_2 is shown in Figure 2.12. The majority of CH_4 is consumed above 1000 K. The formation of COS is also only slightly favored above this temperature for this reacting mixture. Whether or not COS formation will occur in the reaction furnace via interaction of CH_4 and SO_2 will depend on the availability of methane. It is expected that methane will be consumed rapidly via the oxidation reaction within the flame region.

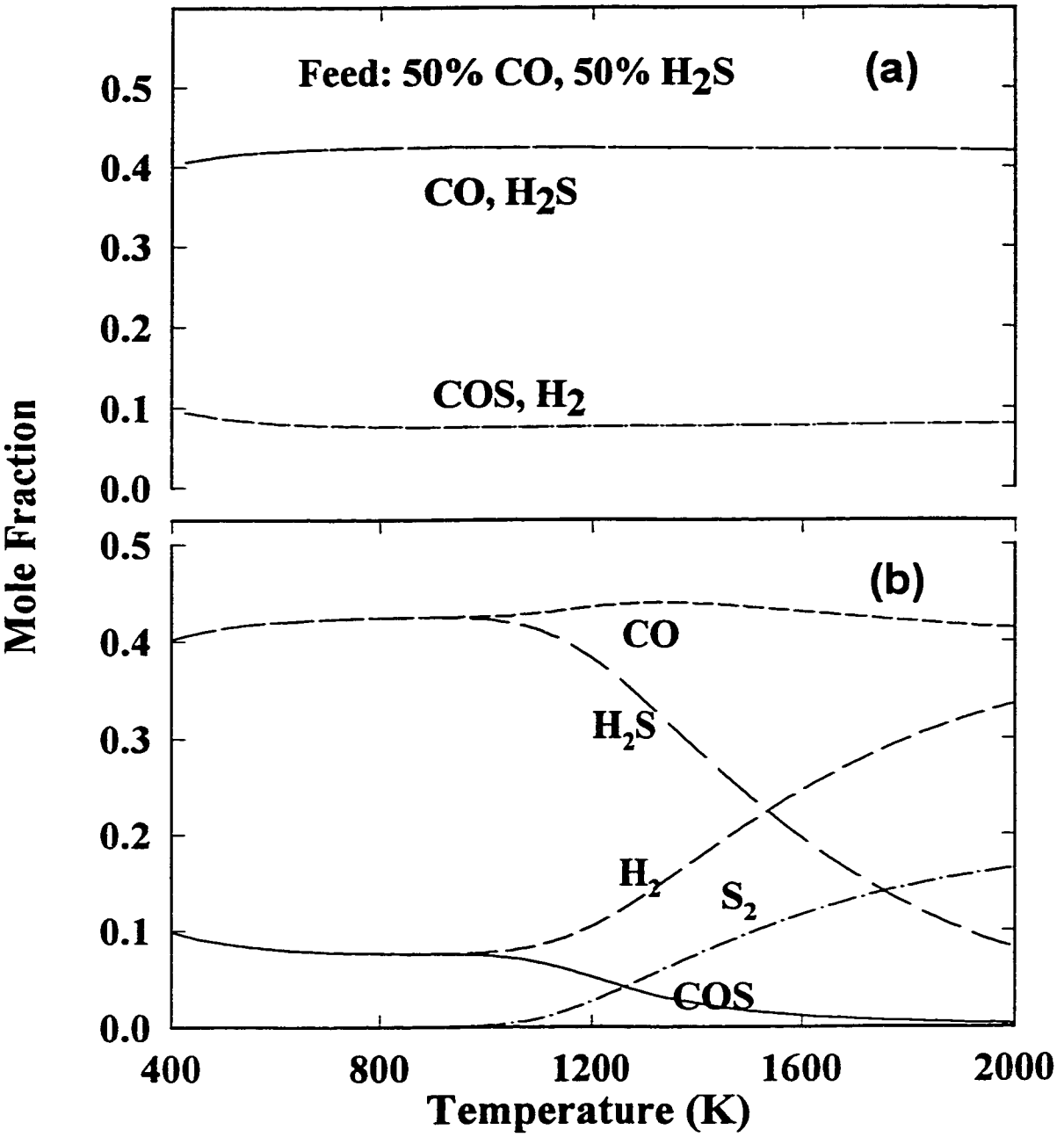

Figure 2.11 Equilibrium gas compositions for an equimolar feed of CO and H_2S. (P=101.3 kPa).
(a) $CO/H_2S/COS/H_2$ system.
(b) $CO/H_2S/COS/H_2/S_i$ (i=1,2...8) system.

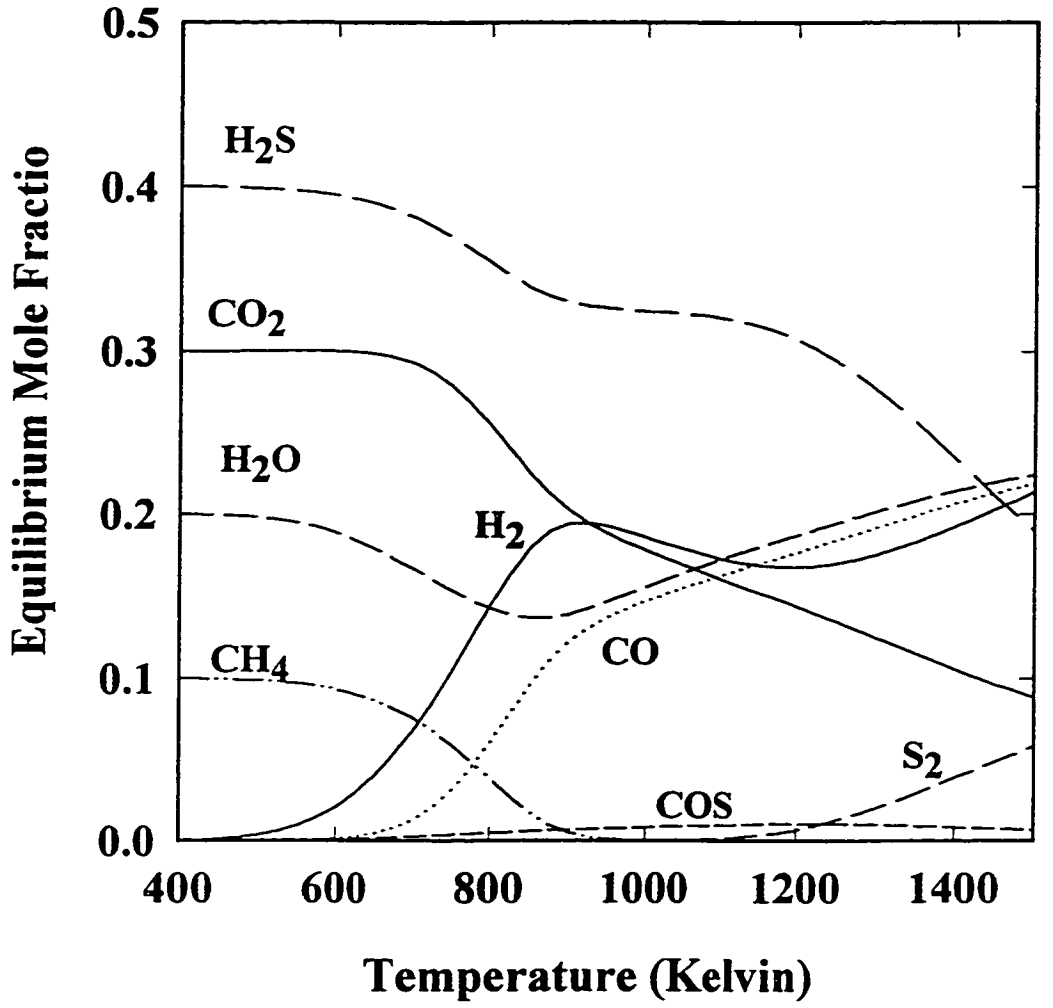

Figure 2.12 Equilibrium distribution for various species for an equimolar feed of CH_4 and SO_2. (P=101.3 kPa)

2.9 CS_2 Formation and Consumption Reactions

The presence of CS_2 in the furnace product stream has been attributed to the hydrocarbons in the RF feed. Hence, it is not surprising to see that four of the six possible CS_2 forming reactions [see Table 2.5] have alkanes as one of the reactants. The two other reactions involve reactions of sulfur with carbon and CO_2 , respectively. The feasibility of reaction between CO_2 and S_2 to produce COS has already been discussed in the previous section. It is suggested that these two components can react to form CS_2 according to the reaction (2.24). Moreover, coke is known to be produced during hydrocarbon combustion process under lean conditions. It can be present in a solid as well as in the gaseous state at high temperatures. A possible route for CS_2 formation can be that via reaction (2.25).

Equilibrium predictions for the reactions between CO_2 and S_i. Equilibrium calculations were carried out to compute the equilibrium yield of CS_2 from reaction (2.24). Only the molecular species involved in this reaction were included for the calculation. The result of the calculations for the above system with a equimolar feed of CO_2 and S_2 feed showed (results not given here) that CS_2 formation is not at all favored via reaction (2.24). Although the CS_2 yield increases with temperature, it is less than 1% even at its maximum value at 2000 K. Thus, this reaction is unimportant as far as contribution to CS_2 formation is concerned.

Equilibrium prediction for reaction between C(g) and S_i. Equilibrium calculations were performed to predict the formation of CS_2 via the reaction between carbon and sulfur. It is known that carbon exists in a number of allotropic forms and also in various phases; most commonly it is present in liquid

Table 2.5 Possible CS_2 Reactions Occurring in RF/WHB (based on Paskall, 1979)

$CO_2 + 3/2S_2$	$\leftrightharpoons$	$CS_2 + SO_2$	(2.24)
$C + S_2$	$\leftrightharpoons$	CS_2	(2.25)
$CH_4 + 2H_2S$	$\leftrightharpoons$	$CS_2 + 4H_2$	(2.26)
$CH_4 + 4/i\ S_i$	$\leftrightharpoons$	$CS_2 + 2H_2S$	(2.27)
$C_2H_6 + 7/2S_2$	$\leftrightharpoons$	$2CS_2 + 3H_2S$	(2.28)
$C_3H_8 + 5S_2$	$\leftrightharpoons$	$3CS_2 + 4H_2S$	(2.29)

and solid phases as coke. Since we are interested in homogeneous gas phase reactions, the carbon species included for the calculation (C_1 to C_5) were assumed to be present in the gaseous state. The calculation results shown in Figure 2.13, predict essentially complete or 100 percent conversion to CS_2 over the temperature range of 400-2000 K.

Equilibrium prediction for reacting feeds of hydrocarbons and S_i/H_2S. The results of the equilibrium calculations for C-H-S system are presented in Figure 2.14. Calculations were performed for six sets of equimolar feed: CH_4+H_2S, CH_4+S_2, $C_2H_6+S_2$, $C_2H_6+H_2S$, $C_3H_8+S_2$, $C_3H_8+H_2S$. The molecular species included for each set of calculation were C_nH_{2n+2}, H_2S, H_2, CS_2 and S_1-S_8, where the hydrocarbon present in the feed only was considered. The results are plotted in Figure 2.14 as equilibrium yield of CS_2, which is the moles of CS_2 produced per mole of carbon in feed. For hydrocarbon-sulfur feed, significant equilibrium conversions to CS_2 are predicted. However, for a hydrocarbon-hydrogen sulfide feed, the CS_2 formation is not favored below a temperature of 1000 K.

The CS_2 formation reaction for hydrocarbon-hydrogen sulfide feed can be explained via a two step reaction scheme. In the first step, hydrogen sulfide dissociates into hydrogen and sulfur. The sulfur produced then reacts with the alkane to form carbon disulfide and hydrogen sulfide. This can be represented as follows:

$$(2n)\ H_2S \rightleftharpoons (2n)\ H_2 + (n)\ S_2 \qquad (2.30)$$

$$C_nH_{2n+2} + (3n+1)/2\ S_2 \rightleftharpoons n\ CS_2 + (n+1)\ H_2S \qquad (2.31)$$

$$C_nH_{2n+2} + (2n)\ H_2S \rightleftharpoons n\ CS_2 + (3n+1)\ H_2 \qquad (2.32)$$

This reaction sequence also explains the increase in CS_2 yield at temperatures above 800 K for a hydrocarbon-sulfur feed. Hydrogen sulfide is a product of the reaction between sulfur and an alkane. Now, it was observed that H_2S

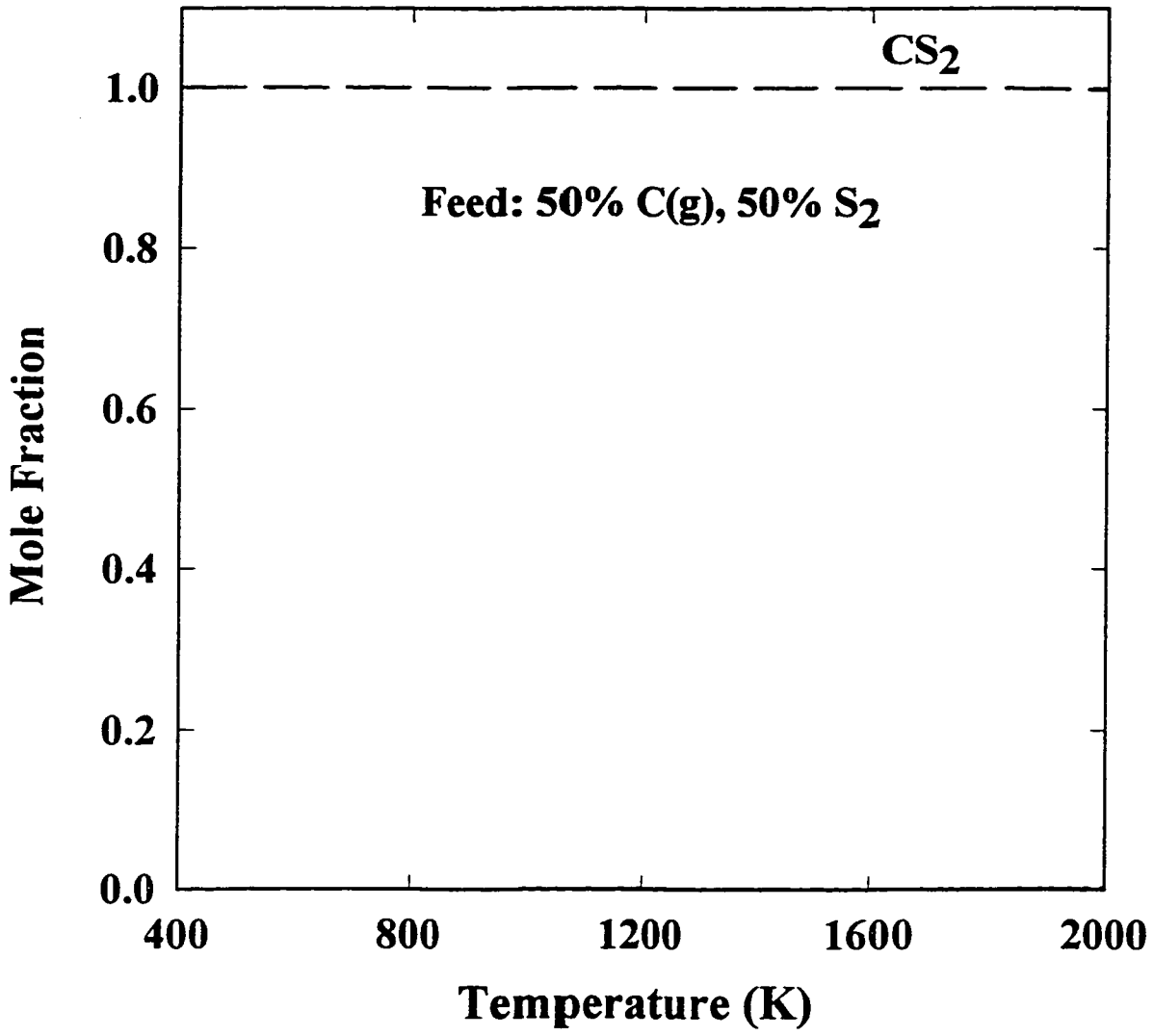

Figure 2.13 Equilibrium CS_2 yield for an equimolar feed of C(g) and S_2. (P=101.3 kPa)

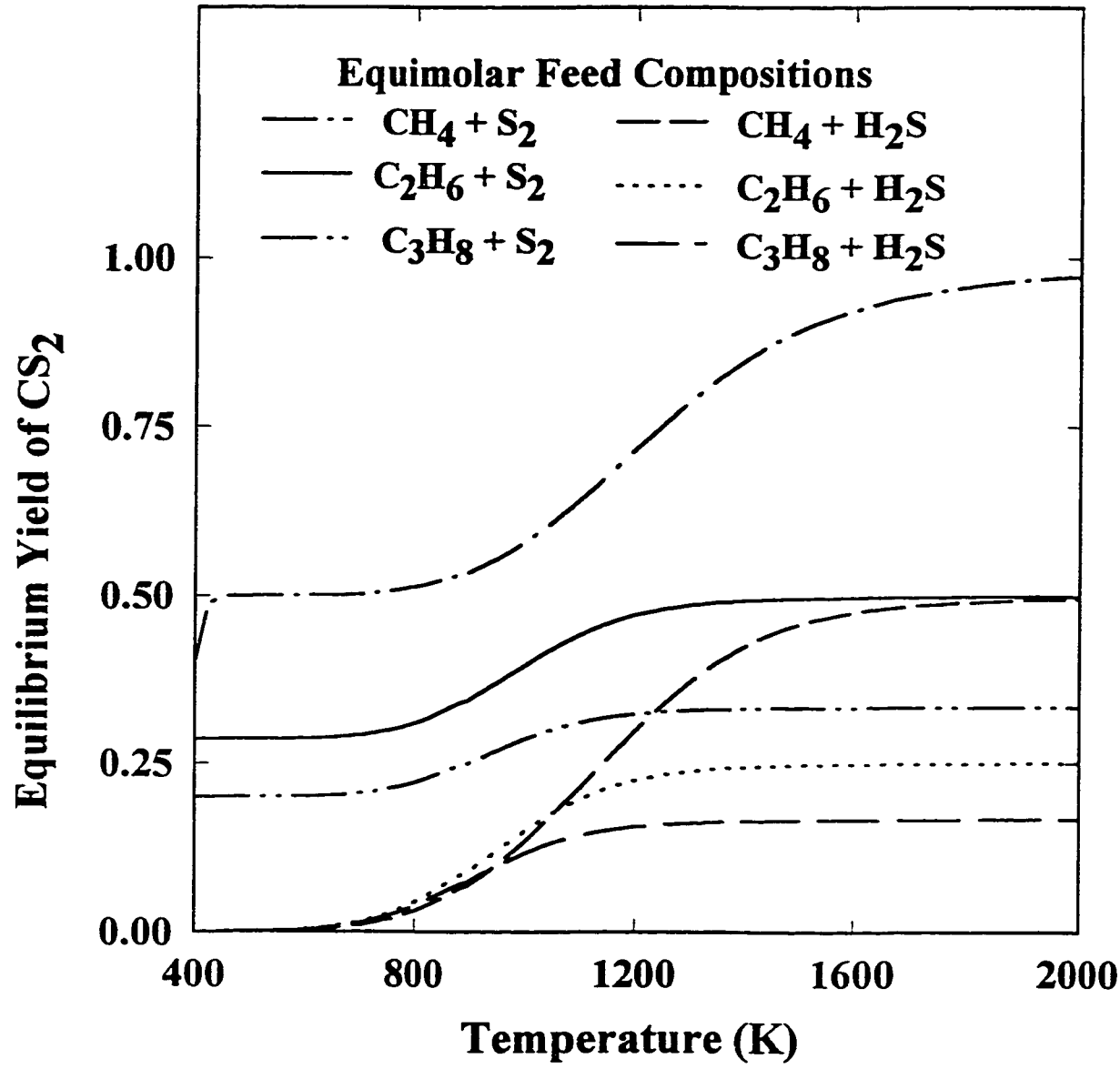

Figure 2.14 Equilibrium yields of CS_2 for equimolar feeds of following:
CH_4 and S_2, CH_4 and H_2S, C_2H_6 and S_2, C_2H_6 and H_2S, C_3H_8 and S_2, C_3H_8 and H_2S.
(P=101.3 kPa).

dissociation into sulfur and hydrogen is favored above 800 K. Thus, dissociation of H_2S in the C-H-S system shifts the equilibrium towards right of reaction (2.30), resulting in production of more CS_2.

From the results for these two feed systems, it can be observed that the presence of elemental sulfur is very important for the formation of carbon disulfide from methane. In the reaction furnace operations, a significant amount of sulfur is produced from the thermal cracking of hydrogen sulfide. Thus, the H_2S cracking reaction could possibly be the limiting step for the formation of carbon disulfide.

2.10 Summary

The results of this equilibrium study can be coupled with simple mass balance consideration to gain useful insight into the probable sources for production of the four species of interest, H_2, CO, COS and CS_2.

For example, from material balance considerations, some unimportant H_2 reactions can be eliminated. H_2 in the RF has to be produced from reactions that involve one or more of the H_2 containing species. In the RF feed, the major H_2 containing species are H_2, H_2S, H_2O and hydrocarbons. In Alberta (Canada), the Claus plant feeds have a relatively low hydrocarbon content and even a complete conversion to H_2 would still not be able to account for all of the H_2 observed in the furnace product gas. In fact, for the field data of Sames et al. (1990), the H_2 in the hydrocarbons constitutes less than 6% of the H_2 observed at WHB inlet. Moreover, significant amounts of H_2 have been measured in plants with negligible hydrocarbons in the RF feed. Dissociation of H_2O to H_2 occurs at very high temperatures and is not expected to occur at temperatures encountered in the furnace. Thus, it can be inferred that the major H_2 source is H_2S.

A similar reasoning can be applied to deduce the source of CO. The carbon containing species in the RF feed are hydrocarbons and CO_2. Since the

conversion of all of hydrocarbons can account for only a small fraction of CO present at RF/WHB exit, it can be inferred that CO_2 is the major source for CO.

Proposed reaction network

From, the results of equilibrium study results and the material balance consideration, a simplified reaction network for formation of H_2, CO, COS and CS_2 is being proposed. It must be emphasized that this proposed network is strictly based on the thermodynamic feasibility study of this thesis and, does not necessarily reflect the actual reaction pathway. The proposed scheme is presented in Figure 2.15.

The key observations from Figure 2.15 are that hydrogen sulfide dissociation is the most important reaction at high temperatures. This reaction is favored at temperatures greater than 1200K such as those observed in the RF. Apart from being the direct source of hydrogen and sulfur, this reaction is also the limiting step for the production of carbon monoxide. The majority of the carbon monoxide is hypothesized to be formed by the reverse of the water gas shift reaction, which is favored at higher temperatures. CO, in turn, is the primary reactant for the formation of carbonyl sulfide via the reaction between CO and sulfur. This reaction is favored, thermodynamically, to occur at temperatures lower than 800 K such as those encountered in the WHB. At low temperatures, CO is also expected to react with H_2S to form COS. Significant equilibrium yields of CS_2 are predicted over 800-2000 K from the hydrocarbon-sulfur reactions. The CS_2 consumption reaction via hydrolysis reaction is also favored at higher temperatures. Both the CS_2 formation reaction and the CS_2 consumption reaction are favored at higher temperatures. Therefore, the net production of CS_2 in the reaction furnace will depend on the relative rates of the two opposing reactions.

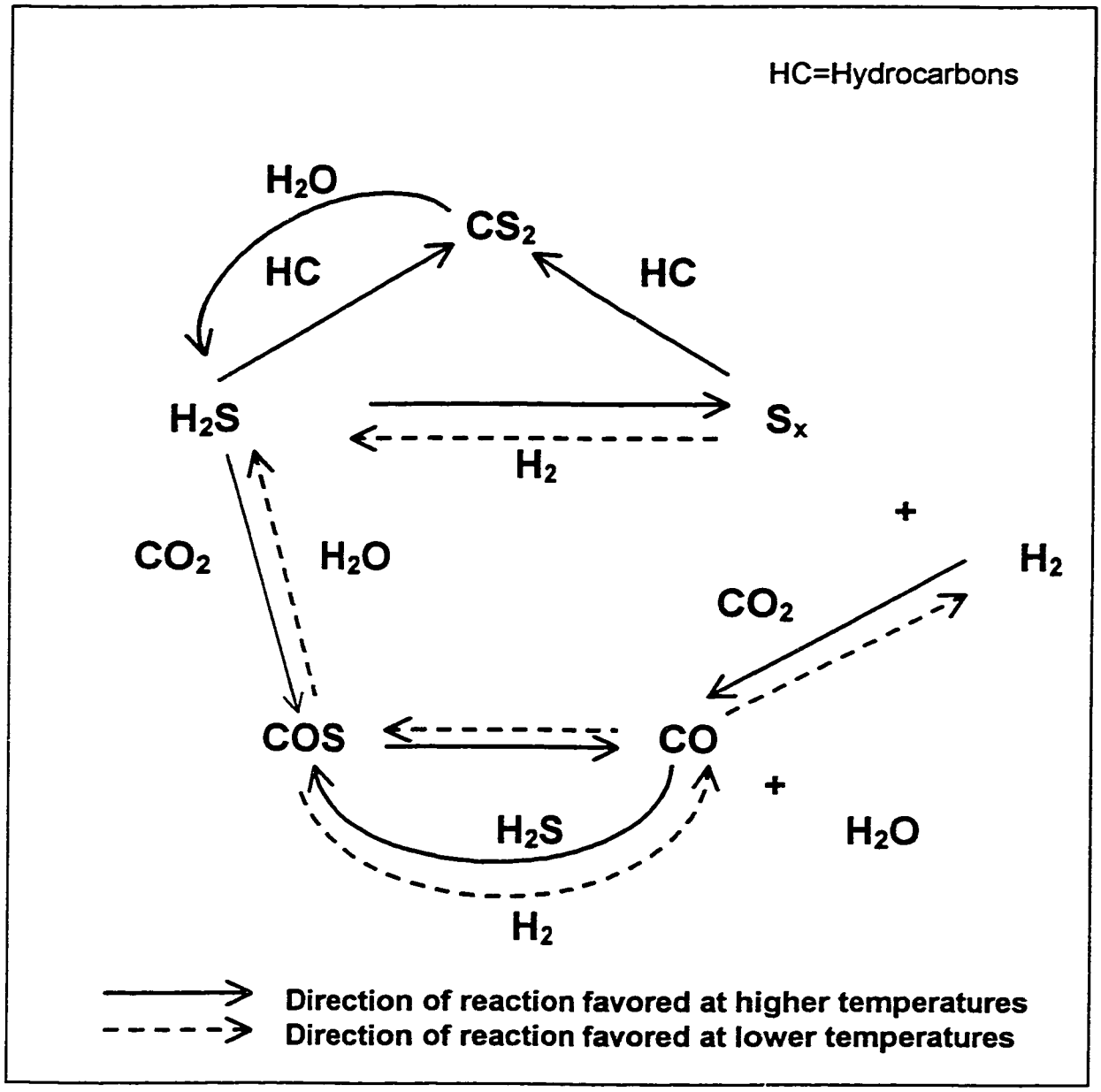

Figure 2.15 Proposed simplified reaction network for CO, H_2, COS and CS_2 formation and consumption in the front-end of a Claus Plant.

Chapter 3

Experimental Apparatus

3.1 Introduction

The details of the apparatus used in the experimental study are provided in this chapter. Most of the apparatus design as well as the procurement of the apparatus had already been completed when this research started. Much of the initial conceptual design for the reactor and the associated equipment was done under the guidance of Professor Leo Behie of the University of Calgary. Robert Fookes, an MSc student at that time, was involved in the development of the reactor system (Fookes, 1996). The author worked extensively with Mr. Fookes in testing and in assembling the reactor system.

In this chapter, the description of the apparatus has been divided into three sections, namely, major equipment, fabricated equipment and auxiliary equipment. A schematic diagram of the experimental set-up showing the key units of the apparatus is presented in Figure 3.1

3.2 Major equipment

High Temperature Muffle Furnace

A 46200 series electric muffle furnace manufactured by Thermolyne was used in the study. The furnace had an overall or outside dimension of (80 cm × 85 cm × 40 cm). The inside refractory chamber was (48 cm × 47 cm × 27 cm) in dimensions. The normal recommended temperature range for the operation of the furnace was 800 to1700 °C. The minimum allowable operating temperature was 600 °C. For furnace operation in the temperature range of 600-800 °C, the only modification required was to reduce the heating rate. This was done by restricting the input current to the furnace to 16 mA instead of the 32 mA setting for the normal operation.

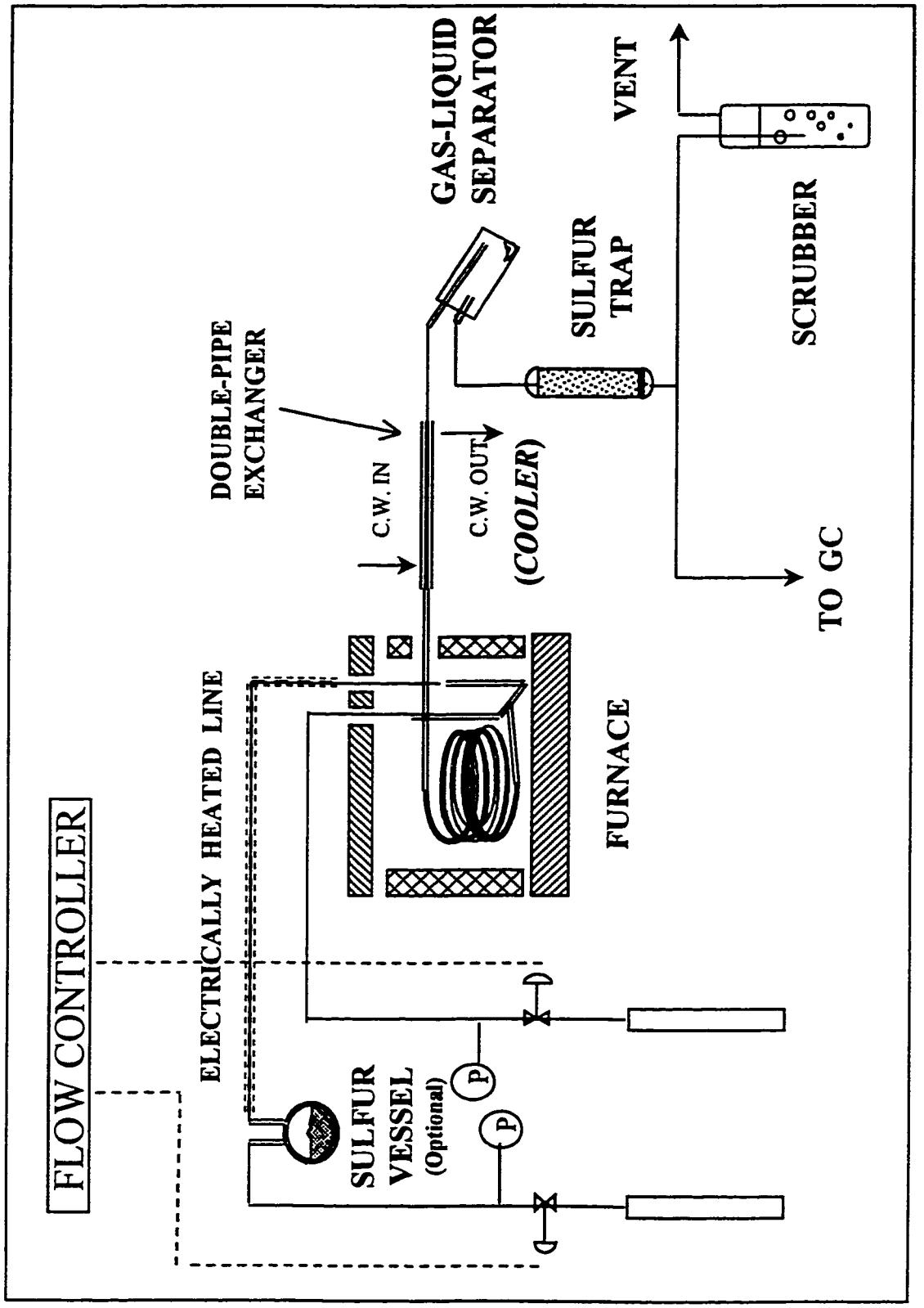

Figure 3.1 Schematic diagram of the experimental set-up.

Gas chromatograph

Initially, a Varian 3400 gas chromatograph along with a Varian DS 651 Data system, donated by Shell Canada Limited, was employed for the analysis of gas composition. This equipment was already twenty years old when it was acquired. Towards the end of the first year of this study, the gas chromatograph broke down and had to be replaced with a Varian Star 3400 C_x gas chromatograph. The new gas chromatograph was equipped with both a thermal conductivity detector (TCD) and a pulsed flame photometric detector (PFPD). The TCD could be tuned to measure concentrations as low as 100 ppm. The PFPD, could detect very low levels of sulfur species concentrations (estimated to be less than 10 ppb). In the majority of the experiments, the gas compositions were analyzed with the TCD. For some experiments involving gas mixtures, the sulfur species that were not detected with the TCD were detected with PFPD.

Flow controller

An eight channel FM 4660 Linde mass flow controller was employed to meter and control the flow of gases. The range of flow rates of each channel could be preset. The maximum and minimum ranges of flow rates preset were 10 L/min and 200 mL/min, respectively. The accuracy of the flow rate was ±1 percent of the full scale when operated within 103.32 kPa of the calibration pressure (206.6 kPa inlet and 34.4 kPa outlet).

Data acquisition system

A Sciemetric Instruments System 200 data acquisition system was used for the display of the temperature and pressure reading. The interface for the data acquisition system was developed using Paragon 500 software by Fookes (1996).

3.3 Fabricated equipment

Quartz coiled reactor

The heart of the experimental system is the coiled quartz tube reactor. The quartz reactor coil was fabricated at Rocky Mountain Enterprise in Colorado Springs, Colorado, USA (Fookes, 1996). The attachments to the reactor, i.e. the inlet and the exit of the reactor were fabricated by John Toonen Glassblowing Services Ltd., Edmonton, Alberta, Canada. A schematic diagram of the reactor is shown in Figure 3.2. The reactor was made of quartz tubes 5.0 mm inside and 8.2 mm outside diameter. The coil diameter was approximately 20.0 cm. An important feature of the reactor was the existence of the two vertical pre-heat sections (inlets) approximately 30 cm in length. This design ensured that the reactant streams flowing through the two inlets or pre-heat sections were rapidly heated up and reached a temperature close to the furnace set point temperature prior to being mixed at the mixer. This was especially useful in studying a reaction involving two different reactants, because the reaction was minimized during the heating period.

Double pipe heat exchanger

To quench the reaction and the gases at the exit of the reactor, a double pipe co-current heat exchanger was employed. The heat exchanger was fabricated by John Toonen Glassblowing Services Ltd. A schematic diagram of the heat exchanger in shown in Figure 3.3. The water was flowed through the annulus and the gases through the inside tube. The length of the heat exchanger was 45 cm. Three different heat exchangers of inside diameters 2.0, 3.0 and 4.0 mm were available. The heat exchangers with different tube diameters were designed to obtain varying rate of quenching in the heat exchanger. However, as will be shown later in Chapter 4, the reactions were actually quenched substantially prior to the gas entering the heat exchanger.

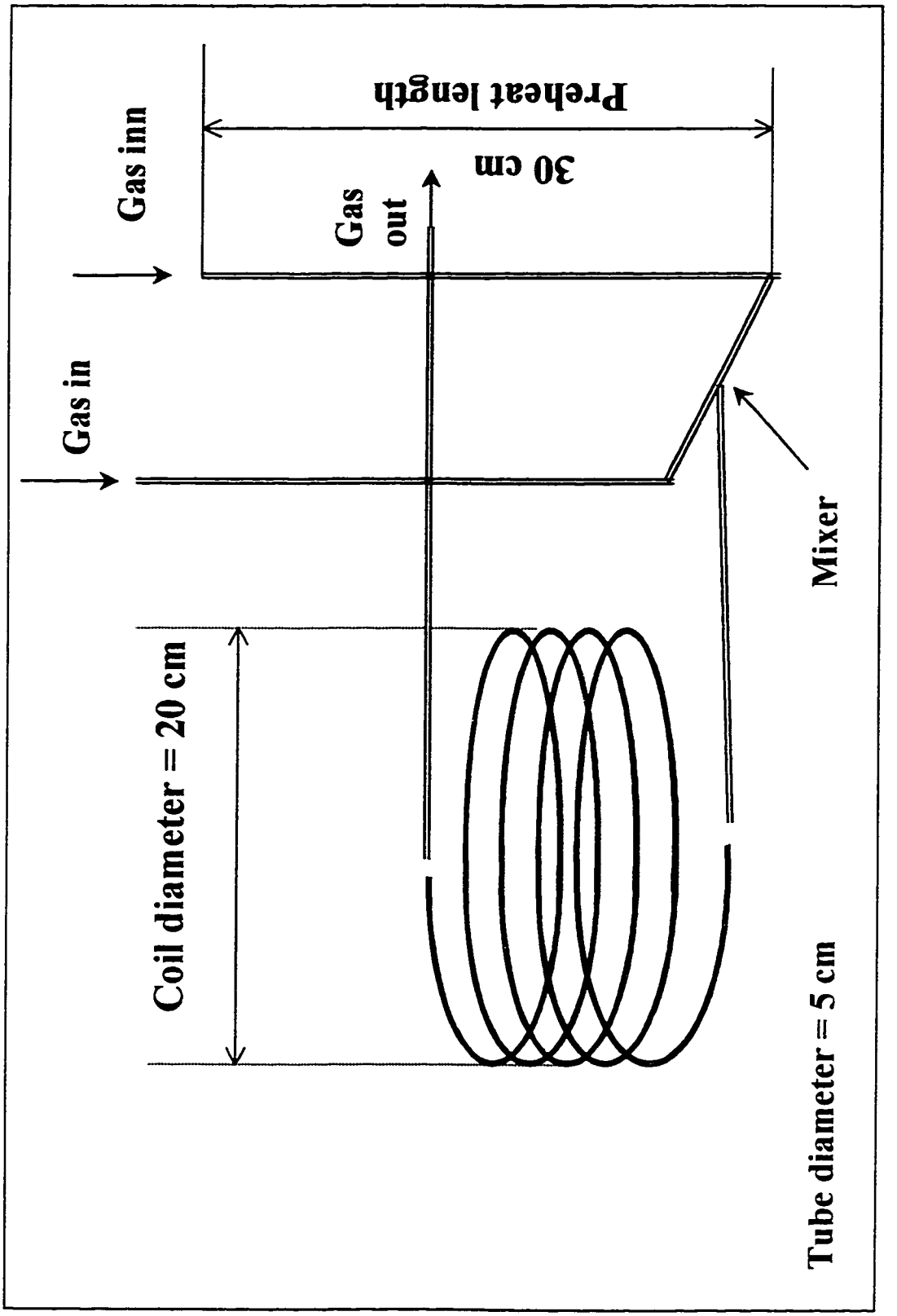

Figure 3.2 Schematic diagram of the coiled quartz tube reactor.

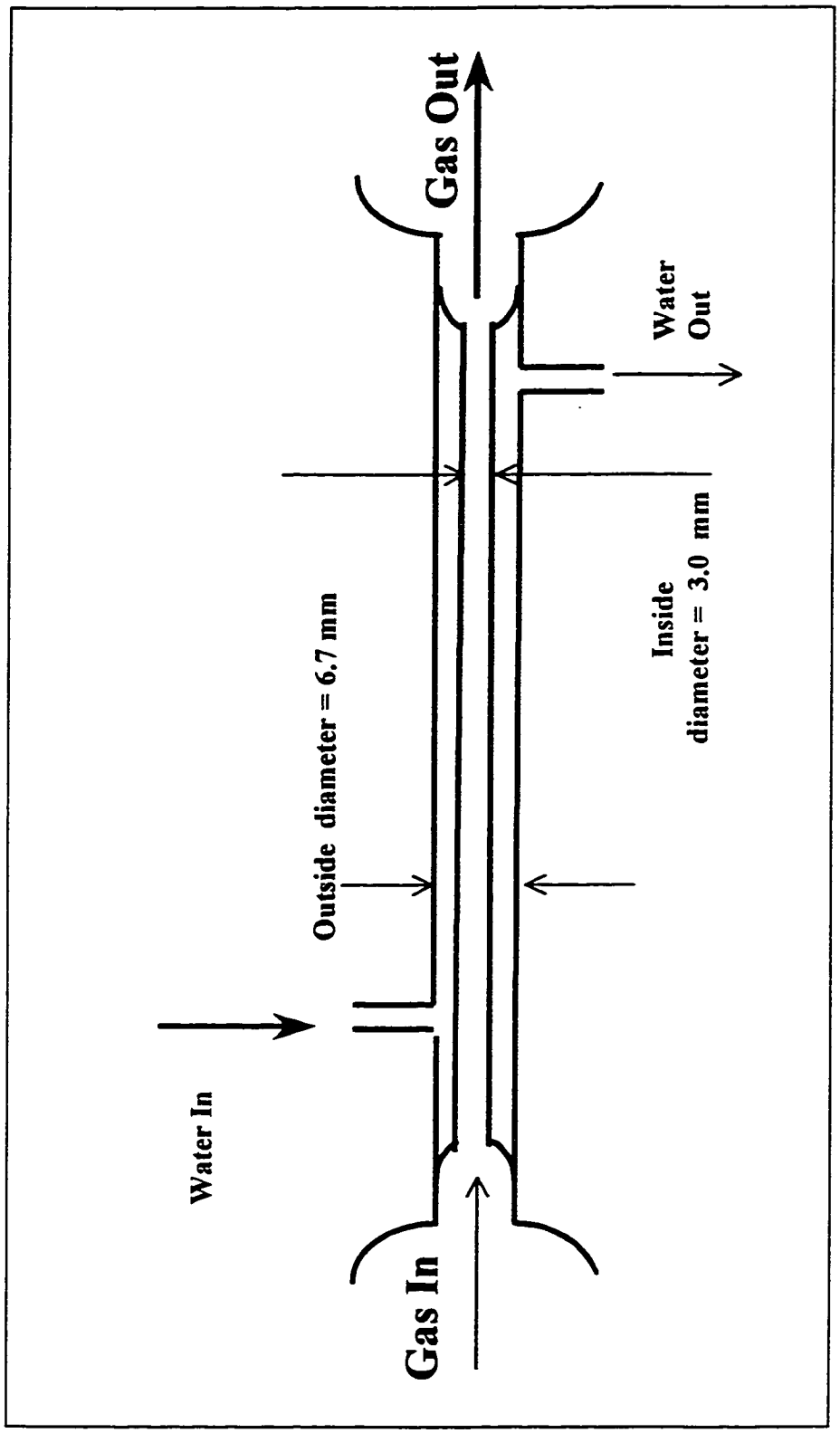

Figure 3.3 Schematic diagram of the double pipe heat exchanger located at the exit of reactor.

Sulfur separation system

The sulfur, present in the product stream, had to be removed prior to the analysis of the product gas stream. The sulfur separation was designed to be achieved in the two individual units, the gas-liquid separator and a fine solid separator (Fookes, 1996). It was found during experimental runs that partial removal of sulfur was attained in the heat exchanger. The schematic diagrams of the units are shown in Figure 3.4 and 3.5

Gas-liquid separator: The gas-liquid separator consisted of a 7.5 cm diameter vessel with a 4.0 mm inlet tube extending to the vessel bottom. The separator was designed for being placed at an angle so that the liquid collected at the bottom due to gravity leaving the gases to flow upwards.

Sulfur and water trap: A single separator unit was used as a sulfur-trap or a water-trap or a sulfur-water trap, depending on the gas system being dealt with. The separator was a tube of 2.54 cm inside diameter. At the downstream end of the tube, a glass frit was attached that served to hold the glass wool in place. The tube was packed with glass wool when separation of only sulfur was required and packed with glass wool in the bottom half and P_2O_5 in the top half when separation of water only or sulfur and water together were required.

3.4 Auxiliary equipment

Thermocouples

R-type thermocouples were used for measuring higher gas temperatures such as those in the electric furnace. At these temperatures radiation heat transfer becomes important. To estimate the radiative heat transfer, a set of no-flow experiments was conducted with shielded and unshielded R-type thermocouples. The difference in the temperature between the two thermocouples was less than 9 K. For the measurements of lower temperatures K-type thermocouples were used.

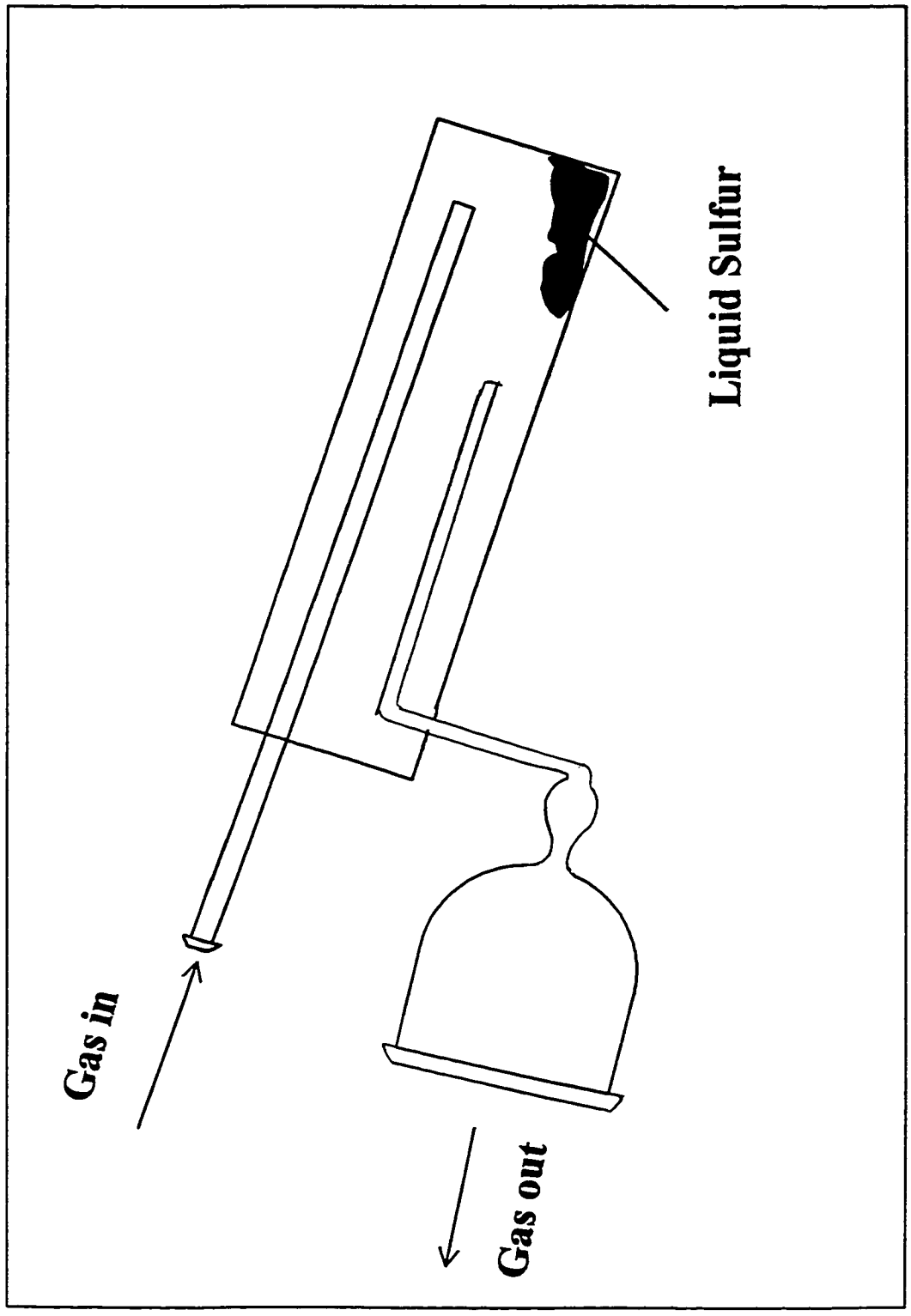

Figure 3.4 A schematic diagram of the gas-liquid separator.

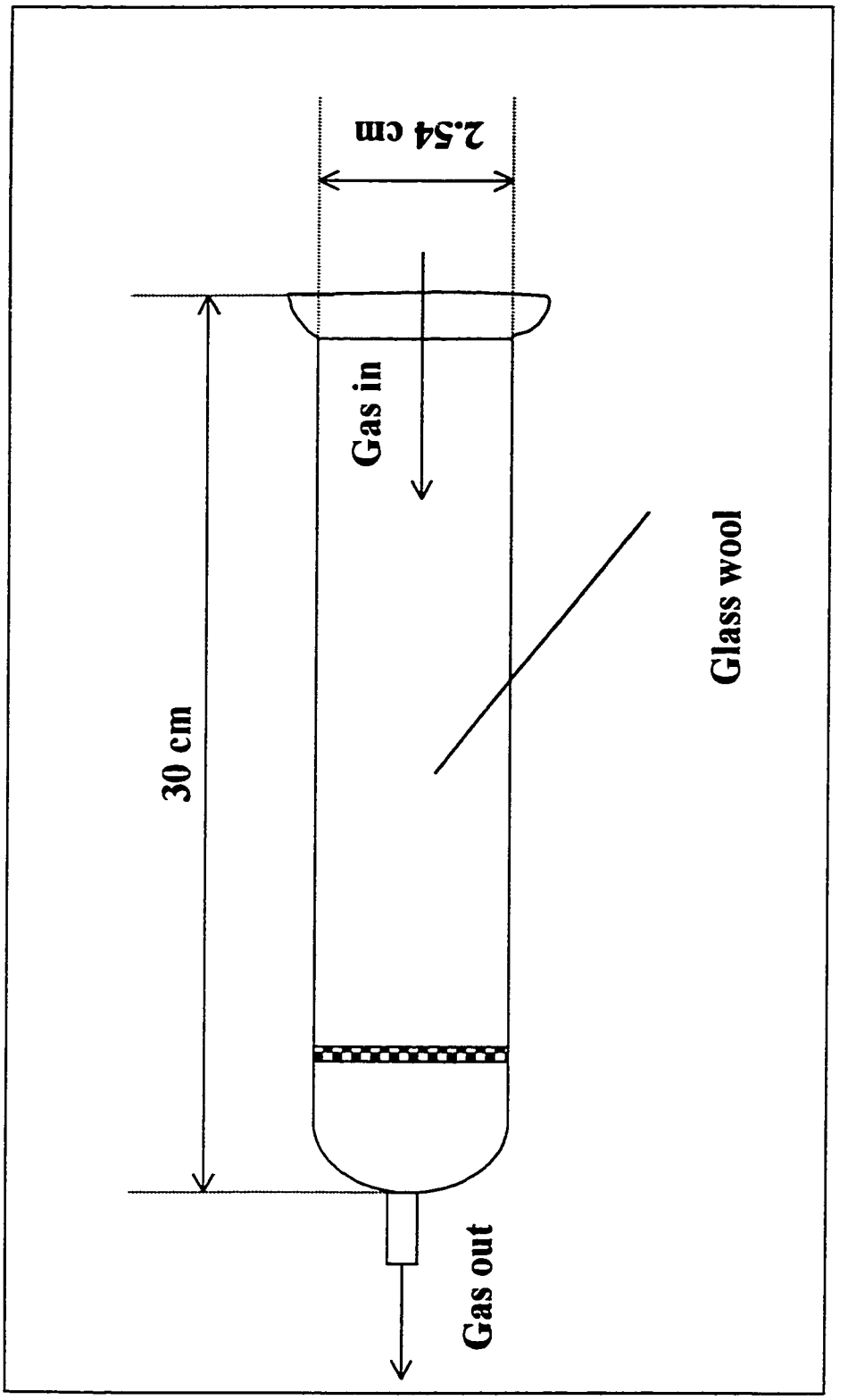

Figure 3.5 A schematic diagram of the sulfur and water trap

Wet type gas flow meter

A DM3D wet test meter manufactured by Alexander Wright and Company was used to measure the total gas flow rate. This also proved as a double check for the Linde mass flow controller. The fluid used in the wet test meter was water. The inside of the wet test meter was coated with special corrosion-resistant polymer to take care of the acid gas components. The wet test meter was rated for a normal flow rate of 10 L/min. The accuracy of measurement was rated to be within ± 0.25 % of the reading.

Sulfur pick up vessel

For experiments involving sulfur as a reactant, the gas stream containing sulfur vapor had to be prepared. Sulfur is solid at room temperature and remains liquid below 460 °C. To prepare a gas stream containing sulfur vapor, the sulfur was heated in a round bottom flask and nitrogen flowed over the molten sulfur. A schematic of the setup is shown in Figure 3.6 The amount of sulfur in the gas stream was found to be a function of flask temperature and the nitrogen flow rate. The flask temperature was dependent upon the Variac setting. The amount of sulfur picked up by the flowing nitrogen was measured gravimetrically, by collecting the condensed in the sulfur trap described earlier. Approximately, 12-15 runs were conducted for a fixed flask temperature. In each run, the nitrogen was flowed for 10 minutes and sulfur collected in the sulfur trap. At least 3 runs were performed by flowing nitrogen for 20 minutes or greater, this was done to check the consistency of sulfur being picked up. The average standard deviation in the amount of sulfur in the gas stream was found to be 10 percent.

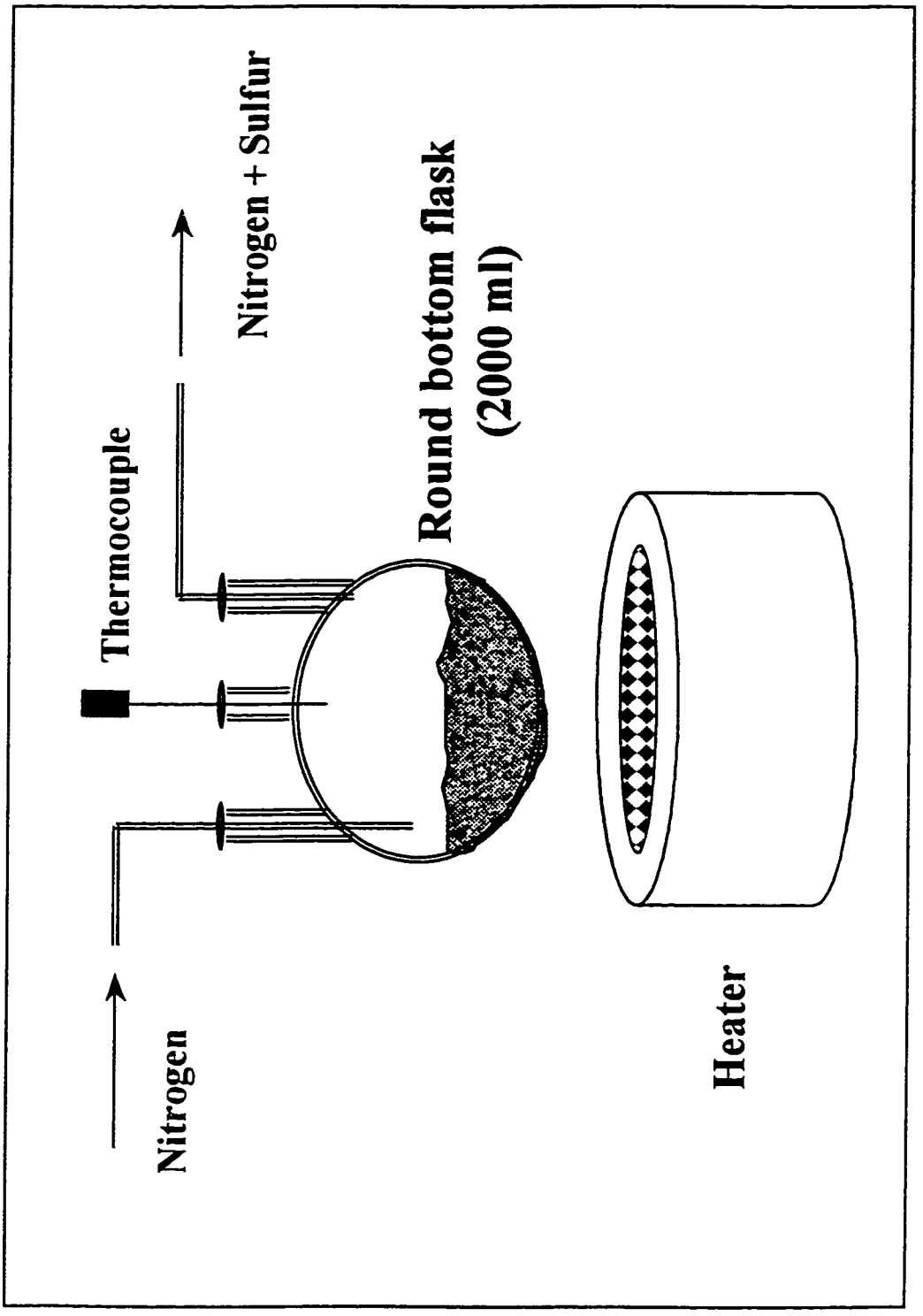

Figure 3.6 A schematic diagram of the sulfur pickup vessel

Chapter 4

Characterization of the Tubular Reactor

4.1 Purpose of the study

In a chemical kinetic study, an appropriate description of the reactor used in the study is important. The experimental data are processed using a well-defined reactor model (known) to obtain the chemical reaction kinetics (unknown). This is contrary to a reaction engineering study where a well-defined kinetic model (known) is used to design the optimum reactor (unknown). Now, to select an appropriate model for the reactor, characterization of the reactor is necessary. The purpose of this particular study was to establish the key operational characteristics of the reactor used in this kinetic study and to develop an acceptable reactor model in order that intrinsic rate data could be measured for a number of reactions of interest.

4.2 Key elements of a flow reactor

In general, to develop an appropriate reactor model or to characterize a flow reactor, the following key elements of the reactor system must be described:

- Temperature profile in the reactor
- Temperature profile in the quench
- Pressure drop across the reactor
- Flow pattern

Before a brief discussion on each key element of the reactor is presented, the reader must be reminded that the reactor used in this study is a coiled tubular reactor. Berger et al. (1983) have published an excellent review on "*flow in*

curved tubes". The secondary flow in the coiled or curved tubes is known to enhance the heat transfer, increase the pressure drop and, generally, reduce the axial dispersion.

Temperature profile in the reactor

For a kinetic study, it is desirable that the temperature in the reactor be isothermal or as close to isothermal as possible. This eliminates one variable and one differential equation (energy balance) in the analysis. Gases have low specific heat capacities and, therefore, may rapidly gain or lose heat. Therefore, it may be expected that for the reactor used in this study, a rapid heat up of gases in the initial length of reactor may be achieved. A simplistic analysis can be done to calculate the heat-up of gases in the reactor. The calculations for the temperature profiles of fluids under laminar flow in a straight tube have been dealt with in the book by Kays and Crawford (1980). The solutions to such problem, though not strictly applicable for curved tubes, provide useful insight regarding the expected gas temperature profiles. For a situation such as the experimental setup used in this study, i.e. the reactor being placed in a large thermal reservoir (electric furnace), the assumption of constant wall temperature is reasonable. The mean temperature (mass averaged or mixing cup temperature) along the length of the tube is given as a function of non-dimensional lengths. The solution was obtained with the consideration of the thermal entrance effects. However, it was assumed that the velocity profile is fully developed. For typical experimental conditions used in this study, it can be estimated that at a furnace set point temperature of 900 °C and a superficial gas flow rate of 4.0 L/min (~Re = 300, dt = 0.005 m, T_{inlet} = 25 °C), the gases will reach a temperature of 550 and 730 °C at distances of 0.05 and 1.0 m downstream from the inlet to the tube. These predictions show that the gases would heat-up quite rapidly in the reactor with a heat up time of 30-40 ms.

Two issues that need to be addressed further are the application to a curved tube and the assumption of a fully developed velocity profile. Addressing the latter issue first, it must be mentioned that for low Prandtl number conditions (i.e. for gases), temperature profile develops more rapidly than the velocity profile (Kays and Crawford , 1980). Consequently, the above analysis may not be strictly valid. However, in the absence of available solution for temperature profiles considering simultaneous development of the temperature and velocity profiles, the analysis based on developed velocity profile is the best available tool. Moreover, Kays and Crawford (1980) report that the mean Nusselt number for the case of simultaneous development of the temperature and velocity profiles are higher than the Nusselt number for the case of fully developed velocity profile. This would indicate that a higher rate of heat transfer and, therefore, a faster heat up of fluids. Now, for the other issue regarding the applicability of the analysis done for straight tubes being extended to curved tubes, it is already known that the secondary flows in coiled tubes enhance the heat transfer rate (Berger et al., 1983). Therefore, the analysis for straight tube condition may be considered a worse case scenario, at least from the perspective of gas heat up.

Gas quenching or cooling at reactor exit

A rapid quenching of the product stream from the reactor is also highly desirable. This minimizes the degree to which the reactions may proceed during the quenching and ensures that the quenched gas composition closely resembles the actual product stream composition. As mentioned earlier, the low specific heat capacities of the gases are expected to help in rapid cooling. As it will be shown later, the temperature profile in the quench-zone has been measured experimentally and the results demonstrate the existence of a rapid

quench (see sections 4.3.1.2 and 4.3.4). The gases are cooled from over 1200 °C to less than 600 °C in a time of less than 20 ms.

Pressure drop across the reactor

Another important element of the reactor is the pressure differential across the reactor. A negligible or zero pressure differential often exists in a tubular reactor when gas flow rates are small. Thus, the assumption of isobaric operation can be applied. This also results in the reduction of another variable (total P) and another differential equation (momentum balance) from the kinetic analysis. In the curved tubes, the pressure drops are higher than that for the straight tubes of same length operating under same conditions. For the reactor used in this study, the experimentally measured pressure drops ranged from approximately 5 kPa to 30 kPa which represents approximately 5-20 percent of the inlet pressures. Although, strictly speaking an isobaric condition does not exist, the assumption of isobaric condition is reasonable. For example, in determination of a second order rate constant, for the case of maximum pressure drop an average error of 20 percent may be incurred by assuming the reactor pressure to be constant at the inlet pressure. A large proportion of the experimental runs was conducted under conditions of pressure drops of less than 15 kPa.

Flow pattern in the reactor

For kinetic studies, it is always desirable that the flow in the reactor can be approximated as plug flow. The advantage of using the plug flow assumption is that the analysis of flow in the reactor becomes very simple and a one-dimension reactor model can be employed. The criterion for plug flow assumption to be valid, based on Reynolds number, is that the actual Reynolds number should be greater than the 10000 for straight tubes. For curved tubes, this is dependent on the coil diameter to tube diameter ratio for curved tubes (Ito, 1953). To obtain high Reynolds number large velocities are required, which

in turn requires a larger reactor to achieve desired residence times in the reactor. The length of the reactor is certainly a constraint for laboratory studies. It becomes very difficult to realize turbulent or plug-flow like conditions in laboratory reactors. The result is that, generally, the laboratory reactors operate under laminar flow conditions.

Hence, it is important to estimate the errors introduced due to an incorrect assumption of plug flow for reactors operating under laminar flow conditions. A manifestation of laminar flow is the existence of an effective axial dispersion (Wan and Ziegler, 1970). Several studies have been reported that have included the effect of axial dispersion to estimate the errors that may result due to the assumption of plug flow when an axially dispersed flow exists (Cleland and Wilhelm, 1956; Wissler, 1969; Wan and Ziegler, 1970). For a reactor with axially dispersed flow, the conversion lies between that for plug flow and laminar flow. Now, in the determination of first order rate constant, the errors arising from plug flow assumption for an actual laminar flow condition are 22 percent and 6 percent for measured conversions of 70 and 10 percent, respectively (Cutler et al., 1988). The errors reduce with an increase in the order of reaction. Now, the residence time distribution in the curved tube lies between that for laminar flow and plug flow in a straight tube (Saxena and Nigam, 1979). Therefore, the errors in the determination of first order rate constant using plug flow assumption for curved tubular reactors under laminar flow condition would be less than 22 and 6 percent for measured conversions of 70 and 10 percent, respectively.

The discussion so far has indicated that if the reactor is operated to obtain lower conversions (< 50 percent), the errors due to incorrect reactor model may be restricted to less than 10 percent. Moreover, this is not an outrageously high number, especially when one realizes that the measurement of concentrations itself may be accurate to 2-5 percent.

Finally, the most important point to note is that in the only experimental study on the measurement of axial dispersion for gases in curved tubes under laminar flow condition it has been shown that the axial dispersion is so small that the flow approaches ideal plug flow (van Andel, 1964). This experimental finding was also confirmed by a more recent theoretical study by Daskapoulos and Lenhoff (1988).

Thus, from the discussion above, it may be safe to state that the assumption of plug flow of gases for the reactor used in this study may be reasonable. Nonetheless, it is very important to state here that an extensive experimental verification study was used with the coiled tubular reactor of this study. The propane pyrolysis was chosen as a model reaction for which well-known intrinsic kinetics developed and reported by Professor Froment's group in Belgium (van Damme et al., 1975; Sundaram and Froment, 1977) were used. The details of the experimental verification study have been provided later in this chapter under section 4.4

4.3 Experimental measurements

4.3.1 Temperature measurements

Experiments were conducted to measure the gas temperature profile along the reactor and in the quench zone at the reactor exit. The description of experiments, discussion on radiation effects and the results of temperature measurements are provided in this section.

4.3.1.1 Temperature measurements in the reactor.

The temperature profiles along the reactor were measured using R-type thermocouples. To place the thermocouple sensor (junction) in the reactor tube different procedures were tried. At first, attempts were made to insert the

thermocouple wire through the tube. However, the coiling of reactor provided large resistance to the thermocouple movement. This process proved to be extremely tedious, often resulting in the breakage of the reactor and therefore it was abandoned after a few trials. Next, the direct fusion of the thermocouple wire to the inside surface of the quartz tube was attempted. This effort also proved to be futile because the difference in the thermal expansivities of the two materials resulted in gaps or holes when the reactor was subjected to high temperatures in the electric furnace. This process was also abandoned after a few attempts. Finally, a successful procedure was found in which the thermocouple wires were placed in the reactor tube through holes made on the tube surface and the gap or holes were filled using a ceramic bonding mixture. The ceramic mixture solidified on exposure to ambient conditions. This seal was cured overnight in a furnace to provide strength and proper sealing.

A schematic of the reactor tube with the fused thermocouple is shown in Figure 4.1

4.3.1.2 Temperature measurements in the quench zone

The quench-zone has been already described in the previous chapter under section 3.2. It was comprised of the short length of the reactor extending out of the furnace refractory and the double pipe heat exchanger located downstream to it. A schematic of the quench-zone is shown in Figure 4.2. Now, before the temperature measurements had been carried out, it was assumed that the

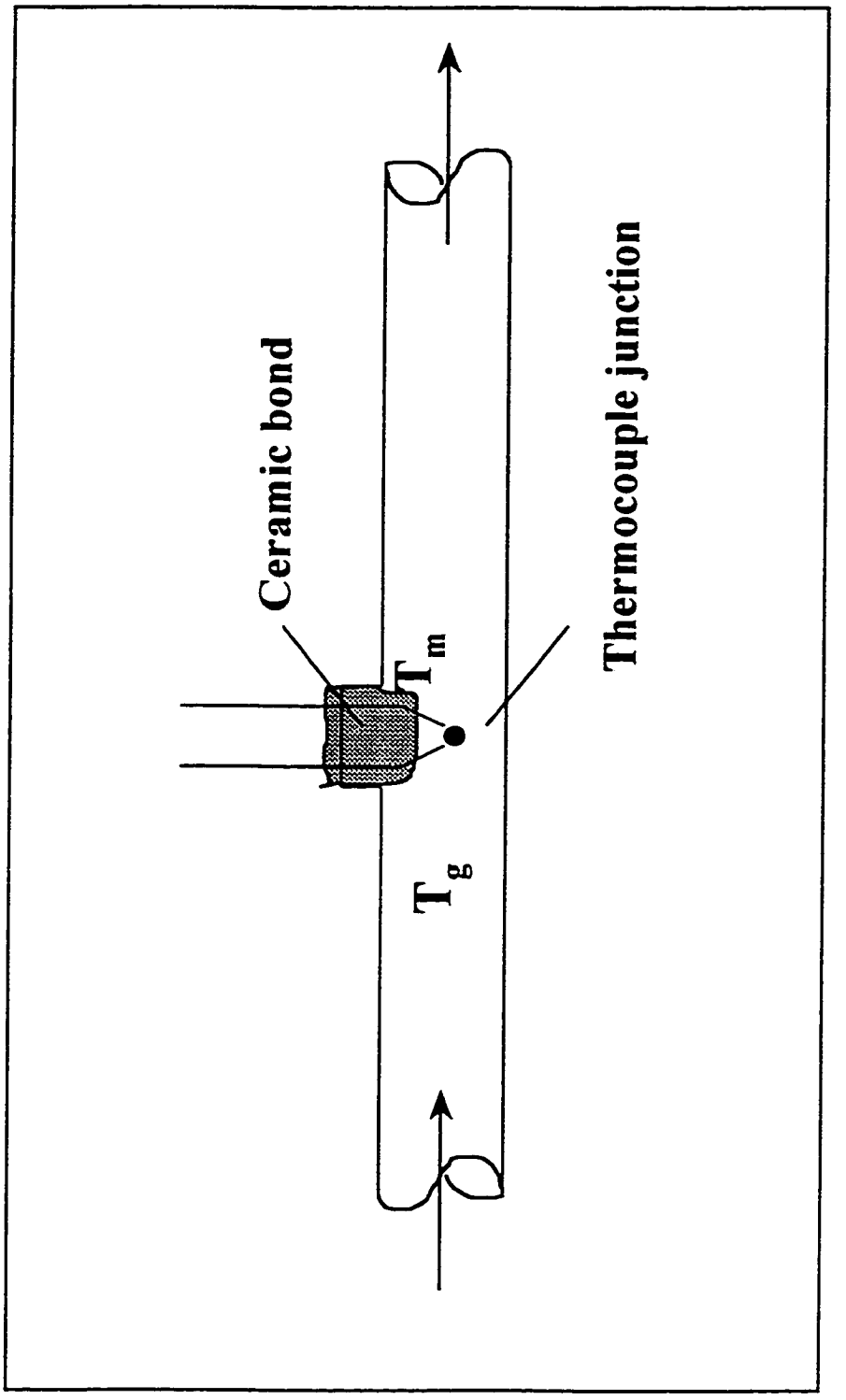

Figure 4.1 Schematic diagram of the reactor tubing showing fused thermocouple.

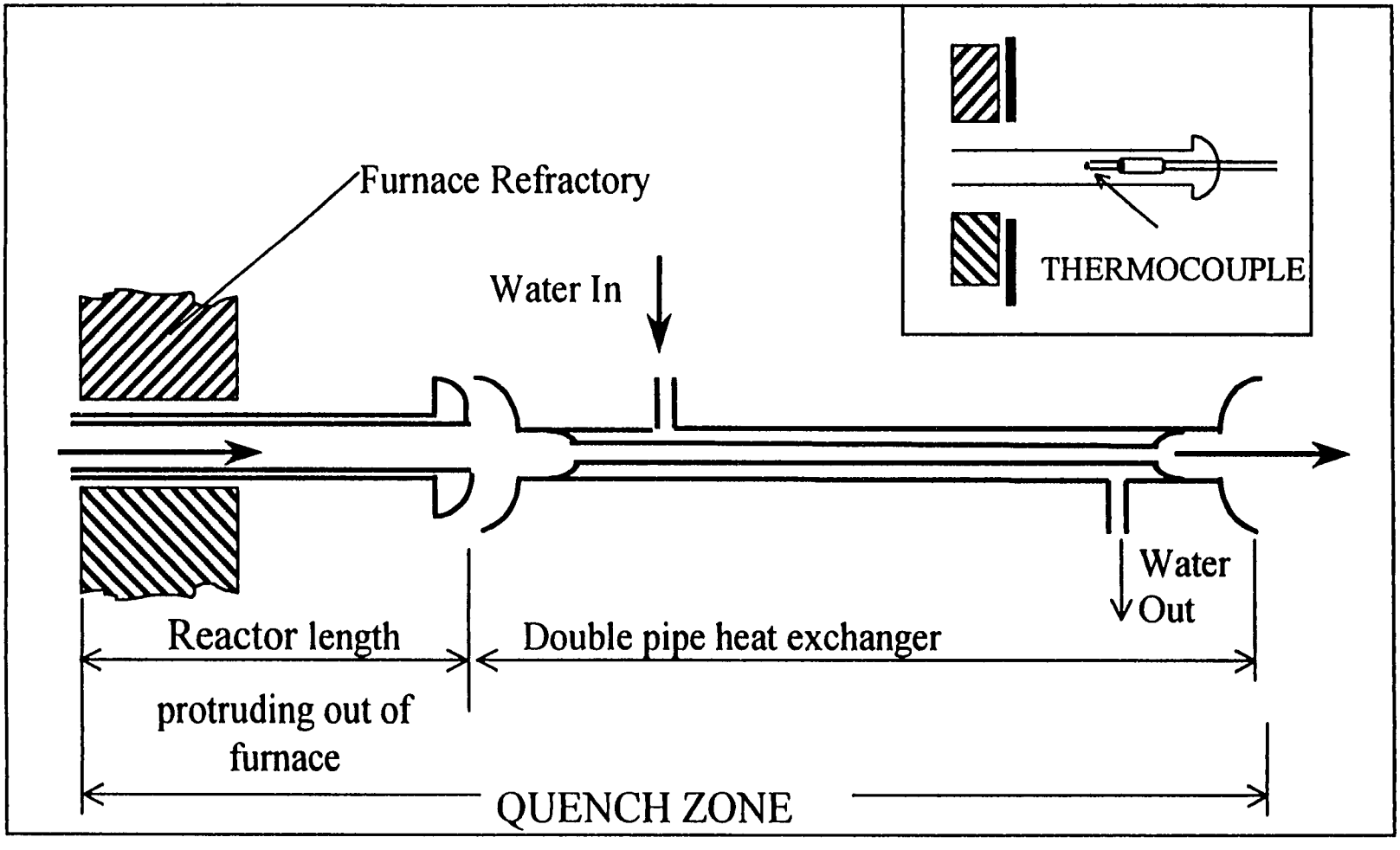

Figure 4.2 Schematic diagram of the quench zone of the reactor system. Inset: Schematic diagram of reactor extension showing thermocouple placement.

product gas from reactor was quenched only in the double pipe heat exchanger (Fookes 1996). However, as it will be shown later this was not the case.

Measurement of the temperatures at the exit of the double pipe exchanger showed that the temperatures were consistently less than 100 °C for gas flow rates up to 16 L/min and for furnace temperatures up to 1250 °C. Although this proved that a fast quench existed, it did not provide information on how fast the quench was. Therefore, it was decided to measure the gas temperature along the heat exchanger. This required placing the thermocouple sensor in the narrow inside tube of the heat exchanger. Now, from the previous experience on the fusion of the thermocouple to the quartz tube (described above in section 4.3.1.1) it was known that this would be a tedious job especially because there were two concentric quartz tubes through which the sensor would have to be inserted. An easier method was devised to measure the gas temperature profiles along the exchanger. Four double pipe heat exchangers of lengths 10, 20, 30, 45 cm were fabricated. The temperatures at the exit of the exchanger were measured and this was used to develop the temperature profile along the exchanger. The results of these measurements are discussed later in section 4.3.4. From these measurements it was estimated that the gas stream was already cooled to temperatures less than 500-700 °C upon entering the heat exchanger in a time of less than 25 ms, effectively quenching the reaction. This meant that the heat exchanger was essentially acting as a "*cooler*" and the actual quenching of the hot product gases occurred in the short length of the reactor extending beyond the furnace refractory.

The gas temperatures were measured in the part of the reactor outside the furnace refractory by placing thermocouple wire through the reactor tube. The schematic of the setup is shown as the inset in Figure 4.2. The temperatures were measured at intervals of 1.0 cm. The results of these measurements are presented and discussed later in section 4.3.4.

4.3.2 Radiation effects

The measurement of the gas temperature at high temperatures (> 1000 C) becomes complicated due to the radiative heat transfer effects. The measured temperatures are expected to be higher than the actual gas temperature when the temperature of the surroundings are greater than the gas temperature, and lower than the actual gas temperature when the temperature of the surrounding is lower than the gas temperature. The former situation prevails during the measurement of temperature profile in the reactor while the latter situation prevails during the temperature measurement in the quench zone.

To estimate the magnitude of the errors associated in the temperature measurements due to the radiation effects, a simple energy balance on the thermocouple junction was done.

4.3.3 Measured gas temperature profile along the reactor

The temperature profiles along the reactor length for four different furnace set points are shown in Figure 4.3. These correspond to the lowest flow rate of 4.0 L/min (measured at 24 ± 1 °C and 101.3 kPa) used in the temperature measurements. At this flow rate and for all temperatures, the maximum error in the measured temperature due to radiation effects was calculated and estimated to be 12 K. It can be observed from Figure 4.3 that an extremely rapid heat of gases are achieved in the reactor and the gases reach temperatures within 20-25 K of the set point temperature in a short length (20-30 cm) downstream of the mixer. The gas measured temperatures clearly demonstrate the flat temperature profiles attained in the reactor and establish that the reactor operates at conditions very close to isothermal.

The measured temperature profile along the reactor length at furnace set point of 1100 °C and for five different flow rates 4, 7, 10, 13 and 16 L/min are shown in Figure 4.4. The maximum error associated with temperature

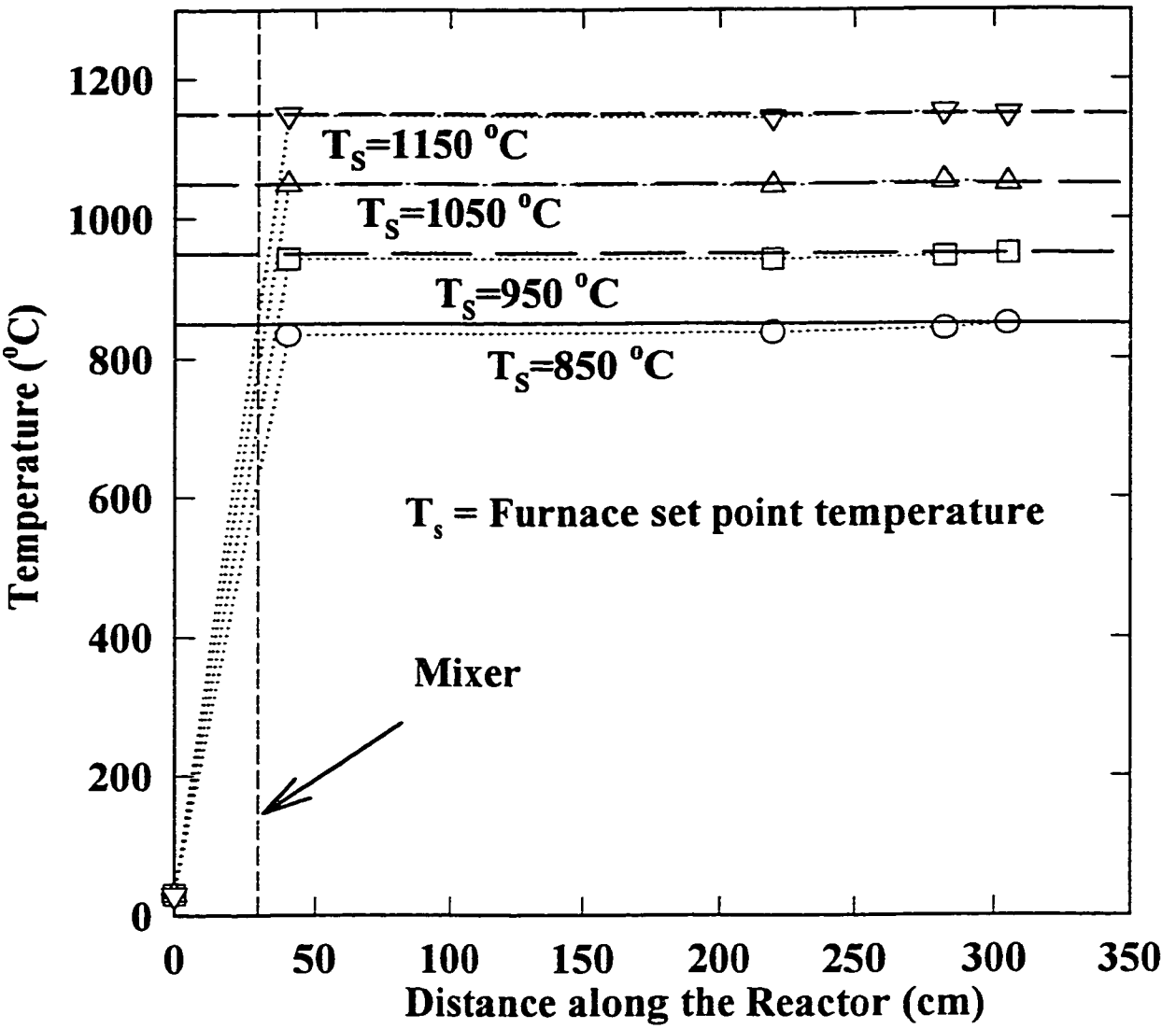

Figure 4.3 Measured gas temperature profile along the reactor length for four furnace set point temperatures at a fixed flow rate of 4.0 L/min. (Re~300-400)

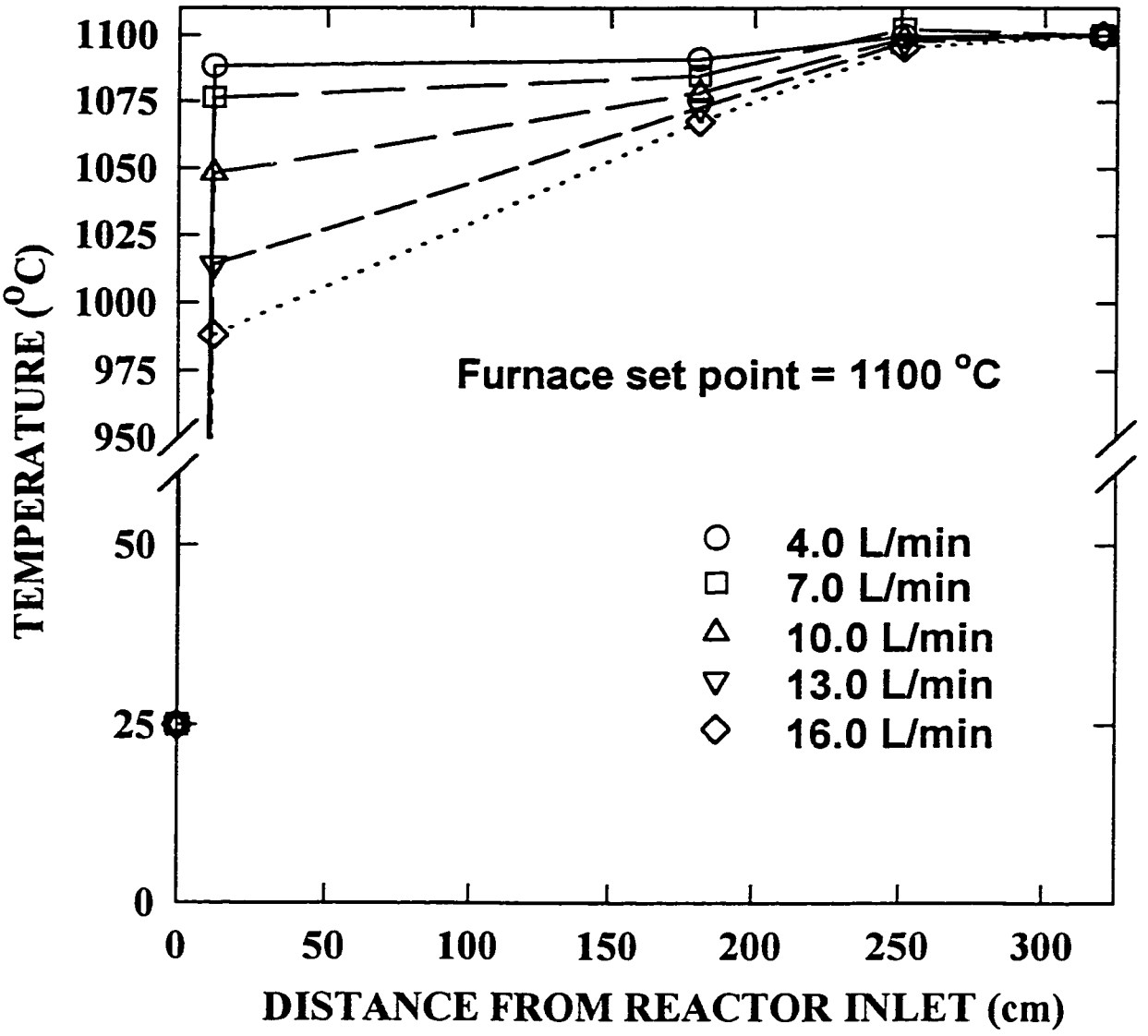

Figure 4.4 Measured gas temperature profile along the reactor length.

Effect of gas flow rate.

measurement was approximately 30 K. This, obviously, was for the highest gas flow rate and at the measurement point nearest to the mixer.

4.3.4 Measured gas temperature profile in the quench zone

The gas temperature profile in the double pipe heat exchanger is shown in Figure 4.5. The temperatures reported at 10, 20, 30 and 45 cm from inlet are the measured temperatures. For a gas flow rate of 4.0 L/min, the gas temperature 10 cm from the entrance of the exchanger is less than 275 °C. It also furthers the credence that the exchanger acts more as a *cooler* than a *quench*. Also it is anticipated that the gases are quenched to temperatures less than 600-700 °C prior to entering the exchanger. It is important to note that a majority of the reactions, studied in this thesis, are effectively quenched at temperatures below 600 °C

The results of temperature measurements in the short length of the reactor extending outside the furnace refractory are presented in Figure 4.6. The errors in the temperature measurements due to radiation effects were estimated to be in the range of 50-70 K. The temperatures reported in the Figure are the radiation corrected values. Nonetheless, it can be seen from Figure 4.6 that the gases are quenched quite rapidly, most likely via a combination of free and forced convection.

4.4 Reactor verification study

To verify the operational characteristics of the reactor, an experimental and simulation study was conducted.

4.4.1 Methodology

The method for verification consisted of the following five steps:

- Selection of a model reaction.

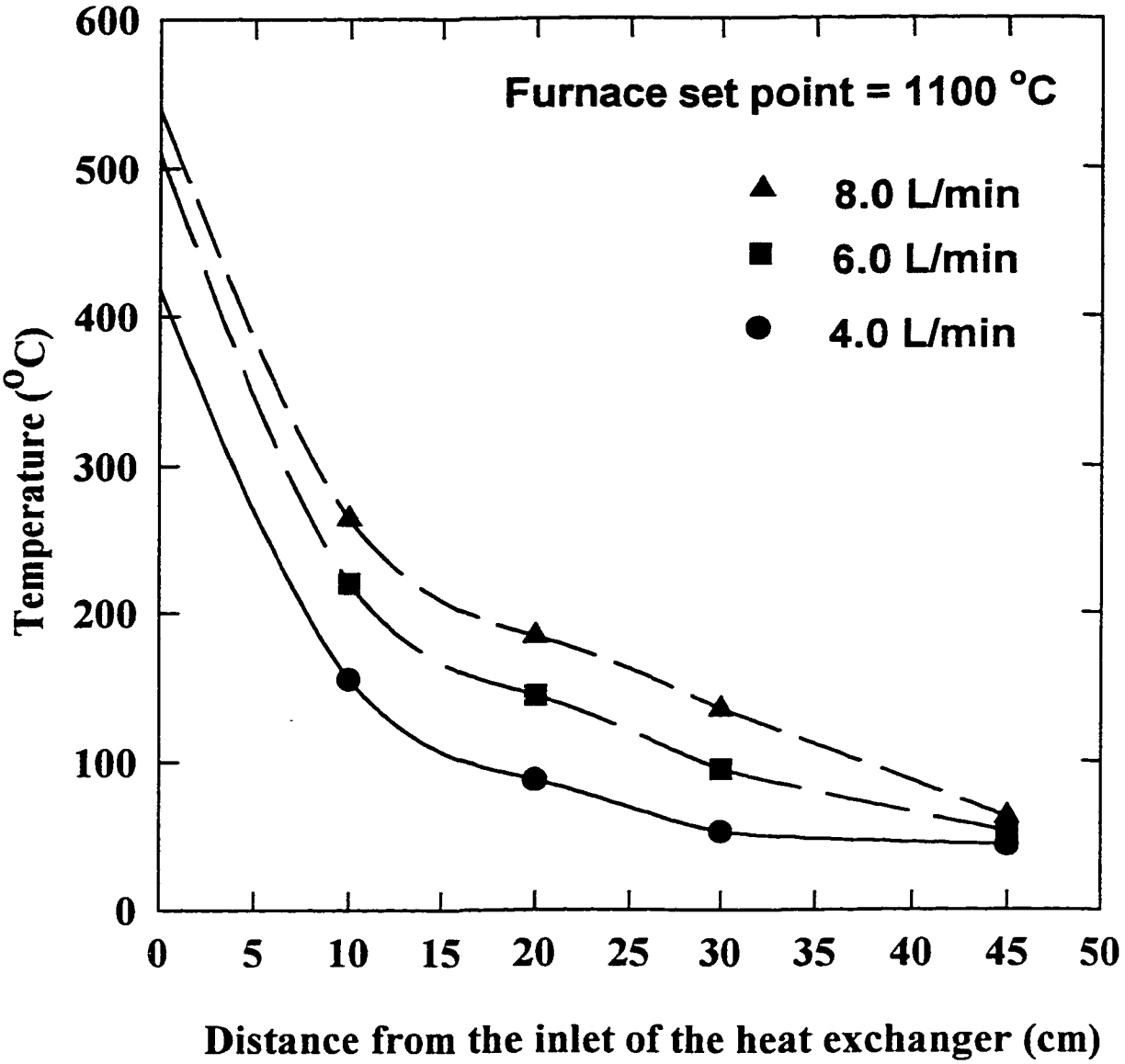

Figure 4.5 Measured gas temperature profile along the length of the double pipe heat exchanger.

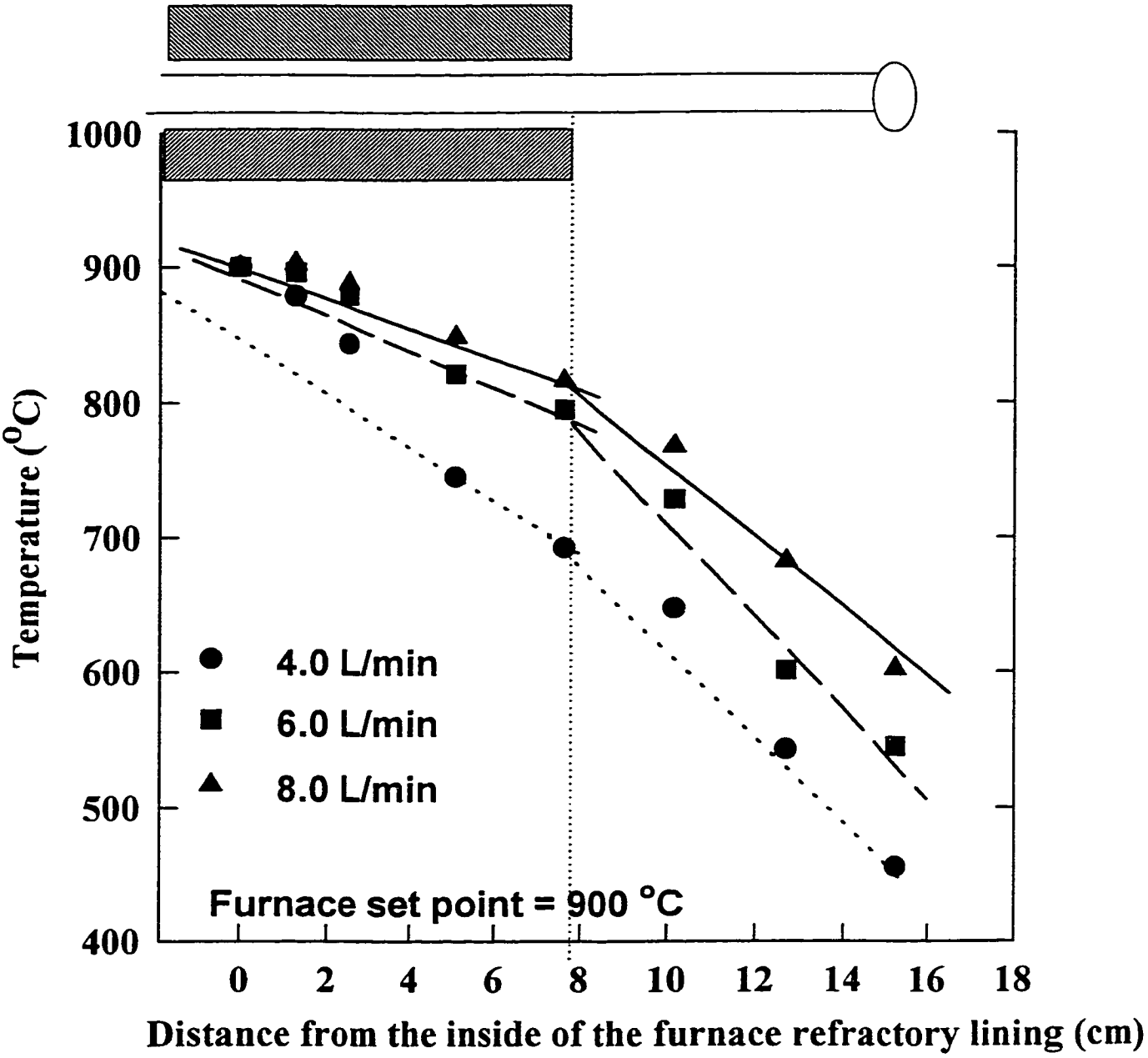

Figure 4.6 Measured gas temperature profile at the exit of the reactor.
Effect of gas flow rate.

- Simulation of the model reaction in a tubular reactor.
- Comparison of the simulation results with the published results.
- Experimental study of the model reaction in the coiled reactor.
- Comparison of experimental results with model predictions.

4.4.2 Selection of model reaction

The primary criterion for the selection of a model reaction was that the intrinsic kinetics for the reaction be well established and readily available in the literature. Additional requirements for selecting the model reaction were that the reaction should be a homogeneous gas phase reaction and that its reaction kinetics be applicable at high temperatures, i.e. between 800 and 1200 °C. It was also desirable that the reaction proceed to a significant degree, at residence times in the reactor, so that the products could be obtained at measurable concentrations.

The gas phase propane pyrolysis reaction meets the requirements for the model reaction. The kinetics of the reaction are well established, available and applicable above 800 °C. From the kinetic information in the literature, it was anticipated that the reaction would proceed rapidly above 800 °C and significant conversion of propane could be achieved at gas residence times of 100 to 400 millisecond. Thus, the propane pyrolysis reaction was selected as the model reaction.

4.4.3 Propane pyrolysis kinetics

Pyrolysis of propane is an important industrial process and the kinetics of the reaction has been studied extensively in the last forty years. Professor Froment in Belgium has done extensive research on propane pyrolysis (Buekens and

Froment, 1968; Sundaram and Froment, 1977a and 1977b; Van Damme et al., 1975; Sundaram and Froment, 1979;). They have proposed kinetic models for propane pyrolyis comprising of 9 molecular reactions (Sundaram and Froment, 1977a). A kinetic model was developed from extensive experimental data obtained from a pilot plant (van Damme et al., 1975) where the data were obtained over a temperature range 700-870 C. The reactor was operated at high velocities with Reynolds numbers varying from 5000-10000, which allows application of the plug-flow assumption. The kinetics for the propane pyrolysis reaction is reported in Table 4.1.

4.4.4 Simulation of propane pyrolysis in tubular reactors

A FORTRAN program was written to compute the gas composition along the reactor length. A set of material balance equations was solved using a fourth order Runge-Kutta integration routine. To simplify the calculations, the following set of assumptions were made:

Assumptions

(a) Isothermal operation

(b) Plug flow of gas

(c) Isobaric operation

These assumption have already been addressed in Section 4.2

The predictions from the program were compared to the published results of Beukens and Froment (1968) and excellent agreement was found between the two. This verified that the predictions from the program were correct.

Table 4.1 Molecular Reaction Scheme and Arrhenius Parameters for Propane Pyrolyis Reaction (Sundaram and Froment, 1977).

Reaction	A (s^{-1} or † $l \cdot mol^{-1} \cdot s^{-1}$)	E_a (kcal/mol)
(1) $C_3H_8 \rightarrow C_2H_4 + CH_4$	4.692×10^{10}	50.60
(2) $C_3H_8 \rightleftharpoons C_3H_6 + H_2$	5.888×10^{10}	51.29
(3) $C_3H_8 + C_2H_4 \rightarrow C_2H_6 + C_3H_6$	2.536×10^{13} †	59.06
(4) $2\ C_3H_6 \rightarrow 3\ C_2H_4$	1.514×10^{11}	55.80
(5) $2\ C_3H_6 \rightarrow 0.5\ C_6 + 3\ CH_4$	1.423×10^{9}	45.50
(6) $C_3H_6 \rightarrow C_2H_2 + CH_4$	3.794×10^{11}	59.39
(7) $C_3H_6 + C_2H_6 \rightarrow C_4H_8 + CH_4$	5.553×10^{14} †	60.01
(8) $C_2H_6 \rightarrow C_2H_4 + H_2$	4.652×10^{13} †	65.20
(9) $C_2H_4 + C_2H_2 \rightarrow C_4H_6$	1.026×10^{12}	41.26

4.4.5 Propane pyrolysis experiments.

4.4.6 Experimental conditions

The propane pyrolysis experiments were conducted in a 3.2 m long reactor at 850 °C for five flow rates that corresponded to five residence times. The feed concentration was 1.97 mol % propane in nitrogen. The reactant gas mixture was obtained from Praxair, Canada. The inlet pressures varied from 96 to 166 kPa.

4.4.7 Experimental results

The results of the experiments are presented in Figures 4.7 The symbols correspond to the experimentally measured concentration of various chemical species. The lines in the figure are simply trendlines. The data exhibit all the expected trends for the propane pyrolysis reaction. The hydrogen, methane and acetylene concentrations increase with an increase in residence time, while the propane concentration decreases with an increase in residence time. The propylene concentration exhibits a maximum.

4.5 Comparison of predictions with data

Finally, in order to verify the reactor system of this study, the predicted gas composition of the product from the reactor is compared with experimental data in the parity plot of Figure 4.8. A majority of the experimentally measured data is within ten percent of the model predictions. The comparison between the measured and the predicted concentrations of individual components as a function of residence time is presented in Figures 4.9. The deviation is larger at smaller residence time. The smaller residence times correspond to reactor operations at higher velocity, which does increase the Reynolds number (but remains under the laminar flow regime) but at the same time affects the

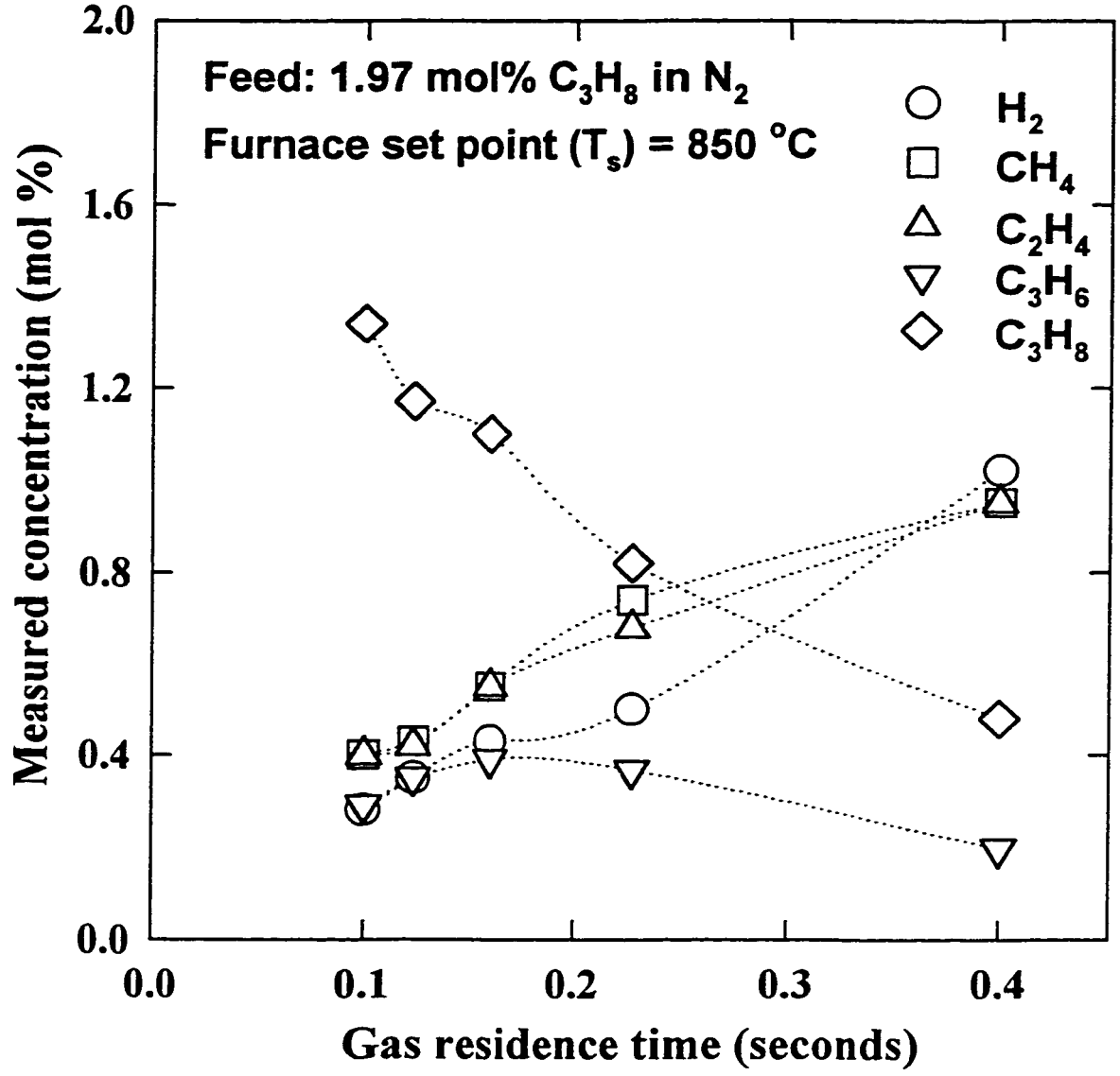

Figure 4.7 Experimentally measured product gas composition at the exit of the reactor for pyrolysis of 1.97 mol% C_3H_8 in N_2 at five different gas residence times.

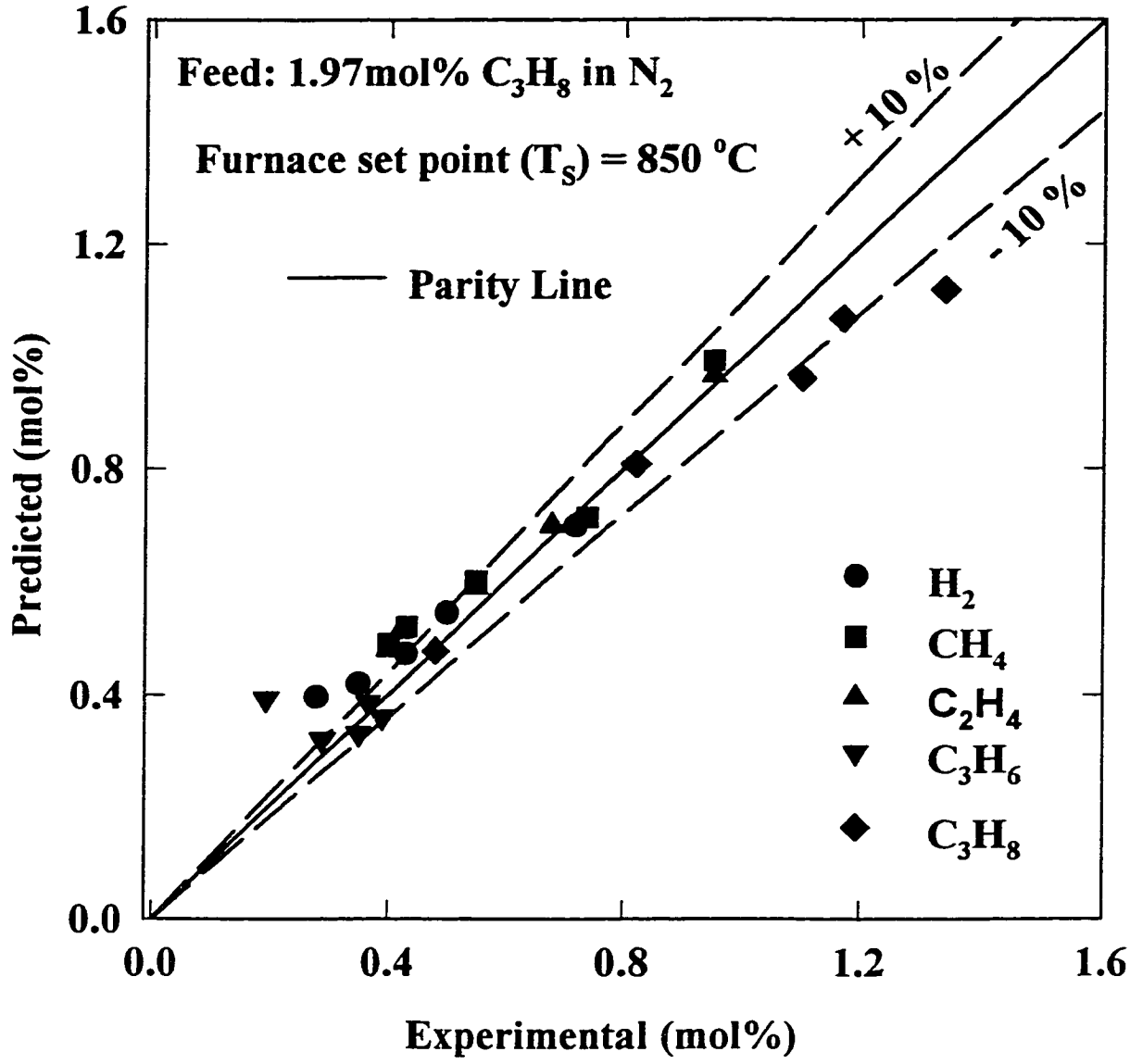

Figure 4.8 Comparison of the experimentally measured and the predicted product gas composition at the exit of the reactor for pyrolysis of 1.97 mol% C_3H_8 in N_2.

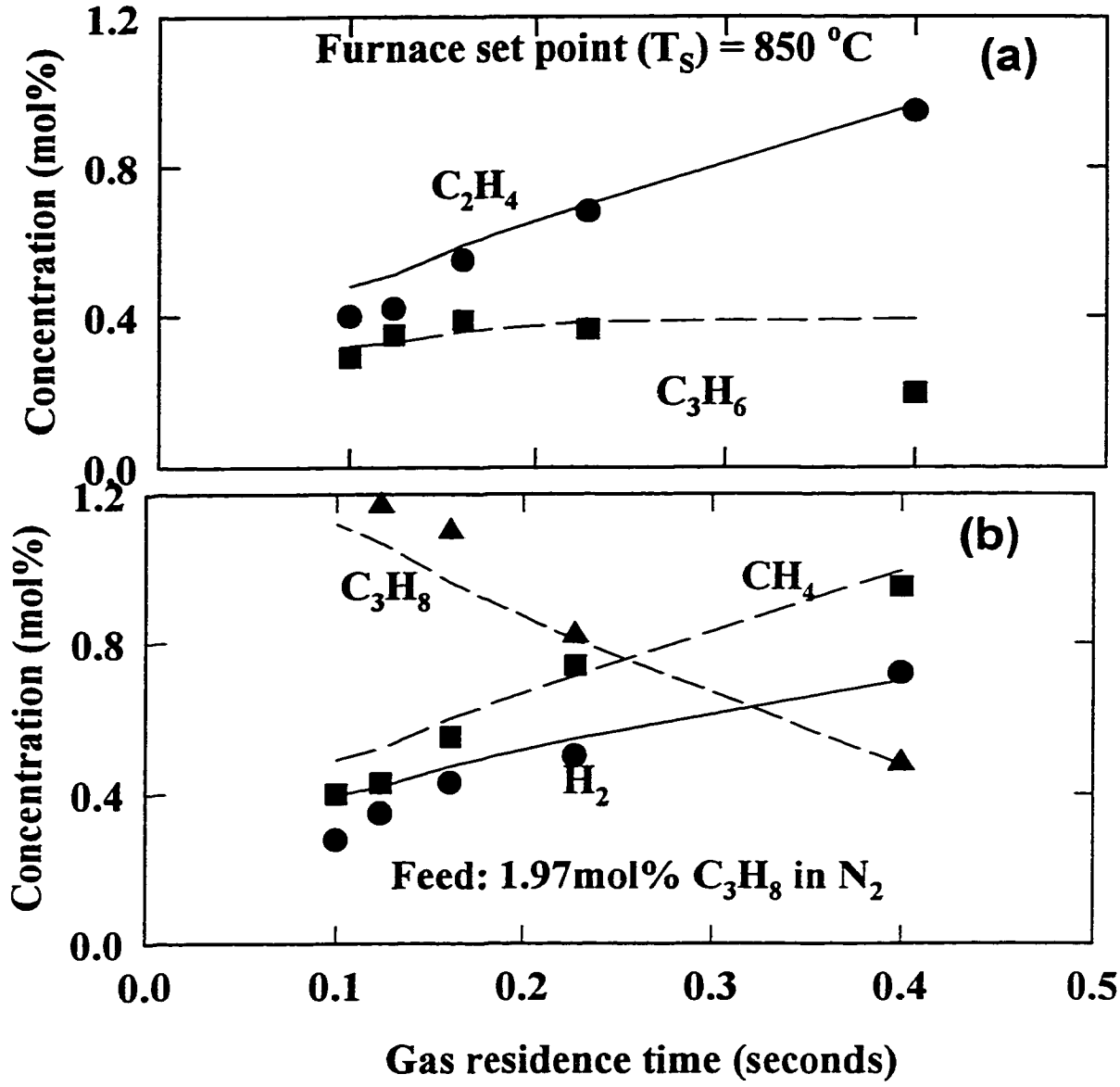

Figure 4.9 Product composition at the reactor exit as a function of gas residence time. Comparison between model predicted and measured gas composition.

(a) Comparison for C_2H_4 and C_3H_6

(b) Comparison for H_2, CH_4 and C_2H_4

temperature profile The differences between the experimental measurements and predictions are therefore expected to be due to temperature effects. The temperature profile in the initial length of the reactor is 25-50 K lower than the set point temperature. This will result in an effective temperature of less than the 850 C that is assumed for the purpose of simulation. The actual propane conversions and the concentrations of the products will be less than the predicted value, which is exactly the case here.

4.6 Summary

A few conclusions can be made based on the observations of the experimental measurements of temperature profile and from the verification study. It may be stated the operation of the reactor can be closely approximated as being isothermal with plug flow of gases, provided gas flow rates are small (< 4.0-6.0 L/min). The assumption of isothermality should hold true for the two longer reactors (6.4 and 16.0 m long) for gas flow rates up to the maximum of 16.0 Li/min. The gases are rapidly cooled, in the short length of reactor extending out of furnace, from over 900-1200 °C to less than 500-700 °C in a short residence time of less than 25 ms, effectively quenching the reaction. The double pipe heat exchanger acts simply as a cooler and not a quench, contrary to the prior claim by Fookes (1996).

Chapter 5

Reaction Kinetic Studies on Individual Reactions

5.1 General Introduction

The reaction kinetic studies have been divided into two parts. In this chapter, the results of the experiments performed for individual reactions have been presented. The results of the experiments on the partial oxidation of acid gas mixtures have been presented in Chapter 6.

In this chapter, the important hydrogen, carbon monoxide, carbonyl sulfide and carbon disulfide reactions have been dealt with. Most of the experiments were performed over a temperature range of 600-1250 C, which covers the typical operational temperature range in the front-end units of a Claus plant, i.e. the reaction furnace and the waste heat boiler. In the experiments, the gas residence time in the reactor ranged from 200 ms to 2.0 seconds. Again, the typical residence time in the Claus reaction furnace is 0.5-2.0 s and that in the waste heat boiler is 1.0-3.0 s. Thus, the residence time in the reactors were of the same order as that in the front-end units of Claus plants. From the data analysis, for a majority of the reactions the rate constants for the overall reactions were determined.

5.2 Basic assumptions employed for kinetic analysis

Some of the basic assumptions employed in the analysis of the data need to be addressed, prior to the presentation of the experimental results. Based on the characterization of the tubular reactor used in this study (Chapter 4). The following assumptions were applied:

Isothermal operation: Experimental measurements of gas temperature profile have verified isothermal operations. Moreover, a majority of the experiments

were conducted under very dilute conditions (dilution > 98%), therefore, the heat of reaction effects were also small.

Isobaric operation: The pressure drop across the reactors range from 5 to 20 percent of the inlet pressure. The average error in determination of a second order rate constant is estimated to be 10 percent when operating at higher inlet pressures (> 150 kPa) and less than 5 percent when operating at inlet pressures below 120 kPa.

Plug flow: A detailed literature review and an experimental verification study (see Section 4.4) show that the plug flow assumption is valid for the reactor used in this study.

Based on the above assumptions, the material balance equation for a flow reactor can be written as:

$$dF_j/dz = A \sum_{i=1}^{r\,max} (\nu_{ij}\, r_i) \qquad (5.1)$$

where, F_j is the molar flow rate of component *j*, A is the cross-sectional area of the tubular reactor, z is the distance along the reactor, r_i represents the reaction rate for reaction *i*, and ν_{ij} is the stoichiometric coefficient of the component *j* in the reaction *i*.

Equation 5.1 can be transformed on the assumption of no effective volume change during the reaction and isothermal operation to an equation of the form:

$$dC_j/dt = (A/Q) \sum_{i=1}^{r\,max} (\nu_{ij}\, r_i) \qquad (5.2)$$

where, C_j is the molar concentration of the j th compoenent, Q is the total volumetric flow of gases and the others symbols are as defined in equation 5.1

5.3 H_2S Decomposition Reaction

5.3.1 Literature Review.

The equilibrium study of Chapter 2 has shown that the hydrogen sulfide decomposition reaction may play a critical role in the formation of hydrogen and also in the formation in carbon monoxide, which is a precursor to carbonyl sulfide. Several studies on the combustion of hydrogen sulfide have been reported that have also included the hydrogen sulfide decomposition reaction [Levy and Merryman, 1965; Merryman and Levy, 1967; Bradley and Dobson, 1966; Muller et al., 1979; Frenkenlach et al., 1981; Cambot et al., 1982; Tsuchiya et al., 1997]. Detailed reaction mechanism comprising several elementary reactions have been proposed (Frenkenlach et al., 1981 and Tsuchiya et al., 1997). The interest in hydrogen sulfide decomposition reaction is not only limited to H_2S combustion systems. In fact, the energy crisis of 1973 led to the initiation of numerous studies on the production of hydrogen from decomposition of hydrogen sulfide. Several of the studies involving catalytic processes for splitting hydrogen sulfide into hydrogen and sulfur were granted patents during the 1980's (Chivers et al., 1980; Berk et al., 1991). Since the interest was mainly in the homogeneous gas phase thermal reaction, these studies are not discussed here.

The reported studies on the homogeneous gas phase H_2S decomposition reaction can be broadly classified into two groups on the basis of the reactor type employed. One group constitutes the experiments conducted in shock tubes. A majority of these experiments were conducted at higher temperatures (> 1800 K). The other group comprises the experiments conducted in conventional flow or batch reactors at lower temperatures (< 1500 K). A review of these studies indicates that the reaction kinetics obtained from the two groups differs significantly. For example, the flow reactor studies (Raymont, 1975; Kaloidas and Papayannakos, 1989, Tesner et al., 1990; Adesina et al., 1995) have reported activation energies in the range of 195-277 kJ/mol while the shock tube studies (Higashihara et al., 1976; Bowman and Dodge, 1981; Roth et al., 1982; Olschewski et al., 1994; Woiki and Roth, 1994; and Shiina et al., 1996) have

reported activation energies varying from 268 to 384 kJ/mol. Moreover, the differences between the rate constants obtained from similar reactor systems were also quite significant. In the most recent study on H_2S decomposition reaction, Shiina et al. (1996) have reported rate constants one-fifth to one-tenth of those reported by Olschewski et al. (1994) and Woiki and Roth (1994). Both of the latter groups in their independent studies came up with almost identical reaction rate constants.

The difference among the reported studies is limited not only to the rate constants. Also there is controversy regarding the overall H_2S decomposition mechanism. While in all the shock tube studies the H_2S decomposition reaction has been considered to be first order with respect to H_2S concentration, the flow/static reactor studies have reported both first and second order dependency on H_2S concentration. Darwent and Roberts (1953) conducted experiments in static quartz reactors over the temperature range of 773-923 K and reported that the homogeneous and heterogeneous reactions were second and first order, respectively, with respect to the H_2S concentration. They estimated that the homogeneous reaction would dominate at temperatures above 923 K. Based on Darwent and Roberts' work (1953), Tesner et al. (1990) assumed that the H_2S decomposition was first and second order with respect to H_2S concentration for the gas-phase homogeneous and the heterogeneous reactions, respectively. They tried to interpret their experimental data based on this assumption, but did not conduct a systematic study to verify the assumption. The hydrogen sulfide concentrations were not directly measured in either of these studies (Tesner et al., 1990; Darwent and Roberts, 1953), although the rate constant for the H_2S decomposition reaction was reported. While Darwent and Roberts (1953) measured the rate of formation of hydrogen, Tesner et al. (1990) measured the rate of formation of sulfur. Another shortcoming of the Tesner et al. (1990) study was that they used nitrogen, as a diluent, containing up to 0.01 % oxygen. This is problematic due to the fact that oxygen present in trace amounts is known to accelerate hydrogen sulfide decomposition reaction (Higashihara et al., 1976).

Since Tesner et al. (1990) did not give consideration to the effects of oxygen in analyzing their experimental data, the rate constants reported for H_2S decomposition in their study may not be considered to be reliable. In other flow reactor studies, Kaloidas and Papayannakos (1989) and Adesina et al. (1995) examined the H_2S decomposition reaction over the temperature ranges of 873-1133 K and 1040-1084 K, respectively. They found the overall reaction rate for H_2S decomposition to be first order with respect to the H_2S partial pressure.

From the review of the literature, it can be inferred that there is a great deal of controversy and discrepancy regarding the overall reaction kinetics and the mechanism for hydrogen sulfide decomposition. Despite the fact that detailed reaction schemes comprising of elementary reactions have been proposed, their application or extrapolation to lower temperatures remains questionable.

The aim of this part of study is to report new experimental data for H_2S decomposition over the temperature range (1073-1523 K) encountered in the front-end of a Claus plant, for which reliable reaction kinetic data are not available. Further, the issue of the order of dependency of H_2S concentration on the overall H_2S decomposition reaction was investigated. And, finally, an attempt was made to reconcile the higher temperature reaction kinetic data (shock tube studies) with our lower temperature data.

5.3.2 Experimental

5.3.2.1 Experimental conditions

A majority of the experiments was performed with 1.0 mol% H_2S in ultra high purity nitrogen over a temperature range of 800-1250 °C. The total gas flow rate was maintained at 4.0 ± 0.1 L/min. The inlet pressures varied from 110 to 165 kPa. The isothermal gas residence time ranged from 200 milliseconds to 2.0 seconds. The gases were analyzed for H_2S concentration using the thermal conductivity detector of the dedicated gas chromatograph. The concentrations were accurate to ± 4 percent of the measured values.

5.3.2.2 Experimental results

5.3.2.3 Effect of Temperature.

The effect of temperature on the H_2S conversion is shown in Figure 5.1. The equilibrium H_2S conversions for a feed of 1.0 mol % H_2S in nitrogen at total pressures of 110 and 165 kPa have also been reported in Figure 5.1. The two pressures correspond to the minimum and maximum inlet pressures for our experiments. The equilibrium conversions were calculated from the Gibbs free energy minimization (see Chapter 2 for details) for a H_2S-H_2-S_x-N_2 system, where S_x represents the sulfur allotropes S_1, S_2,...S_8. It is known that the H_2S decomposition is severely restricted by the thermodynamic equilibrium at lower temperatures (< 500 °C). It can be seen from Figure 5.1, that even at 800 °C the equilibrium conversions are approximately 25 and 30 percent for total pressures of 165 and 110 kPa, respectively. At the highest temperature investigated in this study, i.e. 1250 °C, the equilibrium conversions lie in the range of 79–82 percent. The experimentally measured H_2S conversions in the three quartz reactors of lengths 3.2, 6.4 and 16.0 m is also shown in Figure 5.1. The H_2S conversions below 850 °C are less than 5% even in the longest reactor for gas residence time of approximately 2 seconds. However, at temperatures exceeding 1200 °C, experimental H_2S conversions close to equilibrium conversions were achieved even in the shortest reactor within a residence time of approximately 200 milliseconds. This clearly shows that the H_2S decomposition reaction is very rapid at higher temperatures.

5.3.2.4 Effect of initial H_2S concentration.

To find out the order of dependency of H_2S concentration for H_2S decomposition reactions, experiments were conducted at 900°C and 1000 °C in the 16.0 m long reactor for three initial H_2S concentrations of 0.5, 1.0 and 2.0 mol % and at 1100

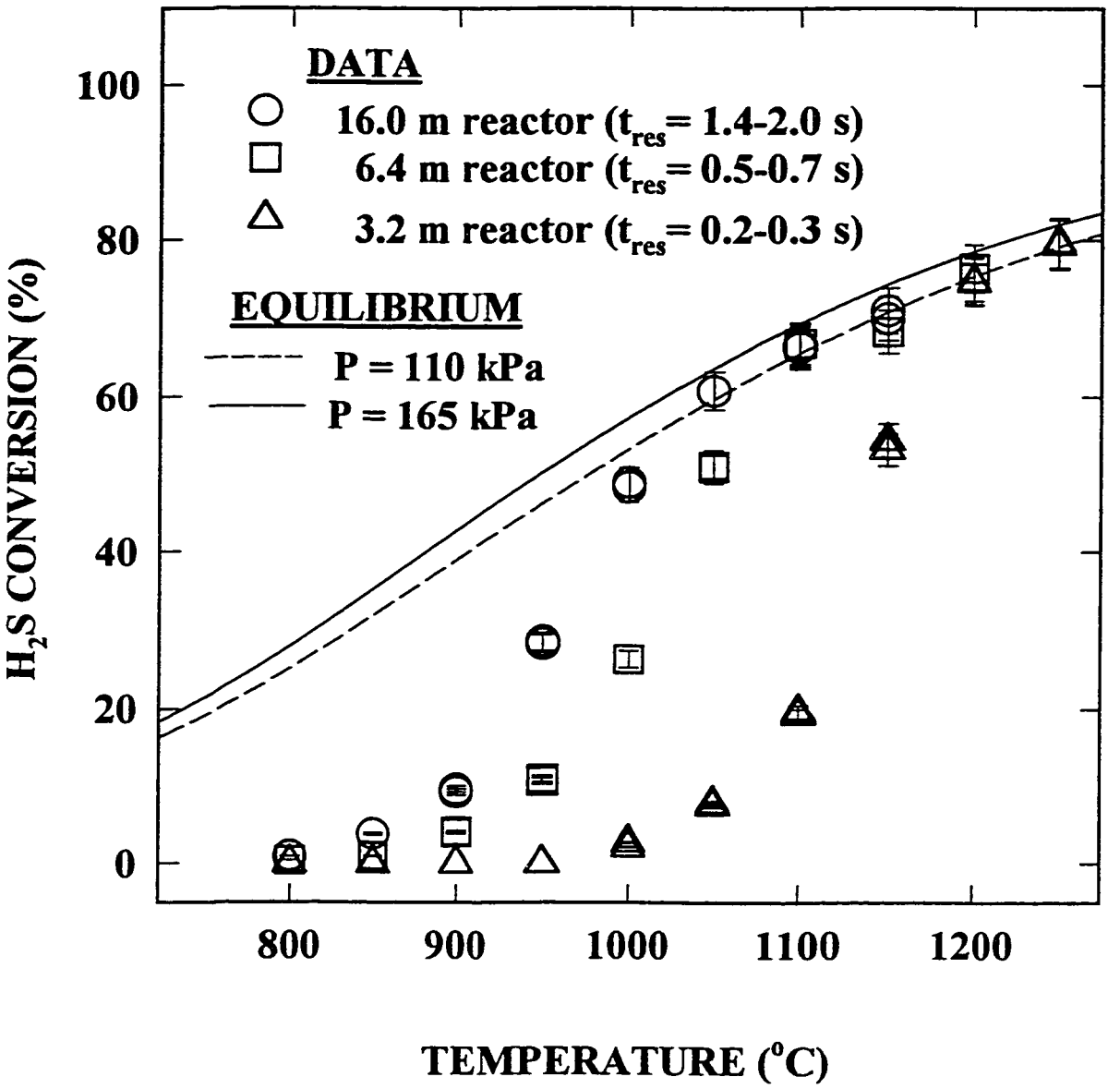

Figure 5.1 Experimentally measured H_2S conversions in three quartz reactors with gas residence times ranging from 0.2 to 2.0 s.

°C in the 3.2 m reactor for four initial H_2S concentrations of 0.2, 0.5, 1.0 and 2.0 mol%. The results of these experiments are presented in Figure 5.2. The measured H_2S conversions for initial H_2S concentrations that varied by four to ten folds were found to yield a constant value within experimental errors. This proves that the reaction rate is first order with respect to the H_2S concentration.

5.3.3 Kinetic model

The initial step in hydrogen sulfide decomposition, until the studies of Woiki and Roth (1994) and Olschewski et al. (1994), was considered to be hydrogen abstraction via the following reaction:

$$H_2S + M \rightleftharpoons SH + H + M \qquad \Delta H_{298} = 377.8 \text{ kJ/mol} \qquad (5.3)$$

where, M is an inert collisional molecule (which in our case is the diluent gas nitrogen) that acts as a energy transfer agent. These two studies, however, reported reaction rate constants that were significantly higher than those reported in the previous shock tube studies. They argued that the initial step for dissociation of H_2S takes place according to the energetically favorable reaction:

$$H_2S + M \rightleftharpoons H_2 + S(^3P) + M \qquad \Delta H_{298} = 297.6 \text{ kJ/mol} \qquad (5.4)$$

where, $S(^3P)$ represents a sulfur atom in a ^3P electronic state. The initial rates of hydrogen sulfide decomposition, according to either of the reaction 5.3 or 5.4, can be expressed as follows:

$$-r_{H2S} = k_1 C_M C_{H2S} \qquad (5.5)$$

where, C_M and C_{H2S} are the concentrations of M and H_2S in kmol/m^3, respectively and k_1 (in m^3/kmol·s) is the reaction rate constant for the reaction 5.3 or reaction 5.4, as the case may be.

Woiki and Roth (1994) measured the initial rates of formation of the H and S atoms and found that the rates of formation of the S atoms were 10-20 times that for the H atoms. Based on these experimental facts, they proposed that reaction (5.4) was the primary step in H_2S decomposition. Irrespective of whether reaction (5.3) or reaction (5.4) dominates the initial decomposition of H_2S, the production of radical SH and atoms S and H is followed by subsequent rapid

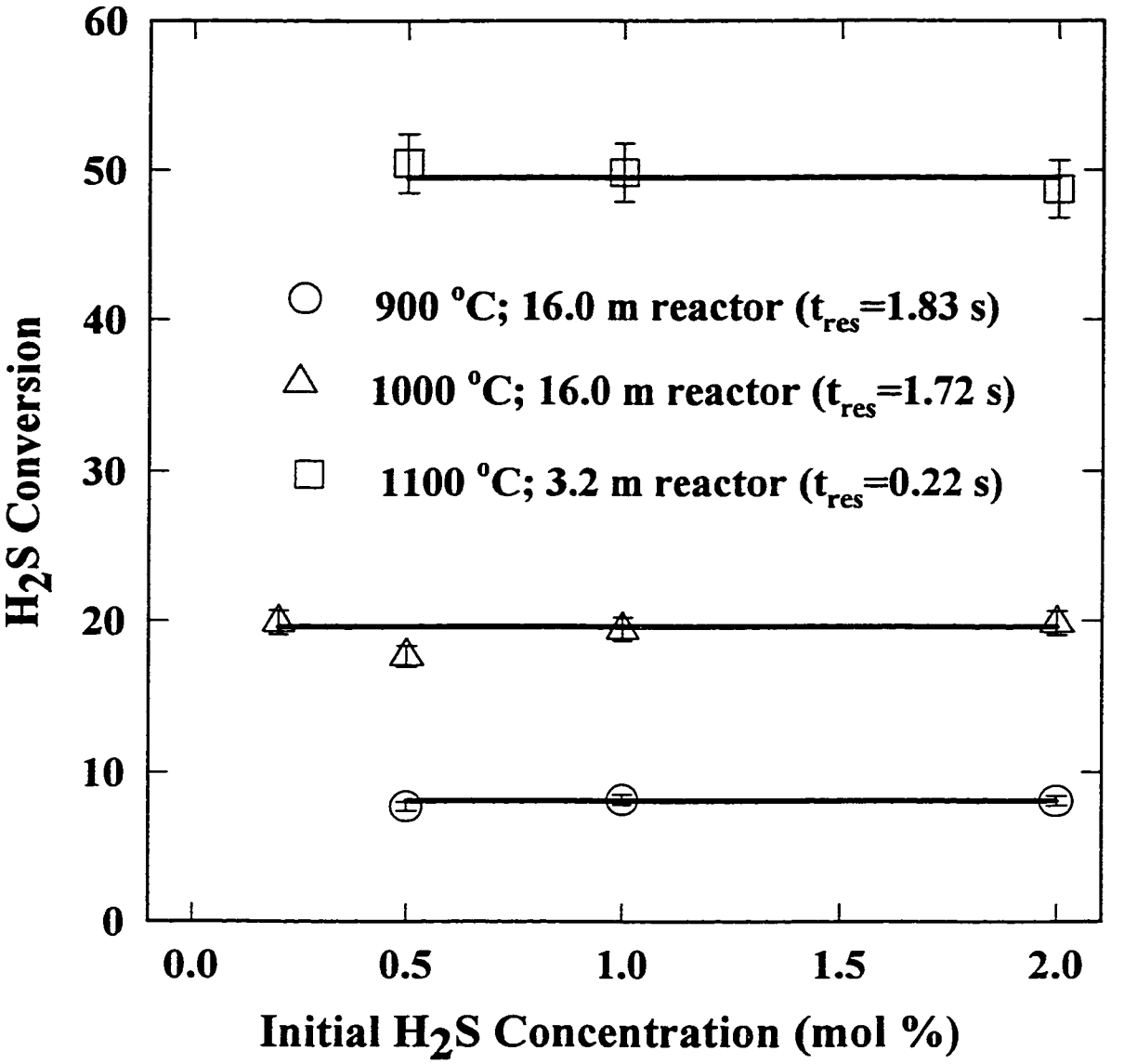

Figure 5.2 Effect of initial H_2S concentration on H_2S conversions measured at three different temperatures.

reactions of H_2S with the atoms. The atoms and radicals also react very rapidly with each other. The net result is that the overall rate of disappearance of H_2S is found to be twice the rate of H_2S consumption via reaction (5.3) or (5.4). Hence, the overall H_2S decomposition rate (in kmol/m^3·s) can be expressed as:

$$-r_{H2S} = k\, C_M\, C_{H2S} \qquad (5.6)$$

where, k (in m^3/kmol·s) is two times k_1 ($k=2k_1$). At very low initial concentrations of H_2S (< 100 ppm), a majority of the H_2S will be decomposed by the primary reaction step and, therefore, the overall rate of H_2S disappearance will equal the initial rate of H_2S decomposition. Some of the important reactions and the associated kinetic parameters reported in the literature are presented in Table 5.1.

5.3.4 Estimation of parameters

From our experiments, we have established the overall H_2S decomposition rate to be first order with respect to H_2S concentration. The rate of disappearance of H_2S was calculated via equation (5.6) and the rate constant k was determined using the experimental data which corresponded to H_2S conversions less than 90 percent of the equilibrium conversions.

The parameters for the irreversible forward reaction rate (k), i.e. the H_2S decomposition reaction, were obtained by least square minimization of the difference between the model predicted and experimentally observed H_2S conversions. The results are reported in the latter part of this thesis in Table 5.2. The regressed rate constant k in m^3/(kmol·s) was found as:

$$k = (1.68 \pm 0.86) \times 10^{11} \exp\left[(-28940 \pm 840)/T\right] \qquad (5.7)$$

Table 5.1 Selected Reactions for H_2S Decomposition

	Reaction	A (m^3/(kmol·s)	E_a (kJ/mol)	Reference
1.	$H_2S + M \leftrightarrow H_2 + S + M$	1.90×10^{11}	274.3	Woiki and Roth (1994)
		2.00×10^{11}	274.4	Olschewski et al. (1994)
		2.18×10^{11}	268.6	Shiina et al. (1996)
2.	$H_2S + M \leftrightarrow H_2 + S + M$	4.64×10^{11}	345.0	Roth et al. (1982)
		1.99×10^{11}	310.0	Bowman and Dodge (1976)
3.	$H_2S + S \leftrightarrow$ products	8.31×10^{11}	30.9	Shiina et al. (1996)
		5.70×10^{11}	63.2	Woiki and Roth (1994)
4.	$H_2S + H \leftrightarrow SH + H_2$	1.90×10^{11}	20.7	Woiki and Roth (1994)
5.	$H_2 + S \leftrightarrow SH + H$	15.84×10^{11}	82.5	Shiina et al. (1996)
		6.00×10^{11}	100.3	Woiki and Roth (1994)
6.	$S + SH \leftrightarrow S_2 + H$	0.20×10^{11}	0	Woiki and Roth (1994)
7.	$S_2 + M \leftrightarrow 2S + M$	0.48×10^{11}	322.16	Woiki and Roth (1994)
8.	$H_2 + M \leftrightarrow 2H + M$	2.20×10^{11}	401.9	Woiki and Roth (1994)

5.3.5 Comparison with previous studies

5.3.5.1 Comparison of activation energy

The activation energy, from equation (5.7), for the overall H_2S disappearance rate corresponds to 240.6 kJ/mol which is in excellent agreement with the recent lower temperature (1030-1070 K) study by Adesina et al. (1995) who reported the activation energy to be 240 kJ/mol. However, it is significantly higher than the 195 kJ/mol value reported by Kaloidas and Papayannakos (1989) who conducted their experiments at temperatures ranging from 873 to 1133 K in tubes made of alumina, in which catalytic effects may have been significant. In a recent study, Harvey et al. (1998) have shown that the surface reactions in alumina reactors may account for up to 70 percent of the total rate. The activation energies of 273.2 kJ/mol, 274.4 kJ/mol and 268.6 kJ/mol reported in the high temperature (1800-3300 K) shock tube studies of Woiki and Roth (1994), Olschewski et al. (1994) and Shiina et al. (1996), respectively, are all somewhat higher than that obtained from our experiments.

The comparison of activation energies is often used to show the relative goodness of one's kinetic data with respect to other published work. This is very misleading because similar activation energies do not ensure similar rate constants. Therefore, we wanted to find out how our rate constants compared to those reported in the literature.

5.3.5.2 Comparison of rate constant

A comparison of the rate constants obtained in our study with those reported in literature is shown in Figure 5.3. It must be noted that we have obtained the rate constant (k) for overall H_2S decomposition reaction defined by equation (5). However, the high temperature shock tube studies have reported the rate constant (k_1) for the initial decomposition reaction, which is equal to one-half the overall rate constant (k). To be consistent in comparison we divided the overall rate constant (k) obtained from our experiments by two.

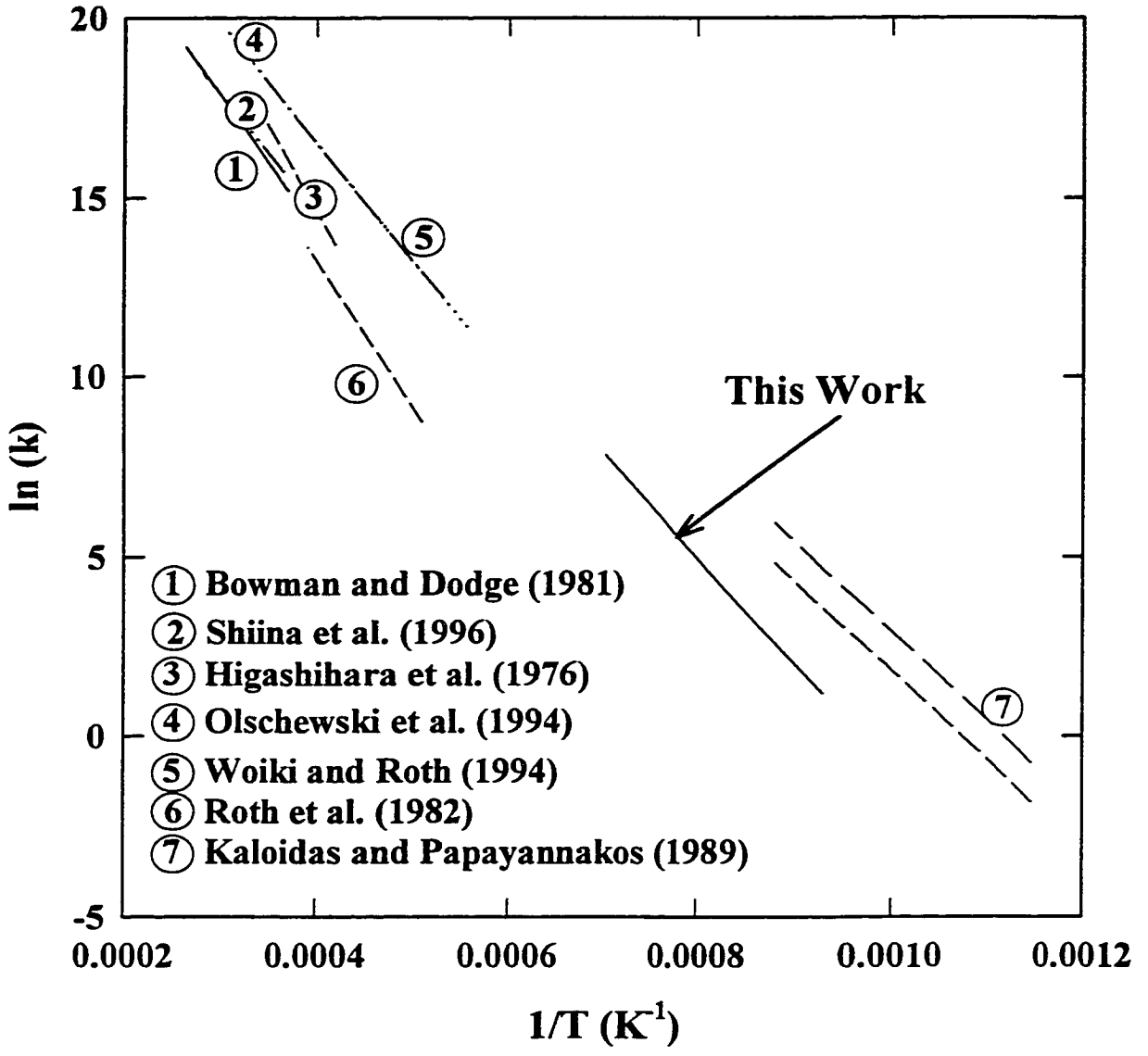

Figure 5.3 Comparison of published rate constant for H_2S decomposition reaction; *k* in m^3 $kmol^{-1}$ s^{-1}.

In their study, Kaloidas and Papayannakos (1989) expressed the rate of disappearance of H_2S (in mol/cm^3·s) in a form different than equation (5.6):

$$(-r_{H2S}) = k_f P_{H2S} \qquad (5.8)$$

where, k_f is in mol/cm^3·s·atm and P_{H2S} (in atmospheres) is the partial pressure of hydrogen sulfide in the reacting mixture. For comparison, this rate expression was transformed into a form consistent with equation (5.6) and expressed as $k_f = 10^{-3} \times k\, P_t / [RT]^2$, where P_t is the total system pressure in atmospheres, T is in Kelvin and the corresponding value of R is 82.0562 cm^3·atm/(mol·K). The rate constant k was then calculated from this expression. However, since the total pressure in their experiments varied from 1.3 to 3 atmospheres, a range of rate constant rather than a single line is shown for the kinetics proposed by Kaloidas and Papayannakos (1989) in Figure 5.3

From Figure 5.3, it can be seen that there is a considerable disagreement among the reported rate constants both in the lower and higher temperature regions. These differences can be attributed partially to the different experimental techniques used in these studies. Among the high temperature shock-tube studies, different research groups have measured different chemical species (e.g. S, H, S_2, H_2 or H_2S) and determined the rate constant from the temporal concentration profiles of these species.

For example, Olschewski et al. (1994) and Woki and Roth (1994) measured the S atom concentration in their experiments. From the S atom production rate at initial times, they obtained the reaction rate constant for the initial decomposition of H_2S, which is expected to proceed via reaction 5.4. In an earlier work, Roth et al. (1982) had monitored the H atom concentrations during H_2S decomposition. They calculated the initial H_2S decomposition rate from the H atom production rates at initial times. The underlying assumption here is that the initial H_2S decomposition proceeded according to reaction (5.3). In their recent study, Woiki and Roth (1994) found the initial H atom production rate to be 10-20 times lower than the initial S atom production rate. This explains why the rate constants reported by Roth et al. (1982), as shown in Figure 5.3, have lower

values than those reported in their recent work (Woiki and Roth, 1994). Among the other studies, the rate constants proposed by Shiina et al. (1996), Bowman and Dodge (1981) and Higashihara et al. (1976) are in good agreement with each other. Both Shiina et al. (1996) and Bowman and Dodge (1981) determined the reaction rate by monitoring the H_2S concentration. While Shiina et al. (1996) used infrared emission spectroscopy to determine the H_2S concentration, Bowman and Dodge (1981) had employed ultraviolet absorption spectroscopy. Although, different techniques were used to monitor the H_2S concentrations in the two studies similar rate constants were obtained. In their experiments, Higashihara et al. (1976) monitored the S_2 concentration by ultraviolet absorption and determined the rate constant from these measurements. The rate constants reported by them lies between the rate constants determined by S atom concentration measurement and that determined by H_2S concentration measurement.

At lower temperatures, the only available first order rate constant was that by Kaloidas and Papayannakos (1989) who measured the H_2S concentrations in the feed stream and product streams of their reactor. It can be clearly seen from Figure 5.3, that the rate constants reported by Kaloidas and Papayannakos (1989) are greater and significantly different than that obtained in this work. It must be mentioned here that Kaloidas and Papayannakos (1989) suggested that quartz had a catalytic effect on the decomposition reaction and therefore performed their experiments in alumina tubes. The fact that the rate constant reported by them are higher than those obtained in this study indicates that the catalytic effect of quartz, if any, is relatively less than that of alumina. Recently, Harvey et al. (1998) conducted experimental studies on H_2S decomposition in tubular alumina reactors over a temperature range of 1350-1600 K. They report that more than 70 percent of the total rate is comprised of the surface reaction. Moreover, in another recent study, Faraji et al. (1998) conducted experiments over a temperature range1273-1473 K in empty and quartz-packed reactors made of quartz. They concluded that at temperatures greater than 1273 K the

homogeneous gas phase reaction is much faster than the catalytic reaction on the silica surface.

5.3.6 Extrapolation of rate constants

The errors involved in modeling H_2S decomposition rates by extrapolating the available high temperature rate constants can be large and the calculated rates may be unrealistically low or high. For example, extrapolation of the rate constants obtained in shock tube studies to the highest temperature (i.e. 1523 K) investigated in this work results in values 3 to 600 times lower than that obtained in this experiment study. These differences are even more pronounced at the lower temperatures. At 1073 K, the extrapolated rate constants are 1/9 to 1/70,000 times that observed in this work. The extrapolation of the rate constant reported at lower temperature also results in values that are significantly higher than those found in this study. For example, the extrapolated rate constant of Kaloidas and Papayannakos (1989) is a maximum of 16 times that found in this study at 1073 K and 8 times at 1523 K.

5.3.7 Proposed reconciliation of rate constant over 1073-3300 K

The differences in high temperature shock tube obtained rate constants and that obtained in this study are too large to be explained by experimental errors or by the different experimental conditions and reactor types used. It is important to reconcile these differences.

This requires an examination of the scatter in the experimental data of this work and other reported studies, and any bias it could have on regression of the parameters. An observation of Figure 5.3 shows that the rate constant obtained from this study falls in line with the rate constants reported by Olschewski et al. (1994) and Woiki and Roth (1994). Fortunately, both Olschewski et al. (1994) and Woiki and Roth (1994) had reported the rate constants and the corresponding temperatures in a tabular form. These data along with the data

obtained in this study are shown in Figure 5.4. The kinetic parameters corresponding to the three sets of data are reported in Table 5.2.

In Figure 5.4, the solid line represents the best fit line obtained by the least square minimization of the three sets of data. The new rate constant (in m^3/kmol-s) is given as:

$$k = (1.12 \pm 0.114) \times 10^{11} \exp [(-28360 \pm 200) /T] \qquad (5.9)$$

The activation energy corresponding to the rate expression (5.9) is equal to 235.8 kJ/mol and is lower than those obtained in all shock tube studies. Figure 5.4 shows that the shock tube study data and our data are in a remarkably good agreement. This plot demonstrates that the rate constants for H_2S decomposition obtained from two entirely different experimental techniques and at vastly different temperature range (T varying from 800 °C to 3000 °C) are indeed highly consistent.

5.3.8 Effect of trace concentrations of oxygen in initial reacting mixture on the H_2S decomposition rates

During the last stages of the experimental study during this doctoral research, it was found that the ultra high purity nitrogen used in experiments contained up to 3 ppm of oxygen. This was found during an investigation on the CO formation rates from the reaction between CO_2 and H_2 which, has been discussed later under section (5.8). Now, as mentioned earlier, it has been reported in the literature that the presence of oxygen accelerates the H_2S decomposition reaction (Higashihara, 1976). Due to time constraints, further experiments on H_2S decomposition reaction after removal of O_2 were not attempted. It must also be noted that removal of these trace quantities of oxygen from highly reactive gas mixture (containing H_2S) may be a difficult task. Therefore, to investigate the role of oxygen during the thermal decomposition of H_2S, a simulation study was carried out. Recently, Tsuchiya et al. (1997) published a reaction scheme comprised of 30 elementary reactions for oxidation of H_2S. The reaction scheme of Tsuchiya et al. has been reproduced in Table 5.3 The forward rates of reaction for the 30 reactions were reported; however, the reverse rates had to be

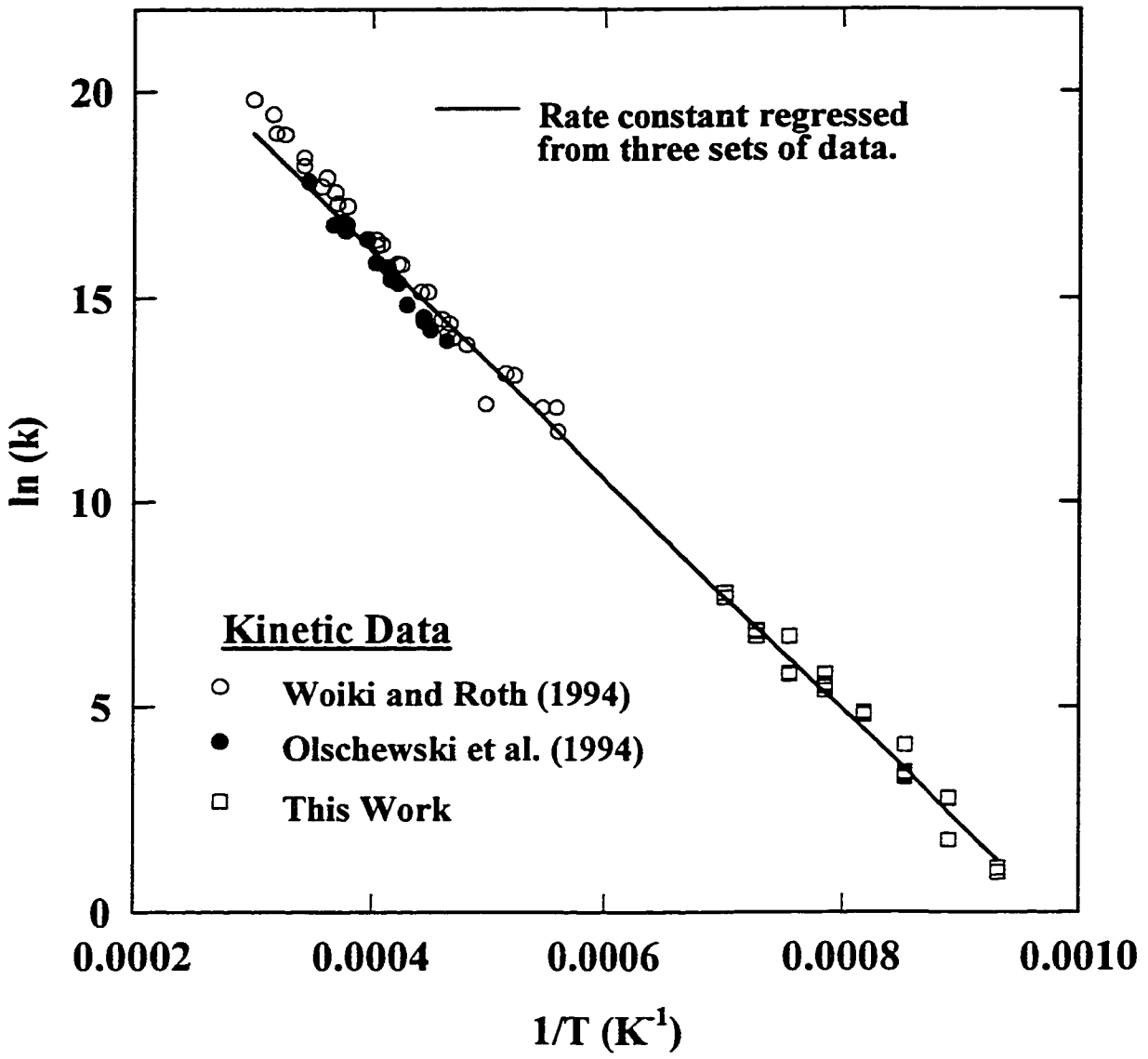

Figure 5.4 New rate constant for H_2S decomposition over the temperature range 1073-3350 K.
***(k* in m^3 $kmol^{-1}$ s^{-1})**

Table 5.2 Kinetic parameters for H_2S decomposition reaction obtained from different sets data.

	Ea_1* (kJ/mol)	A_1* (m^3/kmol·s)	Data Points	Correlation Coefficient (R^2)
Olschewski et al.	274.36 (260.18)**	2.00×10^{14} (2.00×10^{14})**	30	0.9838
Woiki and Roth	273.19 (277.74)**	2.00×10^{14} (2.78×10^{14})**	17	0.9821
This Study	240.12	0.84×10^{14}	38	0.9706
3 sets combined	235.78	0.51×10^{14}	85	0.9959

* Corresponds to the rate constant $k_1 = A_1 \exp(-Ea_1/RT)$ where R equals 8.314×10^{-3} kJ/mol·K and T is in Kelvin.
** Calculated from the data reported in the reference.

Table 5.3 Detailed reaction mechanism for Hydrogen Sulfide oxidation (from Tsuchiya et al., 1997)

Table Reaction Mechanism of H_2S/O_2 System. $k = AT^B\exp[-E(kJ\ mol^{-1})/RT]$ in Molecule cm s Units

Elementary Reactions	A	B	E	Reference
$H_2S + Ar = H_2 + S + Ar$	3.63E-11	0.00	268.4	Shiina (1996) [8]
$H + H_2S = H_2 + HS$	3.20E-10	0.00	20.7	Yoshimura (1992) [9]
$S + H_2S = HS + HS$	1.38E-10	0.00	30.8	Shiina (1996) [8]
$S + H_2 = H + HS$	2.63E-10	0.00	82.5	Shiina (1996) [8]
$S + HS = H + S_2$	4.47E-11	0.00	0.0	Mihelcic (1970) [36]
$HS + HO_2 = H_2S + O_2$	1.66E-12	0.00	0.0	Frenklach (1981) [7]
$O + H_2S = OH + HS$	2.02E-10	0.00	32.0	Tsuchiya (1994) [10]
$O + H_2S = H + HSO$	0.50E-10	0.00	32.0	Tsuchiya (1994) [10]
$H_2S + OH = HS + H_2O$	5.25E-12	0.00	0.0	Perry (1976) [37]
$HS + O = SO + H$	1.26E-10	0.00	0.0	Tsuchiya (1994) [10]
$HS + O_2 = HSO + O$	3.10E-11	0.00	75.0	This work
$S + O_2 = SO + O$	2.53E-11	0.00	15.3	This work
$SO + O_2 = SO_2 + O$	1.70E-12	0.00	34.0	This work
$SO + OH = SO_2 + H$	8.40E-11	0.00	0.0	Jourdain (1979) [38]
$HSO + Ar = H + SO + Ar$	1.40E-08	0.00	245.0	guess
$HSO + O_2 = HO_2 + SO$	1.66E-12	0.00	0.0	Frenklach (1981) [7]
$S_2 + O = SO + S$	1.66E-11	0.00	0.0	Singleton (1988) [39]
$H + O_2 = OH + O$	3.30E-10	0.00	70.3	Baulch (1992) [40]
$O + H_2 = OH + H$	8.49E-20	2.67	26.3	Baulch (1992) [40]
$OH + H_2 = H_2O + H$	1.70E-16	1.60	13.8	Baulch (1992) [40]
$OH + OH = H_2O + O$	2.50E-15	1.14	0.4	Baulch (1992) [40]
$H + O_2 + Ar = HO_2 + Ar$	1.70E-30	−0.80	0.0	Baulch (1992) [40]
$H + HO_2 = OH + OH$	2.80E-10	0.00	3.7	Baulch (1992) [40]
$H + HO_2 = H_2 + O_2$	7.10E-11	0.00	5.9	Baulch (1992) [40]
$H + HO_2 = H_2O + O$	5.00E-11	0.00	7.2	Baulch (1992) [40]
$O + HO_2 = OH + O_2$	5.40E-11	0.00	0.0	Baulch (1992) [40]
$HO_2 + OH = H_2O + O_2$	4.80E-11	0.00	−2.1	Baulch (1992) [40]
$H_2 + Ar = H + H + Ar$	9.88E-06	−1.10	436.8	Cohen (1983) [41]
$O_2 + Ar = O + O + Ar$	3.01E-06	−1.00	494.1	Tsang (1986) [42]
$H + OH + Ar = H_2O + Ar$	2.30E-26	−2.00	0.0	Baulch (1992) [40]

determined from the thermodynamic equilibrium constant. These equilibrium constants were computed from the Gibbs free energy data reported in JANAF thermochemical tables. The free energy data for HSO radical were not available in JANAF tables and had to be obtained from the Burcat's thermochemical data of the Chemkin database (TCC, 1998).

A program written in MATLAB that employed the ODE15S algorithm (better known as the Gear's algorithm) solved the material balance equations involving 30 chemical species and 60 reactions. Tsuchiya et al. reported the concentration profiles for oxidation of H_2S predicted from the Chemkin simulator using their reaction scheme. The mixture had a composition of 4.0% H_2S, 6.0% O_2 and balance Argon and the temperature and pressures were 1800 K and 0.4 atm, respectively. To verify the H_2S oxidation program written in this work, a comparison was made with published results of Tsuchiya et al. for the above mixture. The results of the comparison are presented in Figure 5.5 The shape of the temporal profiles for all the species are almost identical. However, differences exist for the steady state concentrations of OH, SO_2 and SO. Also the H_2S and oxygen depletion rates are higher within the residence time range of 100 to 300 microseconds. The differences could be due to the difference in numerical methods employed in the two studies and also due to the equilibrium constants for the reactions involving sulfur species. Nonetheless, the key features of the profiles are reproducible. For example, the induction time for SO_2 formation (time at which the SO_2 concentrations reach 90% of the final value) is almost identical. It must be mentioned that Tsuchiya et al. (1997) used the criterion of matching the induction period observed in experimental studies reported in the literature as a verification of their model.

After the program developed in the current work was verified, calculations were performed for the conditions employed in this study. The hydrogen sulfide conversions were sensitive to the rate constant of the first reaction of Table 5.3, i.e. the initial step in the decomposition of H_2S. To simulate the experimental conditions of this study, the rate constant k_1 for first reaction in

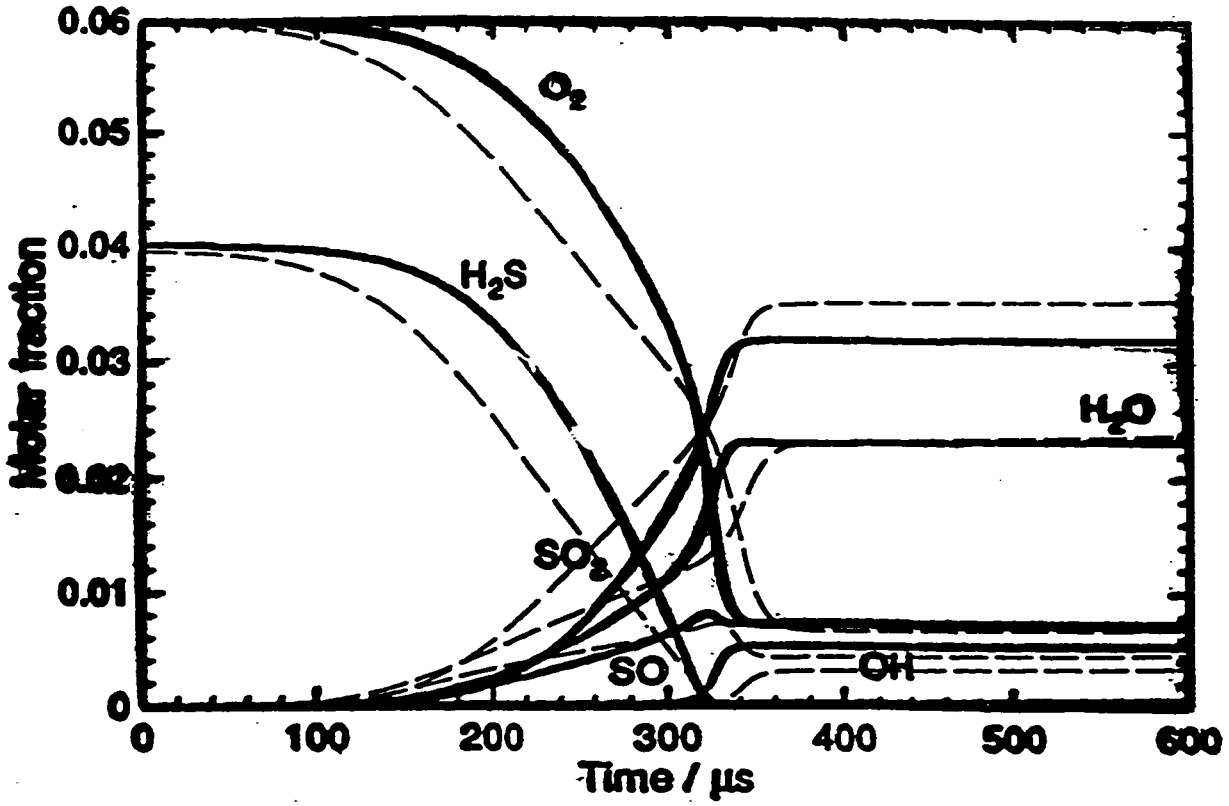

Figure 5.5 Comparison of predicted temporal profiles of chemical species during oxidation of 4% H_2S with 6% O_2 in a batch reactor [T = 1800 K, P= 1.4 atm].

Solid Lines: Reproduced from Figure 10 of Tsuchiya et al., 1997

Dotted Lines: Predicted from computer program written in this study

Table 5.3 was replaced with the rate constant k_1 reported below, where k_1 was obtained by dividing k reported in equation 5.8

$$k_1 = (5.56 \pm 0.507) \times 10^{10} \exp [(-28360 \pm 200) /T] \qquad (5.10)$$

The results of the calculations for the conditions of Figure 5.5 were not affected by this change in the rate constant. The predicted H_2S concentrations using the k_1 from Tsuchiya et al. (1997) and that using k_1 of equation (5.10) are shown in Figure 5.6. It can be observed that using the rate constant of Tsuchiya et al., very small H_2S conversions are predicted. However, on replacing the rate constant with that of equation (5.10) which was obtained by the regression of three sets of data [Olschewski et al., 1994, Woiki and Roth, 1994 and this study), the predicted H_2S conversions are much higher.

Next, the effect of low concentrations of oxygen present in the initial reacting mixtures was investigated by performing calculations for mixtures containing 1, 10 and 100 ppm of O_2. The temporal profiles for H_2S concentration are shown in Figure 5.6 for various initial O_2 concentrations at a fixed initial H_2S concentration. The results indicate that the presence of O_2 in the initial reacting mixture at concentrations up to 10 ppm have little effect on H_2S decomposition rate. Since, the O_2 content for the experimental study was less than 3 ppm, there should be little effect of the presence of O_2 in the initial mixture on H_2S decomposition rate. Consequently, the rate constants obtained from this study can be considered to be reliable. The above conclusions are based on the premise that the reaction mechanism proposed by Tsuchiya et al. (1997) is also reliable.

5.4 Reaction between CO and Sulfur

There is evidence that the reaction between CO and sulfur to form COS is one of the primary COS forming reactions in the Claus process (Sames et al., 1990). There have been references in the past to indicate this reaction was an important

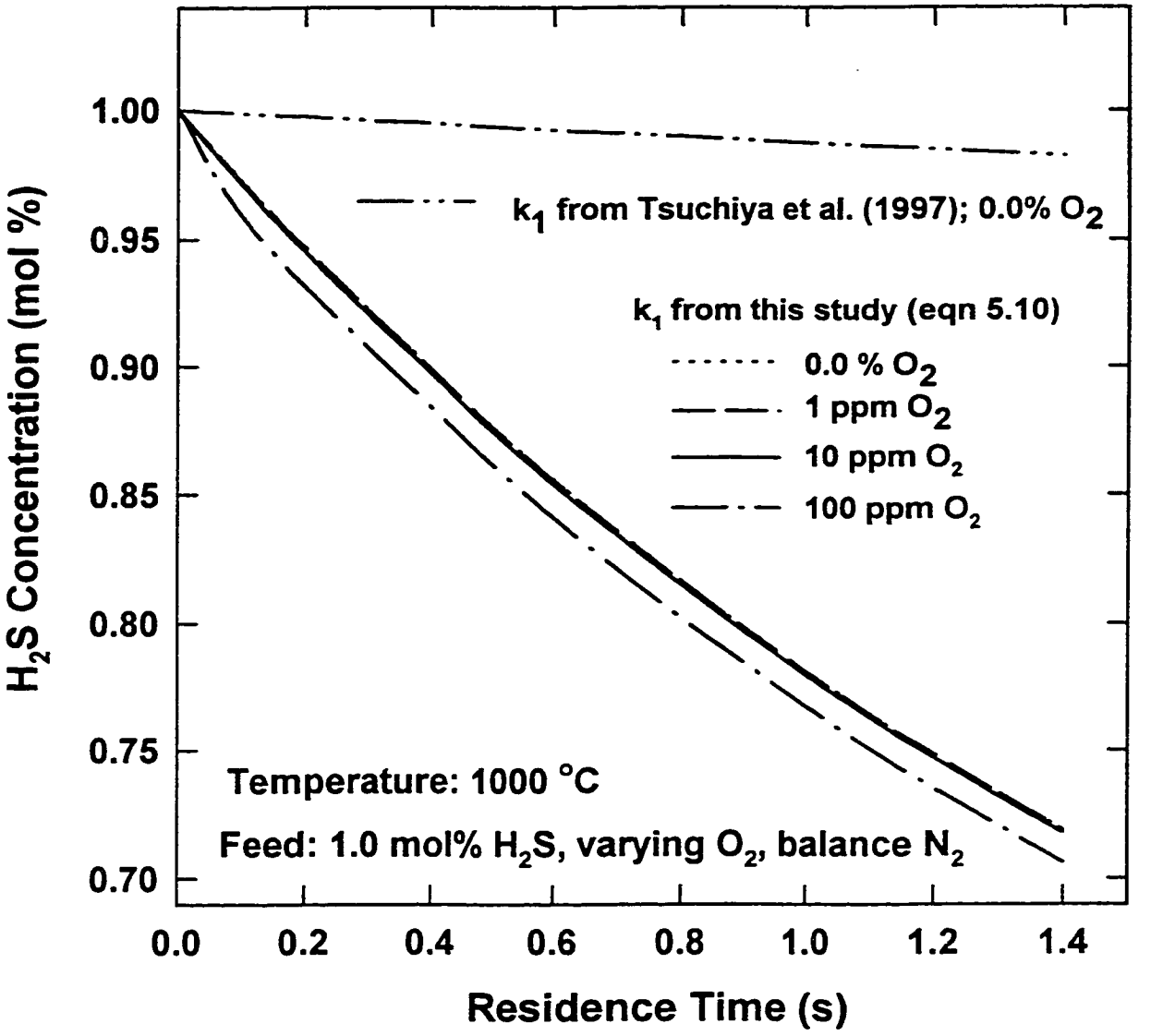

Figure 5.6 Effect of oxygen on H_2S decomposition. Predicted using the 30 reaction mechanism of Tsuchiya et al. (1997)

COS forming reaction (Grancher, 1978; Paskall, 1979). However, there is practically no kinetic information on this reaction.

5.4.1 Literature review

The only published result on an experimental study of the direct reaction between CO and sulfur is that by Dokiya et al (1978). They proposed a two step decomposition process of hydrogen sulfide - (i) the production of hydrogen and carbonyl sulfide via the reaction of carbon monoxide and hydrogen sulfide, (ii) the decomposition of COS via the reverse of the following reaction:

$$CO + 1/x\ S_x \rightleftharpoons COS \qquad (5.11)$$

They were interested in rapidly quenching reaction (5.11), and hence, performed experiments to obtain qualitative information on the rate of this reaction. Their experiments consisted of flowing CO over a sulfur reservoir and continuing the reaction in a pyrex reactor. The effects of CO flow rate, the temperature of the sulfur reservoir and the temperature of the reactor on the COS yield were studied. The sulfur reservoir temperature was varied in a range of 200-400 °C while the reactor temperature was varied in a range of 300-550 °C. As expected, the COS yield were found to be higher for higher reactor and sulfur reservoir temperatures and lower for higher CO flow rate. It was concluded from their study that although reaction (5.11) is very fast, it can be quenched rapidly at higher flow rates. However, the reaction rate kinetics of reaction (5.11) was not reported.

5.4.2 Experimental

5.4.2.1 Experimental conditions.

Experiments were conducted with dilute concentrations of reactants (dilution > 90%) in a temperature range of 600-1150 °C using the 6.4 and 16.0 m long reactors. The flow rate of each reactant stream (i.e. N_2 diluted CO and N_2 diluted sulfur) was maintained at 2.0 L/min (measured at room temperature and

atmospheric pressure) which gave an actual residence times of 0.5-1.0 s and 1.1-2.1 s for the 6.4 m and 16.0 m long reactors, respectively. These residence times were calculated at the furnace set point temperature assuming plug flow of the gases. The total inlet pressure varied from 115 to 130 kPa. A majority of the experiments were conducted by reaction 5.0 mol% CO with 0.9 mol% S_2. To study the effect of CO concentration on COS formation, experiments were conducted with a fixed S_2 concentration of 0.90 mol% while the CO concentration was varied to 0.5, 2.5 and 5.0 mol%. Similarly, the effect of sulfur concentration on COS formation was studied experimentally with a fixed composition of 5.0 mol% CO and by changing the S_2 concentrations to 0.90, 1.60 and 2.45 mol% in N_2.

5.4.3 Experimental Results

5.4.3.1 Effect of temperature on COS formation.

Experiments were conducted by reacting 5.0 mol% CO with 0.90 mol% S_2 in the temperature range of 600-1150°C. The results of these experiments are presented in Figure 5.7 as the amount of COS produced at various furnace temperatures. The two sets of data represents the COS formed in experiments using reactors of length 6.4 and 16 m. Additionally, the equilibrium COS concentration are also plotted as a dashed line in Figure 5.7. The equilibrium concentration of COS in a CO-COS-N_2-S_i (i=1,2..8) system. It can be observed from Figure 5.7 that the COS formation is favored thermodynamically at lower temperatures, with the equilibrium concentration decreasing as the temperature increases. The two distinct features of the experimental plots are the occurrence of a maximum in the COS formed and the greater than equilibrium yield of COS at higher temperatures. The occurrence of maximum in the COS formed is due to the interplay between reaction kinetics and thermodynamic equilibrium.

The experimental COS conversions are limited by chemical thermodynamic equilibrium for temperatures greater than 850 °C and 950 °C for the longer and the shorter reactor, respectively. At lower temperatures (600-950 °C), the experimentally realized conversions are lower than equilibrium

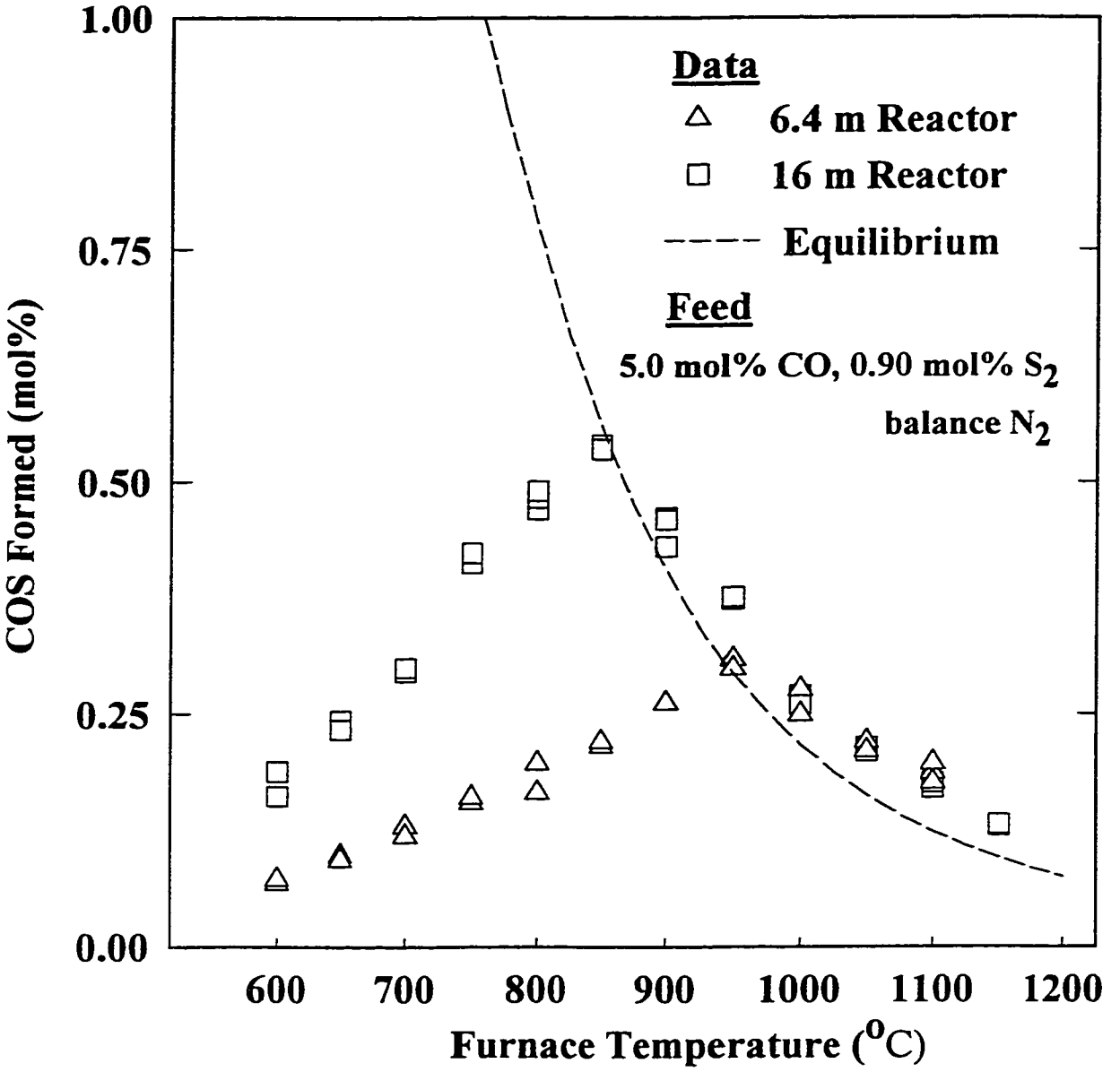

Figure 5.7 Experimentally measured COS concentration at the reactor exit as a function of reactor temperature.

conversion and kinetically limited for the experimental conditions. Within this temperature range, an increase in temperature results in an increased reaction rate and, therefore, in larger COS conversions. At higher temperatures (> 950 °C), the gas residence time or reaction times in either of the reactor are sufficient for attainment of equilibrium conversions. The experimentally obtained conversions are determined by the equilibrium conversion limits, which decrease with the temperature, hence, the experimentally realized conversions are found to decrease with the temperature.

From Figure 5.7, it can be seen that the experimental conversions in the 16.0 m and 6.4 m long reactors exceed the thermodynamic equilibrium conversion for temperatures greater than 900 °C and 1000 °C, respectively. This seemingly odd behavior can be attributed to a combination of experimental errors and limitation of complete reaction quenching. The experimental errors involved in measurement of COS compositions (< 5%) and in determination of sulfur concentration (< 10%) only partially account for the higher than equilibrium conversion. The major reason for this observation lies in the fact that, though an extremely rapid quenching of hot product gases exists (quenching from over 1200 °C to 500 °C in less than 20 ms), it is not instantaneous. The lower temperatures in the quench zone shifts the equilibrium of COS forming reaction (5.10) towards the right (i.e. towards higher COS concentrations). Thus, in the quench zone, due to the shift in equilibrium the CO and sulfur react to some extent before being quenched completely.

5.4.3.2 Effect of sulfur concentration.

To study the effect of the sulfur concentration on COS formation and to determine the order of reaction with respect to the sulfur concentration, experiments were conducted in a 6.4 m long reactor at three temperatures of 600, 700 and 800 °C with a fixed CO concentration of 2.5 mol% and by varying the S_2 concentration to 0.9, 1.6 and 2.45 mol%. It must be pointed out, once again, that the sulfur vapor was considered to be composed entirely of S_2.

Equilibrium calculations have verified that more than 90% of sulfur is present as S_2 at low partial pressures and high temperature (> 500 °C).

At compositions far removed from equilibrium, the reversible reaction is negligible and, under such conditions, the rate of formation of COS can be expressed by the following empirical relation:

$$(r_{cos}) = k_2 C_{co}^{n} C_{s2}^{m} = k_2 P_{CO}^{n} P_{S_2}^{m} / [RT]^{m+n} \quad (5.12)$$

where, "n" and "m" are reaction orders with respect to CO and S_2 concentration. Below 800 °C, the conversion of CO was less than 20% and, thus, its concentration can be assumed to be constant, i.e. $P_{CO}=P_{CO}^{\circ}$. Additionally, the sulfur conversions calculated from the COS formed were calculated to be less than 30%. Thus, for the sake of simplicity, if it is assumed that both the reactants were in excess compared to the product, the relationship $\ln(P_{COS}) = \ln(k' t_{res}) + m \ln(P^{\circ}_{S_2})$ can be derived, where k' is equal to k_2 times $P^{\circ n}_{co}/[RT]^{m+n-1}$ Hence, the slope (m) of a plot of $\ln(P_{COS})$ versus $\ln(P^{\circ}_{S_2})$ would give the order of reaction with respect to the S_2 concentration. In Figure 5.8, $\ln(P_{COS})$ is plotted against $\ln(P^{\circ}_{S_2})$ for three different temperatures. The slopes (m) of the straight lines correlating the data points are also reported on the Figure 5.8 and are 0.981, 0.997 and 1.029 which correspond to temperatures of 800, 700 and 600 °C respectively. These slopes are close to unity which, implies that the order of the reaction with respect to the S_2 concentration is one.

5.4.3.3 Effect of CO concentration.

The effect of the CO concentration on COS production was studied in a manner similar to that employed for studying the effect of the S_2 concentration on COS formation. Experiments were conducted in a 16 m long reactor with CO concentrations of 0.5, 2.5 and 5.0 mol% with a fixed S_2 concentration of 0.90 mol%. The amount of COS formed corresponds to conversions of less than 10% for both CO and S_2. Thus, with the assumption that the reactants were in excess compared to the product, the relationship between COS and CO concentration

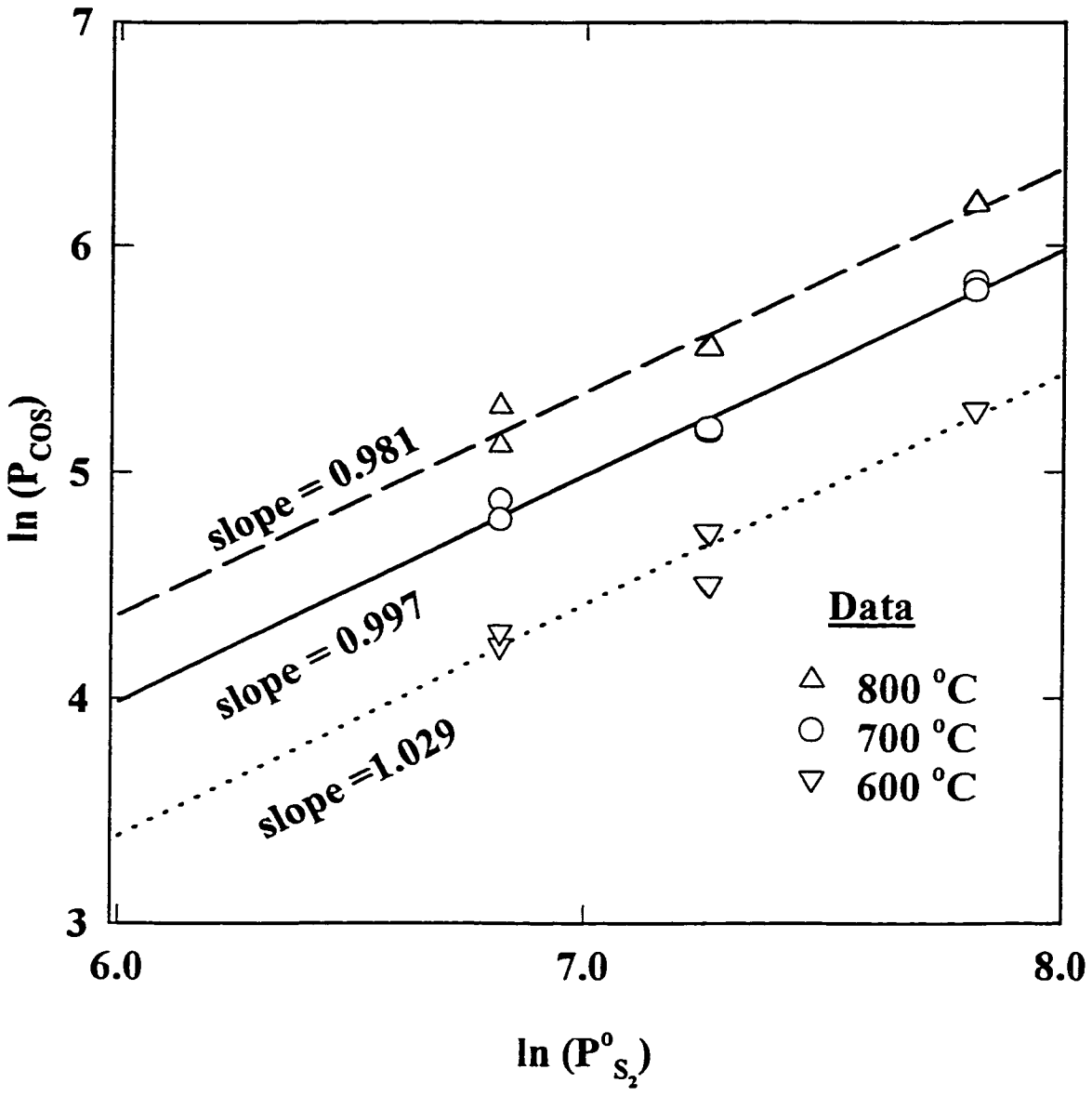

Figure 5.8 Order of dependency with respect to sulfur concentration for COS forming reaction.

can be derived from equation (5.12) to be $\ln(P_{COS}) = \ln(k'' t_{res}) + n \ln(P^{\circ}_{CO})$, where k'' is equal to k_2 times $P^{\circ}_{S_2}/[RT]^{m+n-1}$. In Figure 5.9, the straight line fitted through the data points yield slopes (n) of 1.053, 0.997 and 1.107 for the reaction temperatures of 800, 700 and 600 °C respectively. The order of reaction with respect to the CO concentration is, therefore, equal to unity.

5.4.4 Kinetic modeling

5.4.4.1 Determination of rate constant (k_2)

The reaction rate constant (k_2) for reaction between CO and S_2 was determined by integrating equation (5.12) with both "n" and "m" taken as unity. For the evaluation of the rate constant (k_2), selected data corresponding to COS conversion of less than 80 percent of the equilibrium value were used. The calculated rate constants are presented as an Arrhenius plot of rate constant (k_2) in Figure 5.10. The plot demonstrates linearity for the range of temperature investigated. The activation energy, computed from the slope of the plot, was found to be 55.8 kJ/mol. A least square minimization of calculated rate constants yielded a second order rate expression (k_2 in m^3/kmol·s) :

$$k_2 = (3.18 \pm 0.36) \times 10^5 \exp[-(6700 \pm 108\ K) / T] \qquad (5.13)$$

5.4.5 Possible reaction mechanism.

Since the apparent orders of reaction with respect to the CO and S_2 concentrations are unity, a plausible reaction mechanism for COS formation can be proposed on the basis of following set of reactions:

$$CO + S_2 \rightleftharpoons COS + S \qquad \Delta H_r^{\circ} = 120\ kJ/mol \qquad (5.14)$$

$$S + S \rightleftharpoons S_2 \qquad \Delta H_r^{\circ} = -426\ kJ/mol \qquad (5.15)$$

$$CO + S \rightleftharpoons COS \qquad \Delta H_r^{\circ} = -305\ kJ/mol \qquad (5.16)$$

The initial step involves reaction of CO and S_2 to form COS and atomic sulfur via reaction (5.14). The sulfur atom can subsequently react with another sulfur atom

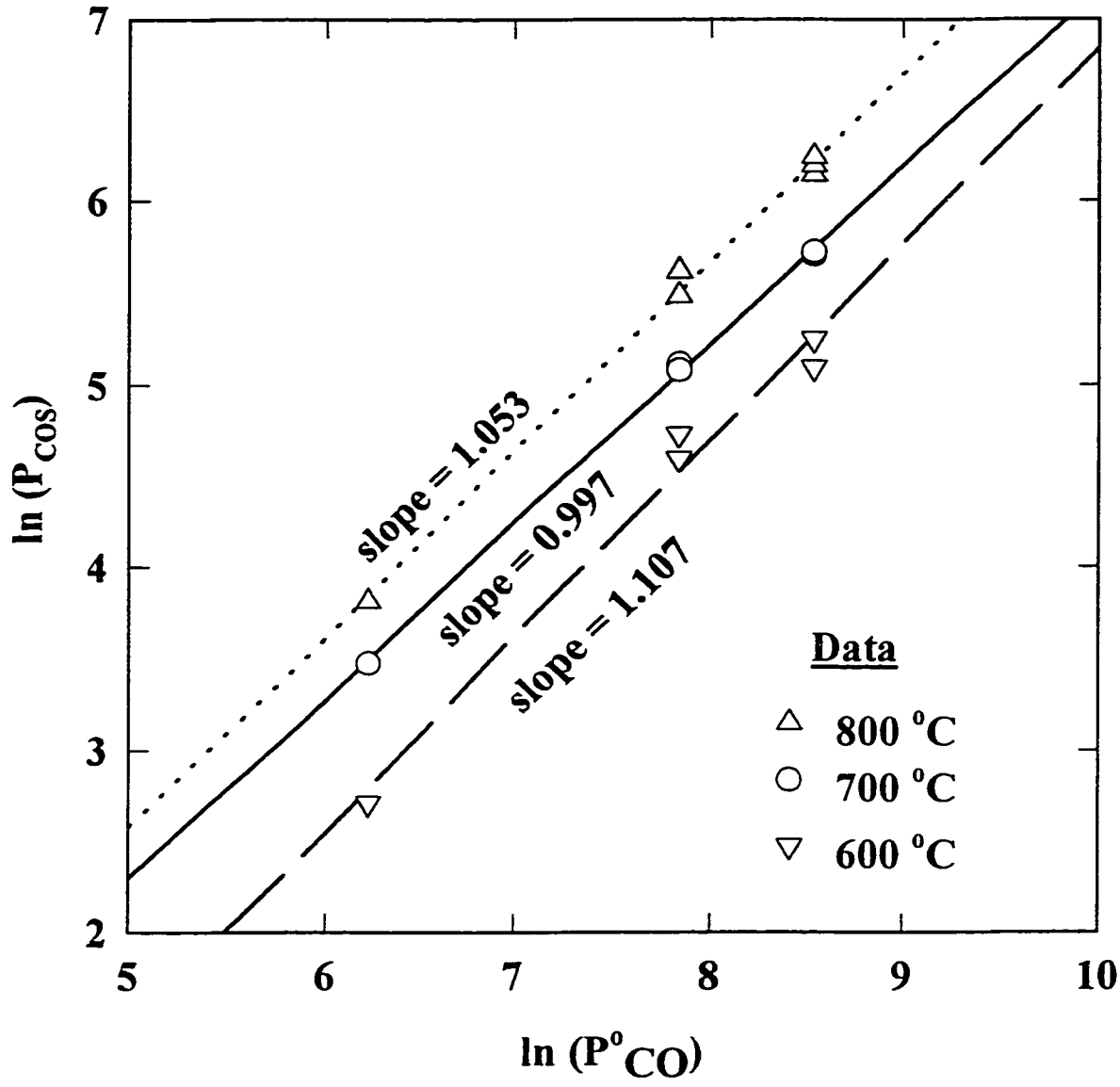

Figure 5.9 Order of dependency with respect to CO concentration for COS forming reaction.

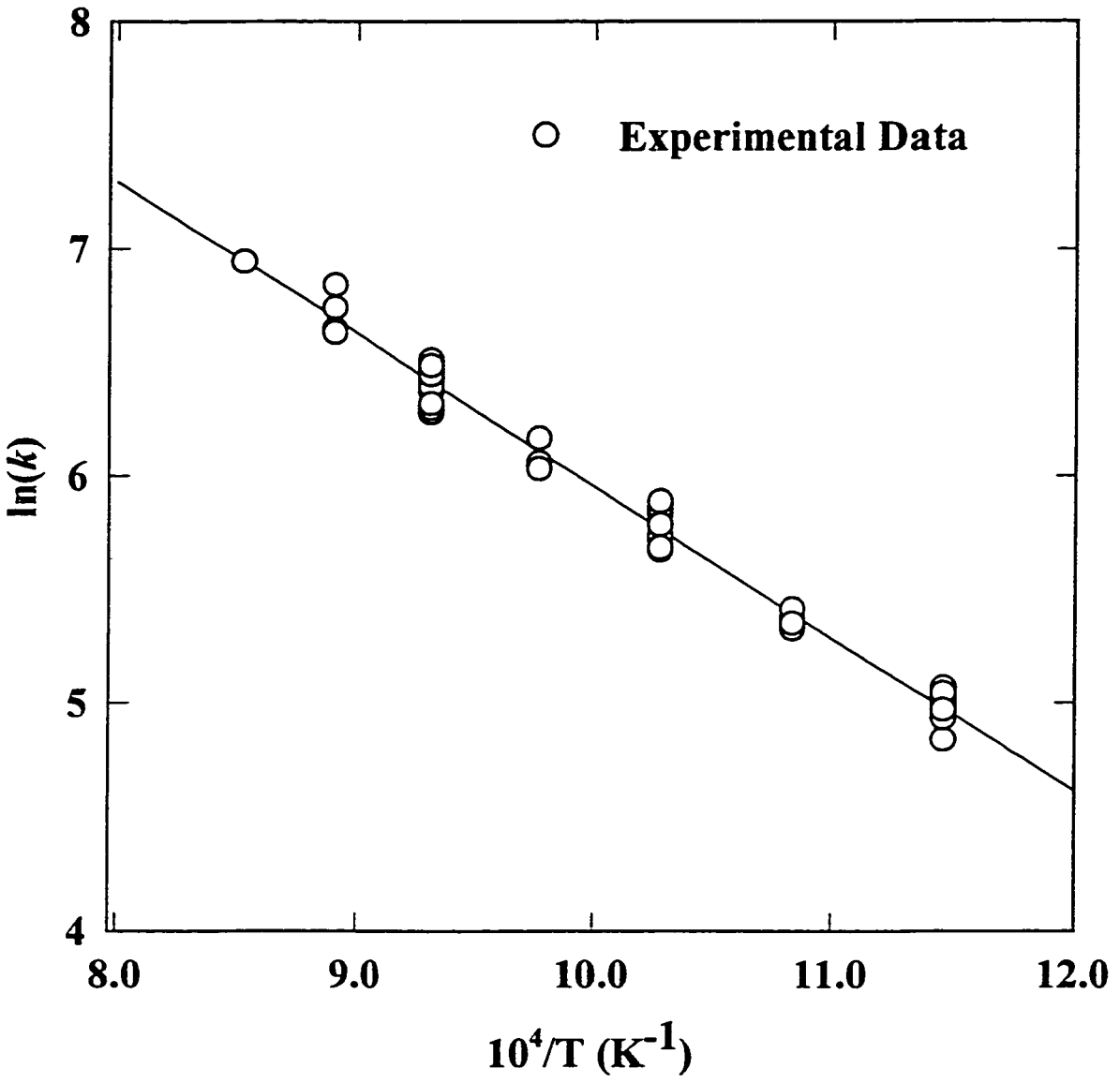

Figure 5.10 Arrnehius plot for the reaction rate constant (k_2) for the COS forming reaction between CO and S_2.

or with CO according to reactions (5.15) and (5.16) respectively. Association of two atoms or an atom and a diatomic molecule are known to proceed via rapid reactions (Benson, 1954 and Kondratev, 1955). Hence, it is expected that sulfur atoms produced from reaction (5.14) will react rapidly and, therefore, the rate-limiting step for the three reaction (5.14-5.16) mechanism is expected to be reaction (5.14). Using the steady state hypothesis for sulfur atom, it can be derived that the rate constant for COS forming reaction (5.14) will be one-half the observed rate constant (k_2), if reaction (5.16) dominates as the subsequent reaction, and equal to the observed rate constant (k_2), if reaction (5.15) dominates as the subsequent reaction. Since, CO concentrations are expected to be greater than two orders of magnitude than S atom concentrations, reaction (5.16) will dominate.

The reverse of reaction (5.14) has been studied recently by Oya et al. (1994) and Woiki et al. (1994) who reported activation energy of 23.8 and 37 kJ/mol respectively. Therefore, the activation energy of the forward reaction would be expected to be in the range of 140-160 kJ/mol (= ΔH_r° - Δn RT + E_r ~ 120+24 or 37 kJ/mol). However, the observed activation energy is approximately 40 percent of that expected. This suggests that the reaction possibly proceeds via the formation of reaction intermediates, which have a lower energy barrier, and possibly the actual reaction mechanism involves other reactions. Also, it is possible that the reaction in the reverse and the forward direction proceeds along different reaction pathways, which involve the formation of different reaction intermediates. For example, the reaction intermediate formed during the reverse reaction could be $[O{=}C{=}S{---}S]^{\#}$ while that formed during forward reaction could be $[O{=}C{---}S{=}S]^{\#}$. Clearly, the location of a single bond associated with the sulfur atom is different in the two postulated reactions intermediates; hence, the energy required to form or to break the relevant bond is expected to be different.

The low pre-exponential factor also needs some discussion. We calculated the pre-exponential or the frequency factor from the collision theory (Glasstone et al., 1938) to be of the order 10^{11} m^3 /kmol·s for the reaction

between S_2 and CO. The observed frequency factor is about 0.3×10^6 m^3/kmol·s, which implies that the steric factor is of the order 10^{-5} or 10^{-6}. This steric factor may seem to be an extremely low value. According to the statistical theory (Glasstone et al., 1938), the steric factor for a reaction involving two diatomic molecules to form a nonlinear complex is of 10^{-3}–10^{-6} and that for reaction between two diatomic molecules forming a linear complex is 10^{-4}–10^{-8}. Since, the observed steric factor lies in the range predicted by the statistical theory the low pre-exponential factor should not be considered to be an anomaly.

5.5 COS Cracking Reaction

5.5.1 Literature review

The COS decomposition is known to occur via two reaction routes, one leading to the formation of CO_2 and CS_2 and the other to the formation of CO and sulfur, according to the following reactions:

$$COS \leftrightharpoons CO_2 + CS_2 \qquad (5.17)$$

$$COS \leftrightharpoons CO + S \qquad (5.18)$$

Reaction 5.17 is favored at lower temperatures and reaction 5.18 at higher temperatures and short reaction times. The decomposition of COS has been studied for over one hundred year, and the reported studies can be classified either as low temperature equilibrium or as high temperature kinetic studies. Early studies (prior to 1950's) on COS decomposition were limited mainly to the determination of the equilibrium in a COS-CO-S_x system (Partington and Neville, 1951). In more recent years, studies have been directed towards kinetics of the high temperature (> 1200 C) decomposition of COS to CO and elemental sulfur.

Partington and Neville (1951) conducted experiments over a temperature range of 400-650 °C to investigate the equilibrium for the two reactions (5.17) and (5.18). They found that the CO_2 reaction could be catalyzed by silica but the CO reaction could not. Haas and Khalafalla (1973) were interested in catalytic conversions of COS. They tested various alumina and

silica catalysts over a temperature range of 400-775 °C. They observed that the main products of COS decomposition below 650 C were CO_2 and CS_2.

The pioneering work on high temperature COS decomposition reaction can be considered to be that of Hay and Belford (1967). They conducted the experiments with 0.5, 2.0 and 4.0 % COS in argon in shock tubes over a temperature range of 2000-3200 K. They proposed that the COS decomposition occurred via a second order rupture according to the reaction (5.19) which was followed by two bimolecular atom abstraction reactions, (5.20) and (5.21).

$$COS + M \xrightarrow{k_3} CO + S + M \qquad (5.19)$$

$$COS + S \xrightarrow{k_4} CO + S_2 \qquad (5.20)$$

$$COS + S \rightarrow CS + SO \qquad (5.21)$$

The secondary reaction 5.21 was found to be important only at temperatures exceeding 2500 C. They reported the reaction rate for reaction (5.19), based on the RRKM (Rice Ramsperger Kassel Marcus) theory and a critical activation energy of 299.15 kJ/mol as $k_3=1.11\times10^{11}$ $(T)^{1/2}[299.15\ (kJ/mol)/RT]^{1.87} \times \exp[-299.15\ (kJ/mol)/RT]$ $cm^3/mol\text{-}s$. One of the important observations in their study, which did not receive much attention was that the rate constants for 2 and 4% COS in Ar experiments were consistently higher than those obtained from 0.5 % COS experiments. Since the rates differed by a factor of only two for an eight fold increase in initial concentration, they argued that the important initiating step for COS decomposition was the collisional activation of COS by an Argon molecule (M).

Schecker and Wagner (1969) also studied the thermal dissociation of carbonyl sulfide in shock waves over a temperature range of 1500-3100 K and at pressure up to 320 atmospheres or 3.22×10^4 kPa. They demonstrated that the reaction mechanism shifted with the total pressure. The reaction proceeded bimolecularly at low pressures according to the reaction (5.19) and

unimolecularly at high pressures according to the reaction (5.18). They determined the rate constant for the bimolecular reaction (5.19) as $k_{30}=10^{11.2}\exp(-30700/T)$ m^3/kmol-s. The unimolecular reaction rate constant at high-pressure limit was calculated to be $k_{3\infty}=10^{11.6}\exp(-34220/T)$ s^{-1}. The primary aim of their study was to find out whether the thermal decomposition of COS proceeded via a "spin forbidden path" and whether the apparent energy barrier was equal to the known ΔH_0° value. They showed that the COS dissociation takes place via energetically favorable reaction path;

$$COS + M \rightarrow CO\ (^1\Sigma) + S\ (^3P) + M \qquad \Delta H_0^\circ = 299.15\ kJ/mol \quad (5.22)$$

where, M is an inert molecule that acts as an energy transfer agent. The apparent activation energy for reaction 5.22 is 255.2 kJ/mol and the energy barrier is 301.25 kcal/mol.

Chenery et al. (1983) studied the vibrational analysis of CO, the product of thermal decomposition of COS in a shock tube. They assumed the reaction to proceed according to reaction (5.19). Their study was conducted over a temperature range of 2400-3500 K. Their reported experimental activation energy of 246.62±12.54 kJ/mol compares well with 255.2 kJ/mol value reported by Scheker and Wagner (1969).

In a recent work, Woiki and Roth (1992) directly measured the $S(^3P)$ atom concentration with time to determine the kinetics of thermal decomposition of carbonyl sulfide behind reflected shock waves. The experiments were conducted in a temperature range of 1750-2990 K at total pressures between 0.5 and 1.5 bar. The initial concentrations of COS in Ar were between 4 and 100 ppm. They determined the COS decomposition kinetics using the method of initial slopes. They report that the slope of the measured $S(^3P)$ atom profile was due to reaction (5.22) for experiments with low initial COS concentration (4-30 ppm). For higher initial concentrations of 100 ppm, they found that $S(^3P)$ atom profile was affected by a secondary sulfur consuming reaction, probably via reaction (5.20). They reported the reaction kinetics for reaction (5.19) to be $k_3 = 2.90 \times 10^{11} \times \exp$ [-32000 K/T] m^3/kmol-s. In a subsequent work, their group (Woiki et al., 1993)

reported the reaction rate constant (k_4) of flash photolysis reaction (5.20) as $6.0 \times 10^{10} \times \exp [-4560K/T]$ $m^3/kmol{\cdot}s$.

Oya et al. (1994) have determined the rate constants for reaction (5.19) as well as the consecutive reaction (5.20). The first reaction (5.19) was studied for 1% COS in Ar over a temperature range of 1900-3230 K and at total pressures between 27 and 123 kPa. The COS concentration was monitored by IR emissions. The kinetics of the secondary reaction between COS and S were determined from separate experiments in which the S atom were generated by laser photolysis of COS and the time dependent S (^3P) concentration was monitored by Atomic Resonance Absorption Spectrometry. These experiments were conducted with low COS concentrations (130-520 ppm in Ar) at total pressures between 124 and 232 kPa over a temperature range of 1140-1680 K. They reported the reaction rate constants as $k_3 = (2.45 \pm 1.10) \times 10^{11} \times \exp [(-257 \pm 24$ kJ/mol)/RT] m^3/kmol-s and $k_4 = (2.35 \pm 0.71) \times 10^{10} \times \exp [(-28.3 \pm 0.9$ kJ/mol)/RT] m^3/kmol-s. The activation energy of 257 kJ/mol for reaction (5.19) obtained by Oya et al. (1994) is in good agreement with Schecker and Wagner's (1969) value of 255 kJ/mol and Woiki and Roth's (1992) value of 266 kJ/mol. The activation energy of 28.3 kJ/mol for reaction (5.20) obtained by Oya's group is somewhat lower than the value of 37.9 kJ/mol found by Woiki's group (Woiki et al., 1993).

From the survey of literature it may be concluded that reaction kinetics studies on the COS decomposition reactions have been studied mainly at high temperatures (> 1500 K). There is little experimental data on the COS decomposition at temperatures encountered in the front-end units of the Claus plants, i.e. over 1000-1525 K. Therefore, an experimental study was conducted to obtain kinetic data under Claus front-end unit conditions.

5.5.2 Experimental

Experiments were conducted in empty tubular reactors over a temperature range of 800-1100 °C. A majority of the reactions was performed with diluted gas

mixture of composition, 2.33 mol % COS in nitrogen. This gas mixture was obtained from Matheson, Canada. To study the effect of COS concentration on the decomposition reaction, COS concentrations were varied from 0.2 to 2.33 mol %. These gas mixtures were prepared by diluting 25.0 mol % COS in N_2 (Matheson) with ultra high purity nitrogen.

5.5.2.1 COS conversion as a function of temperature.

The experimentally measured COS conversion as a function of temperature is presented in Figure 5.11 These data were collected from experimental runs in the 16 m reactor with feed gas of 2.33 mol% COS in N_2. The effective residence time was in the range of 0.88 to 1.15 seconds. The higher residence time corresponds to the lower temperature and vice versa. The equilibrium conversion for COS has been plotted in Figure 5.11. Since the partial pressure of COS in feed is low, the equilibrium conversion of COS is high (> 80 %) even at 800 °C. Under these dilute conditions the COS decomposition can, thus, be considered essentially to be irreversible. From Figure 5.11, it can be seen that the reaction rate increases rapidly with temperature and above 950 °C, the COS conversion equal to or greater than 90% of equilibrium conversion is reached in less than 1.2 seconds.

5.5.2.2 Effect of initial concentration on COS conversion.

The initial concentration of COS was varied greater than ten folds from 0.20 mol% to 2.33 mol %. The data of these experimental runs have been plotted in Figure 5.12. It can be seen from Figure 5.12 that the COS conversion increases steadily with the initial COS concentration. For a first order or a pseudo-first order reaction, the conversion is independent of the initial concentration of the reactant provided the temperature and the reaction time is held constant. The data presented in Figure 5.12 conclusively show that at conditions used in our experiments that overall rate of COS decomposition is not first order with respect to COS concentration.

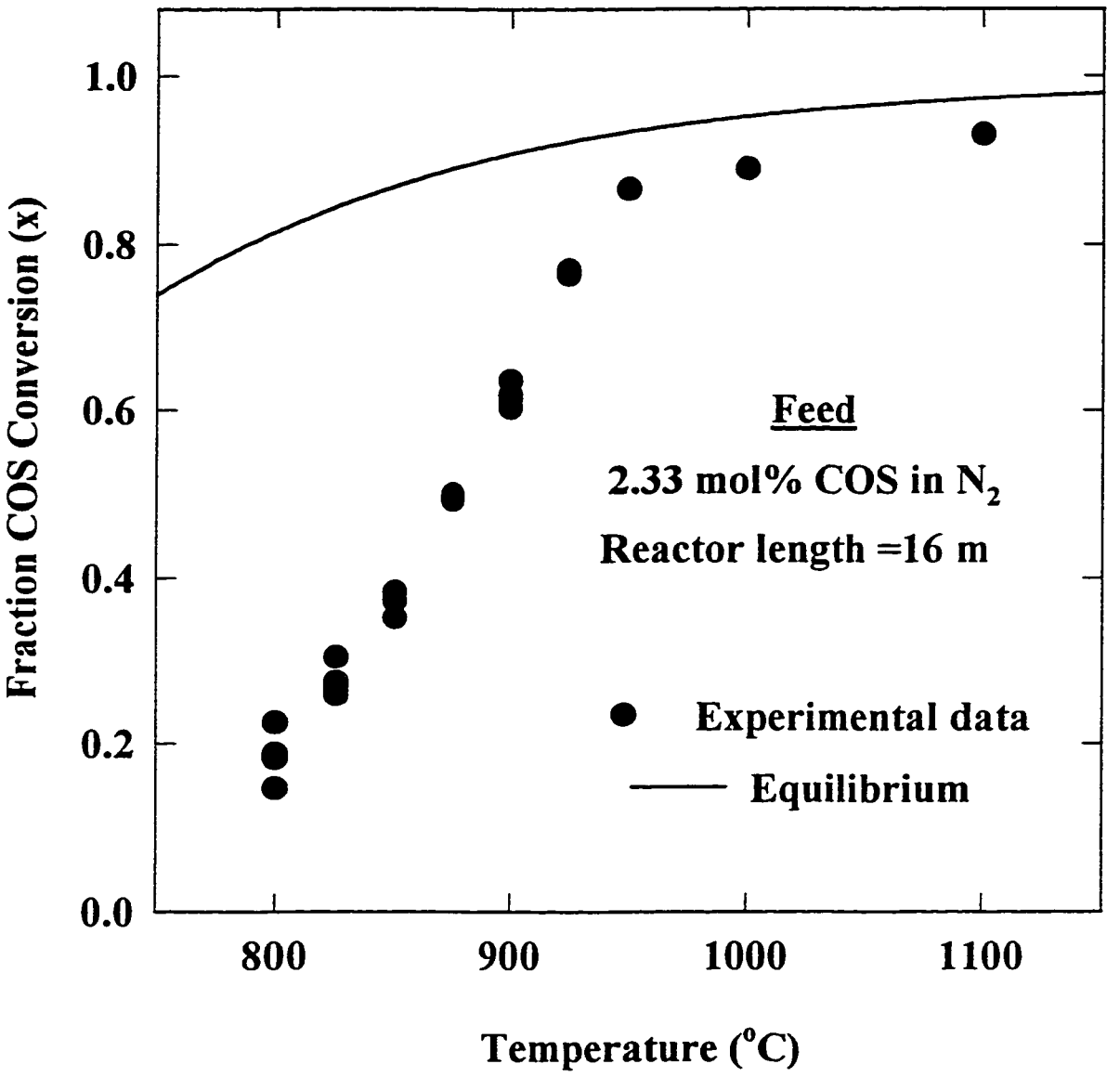

Figure 5.11 Experimental COS Conversion as a function of temperature.

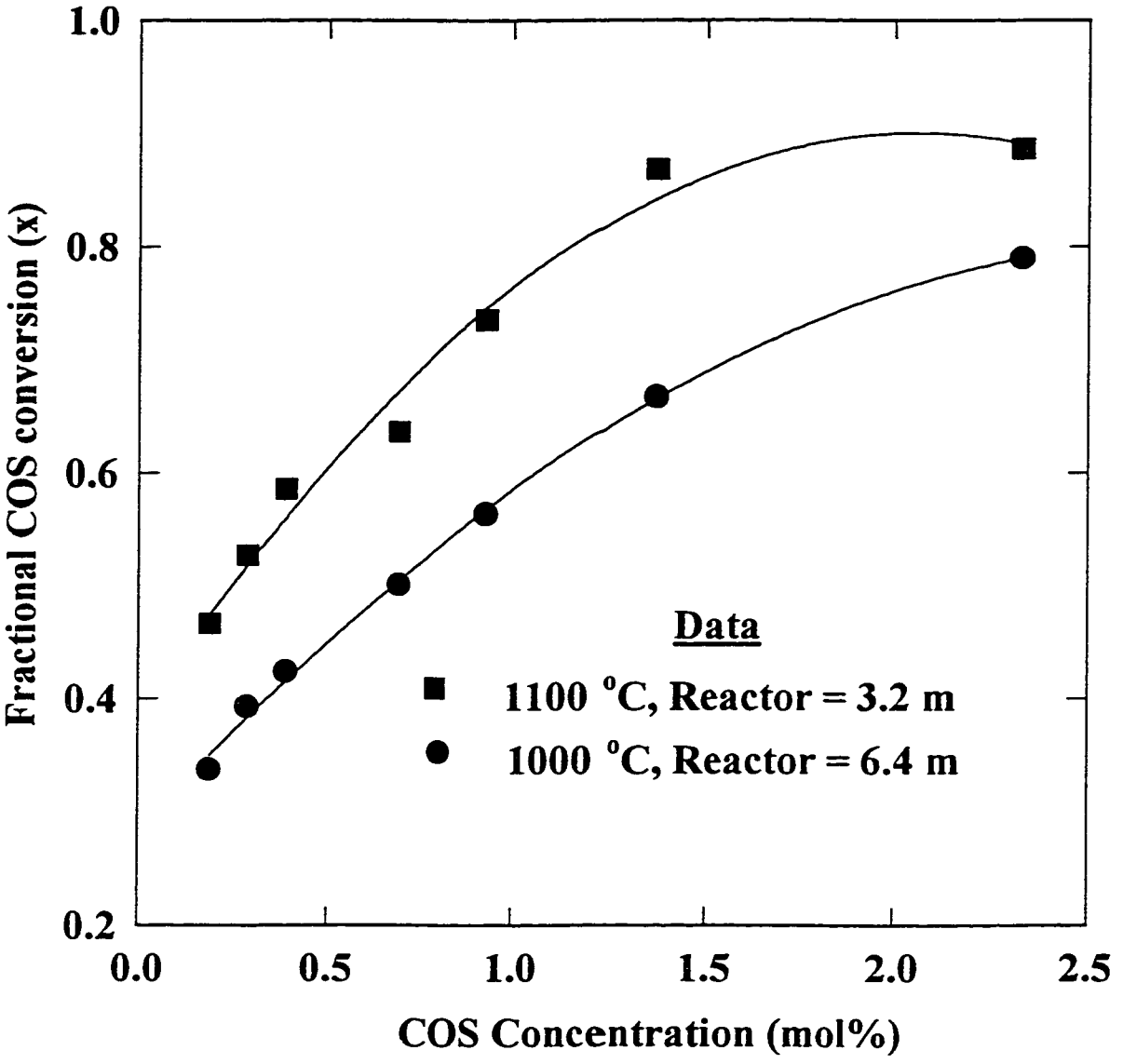

Figure 5.12. Effect of initial COS concentration on COS conversion.

[Lines are simply trendlines]

5.5.2.3 Surface effects

The estimates of COS conversions obtained from the calculations based on extrapolation of published rate constants for reaction 5.19 at the temperatures employed in this study showed minimal conversions for the residence time in our reactors. Since the observed COS conversions were significantly higher, it was suspected that the reaction was catalyzed by the quartz reactors. To study the catalytic/wall effects, experiments were conducted in an empty and quartz wool packed tubular reactors. A new reactor was fabricated for this purpose. The reactor was L-shaped, 10 mm inside diameter and approximately 1.0 m long The results of these experiments are reported in Table 5.4. From the results of these experiments, it can be seen that there is a significant increase in COS conversions when a reactor is packed with quartz wool. It must be mentioned that the packing covered one-third the length of reactor and the effective porosity in the packed length of the reactor was estimated to be less than 40 per cent. The quartz wool has an enormous surface area, the estimated increase in surface area is of the order of 10^3 to 10^4 compared to the empty tubular reactor. If we consider, that the reaction is catalyzed and occurs completely at the surface, we can estimate the contribution of the heterogeneous reaction towards the COS conversion according to the following relationship used by Tesner (1990):

Degree of heterogeneity =

$$[\ X_{COS}\ ]_{packed} \times 100 \,/\, \{[X_{COS}]_{empty} \times \text{Increase in surface area}\} \quad (5.23)$$

The degree of heterogeneity calculated from the above expression is presented in Table 5.4. The numbers indicate that under our experimental conditions the majority of reaction occurs in the gas phase with the contribution of heterogeneous reaction estimated to be less that 2-3 percent. However, the exact cause of the difference in conversions observed from the packed and empty reactors cannot be determined. A number of possible reasons may exist

Table 5.4 Experimental results on COS decomposition experiments to study the catalytic/wall effects

	COS CONVERSIONS		
TEMPERATURE (°C)	PACKED REACTOR	UNPACKED REACTOR	DEGREE OF HETEROGENEITY (%)
900	0.14	0.03	0.5
1000	0.28	0.07	0.4
1050	0.84	0.56	0.15

for the difference. The reactor used for studying the catalytic/wall effect was not characterized. Therefore, it is difficult to conclusively state that the increase in conversion observed for COS decomposition is totally due to catalytic effect. For example, the packing may significantly affect the hydrodynamics and also the temperature profile of the gas. The glass wool which is at furnace temperature and has a thermal mass much greater than the flowing gas may act as a very effective heat transfer agent. Thus the effective gas temperatures in packed reactors may be greater than that in empty reactor. Another possible reason for the enhanced COS conversion in packed reactor could be an increased collision with quartz surface which acted as an effective energy transfer partner.

Due to the lack of any conclusive evidence, for the present study it will be assumed that the although the COS decomposition reaction may proceed via both heterogeneous and homogeneous reaction pathways, for the reactors used in the study and under the experimental conditions the major contributing reaction is homogeneous.

5.5.3 Kinetic model

It may be recalled that in the published literature, the development of the kinetic model for COS decomposition have been based on two reactions (5.18) and (5.19). Since the reaction rate of the subsequent reaction is fast it is assumed that any sulfur produced via reaction (5.18) is rapidly consumed according to reaction (5.19). On applying the steady state assumption for sulfur atom, it can be derived that:

$$[S]_{SS} / [M] = k_1 / k_2 \qquad (5.24)$$

where $[S]_{ss}$ represents the steady state concentrations of S and [M] is the concentration of the inert molecule acting as an energy transfer agent.

Since, the RHS of equation (5.24) is a function of temperature only, the steady state concentration of sulfur atom ($[S]_{SS}$) should also be solely a function of temperature. However, the experimental results of Woiki and Roth (1992) showed that the steady state concentration for S atom was dependent on initial

COS concentration for lower temperatures (<2200 K) and higher initial concentrations (>15 ppm). In fact, it was found that the ratio of $[S]_{ss}/[M]$ for various initial concentration of COS approximately obeyed the relationship: $[S]_{ss} / [M] \propto ([COS]_o / [M])^{1/2}$.

This may be explained from the fact that the final sulfur atom concentration was in equilibrium with S_2 molecule. The final concentration of S_2 obtained at complete conversion of COS can be approximated as half of the initial concentration of COS.

Now, since the variation of the steady state sulfur atom concentration with the initial concentration of COS cannot be explained with a two reaction mechanism such as those discussed earlier, it may be indicative of the occurrence of another side reaction. It is possible that the following sulfur reaction may occur:

$$S_2 + M \leftrightharpoons S + S + M \qquad (5.25)$$

This reaction may be used to explain the variation of steady state sulfur atom concentration with change in the initial COS concentration.

The experimental results in this study shows that the COS conversions are affected by the initial COS conversion. This behavior may be partially explained by the occurrence of the bimolecular reaction between two COS molecules, which was alluded but discounted by Hay and Belford (1967). The reaction may be written as:

$$COS + SCO \leftrightharpoons S_2 + 2CO \qquad \Delta H_r^\circ = 179.9 \text{ kJ/mol} \qquad (5.26)$$

The experimental data of this study were modeled assuming the occurrence of reaction 5.19, 5.20 and 5.26. The rate of consumption of COS can be written as:

$$(-r_{COS}) = 2k_3 C_M C_{COS} + k_4 C_{COS}^2 \qquad (5.27)$$

where, k_3 is the rate constant for the forward reaction 5.19 and k_4, the rate constant for forward reaction 5.26 and C_M, the concentration of the energy transfer molecule (nitrogen in this case). In this study all the molecules were

considered to be an equally effective energy transfer agent and therefore C_M was essentially calculated as the total concentration of all the molecules in the gas mixture. The factor 2 in the first term of the right hand side of equation 5.27 is due to the fact that for every sulfur atom produced via reaction 5.19, a COS molecule is rapidly consumed via reaction 5.20. Therefore, effectively for every molecule of COS decomposed by reaction 5.19, the net effect is consumption of two molecules of COS.

5.5.4 Estimation of parameters

The reaction rate constants k_3 and k_4 were determined by minimizing the objective function X^2, where X^2 is defined as $\sum (x_{expt} - x_{model})^2/\sigma$. The data points corresponding to conversions less than 75 percent of equilibrium conversions were only selected for regression of data. The weight factors for all data points were kept one. The function was minimized using the Levenberg-Marquardt method. The results of the analyses are presented in Table 5.5.

5.5.4.1 Comparison of the predictions with data

The COS conversions were predicted from the integrated form of equation 5.27 and using the regressed parameters. The predictions are compared with the experimental data in Figures 5.13 and 5.14. In Figure 5.13, the predictions are compared with experimental data obtained from the longest reactor 16.0 m long over a temperature range of 800-950 C for two initial COS concentration. The model predictions compare well with the data for initial COS concentration of 2.33 mol%, however, they are significantly lower than the experimental data for initial COS concentration of 0.20 mol%. In Figure 5.14, the effect of initial COS concentration on COS concentration is observed. For the given set of data at 1100 °C, the model significantly over-predicts the COS conversions for lower initial COS conversions and under-predicts COS conversions for higher initial COS concentrations. The model predictions are in reasonably good agreement with the whole range of data obtained at 1000 C.

Table 5.5 Results of parameter estimation for COS decomposition reactions

Data points (n)	53
Number of parameters (n_p) optimized at a time	2
A_3 m^3 /kmol-s	7.67×10^{11}
Ea_3 (kJ/mol)	251.24
A_5 m^3 /kmol-s	1.71×10^{11}
Ea_5 (kJ/mol)	181.10
$\sqrt{\sum(x_{expt} - x_{calc})^2/(n-n_p)}$	0.066

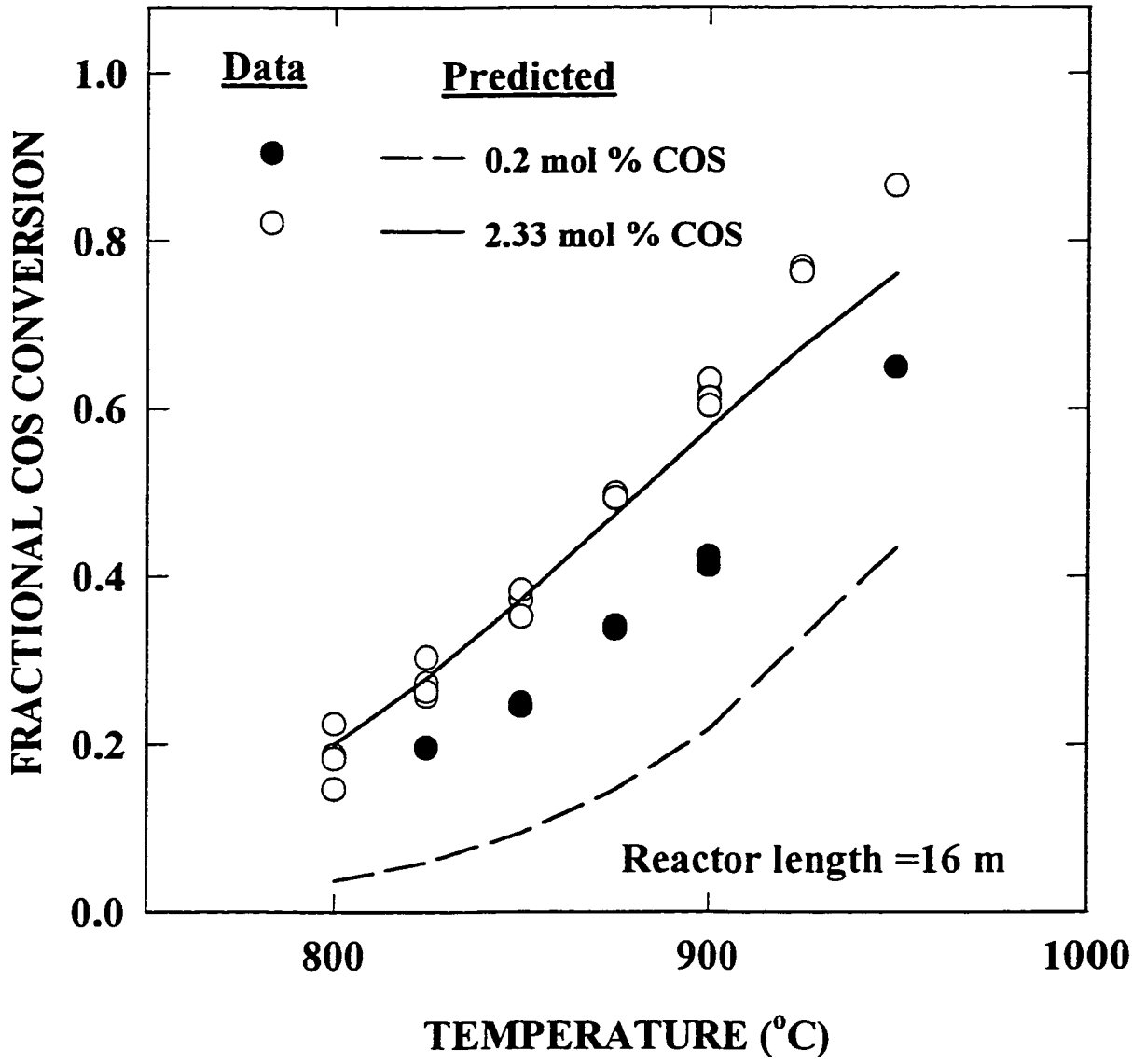

Figure 5.13 Comparison of predicted and measured COS conversions as a function of temperature for two different initial concentrations of COS.

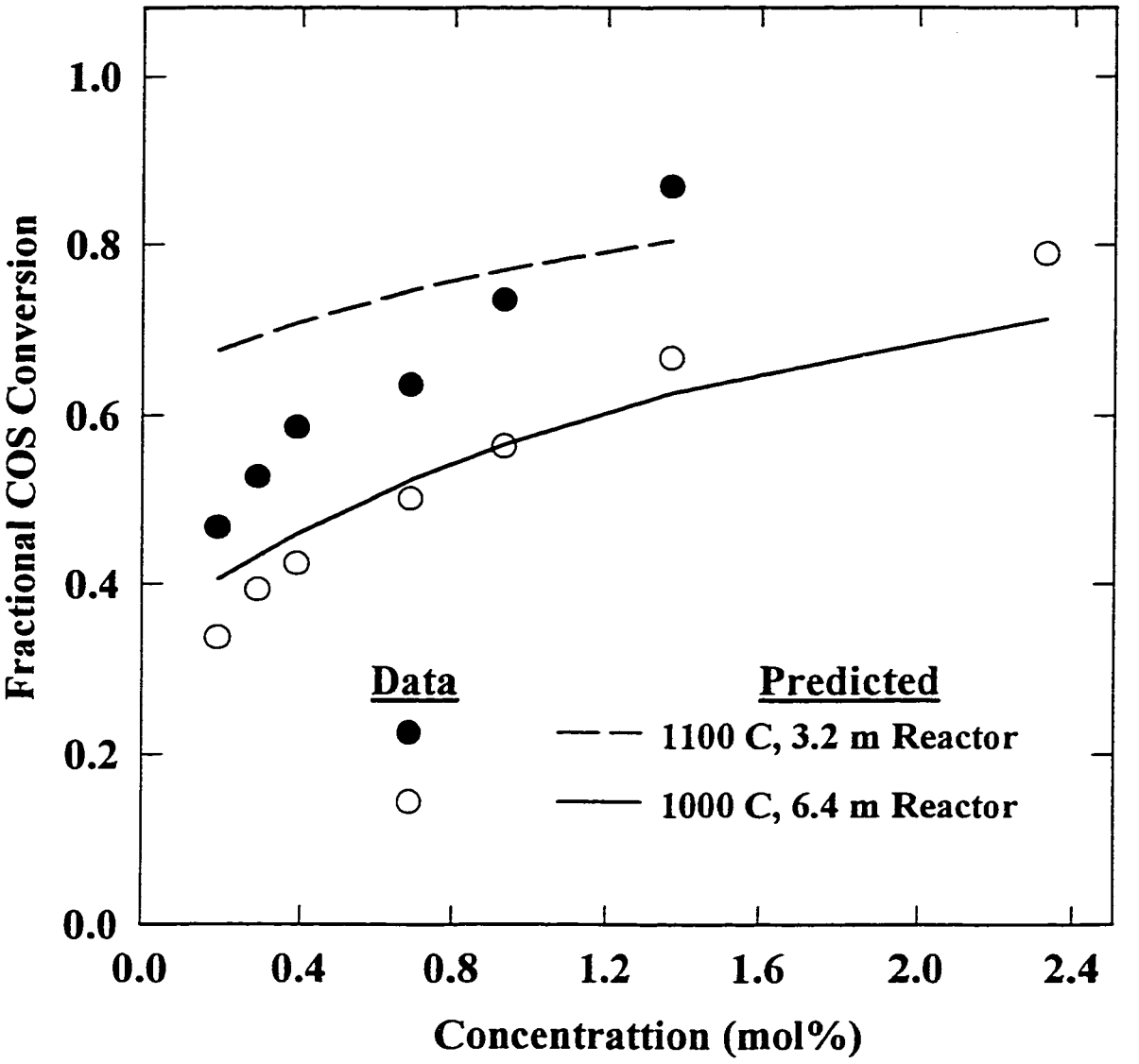

Figure 5.14 Comparison of predicted and measured COS conversions as a function of initial COS concentrations for two reactors at two different temperatures.

From the above mentioned results, it is observed that the model exhibits a strong concentration dependence for longer residence times at temperatures lower than 1000 C. At shorter residence times and higher temperatures (1100 C), the model shows lesser concentration dependence. At higher initial concentrations (1.4-2.33 mol% COS), however, the model performs well over the complete range of temperature tested.

5.5.4.2 Comparison of the rate constant

The rate constant for reaction 5.19 or the initial step in COS decomposition obtained in this study is compared with the literature values. The activation energy of 251 kJ/mol may be comparable to the 255, 257 and 266 kJ/mol values by Schecker and Wagner (1969), Oya et al. (1991) and Woiki and Roth (1992, respectively. The reported rate constants are also presented as Arrhenius plots in Figure 5.15 and compared with the rate constant obtained from this study.

The rate constant for reaction 5.26 has not been reported in literature and, therefore, the value obtained in this study could not be compared with any published work. The activation energy of 181 kJ/mol compares well with the heat of reaction of 179 kJ/mol suggesting zero energy barriers for the termolecular reaction between two CO molecules and a S_2 molecule.

5.5.5 Summary

The data show that COS decomposition is very rapid at higher temperatures. At temperatures greater than 1100 C, it is expected that COS will rapidly dissociate to reach equilibrium conversions. This implies that the higher than equilibrium levels of COS observed at the front-end of Claus plant, i.e. in the waste heat boiler exit is not as a result of slow COS consuming reactions in the furnace. The assumption being that COS is formed rapidly but not consumed fast enough and therefore, a higher than equilibrium level COS is observed.

The kinetic model for COS decomposition is not adequate to represent the complete set of experimental data obtained in this study. Further work needs to be done to clarify a number of issue, on the occurrence of other COS consuming reactions and their associated kinetics as well as the heterogeneity of

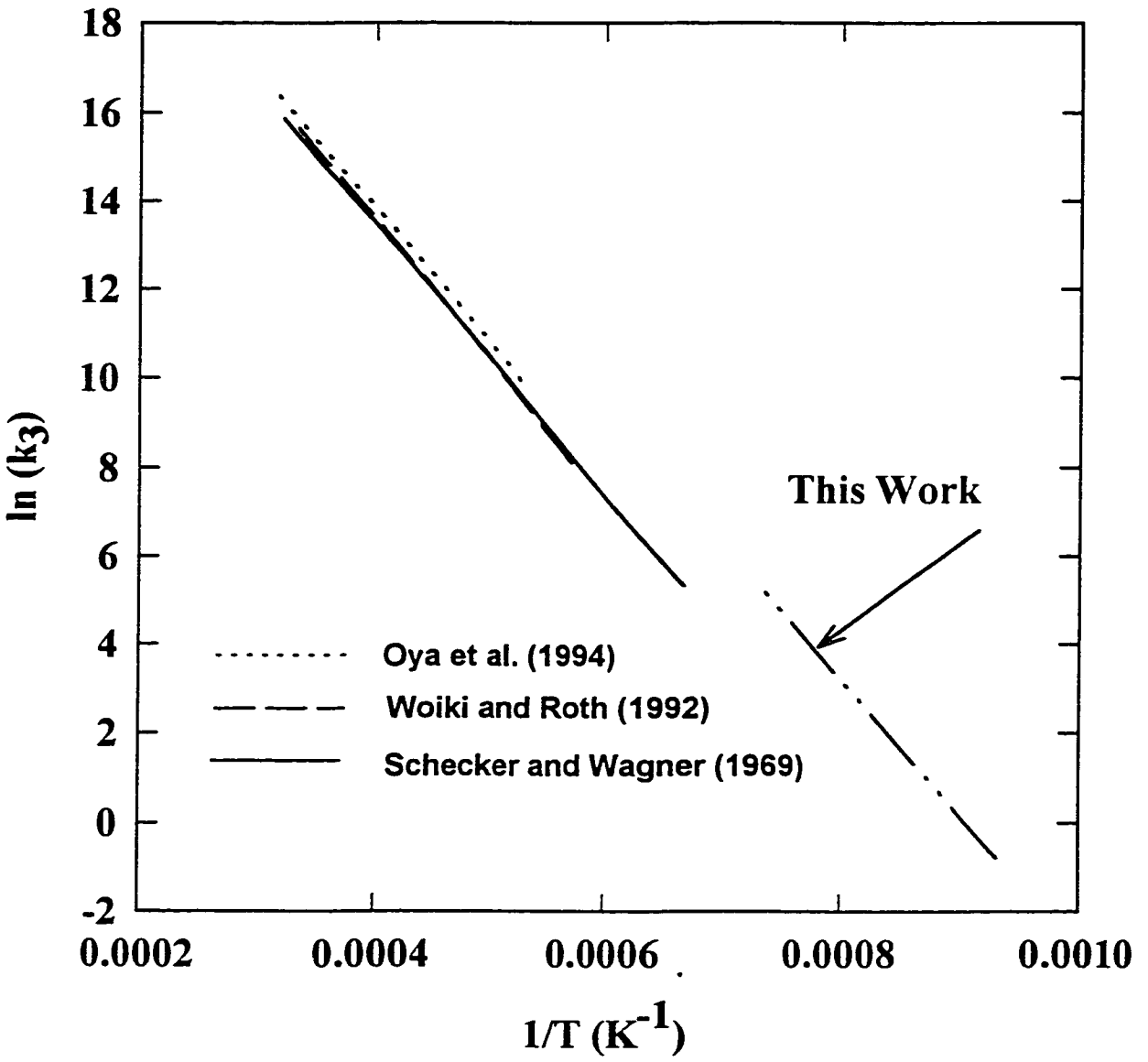

Figure 5.15 Comparison of published rate constant for for COS decomposition reaction.
(k_3 in m^3 $kmol^{-1}$ s^{-1})

the COS decomposition reaction. However, the kinetic modeling done in this thesis may be considered to be good as a first approximation.

5.6 Reaction between CO_2 and H_2S

5.6.1 Literature review

It is not uncommon to find references in the literature that attribute the COS formation in a Claus reaction furnace to the reaction between CO_2 and H_2S [Hyne and Goar, 1996, Chiari et al., 1997]:

$$CO_2 + H_2S \rightleftharpoons COS + H_2O \qquad (5.28)$$

However, there is no direct experimental evidence in the literature to prove or to disprove the occurrence of reaction (5.28). In a recent experimental study on CO_2 and H_2S mixtures at high temperatures, Towler and Lynn (1993) attempted to explain the COS observed in their experiments via the reaction between CO and sulfur and that due to reaction (5.28). They conducted a flow reactor study with mixtures of 5% and 10% H_2S with the balance made up of CO_2 at two temperatures of 900 and 950 °C. The gas residence time in their reactor was in the range 5-10 seconds. In their experiments, they observed a significant amount of CO but very low levels of COS. They were able to predict CO concentration assuming that the water gas shift reaction was at equilibrium. No conclusive reaction pathway for COS formation could be deduced from the simulation and experimental studies.

In the current study, experiments were conducted with dilute CO_2 and H_2S mixture to obtain information on the formation of COS formation via reaction 5.28

5.6.2 Experimental

5.6.2.1 Experimental conditions

The experiments were carried by reacting 1.0 mol% CO_2 with 1.0 mol% H_2S, where both reactant streams were diluted with ultra-high purity nitrogen. The gas flow rate was maintained at 4.0 ± 0.1 L/min. Experiments were carried in two quartz reactors of lengths 6.4 m and 16.0m over a temperature range of 800-1200 C. The inlet pressure in the experiments varied over the range 120-160 kPa.

5.6.2.2 COS Formation

The concentration of COS measured at the exit of reactor for various reactor temperatures are presented in Figure 5.16. The results in the Figure represent data from two quartz reactors. However, owing to the overlap of the two sets of data, it is difficult to discern the difference. It can be observed from Figure 5.16 that the amount of COS produced from the reacting mixture was almost negligible. The COS formed increased slightly with the temperature but remained far below the equilibrium concentrations, which decreased with increasing temperature. The maximum yield of COS (i.e. moles COS / moles of CO_2 in the feed) was less than 0.3 percent.

5.6.2.3 H_2S Conversion in the Presence of CO_2

H_2S conversions measured from the experiments conducted in the two quartz reactors of length 6.4 m and 16.0 m for the feed mixtures of (1.0 mol% CO_2+ 1.0 mol% H_2S) in N_2, and 1.0 mol % H_2S in N_2 are presented in Figure 5.17. The predicted equilibrium H_2S conversions for the two feed mixtures are also presented. The H_2S conversion here is calculated as the amount of H_2S consumed divided by the amount of H_2S in the initial mixture. The equilibrium H_2S conversions for (H_2S+CO_2) mixtures are greater than that for H_2S in N_2 for all temperatures.

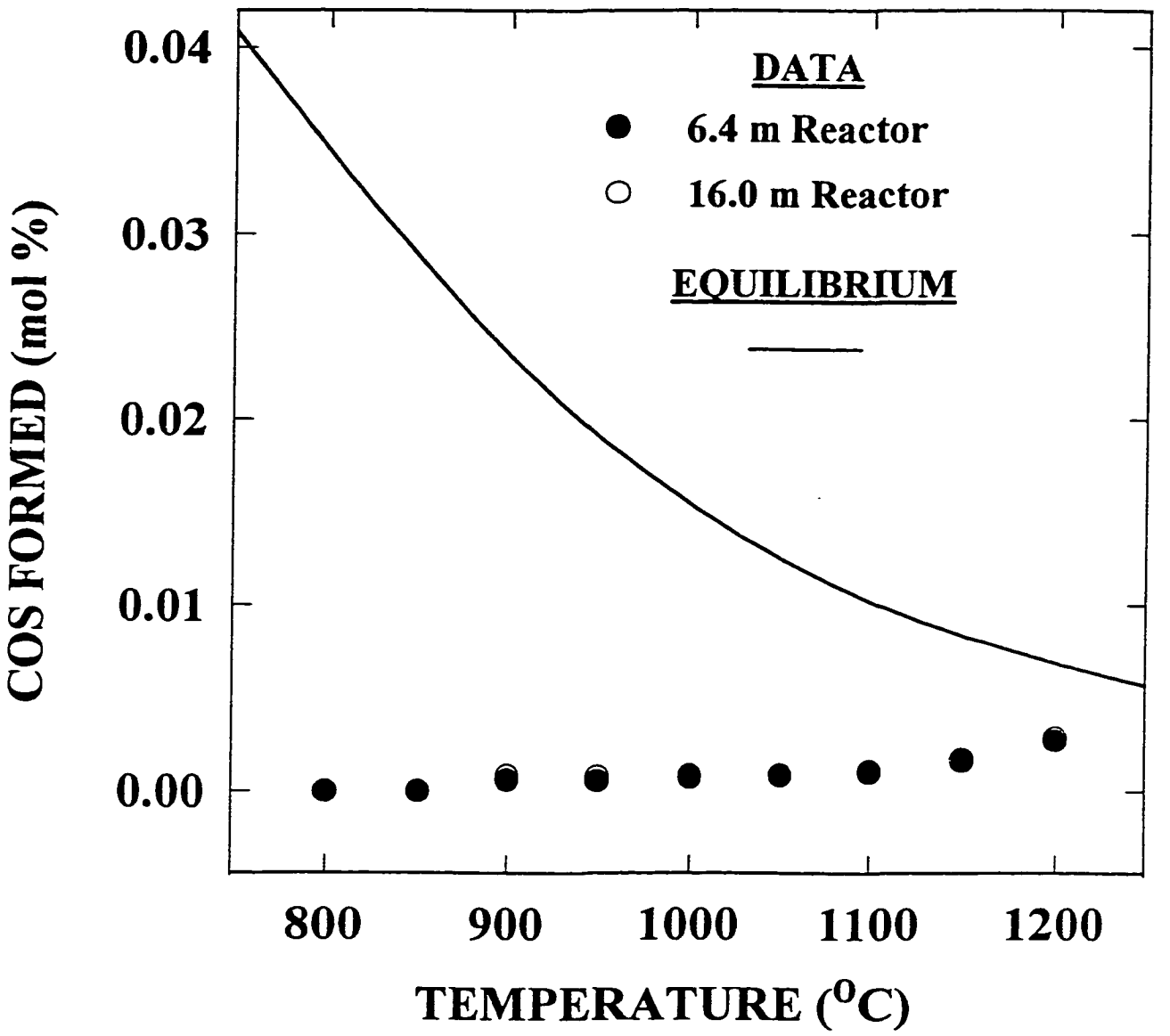

Figure 5.16 COS produced from two quartz reactors from a feed mixture of 1.0 mol % CO_2 and 1.0 mol % H_2S.

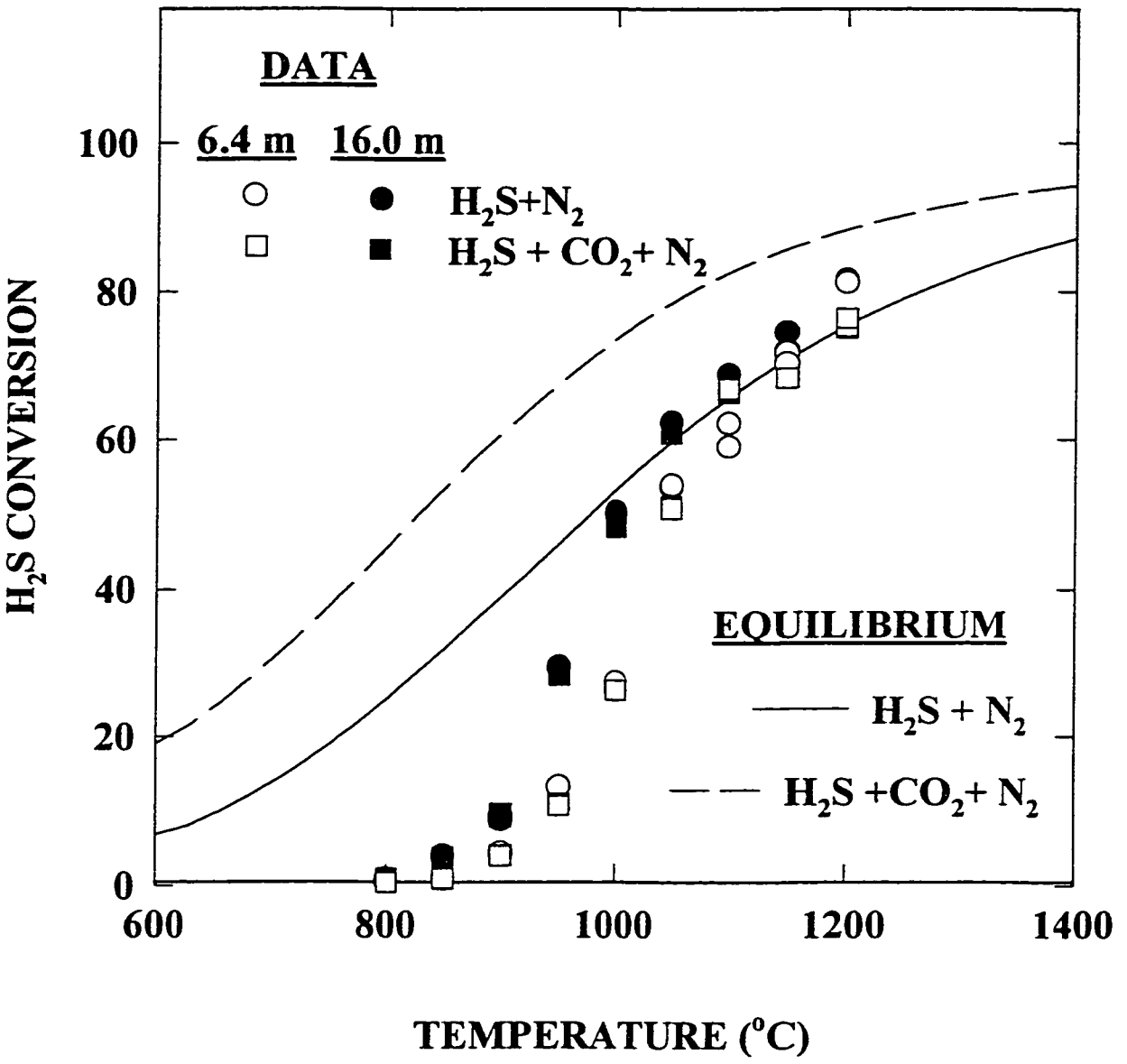

Figure 5.17 H_2S conversions for two feed mixtures from two reactors.

Mixtures: 1.0 mol% H_2S + 1.0 mol% CO_2 in N_2
1.0 mol% H_2S in N_2.

The experimental data show that the hydrogen sulfide conversions in (H_2S+CO_2) mixtures increase rapidly with temperature and attain conversions close to the equilibrium conversion for H_2S in nitrogen. The hydrogen sulfide conversions from the two mixtures for a fixed residence time and temperature do not differ significantly with each other which implies that the H_2S decomposition reaction in the presence of the reacting components, CO and CO_2, is not affected significantly by side reactions.

5.6.2.4 CO formation from (CO_2 + H_2S) feed

In the experiments with CO_2 and H_2S mixtures, significant amounts of CO were observed at temperatures exceeding 1000 °C. The experimentally measured and equilibrium predicted CO yields from (CO_2+H_2S) feed are presented in Figure 5.18. The yield is calculated as the moles of CO produced divided by the moles of CO_2 in the feed. The equilibrium CO yield increases from over 20 percent at 800 °C to about 60 percent at 1200 °C. The experimental CO yields for actual gas residence times of 0.5-0.75 s and 1.2-2.0 s in the 6.4 m and 16.0 m reactors, respectively, are significantly lower than the equilibrium yields for the complete range of temperatures investigated. At temperatures below 1050 °C, the measured CO yields are less than 5 percent, but increase rapidly with temperature attaining values over 12 and 25 percent in 6.4 m and 16.0 m long reactors, respectively.

5.6.3 Kinetic modeling

5.6.3.1 Reaction mechanism

COS Formation

In view of the experimental finding that the direct reaction between CO_2 and H_2S contributes little to the formation of COS, the mechanism of the formation of COS is not being discussed here. It may be that the small amount of COS observed at

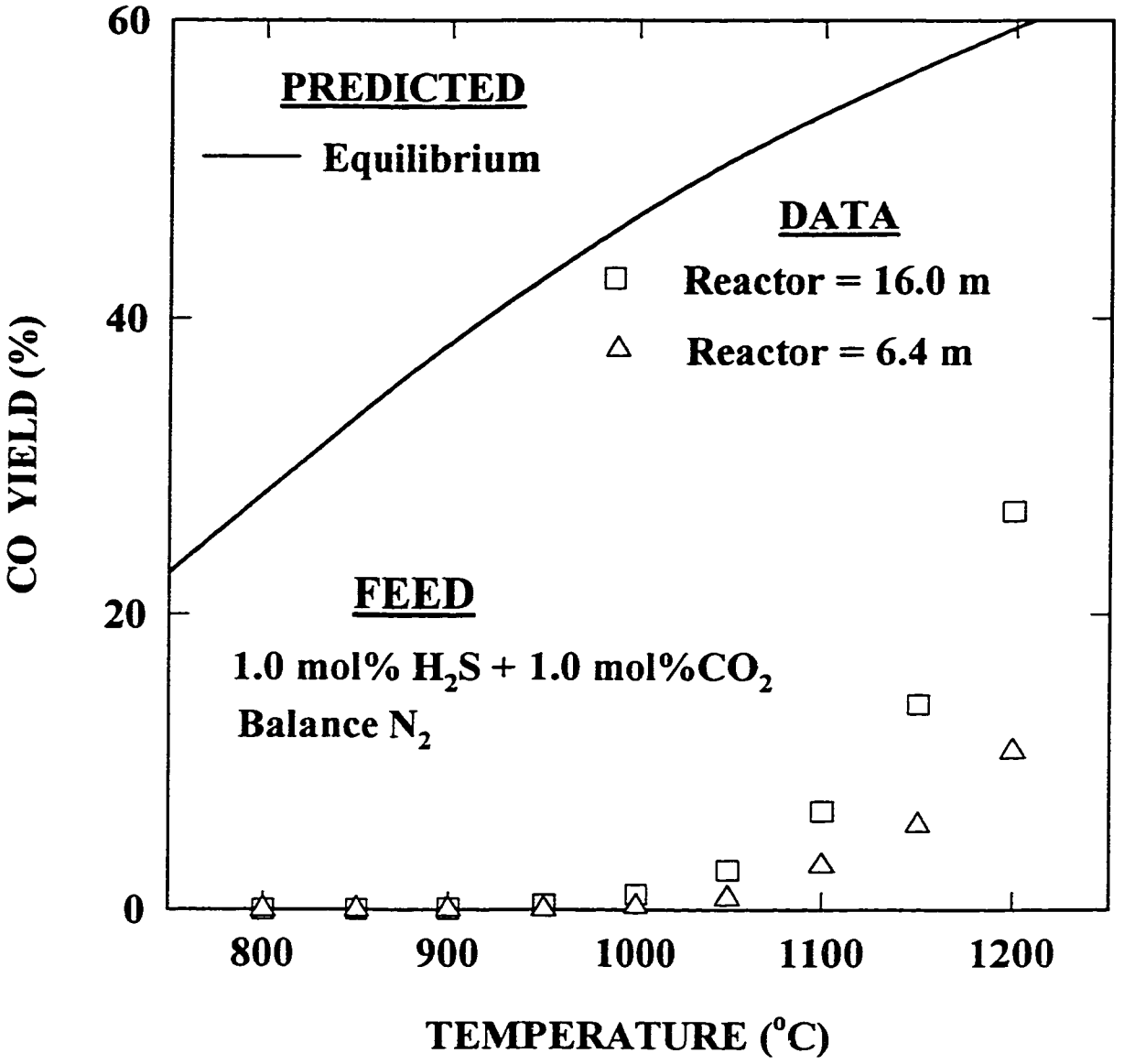

Figure 5.18 Experimentally measured CO concentrations at the reactor exit as a function of temperature.

higher temperatures (> 1050 °C) is probably produced from the reaction of CO with sulfur or hydrogen sulfide.

H_2S Consumption

The consumption rates of H_2S in (CO_2+H_2S) mixture in nitrogen and that in H_2S in N_2 are similar for a fixed residence time. Therefore, under such conditions, it may be considered that the consumption of H_2S in (CO_2+H_2S) mixtures proceeds independently of the other side reactions. The H_2S decomposition mechanism may be similar to that discussed in section 5.3

CO Formation

The formation of CO from a (CO_2+H_2S) feed has been typically attributed (Towler and Lynn, 1993) to the water gas shift reaction:

$$CO_2 + H_2 \leftrightharpoons CO + H_2O \qquad (5.29)$$

Towler and Lynn (1993) argued that this reaction was rapid and the hydrogen produced from the H_2S decomposition reaction equilibrated to form CO. Our experimental results indicate that the CO forming reaction is not rapid and is limited kinetically. However, the residence times in Towler and Lynn's experiments were higher than those found in this study, the difference being at least a factor of three. Therefore, it may be possible that in their reactor, there was enough time for the equilbria of reaction 5.29 to be established. The formation of CO may be described via the overall water gas shift reaction 5.29. This reaction may be considered to be comprised of the following three reactions (Baulch *et al.*, 1992):

$$H_2 + M \leftrightharpoons 2H + M \qquad (5.30)$$

$$CO_2 + H \leftrightharpoons CO + OH \qquad (5.31)$$

$$H + OH \leftrightharpoons H_2O \qquad (5.32)$$

where, M is a collisional partner, which is the diluent nitrogen in this study. It must be mentioned that many other elementary H-O reactions will occur simultaneously, but are not discussed here for sake of brevity.

5.6.3.2 Modeling CO formation from (CO_2 and H_2S) mixtures

The rate-determining step for CO formation is reaction (5.31). Assuming that the H radical is always in equilibrium with hydrogen molecule according to the reaction (5.30), the rate of formation of CO can be described appropriately by equation (5.33)

$$(r_{CO}) = k_6 [C_{CO2} C_{H2}^{0.5} - (C_{CO} C_{H2O} / C_{H2}^{0.5}) / K_{EQ6}] \qquad (5.33)$$

where, r_{CO} is the net rate of formation of CO in kmol/m^3·s

For sake of simplicity, two reactions were considered to occur in a CO_2 and H_2S mixture, the hydrogen sulfide decomposition reaction and the reaction between hydrogen and carbon dioxide. The rate of hydrogen sulfide decomposition had already been obtained. The reverse reaction was obtained from equilibrium consideration. The rate constant (k_6) was obtained by matching the CO concentrations for the data from two reactors over 1000 to 1200 C. The rate constant (k_6) was then regression to obtain the Arrhenius expression k_6 = $3.95 \pm 0.35 \times 10^{10}$ exp [(-31220 ± 180) /T] $(m^3/kmol)^{0.5}/s$. The corresponding activation energy value of 259 kJ/mol compares well with the activation energy of 238 kJ/mol reported by Graven and Long (1967). However, the collision factor or pre-exponential is greater by a factor of 2.5.

5.6.3.3 Detailed modeling

The formation of CO was also predicted with a detailed kinetic model. The kinetics of the reaction 5.33 reported by Yetter et al. (1993) was added to the existing kinetic scheme for H_2S oxidation reaction (discussed in section 5.3.5). The rate constant for the reaction was $K_{CO2\text{-}H} = 1.51 \times 10^{11}$ exp [-110.58 (kJ/mol)/RT] m^3/kmol·s. To improve the match between the data and predictions, the rate constant for reaction 5.33 had to be multiplied by 1.3.

5.6.4 Comparison of prediction with data

The predictions of the CO yields obtained from the simple two-reaction model are compared with the experimental data in Figure 5.19. The predicted CO yields are in excellent agreement with data for the 16.0 m reactor. The model predictions, however, are slightly lower than the data obtained from 6.4 m reactor for temperatures below 1050 °C.

The predictions of CO yields from the detailed kinetic model are compared with experimental data in Figure 5.20. The effect of the initial trace oxygen (< 3 ppm) content was also investigated. The model predictions showed no sensitivity to the presence of trace oxygen in initial mixture on CO production rate. It can be observed from Figure 5.20 that the predicted CO concentrations are consistently lower than the experimentally measured CO concentrations. If it is assumed the detailed kinetic model correctly accounts for the main reactions, then it may be possible that the CO formation reaction is being accelerated. At present, the probable cause has not been established. Moreover, only one CO_2 or CO reaction was included in the detailed model and the occurrence of other reactions in H-C-S-O system is certainly possible.

5.7 Reaction between CO and H_2S

5.7.1 Literature review

Thermodynamic equilibrium study indicates that the formation of COS via the reaction between CO and H_2S may be important. The overall reaction between CO and H_2S can be represented as follows:

$$CO + H_2S \rightleftharpoons COS + H_2 \qquad (5.34)$$

This overall reaction between CO and H_2S to produce COS and H_2 has been studied by a number of researchers (Faraji *et al.*, 1996; Fukuda *et al.*, 1977; Dokiya *et al.*, 1977). These studies, however, have been limited to low temperature catalytic reactions. There is little information on the kinetics of the

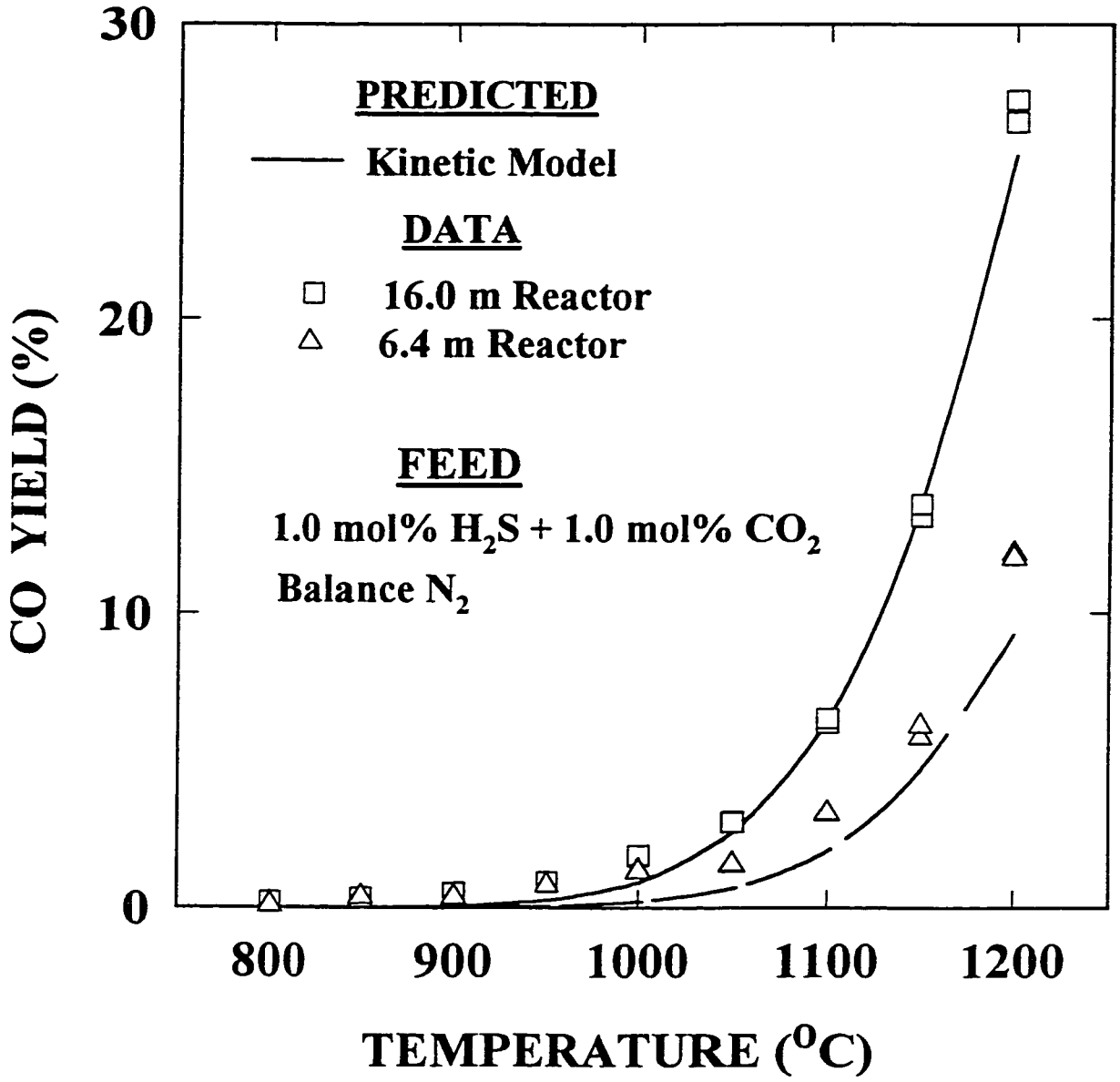

Figure 5.19 A comparison of model predicted CO yield with experimental data

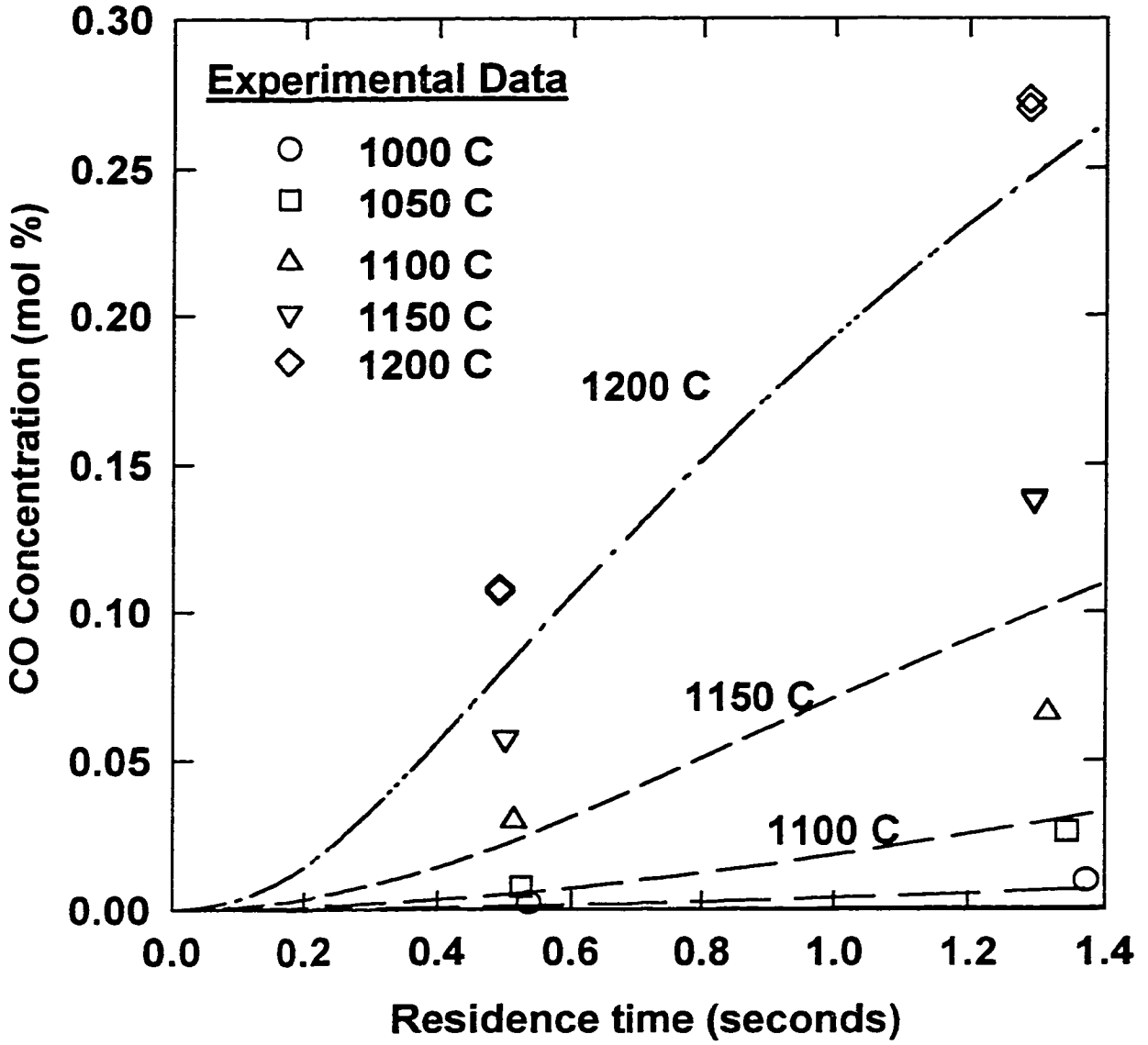

Figure 5.20 Comparison of the CO concentration predicted from detailed kinetic model with experimental data.

high temperature homogeneous gas phase reaction. Kurbanov and Mamedov (1995) studied this reaction in the temperature range of 300-650 °C. However, they were interested primarily in investigating the contribution of the reaction between CO and SH radical to produce COS and H radical. In their experiments, the SH radical was produced by photochemical initiation method, hence, the overall reaction between CO and H_2S was not completely a thermal reaction.In this study the thermal reaction between CO and H_2S was studied to obtain kinetic information on the COS formation via the reaction (5.34).

5.7.2 Experimental

5.7.2.1 Experimental conditions

Experiments were carried in two quartz reactors of lengths 6.4 m and 16.0m over a temperature range of 800-1000 C. Experiments were conducted by reacting 1.0 mol% CO with 1.0 mol% H_2S, the balance in both reactant stream made up of ultra-high purity nitrogen. The gas flow rate was maintained at 4.0 L/min. The inlet pressure varied from 120 to 160 kPa.

5.7.2.2 COS formation.

The experimentally measured COS concentrations show the typical trend expected of the conversions obtained in a tubular reactor for an exothermic reversible reaction. The measured conversions initially increase with temperature until they attain equilibrium conversion. With further increase in temperature, the measured conversions decrease as the equilibrium conversions decrease. From the experimental data reported in Figure 5.21, it can be seen that the COS formation from the ($CO+H_2S$) mixture at our experimental conditions is limited kinetically at lower temperatures and thermodynamically at higher temperatures. At temperatures greater than 1000 °C, the formation of COS is rapid and the COS concentration in either of the reactor reach equilibrium concentration. Another point to note is that at these temperatures, the measured COS concentrations slightly exceed the equilibrium concentration. This increased COS

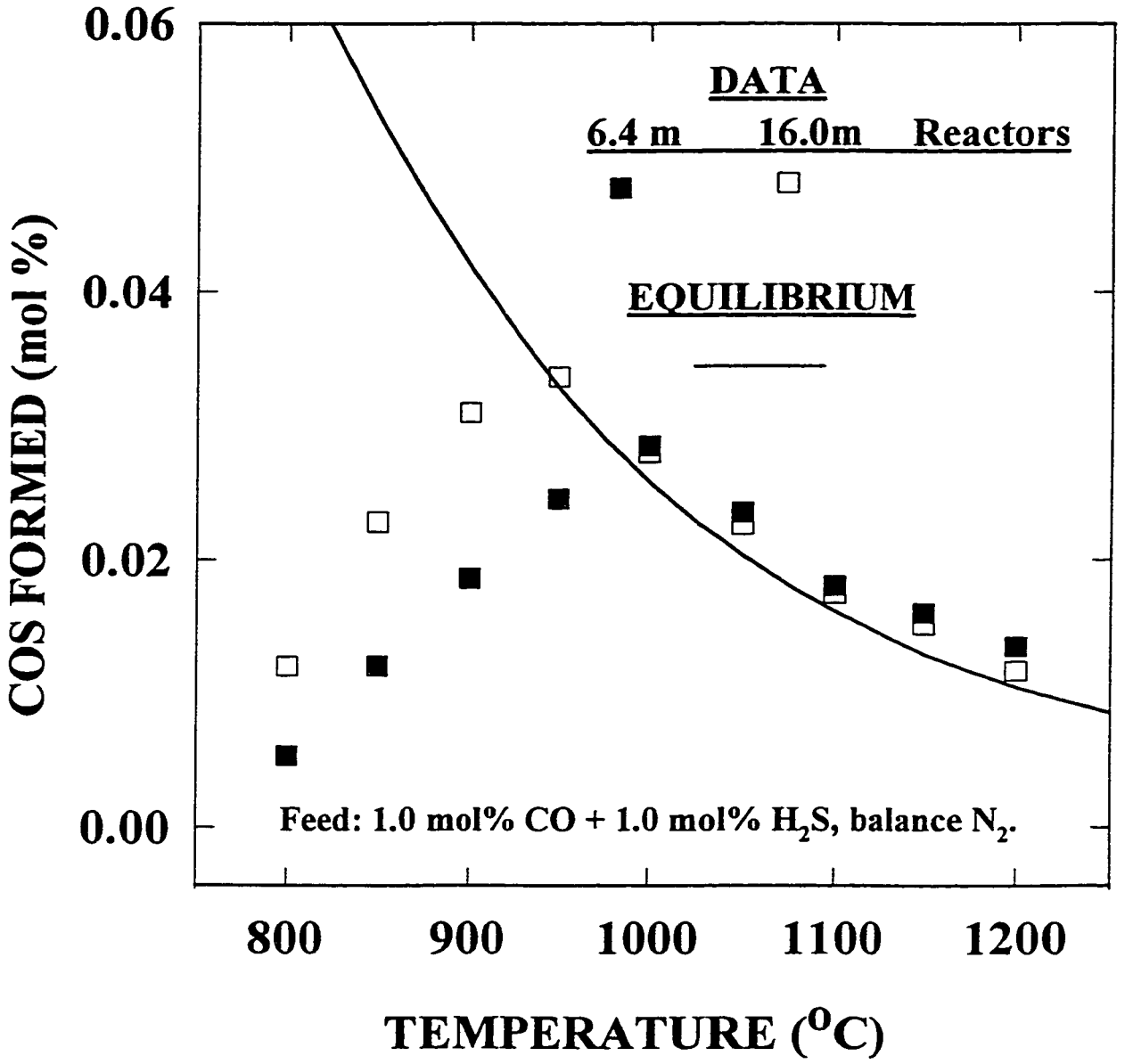

Figure 5.21 Measured COS concentration at the exit of two quartz reactors as a function of temperature.

concentration, as discussed under 5.4.3.1, is a result of the COS formation during the gas quenching process. At these high temperatures, the reactions are fast, and, although the reaction quenching is rapid it is not instantaneous. Nonetheless, the differences between the equilibrium and the measured concentrations of COS are small and lie within the limits of experimental accuracy.

5.7.2.3 Effect of CO and H_2S concentrations.

The effect of CO concentrations on COS formation was studied by conducting experiments at a fixed H_2S concentration of 1.0 mol% and varying the CO concentration to 1.0, 2.5 and 5.0 mol%. Similarly, the effect of H_2S concentration was studied by reacting 1.0 mol% CO with 0.5 mol%, 1.0 mol % or 2.0 mol% H_2S. The results of these experiments are presented in Figure 5.22. The slopes of these log-log plots give an estimate for the order of reaction with respect to the relevant reactant for the COS forming reaction between CO and H_2S.

5.7.3 Kinetic modeling

At lower temperatures (<900 °C), when insignificant H_2S decomposition takes place, the experimental data indicates that the formation of COS from a mixture of CO and H_2S is a result of the following molecular reaction between CO and H_2S:

$$CO + H_2S \rightleftharpoons COS + H_2 \qquad (5.34)$$

At higher temperatures, the decomposition of H_2S via reaction (5.35) results in the formation of sulfur, which in turn may react with CO to form COS according to reaction (5.36):

$$H_2S + M \rightleftharpoons H_2 + \tfrac{1}{2} S_2 + M \qquad (5.35)$$

$$CO + \tfrac{1}{2} S_2 \rightleftharpoons COS \qquad (5.36)$$

where, M is an inert collisional partner, which is the diluent gas nitrogen. The collisional partner essentially acts as an energy transfer agent that provides the

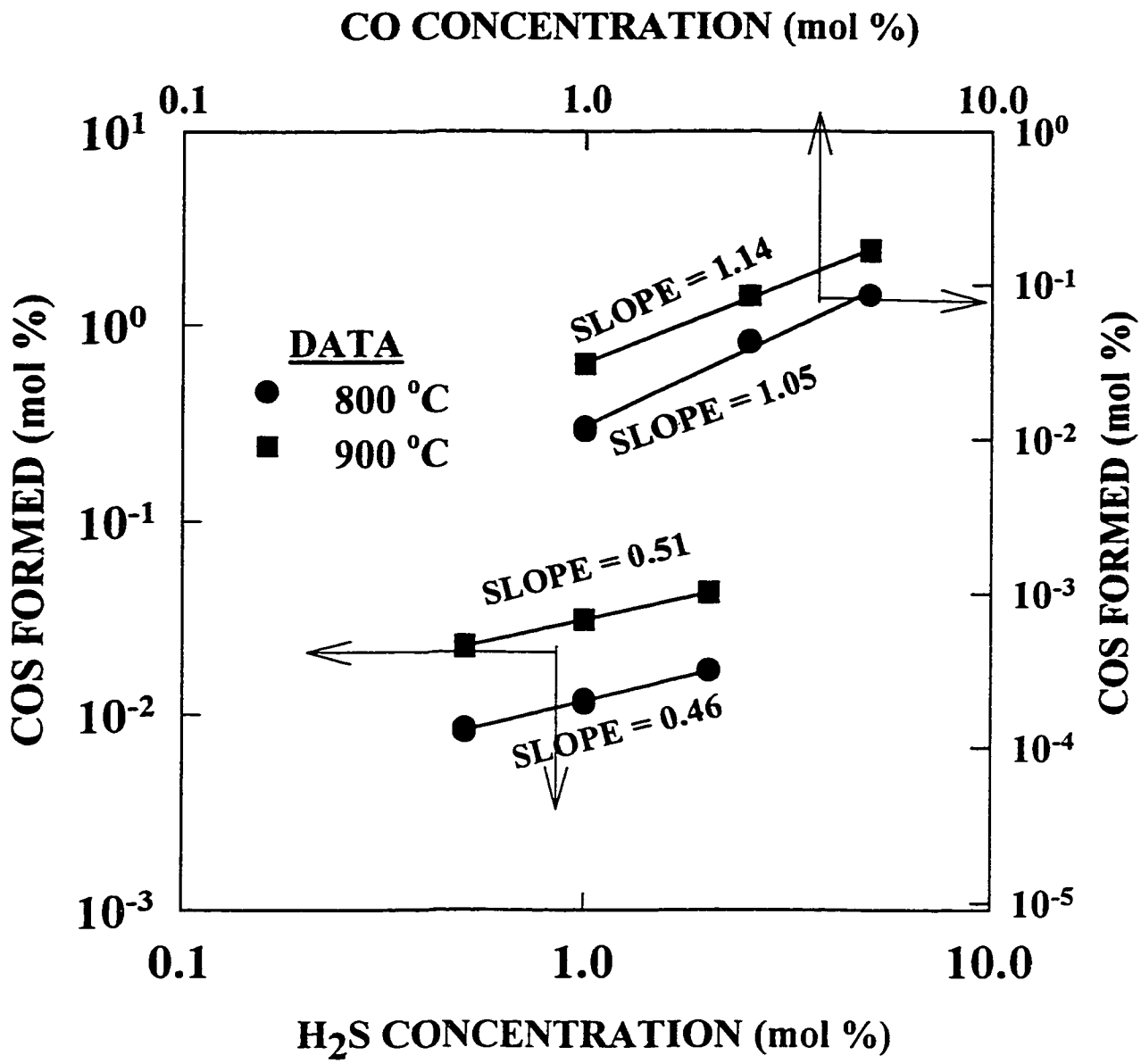

Figure 5.22 Effect of CO and H_2S concentrations on COS formation.

necessary energy required for decomposition of the H_2S molecule. The degree of contribution of either reaction (5.34) or (5.36) towards the formation of COS requires kinetic information on these reactions. The results of the study for the reaction between CO and sulfur indicate that the reaction can be quite rapid especially at temperatures exceeding 1000 °C. Whether this reaction contributes significantly to the COS formation can be established from a simulation study that has been reported later in this section.

As mentioned earlier, the formation of COS from a mixture of CO and H_2S is complicated by the two parallel reactions (5.34) and (5.36). Since the reaction kinetics for reaction (5.36) has already been measured (section 5.3), it was important to ascertain whether this reaction could solely account for the observed COS.

Therefore, the COS formation from (CO+H_2S) feed was first calculated from the consideration that only reaction (5.35) and (5.36) occurred, where the rate of H_2S decomposition was given by equation (5.37) and that of COS formation was given by:

$$-r_{H2S} = 2\, k_1 \left[C_M\, C_{H2S} - (C_{H2}\, C_{S2}^{0.5})/K_{EQ1}\right] \qquad (5.37)$$

$$(r_{COS}) = k_2 \left[C_{CO}\, C_{S2} - (C_{COS}\, C_{S2}^{0.5})/K_{EQ2}\right] \qquad (5.38)$$

It must be noted that the orders of dependency of the reactant concentrations for the forward reaction were based on experimental observation, however the form of the reverse reactions were derived from thermodynamic equilibrium constraints and do not necessarily represent the actual reaction mechanism.

The COS predictions from equation (5.38) for experiments in the 16.0 m long reactor are presented in Figure 5.23 as dotted line. It can be clearly seen that the COS formation via reaction between CO and sulfur cannot account for the measured amount of COS. At temperatures lower than 900 °C, there is little sulfur produced from H_2S decomposition, hence the COS production is negligible. At temperatures above 1100 °C, significant amounts of sulfur are produced increasing the reaction rate for COS formation. In fact, at temperatures

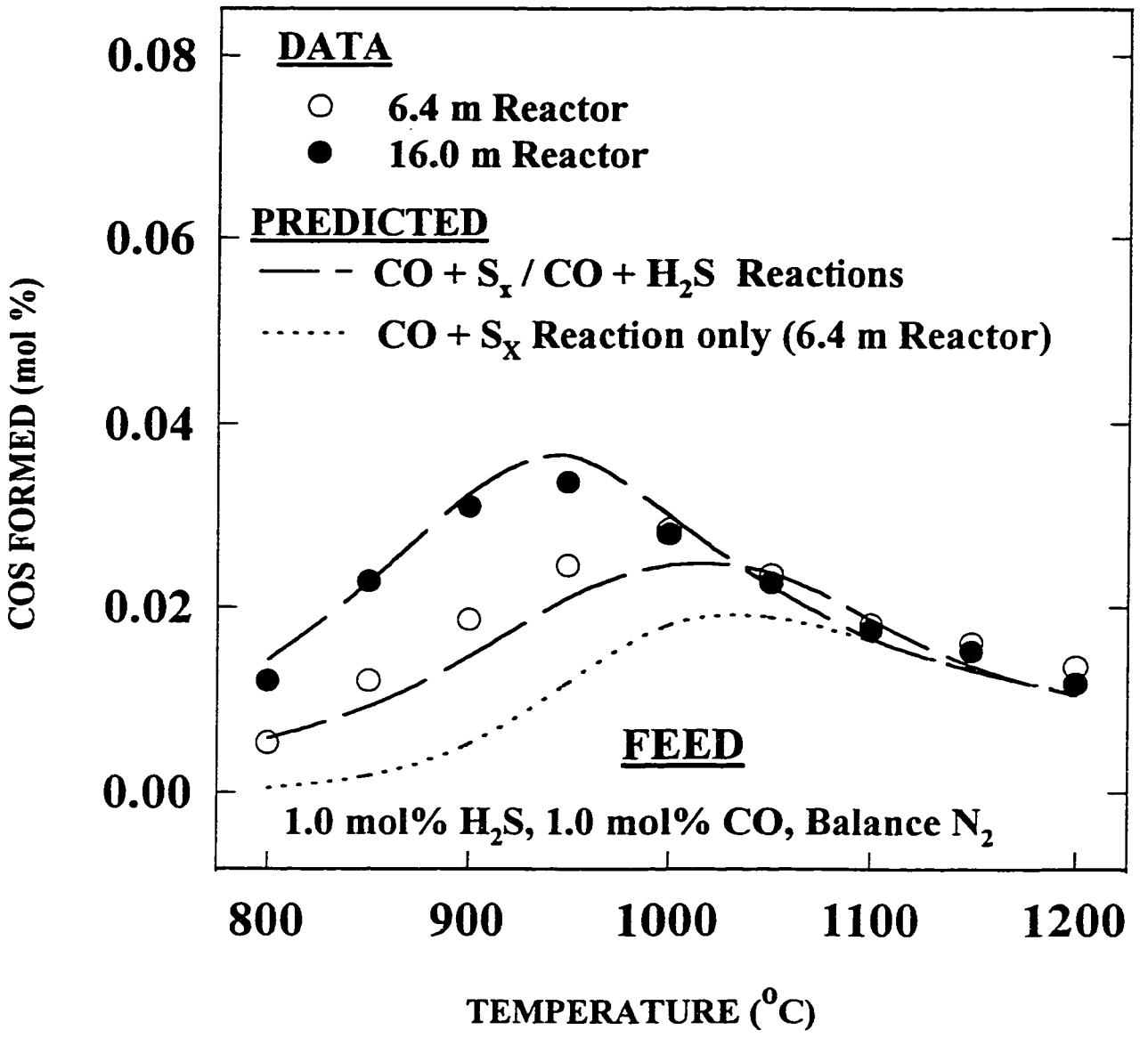

Figure 5.23 COS production from 1.0 mol% CO + 1.0 mol% H_2S mixture. Comparison of model predictions with data.

above 1100 °C, the measured COS concentration can be explained via reaction (5.36) only.

The results of simulation confirmed that another COS forming reaction apart from reaction (5.36) needs to be included in the reaction scheme to explain the observed amount of COS. Thus, the reaction (5.34) was included as a possible COS forming reaction, and the net rate of COS formation was given by:

$$(r_{COS}) = k_2 [C_{CO} C_{S2} - (C_{COS} C_{S2}^{0.5})/K_{EQ2}] + k_7 [C_{CO}C_{H2S}^{0.5} - (C_{COS}C_{H2}/ C_{H2S}^{0.5})/ K_{EQ7}] \quad (5.39)$$

The appropriate orders for reactant concentrations for CO and H_2S reaction were obtained from the experimental data reported in Figure 5.22. For the reaction between CO and H_2S, the half-order dependency of the reaction rate with respect to the H_2S concentration clearly indicates that the overall reaction comprises of other elementary reaction steps.

For the reaction between CO and H_2S, the rate constant k_6 was regressed to match the experimental data and found to be $k_7 = 1.59 \pm 0.86 \times 10^{05}$ exp [(-13340 ± 930 K) /T] $(m^3/kmol)^{0.5}/s$. The predicted COS concentrations are shown as dashed lines in Figure 5.23. The model predictions are in good agreement with the data for 16.0 m reactor. The predictions for 6.4 m reactor are slightly lower than the data in the temperature range 850-1000 °C.

5.7.4 Possible reaction mechanism

One of the possible reaction mechanism for COS formation in CO and H_2S mixture may be via the production of SH radical via decomposition of H_2S and its subsequent reaction with CO to produce COS and H radical. Such a reaction scheme is possible as alluded by Kurbanov and Mamedov (1995). Moreover, the concentration of SH radical can be shown to be proportional to the square root of the H_2S concentration which explains the half order dependency of the reaction rate with respect to the H_2S concentration (Adesina et al., 1995). Therefore, the main step for COS formation for the overall reaction between CO and H_2S may be that via reaction between CO and SH.

5.8 Reaction between CO_2 and H_2.

5.8.1 Introduction

The importance of the CO forming reaction between CO_2 and H_2 has already been addressed in section 5.7. The overall reaction between CO_2 and H_2 to form CO and water is easily recognized as the reverse of the water gas shift reaction:

$$CO_2 + H_2 \leftrightharpoons CO + H_2O \qquad (5.29)$$

The reaction kinetics for the elementary reactionz leading to the overall reaction (5.29) have also been studied in various types of reactor systems (flow reactor, flames, shock tubes) over a wide range of temperature (1000-3000 K). Before the detailed kinetic model was (see section 5.6.3.3) used to simulate the CO formation from CO_2 and H_2S mixtures, it was thought that kinetic parameters obtained for the CO forming reaction from simple reaction model (5.7.3.2) were too high. Therefore, an experimental study for the reaction between CO_2 and H_2 was conducted.

5.8.2 Literature review

As mentioned above the kinetics of this reaction has been studied in various reactor types and over a large range of temperature. Baulch et al. (1976) provide a concise summary of the reported kinetics for the forward and the reverse elementary reactions involved for this reacting system and need not be reviewed once again here.

5.8.3 Experimental

5.8.4 Experimental conditions

Experiments were conducted in two reactors of lengths 6.4 and 16.0 m over a temperature range of 950-1250 °C. The reactant stream consisted of 1.0 mol% CO_2 and 1.0 mol % H_2 with the balance made up of ultra high purity nitrogen. To study the effect of CO_2 and H_2 concentrations and also to determine the orders of

the reaction with respect to their concentrations on CO formation, experiments were performed by varying the CO_2 or H_2 concentrations over 4 fold while keeping the concentration of other species fixed. The product stream was analyzed for CO and CO_2 concentrations only. The water from the product stream was removed by passing the quenched and cooled product stream through a water-trap, a glass tube filled partially with phosphorous pentoxide. P_2O_5 was chosen as a dessicant because it does not react with sulfur compounds like most of the other dessicants. However, for this set of experiments, i.e. between CO_2 and H_2, other dessicant could as well have been used.

5.8.5 Results.

5.8.5.1 Effect of temperature

The experimentally measured CO concentrations at the reactor exit are presented in Figure 5.24. The equilibrium CO concentration calculated for the $CO\text{-}H_2\text{-}CO_2\text{-}H_2O$ system is also shown as solid line. Clearly, the experimental results prove that the formation is kinetically limited below 1000 °C.

5.8.5.2 Effect of initial concentrations of CO_2 and H_2 on CO formation

To determine the order of reaction with respect to CO_2 concentration, experiments were conducted with a fixed concentration of H_2 equal to 1.0 mol% and varying the CO_2 concentrations to 0.5, 1.0 and 4.0 mol %. Similarly, for determining the order of reaction with respect to H_2 concentrations, experiments were conducted with a fixed CO_2 concentration of 1.0 mol% and varying the H_2 concentrations to 0.5, 1.0 and 2.0 mol%. All the above experiments were conducted in a 6.4 m long reactor at 1100 °C at a total flow rate of 4.0 L/min

For simplicity, it may be assumed that the concentration of the product CO is proportional to the reactant concentration raised to the power of reaction order (similar to the assumption employed in section 5.4.3.2). With this assumption the plots of the concentration of product CO against the initial concentrations of

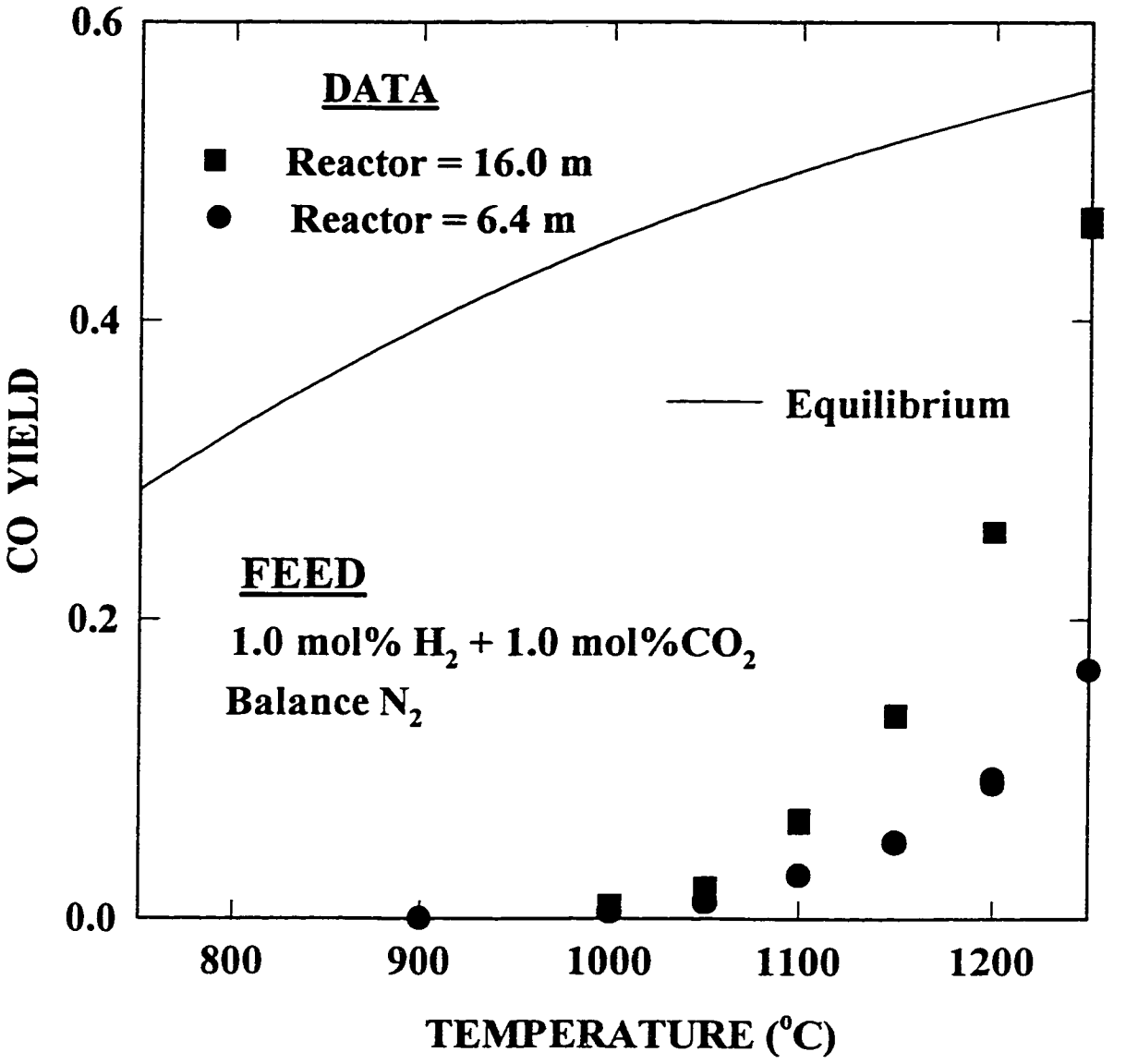

Figure 5.24 Experimentally measured CO concentrations at reactor exit as a function of temperature.

reactants CO_2 and H_2 should give information on the orders of the reaction. The log-log plot of the partial pressure of CO against the initial partial pressures of CO_2 and H_2 is presented in Figure 5.25. The slopes of these plots show an order of dependency with respect to H_2 and CO_2 concentrations to be 0.58 and 1.14, respectively. The orders of reactions will be considered to be 0.5 and 1.0 for H_2 and CO_2, respectively.

5.8.6 Kinetic modeling

5.8.6.1 Reaction mechanism

The important steps in CO formation from reaction between CO_2 and H_2 has already been discussed in 5.6.3. The experimentally determined orders of reaction with respect to CO_2 and H_2 concentrations are consistent with the reaction mechanism discussed in 5.6.3. The CO producing reaction is that between CO_2 and the H atom. The H atom is in equilibrium with H_2 molecule. Therefore, the overall rate of formation of CO from a mixture of CO_2 and H_2 which, has already been used earlier in section 5.6.3 may be expressed as:

$$(r_{CO}) = k_6 C_{CO2} C_{H2}^{0.5} - k_6/K_{eq} C_{CO} C_{H2O}/ C_{H2}^{0.5} \qquad (5.33)$$

To include the effect of reverse reaction, the second term on the right hand side has been added.

5.8.7 Parameter estimation

The parameters for the forward rate constant (k_6) were determined by regressing the experimental data for which the CO conversions remained below 75 percent of the equilibrium value. The one and half order rate constant, k_6 in $(m^3/kmol)^{0.5}/s$, was found to be: $k_6 = (8.59 \pm 3.33) \times 10^{10} \exp [(-32535 \pm 680K)/T]$.

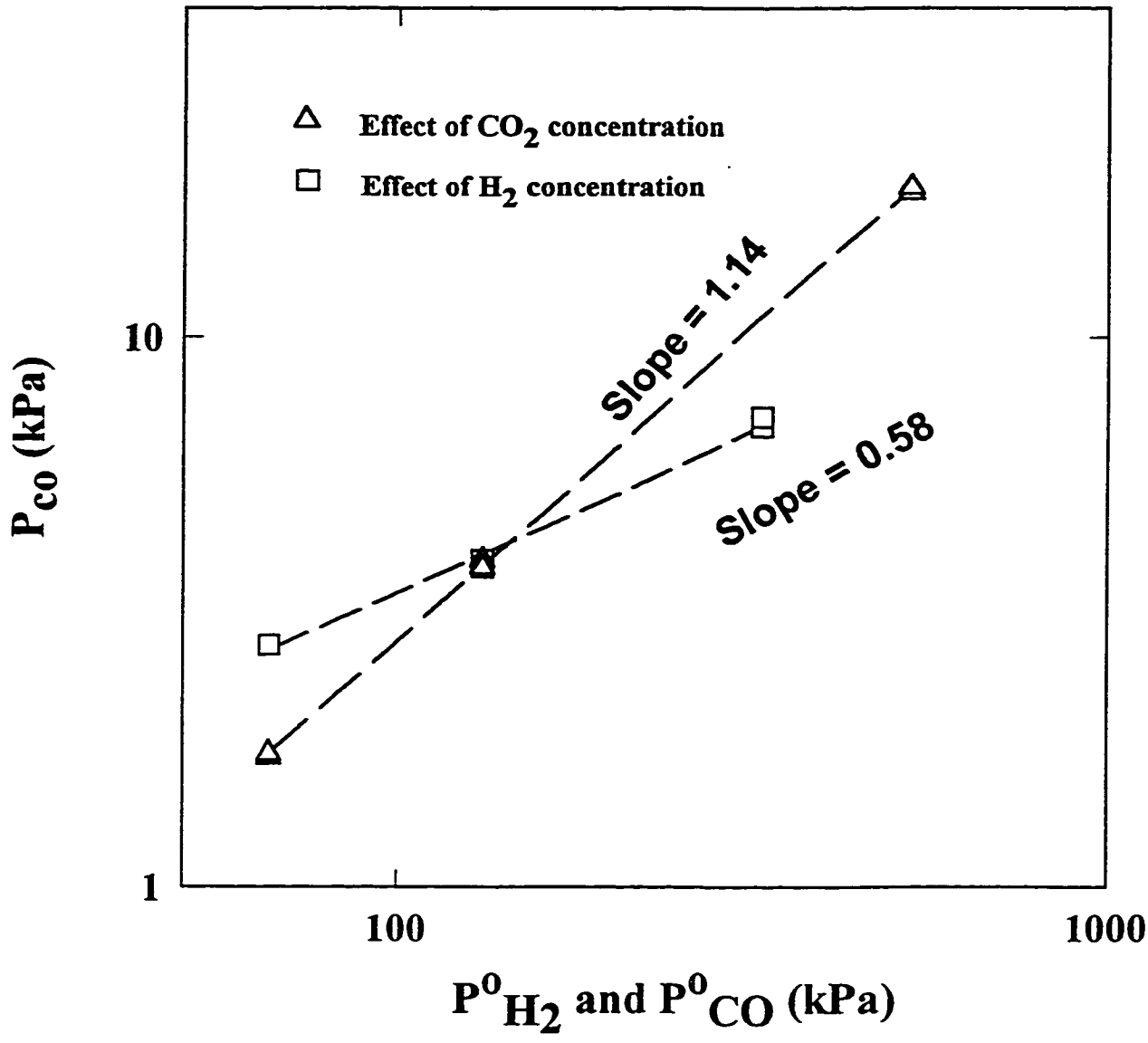

Figure 5.25 Effect of initial concentrations of CO_2 and H_2 on CO formation.

5.8.8 Comparison of rate constant

A plot of the rate constant obtained from the two reacting mixtures (CO_2 + H_2S) and (CO_2 and H_2) are presented in Figure 5.26. It can be observed from the Figure that the rate constants obtained from the experiments with (CO_2 and H_2) were highly consistent with those determined from the experiments with (CO_2 and H_2S) mixtures

5.8.9 Simulation of CO formation with detailed reaction kinetic scheme

Simulations performed with the detailed kinetic model as referred to in section 5.6.3.3 showed that very low amounts of CO were formed. The detailed kinetic model was based on the reaction mechanism proposed for H_2S oxidation. In this mechanism all the important elementary H-O reactions had been included. As mentioned in section 5.6.3.3, the primary step for CO formation reaction, i.e. the reaction between CO_2 and H, was added to the reaction scheme proposed for H_2S/O_2 system.

The results of the simulation are discussed in the following subsection. The simulation results indicated that, in the experiments, somehow the CO formation rate was being accelerated. This may happen only if the rate of formation of H atom was enhanced, because the CO forming step involves reaction between CO_2 and the H atom. It was thought that some impurity was causing the enhancement of the H atom formation reaction, which in case of pure mixtures of CO_2 and H_2 would be H_2 dissociation into H atoms.

5.8.9.1 Role of trace amounts of oxygen on CO formation rates

One of the reactions in the detailed kinetic model involving the starting reactant H_2 is that between H_2 and O_2 to produce H and HO_2. This reaction was narrowed down to be the probable cause for enhancement in CO formation rates.

Next, an investigation of the quality of the reactant gases was conducted. It was found that the ultra high purity (UHP) nitrogen gas, which was used as the diluent gas contained trace amounts of oxygen. According to Praxair, the

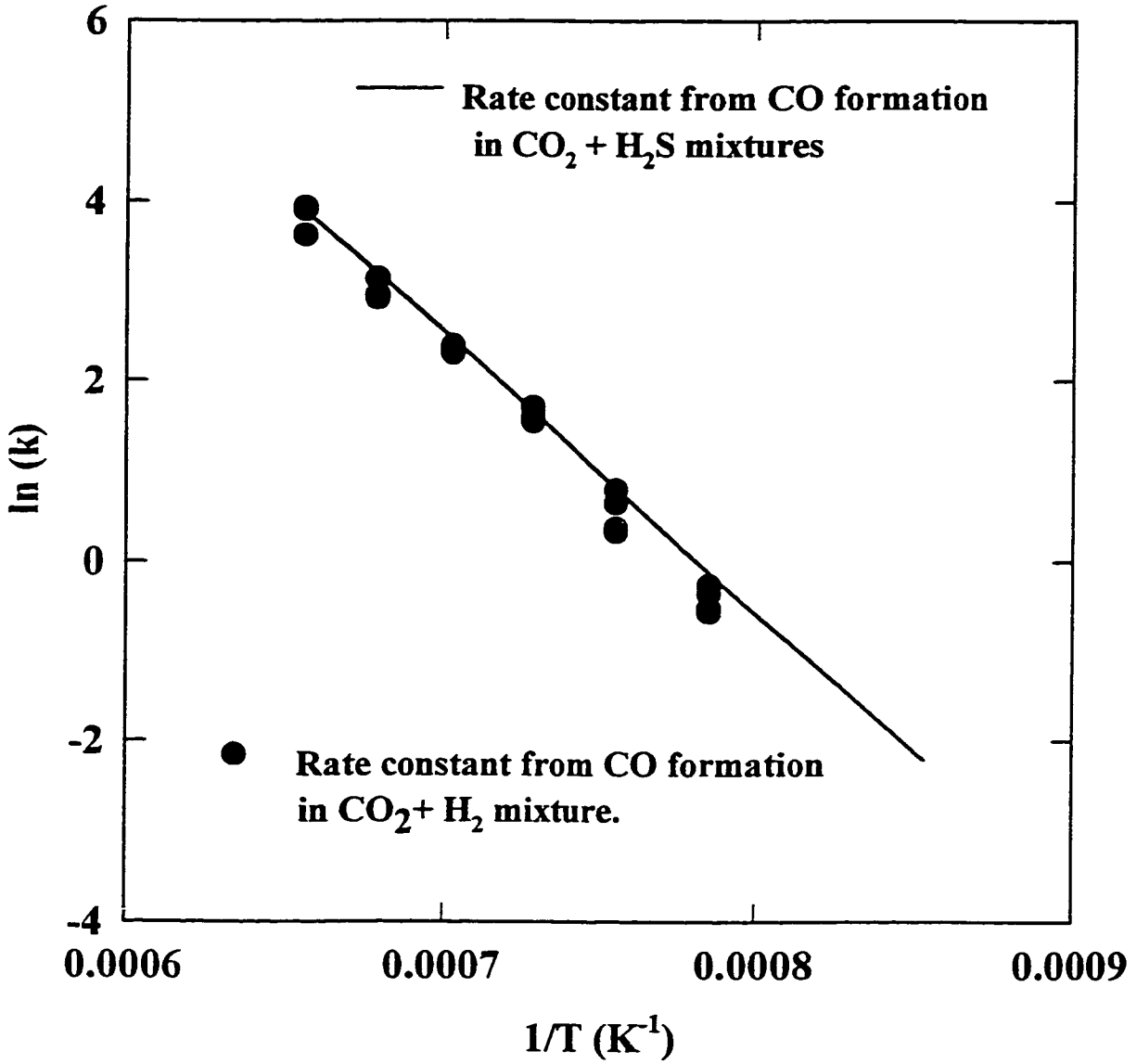

Figure 5.26 Comparison of rate constant for CO forming reaction obtained from two different reacting mixture systems.

Mixtures: 1.0 mol % CO_2 + 1.0 mol % H_2S;
1.0 mol% CO_2 + 1.0 mol % H_2.

maximum assay on the O_2 content for the UHP nitrogen is less than 3 ppm. However, there will always be trace amounts in their UHP nitrogen.

The 3 ppm O_2 content may seem to be too low a concentration to enhance the H forming reaction. Whether these levels of O_2 content in CO_2 and H_2 mixtures would affect the CO formation drastically remained to be tested.

The results of simulation showing the amount of CO formed from a mixture containing 1.0 mol% CO_2 and 1.0 mol% H_2 with varying initial amounts of oxygen are shown in Figure 5.27. The simulation results show the dramatic effect that trace amounts of oxygen can have on the enhancement of CO formation. The experimental data at 1200 C obtained from two reactors have also been shown. To match the experimental, approximately 0.7-0.8 ppm of O_2 in feed mixture is required. This is well within the maximum assay reported by Praxair Canada Limited. This is a convincing reason for the observed accelerated rates of the reaction.

5.9 Reaction between CH_4 and Sulfur/Hydrogen Sulfide

5.9.1 Literature Review

Methane and Sulfur Reaction

The reaction between methane and sulfur has been long considered as a viable route for production of CS_2 industrially. There was a considerable interest in the early fifties and sixties to establish the viability of the process. The thermodynamic feasibility of CS_2 formation from reaction of methane and sulfur was studied by Stull (1949). The overall reaction between methane and sulfur to produce CS_2 may be written as:

$$CH_4 + 2S_2 \rightleftharpoons CS_2 + 2H_2S \qquad (5.40)$$

Kinetic studies on the catalytic and non-catalytic reactions have also been reported [Fisher and Smith, 1950; Nabor and Smith, 1953; Folkins et al., 1950; Thacker and Miller, 1944]. A majority of these studies were conducted at temperatures less than 700 °C. In a recent study, Anderson et al. (1993) reported experimental data on the reaction of methane and sulfur over a temperature

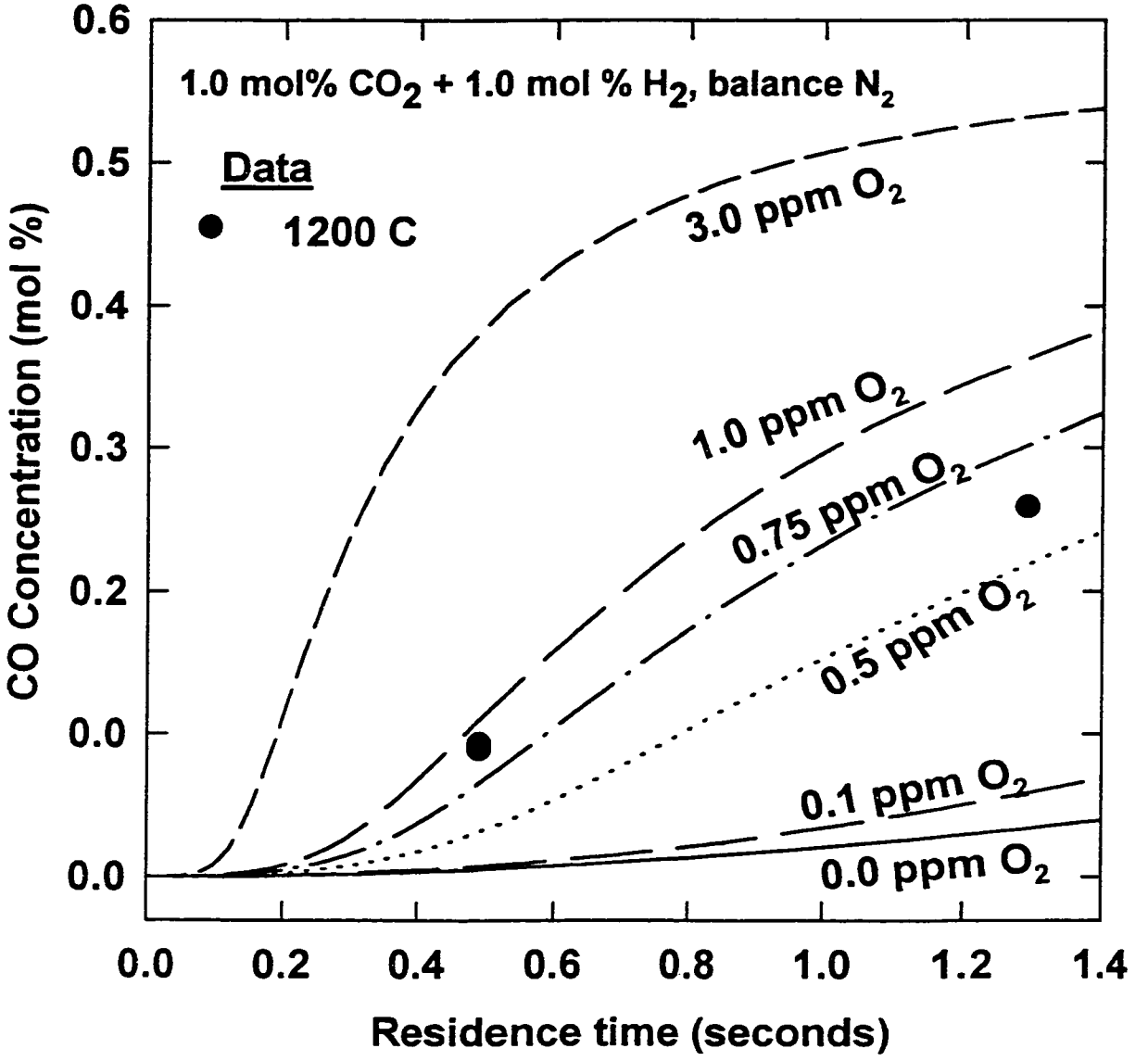

Figure 5.27 Results of simulation showing the effect of trace oxygen content on enhacement in CO formation.

(Lines: Predicted from detailed kinetic model)

range 500-800 °C. They were primarily interested to find whether sulfur would act as an effective oxidative coupling agent. They performed most of the experiments in a catalytic reactor but reported data with experimental runs in empty reactors. Experimental data at higher temperatures (> 1000 °C) on the reaction between methane and sulfur are not readily available and, therefore, an experimental study was conducted in this research to find how rapid the reaction is.

Methane and Hydrogen Sulfide Reaction

The effect of hydrogen sulfide on the pyrolysis of hydrocarbons has been studied extensively. An excellent review on this topic was published by Rebick (1980). In his paper, Rebick refers to the pyrolysis of hydrocarbons other than methane. Industrially, the pyrolysis of methane has not been found to be a feasible process and, hence the effect of hydrogen sulfide during methane pyrolysis has not been studied either. Folkins et al. (1950) have referred to an earlier study by Waterman and Vlodrop (1939) who have reported thermal reaction of methane with hydrogen sulfide at temperatures up to 1125 °C. The reaction between methane and hydrogen sulfide may be written as:

$$CH_4 + 2H_2S \rightleftharpoons CS_2 + 4H_2 \qquad (5.41)$$

In the present research, experiments were conducted to obtain information on the formation of CS_2 via the reaction between methane and hydrogen sulfide.

5.9.2 Experimental

5.9.3 Experimental conditions and analysis

Experiments were conducted by reacting 0.9 mol% sulfur with 2.45 mol% methane in three reactors of lengths 1.6, 3.2 and 6.4 m. The determination of the concentration of sulfur in the feed stream has been described under Section 3.3. The experiments with methane and hydrogen sulfide mixtures were conducted by reacting 1.75 mol% H_2S with 2.45 mol% CH_4.

The gas chromatographic analysis of carbon disulfide required the use of a special separation column. The separation and analysis of product stream showed existence of chromatograph peaks other than H_2S, CH_4 and CS_2. A further analysis showed that these peaks corresponded to those for ethylene and ethane.

5.9.4 Experimental results

CS_2 formation from CH_4 + sulfur reaction

The experimental data on the measured concentrations of CS_2 at the exit of three reactors as a function of reactor temperature are presented in Figure 5.28. The CS_2 formation is found to increase steadily with temperature and reach a maximum value at temperatures exceeding 1150 °C. This maximum CS_2 concentration is the maximum CS_2 concentration possible from a complete conversion of all sulfur (limiting reactant) to CS_2.

CS_2 formation from CH_4 + H_2S reaction

The data on CS_2 formation from CH_4 and H_2S mixtures are reported in Figure 5.29. These data were obtained from the reactors of lengths 6.4 and 16.0 m. It must be mentioned that the longest reactor used for CH_4-Sulfur reaction was 6.4 m. The CS_2 formation show a similar trend as that observed for the CH_4-Sulfur system. However, the rates of formation of CS_2 in CH_4-H_2S system were much smaller than that in CH_4-Sulfur system. Moreover, little CS_2 was observed at temperatures below 900 C, when insignificant amount of H_2S decomposition is expected.

C_2H_4 yields from CH4 + Sulfur mixtures

During the reaction of methane with sulfur and with hydrogen sulfide, the main product of methane pyrolysis, C_2H_4 was also observed. The yield of C_2H_4, i.e. moles of C_2H_4 produced per mole of CH_4 in the feed, has been plotted in Figure 5.30. These data are for reacting mixture of methane and sulfur. The ethylene

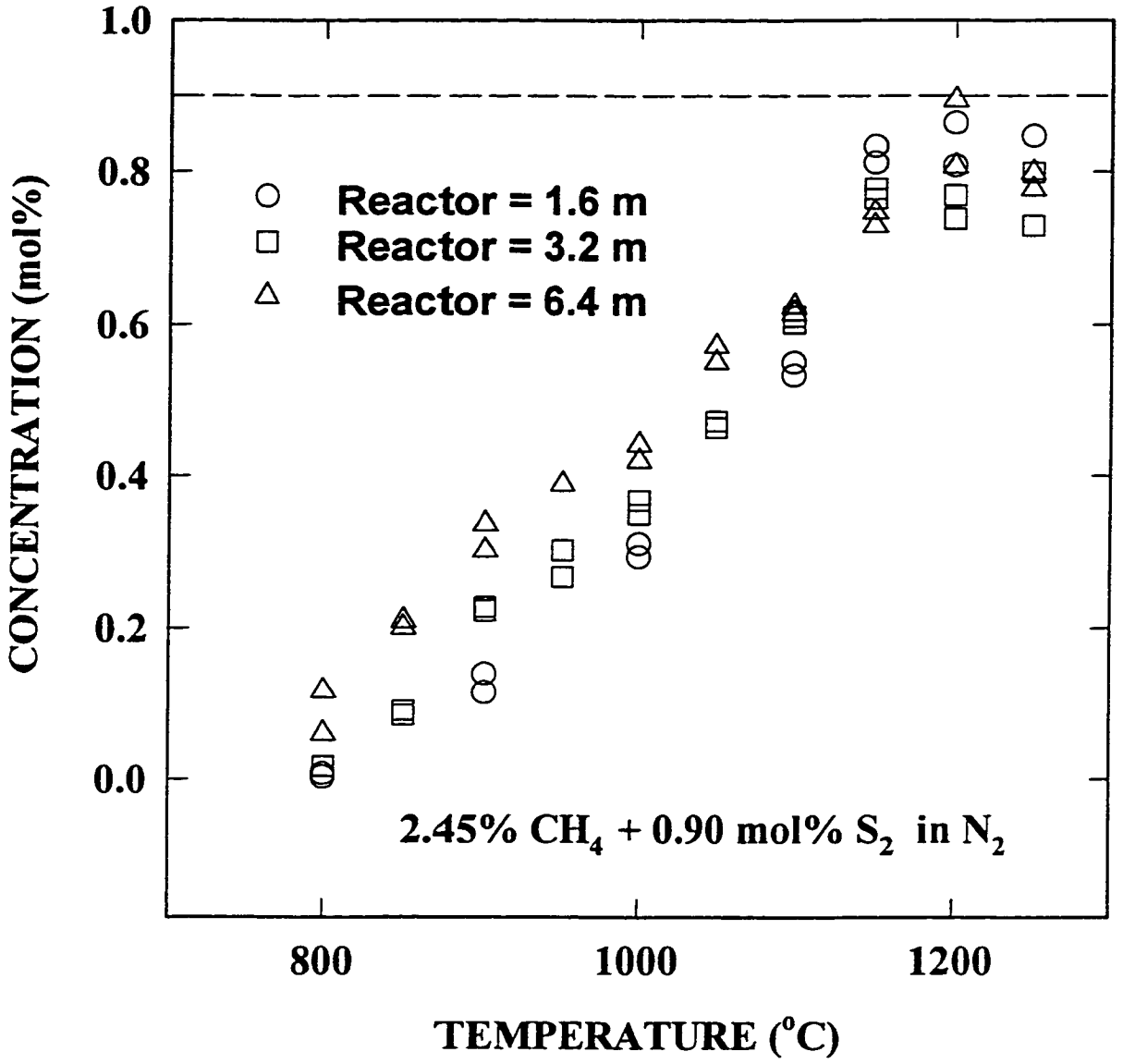

Figure 5.28 Experimentally measured CS_2 concentrations concentrations from three quartz reactors for reacting mixtures of CH_4 and S_2.

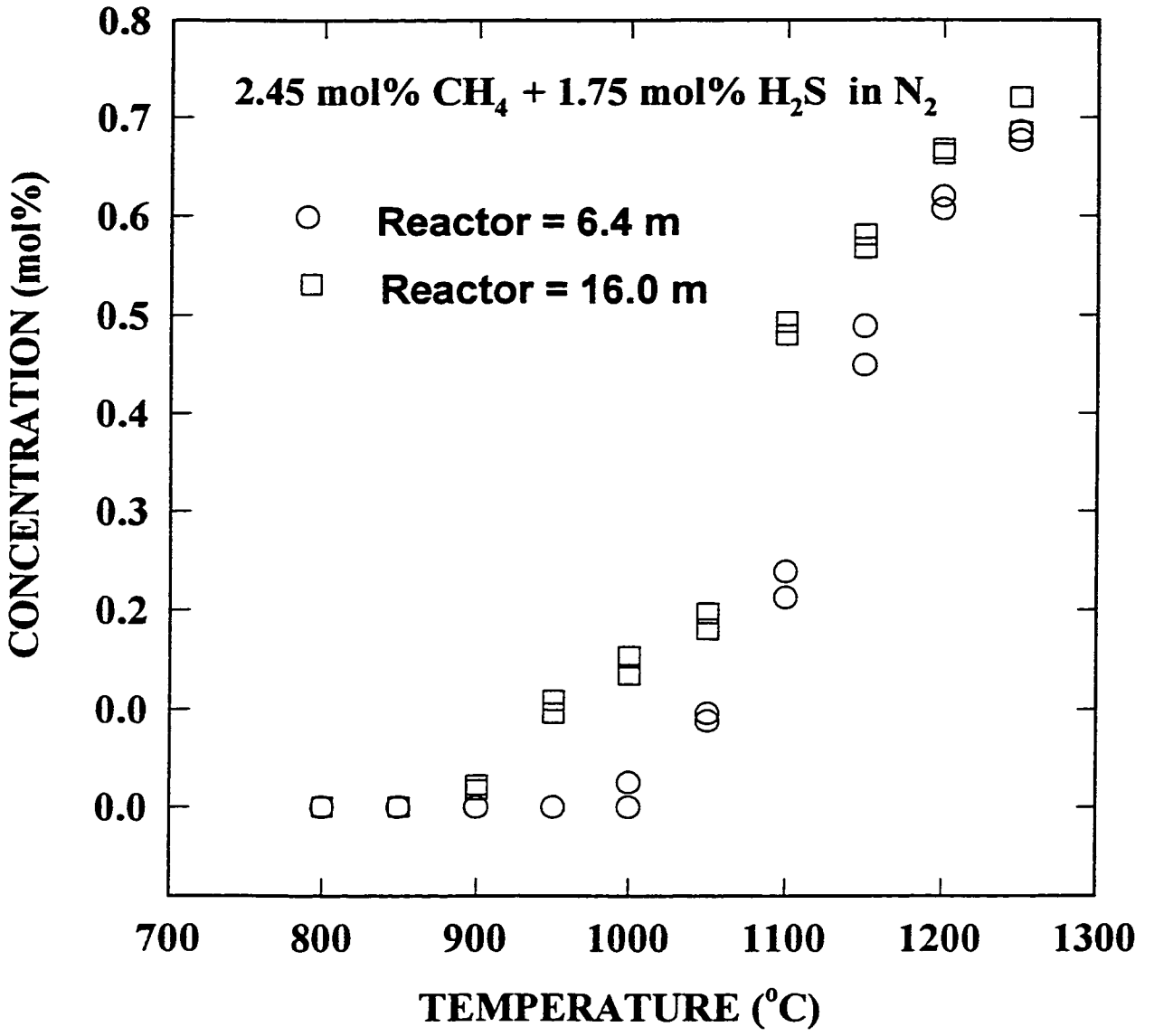

Figure 5.29 Experimentally measured CS_2 concentrations from two quartz reactors for reacting mixtures of CH_4 and H_2S.

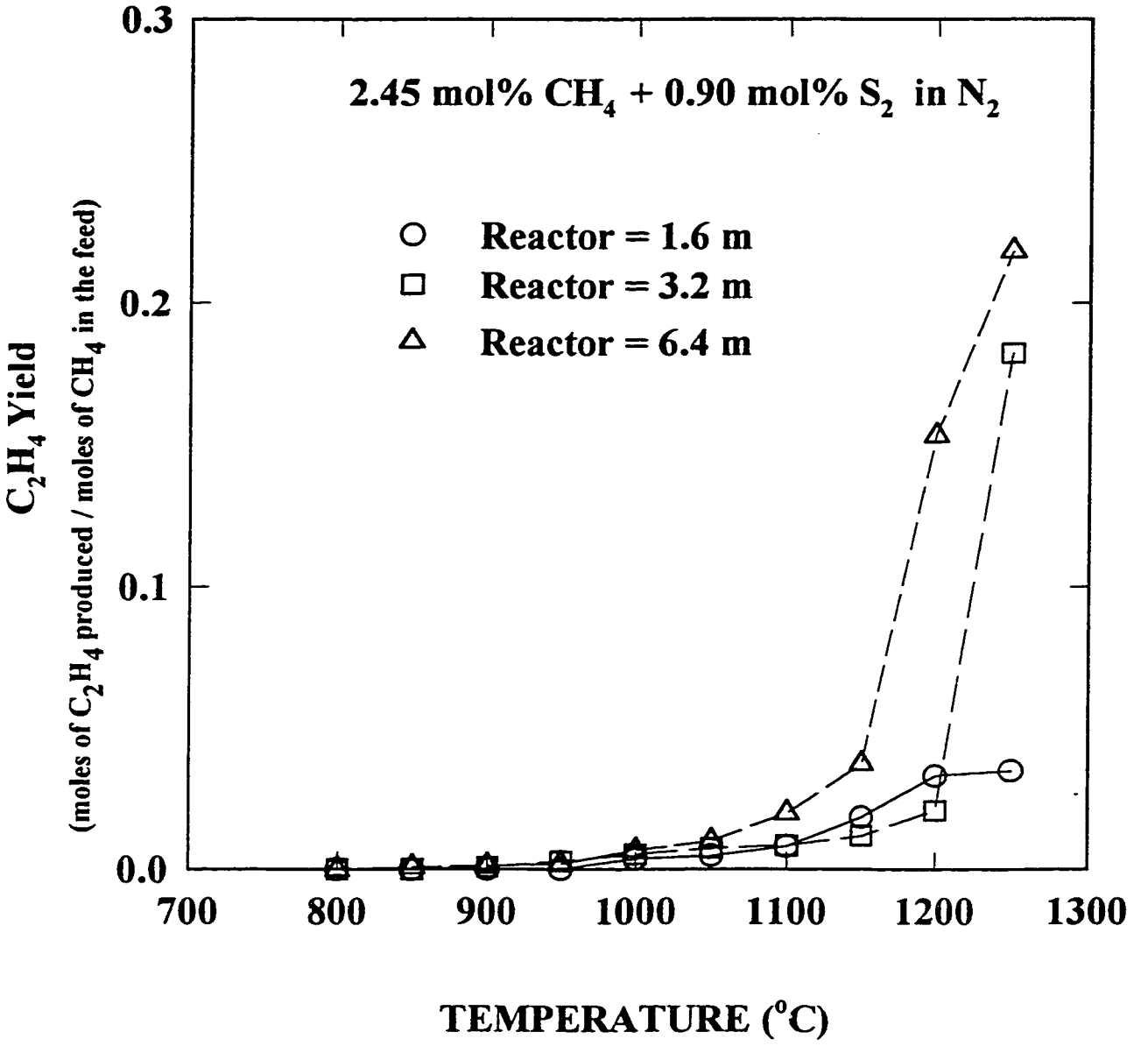

Figure 5.30 Yields of C_2H_4 from reacting mixtures of CH_4 and S_2 (Lines are trendlines)

yield are low for all the three reactors for temperatures up to 1100 C. Above this temperature, the ethylene yields from the longest reactor increases rapidly to a value of 22% at 1250 °C. However, the ethylene yield in the shortest reactor used does not increase as sharply.

These observations can be explained by the fact that at lower temperatures, there is still sulfur present in the product stream and this inhibits the reaction leading to the formation of ethylene. Once, all the sulfur is consumed the side reactions continue leading to formation of ethylene.

Coke deposition

At temperatures exceeding 1050 C, coke deposition was observed in the reactors. The pictures of the reactor clearly showing coke deposition along the reactor are shown in Figure 5.31 and 5.32.

Figure 5.31 shows the pictures of the coke deposition in the reactors for reaction between methane and sulfur. It can be seen that coking has already occurred during the heat-up period. This can be inferred from the coke deposition in the vertical inlet section through which methane was flowed. An interesting feature to note is that no coke deposition is observed in the short length of reactor after the mixer. This indicates that either the coking reaction is inhibited or the deposition is inhibited when the methane stream comes in contact with sulfur laden gas stream. Once, a majority of sulfur is consumed, the coke deposition starts to occur again.

In Figure 5.32, the coke deposition in the reactors during the reaction between methane and hydrogen sulfide is shown. The coking in the reactor can be observed in the inlet to the reactor through which methane was flowed. The coke deposition is observed at the mixer and downstream of the mixer as well. These results indicate that the coking as well as the coke deposition in unaffected by the presence of hydrogen sulfide. It may also be inferred that sulfur acts as a more effective coking/coke deposition inhibitor.

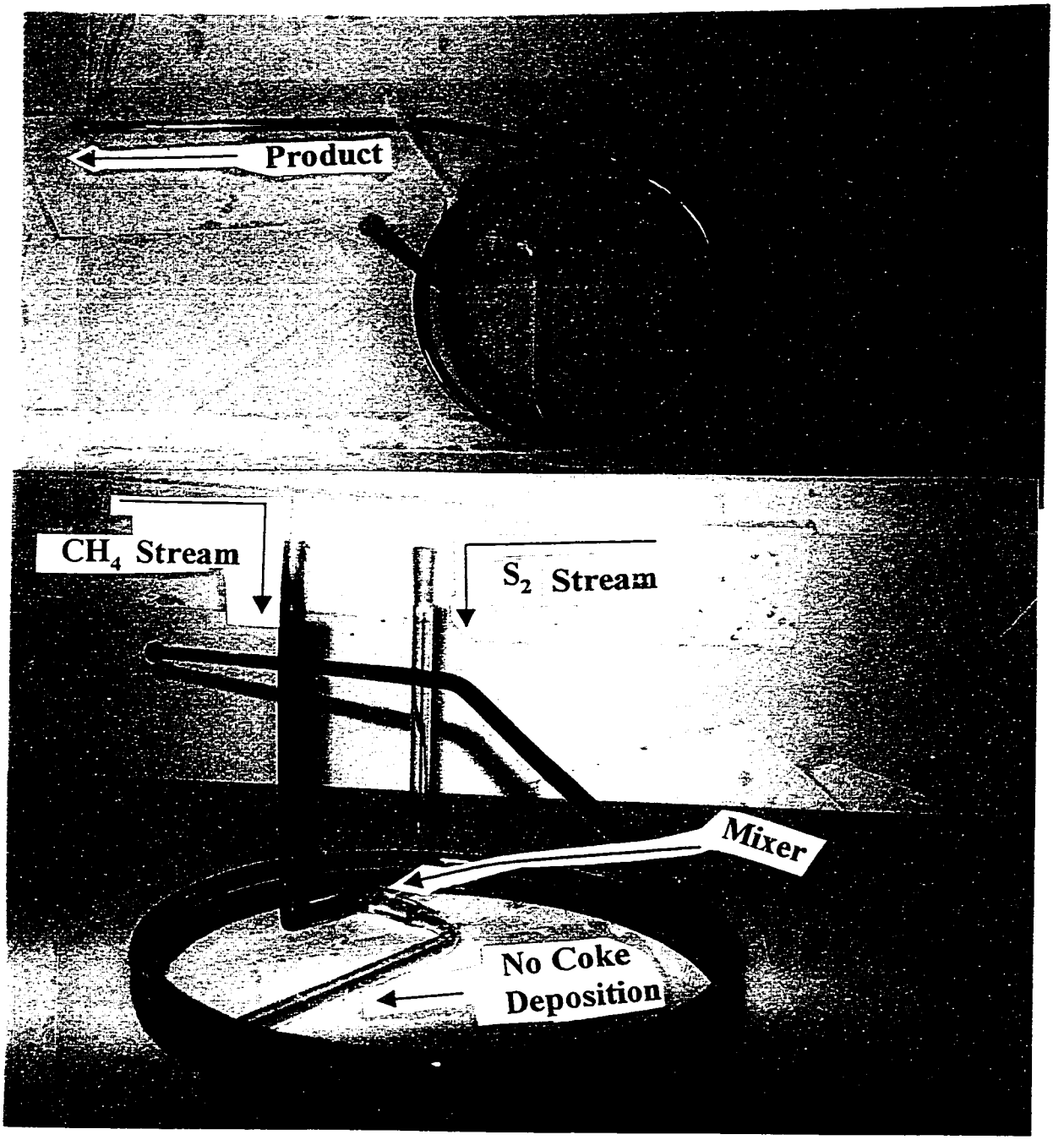

Figure 5.31 Pictures of the reactor showing coke deposition during reaction between CH_4 and sulfur.

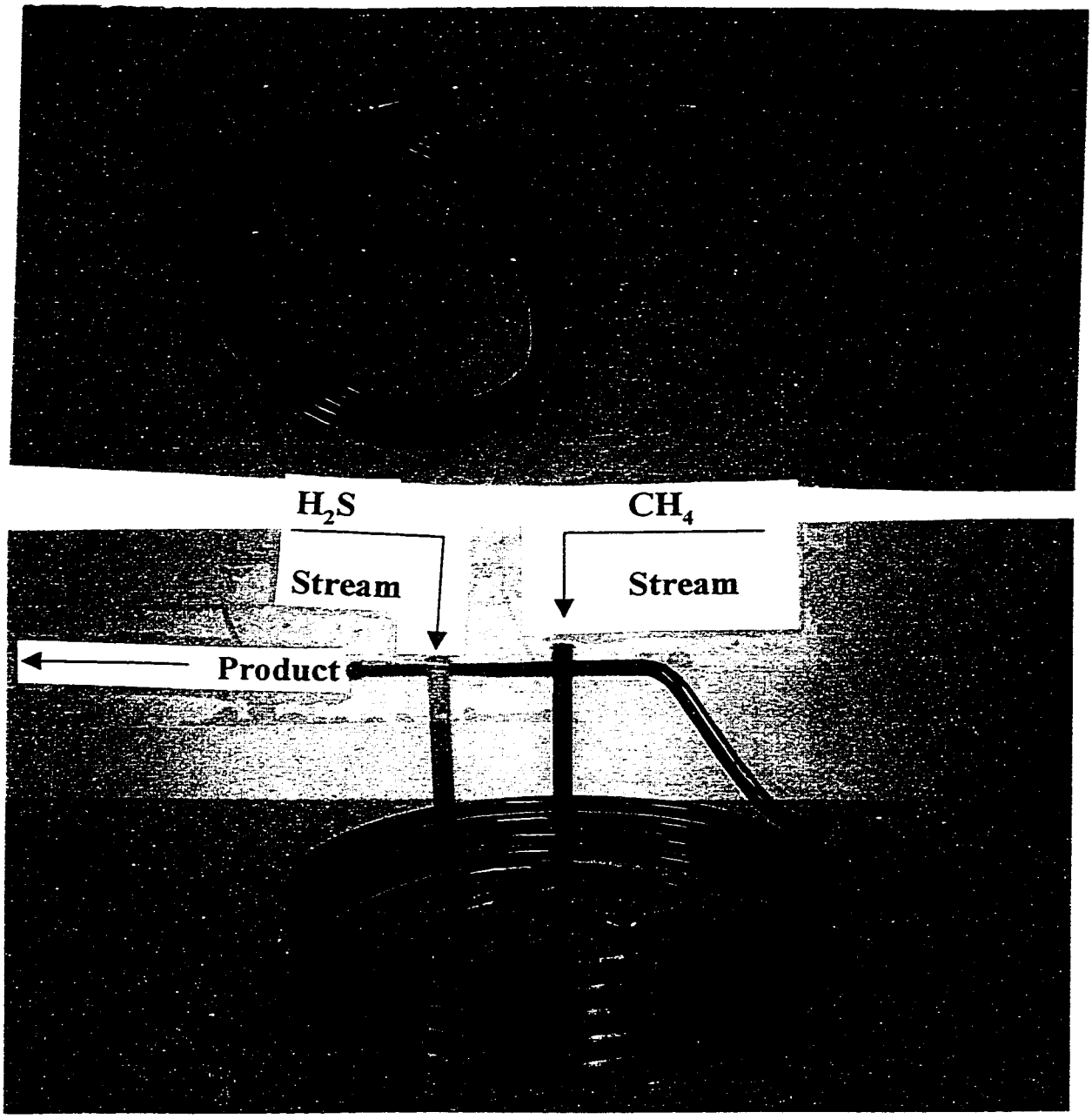

Figure 5.32 Pictures of the reactor showing coke deposition during reaction between CH_4 and H_2S .

Further experimental evidence is required to find out whether sulfur actually acts as an inhibitor to the coking reaction or it acts as an inhibitor to the coke deposition mechanism. Moreover, investigation into the reaction mechanism involved also needs to be conducted.

5.10 Material balance on the reacting systems

Material balance on the reacting systems were done to improve the level of confidence on the experimental data obtained. For simple systems such as H_2S cracking reaction, COS decomposition reaction and reaction between CO_2 and H_2 where only limited chemical species were present in the product, the material balance was relatively easy. For reacting systems such as reaction between CO_2 and H_2S where a relatively larger number of chemical species were present in the product stream (CO, COS, H_2, H_2O, S_2, CO_2, H_2S) the material balance was complicated because all species were not analyzed (H_2O and elemental sulfur). Material balances for both simple and complex systems are provided below.

Simple systems

The hydrogen balance for the reacting system relevant to H_2S decomposition reaction showed a maximum deviation of 6 percent. The hydrogen balance was done by calculating the total mole fraction of H containing species (i.e. H_2 and H_2S) measured in the product stream and comparing that with the total mole fraction of H containing species in the feed (i.e. H_2S). Only a few experimental runs were conducted for which both H_2 and H_2S concentrations in the product stream were measured. The carbon balance done on the reacting system involved in the COS decomposition reaction showed agreement to within 4 percent. The material balance was done by calculating the total mole fraction of C containing species (i.e. CO and COS) in the product and comparing it with the mole fraction of C containing species in the feed (i.e. COS).

Complex systems

The carbon balance for the reacting system of CO_2 and H_2S were done by calculating the total mole fraction of C containing species (CO_2, CO, COS) in the product and comparing it with the mole fraction of C containing species in the feed (CO_2). The agreement between the two was less than 5 percent on an average and the maximum difference was less than 10 percent.

For reacting systems containing CH_4 as a reactant (CH_4 + H_2S and CH_4 + S mixtures), the carbon balance ranged from poor (greater than 20 percent) to good (less than 4 percent). Some of the causes of poor material balance on carbon were the formation of coke that was not analyzed, and formation of a number of products of methane pyrolysis , all of which were not analyzed.

Chapter 6

Reaction Kinetic Studies on Acid Gas Mixtures

6.1 General Introduction

In the previous chapter, the results of the experiments performed for individual reactions were presented. In this chapter the results of the experiments on the partial oxidation of acid gas mixtures are presented. It is important to realize that experimental data on the partial combustion of acid gas components and mixtures are scarce. It is, therefore, essential to conduct experiments under controlled conditions to obtain reliable information that may elucidate the important reaction mechanism involved in acid gas combustion. A systematic approach was, therefore, taken to conduct a series of experiments on partial oxidation of acid gas mixtures and their components. An effort was made to simulate the experimental conditions using a detailed kinetic reaction mechanism.

In this Chapter, the experimental and simulation results have been presented in four sections. The first dealing with the partial oxidation of H_2S, the second with the partial oxidation of CH_4 and H_2S, the third with the partial oxidation of CO_2 and H_2S mixtures and finally a fourth with the partial oxidation of CO_2, H_2S and CH_4 mixtures. Experiments were conducted at three temperatures 1000 °C, 1100 °C and 1200 °C, which covers the typical operational temperature range of the Claus furnaces. The gas residence time in the reactors ranged from 100 ms to 1.35 s.

6.2 Oxidation of H_2S

6.2.1 Literature review

Several experimental studies on the oxidation of hydrogen sulfide in flames and in shock tubes have been reported in the literature [Levy and Merryman, 1965; Merryman and Levy, 1967; Bradley and Dobson, 1967; Muller et al., 1979; Frenkenlach et al., 1981; Cambot et al., 1982; Tsuchiya et al., 1997]. In fact, detailed reaction mechanism comprising several elementary reactions have also been proposed (Frenkenlach et al., 1981 and Tsuchiya et al., 1997). The studies by Levy and Merryman [Levy and Merryman, 1965; Merryman and Levy, 1967] and by Bradley and Dobson [1967a, 1967b] were carried out during the same period. Levy and Merryman reported studies on actual hydrogen sulfide flames in an H_2S-O_2-N_2 system whereas Bradley and Dobson studied the oxidation of hydrogen sulfide in shock tubes. Muller et al. (1978) conducted their experiments with fuel rich flames doped with low concentrations of H_2S. They also reported a detailed kinetic analysis of the sulfur chemistry involved in such flames. Cambot et al. (1981) conducted experiments on hydrogen sulfide flames in air with an objective to develop sulfur formation mechanism in the Claus process. Their experiments involved a study on H_2S diffusion flames. Frenkenlach et al. (1981) conducted shock tube experiments with 4 to 22% H_2S in air at temperatures ranging from 950 to 1200 K. They reported a very detailed reaction mechanism for the H-S-O system. The reaction mechanism comprised of 56 forward and their associated reverse elementary reactions. Recently, Tsuchiya et al. (1997) have reported a study in which the hydrogen sulfide oxidation mechanism was developed. They proposed a thirty-reaction mechanism, which was briefly discussed in Chapter 5.

From the review of literature it was found that a considerable amount of kinetic information on hydrogen sulfide oxidation is available both in form of experimental data and as reaction kinetics. For this study, it was thought that it might be useful to gather experimental information on H_2S oxidation prior to obtaining information on partial oxidation of acid gas mixture containing H_2S presence of either CO_2 or CH_4 or both.

6.2.2 Experimental

Experiments on hydrogen sulfide oxidation were conducted by reacting 1.65 mol% H_2S with 1.0 mol% O_2 at three different temperatures of 1000 °C, 1100 °C and, 1200 °C in the four reactors of lengths 1.6 m, 3.2 m, 6.4 m and 16.0 m. The total flow rate of gases were maintained at 4.0 L/min and the inlet pressures varied from 98 kPa to 125 kPa. Two of the products of the hydrogen sulfide oxidation, water and sulfur were removed in the water-sulfur trap prior to the analysis of the product stream for gas composition. The product stream was analyzed for H_2S and SO_2. For the analysis of hydrogen duplicate runs were performed and analysis performed on GC with Argon as carrier gas.

6.2.2.1 Experimental results

H_2S and SO_2 concentration profiles

The plots of H_2S and SO_2 concentrations measured at the exit of the four reactors are presented in Figures 6.1 for the three temperatures of 1000 °C, 1100 °C and 1200 °C. The results indicate that the actual H_2S oxidation reactions are extremely rapid. No measurable trace of oxygen was observed in the product stream for the shortest reactor, which means that a complete O_2 consumption was achieved in less than 115 ms.

It can be observed from Figure 6.1 that a maximum in SO_2 concentration is reached at a value of 0.8 mol%, this indicates that 80 percent of the oxygen is consumed to form SO_2 via the following overall reaction.

$$H_2S + O_2 \quad \leftrightharpoons \quad SO_2 + H_2 \qquad (6.1)$$

It can also be observed that both the H_2S and SO_2 concentrations show a decreasing trend with an increase in residence time. It may be tempting to believe that the perhaps the main Claus reaction is occurring:

$$2H_2S + SO_2 \quad \leftrightharpoons \quad 3/x\ S_x + 2H_2O \qquad (6.2)$$

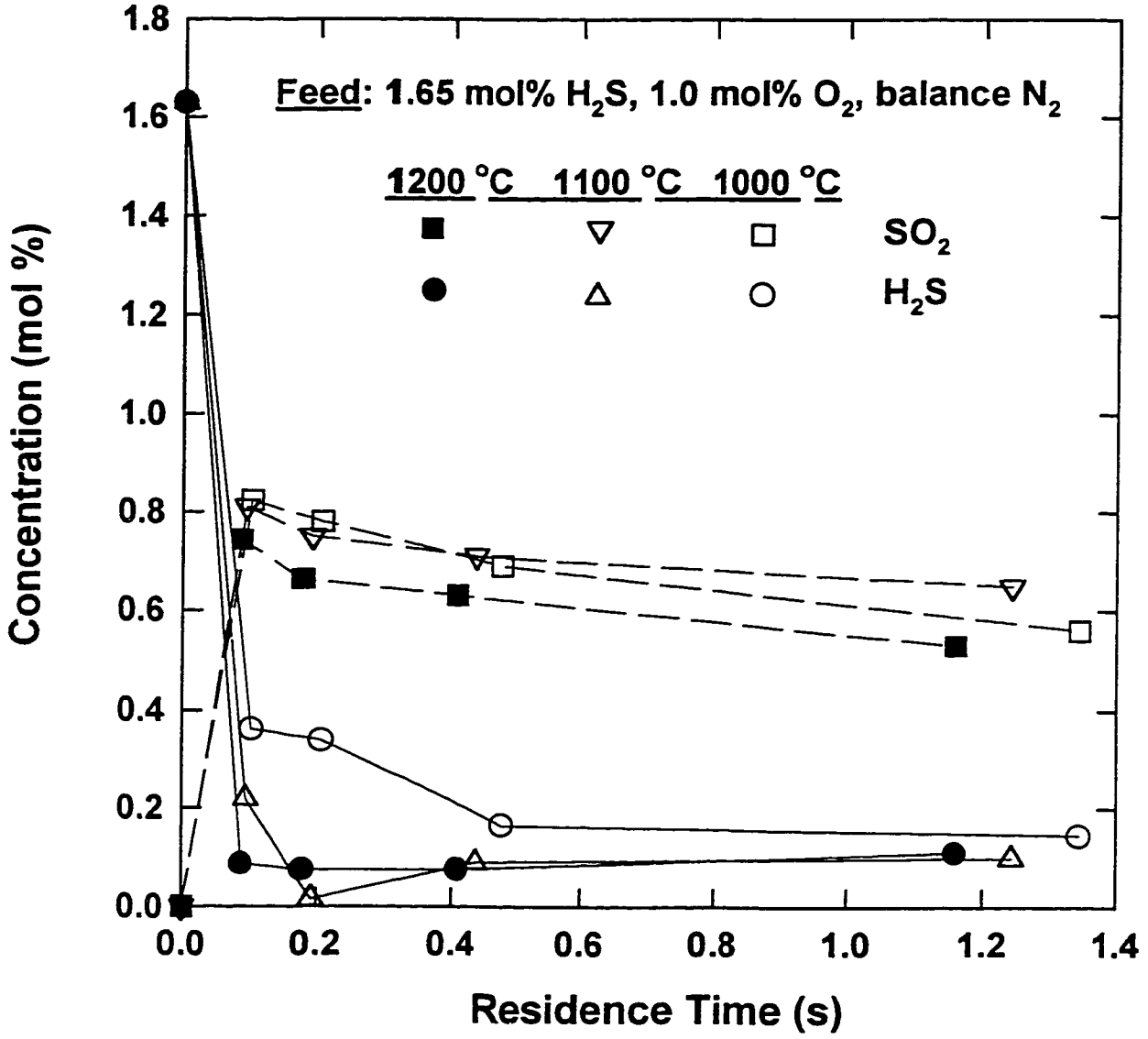

Figure 6.1 Measured concentrations of SO_2 and H_2S as a function of gas residence time for a feed of 1.65 mol% H_2S, 1.0 mol% O_2 and balance N_2.

However, the consumption of SO_2 may be due to another reaction, as it is discussed later.

H_2 concentration profile

For the same feed conditions, the hydrogen concentration is also plotted as a function of the residence time in the reactor for three furnace temperatures in Figure 6.2 The results indicate that a majority of the hydrogen is produced during the initial reaction times when oxidation reactions are occurring. At the lowest temperature (1000 °C), the least hydrogen concentrations are observed. This may be due to the fact that hydrogen sulfide decomposition is limited at lower temperatures.

For the higher temperatures (>1100 °C), the results indicate that the production of hydrogen is not kinetically limited and also that the decomposition of hydrogen sulfide into hydrogen is accelerated in the presence of oxygen. One of the interesting feature of the Figure 6.2 is the occurrence of a lower hydrogen concentration for temperature 1200 °C than that for 1100 °C. It may be possible that at the higher temperatures, a larger amount of H_2 is produced but is being rapidly consumed by the following reduction reaction:

$$2H_2 + SO_2 \quad \rightleftharpoons \quad 2H_2O + 1/x\ S_x \qquad (6.3)$$

The occurrence of this reaction may also explain increased SO_2 consumption at higher residence times.

SO_2 and H_2O concentration profiles

The plots of H_2O and S_2 concentrations are presented in Figure 6.3 It should be pointed out that these concentrations are estimated and do not represent actual measured concentrations. The key point to note from the Figure is that at 1100 °C, the H_2O concentration at later residence times is the least. This is consistent with the observation of a higher H_2 concentration at 1100 °C, i.e. from the material balance for hydrogen element.

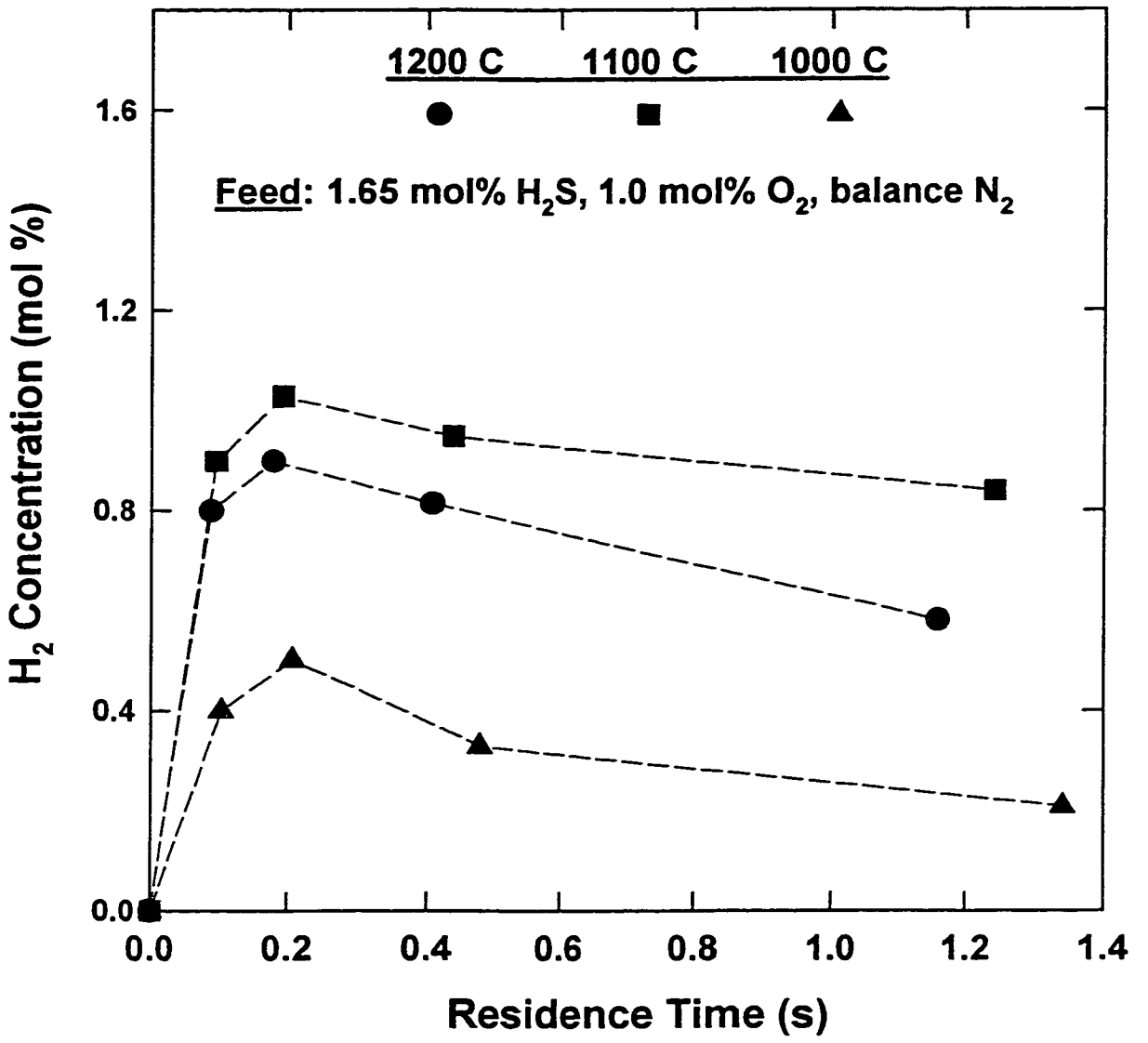

Figure 6.2 Measured H_2 concentrations as a function of gas residence time for a feed of 1.65 mol% H_2S, 1.0 mol% O_2 and balance N_2.

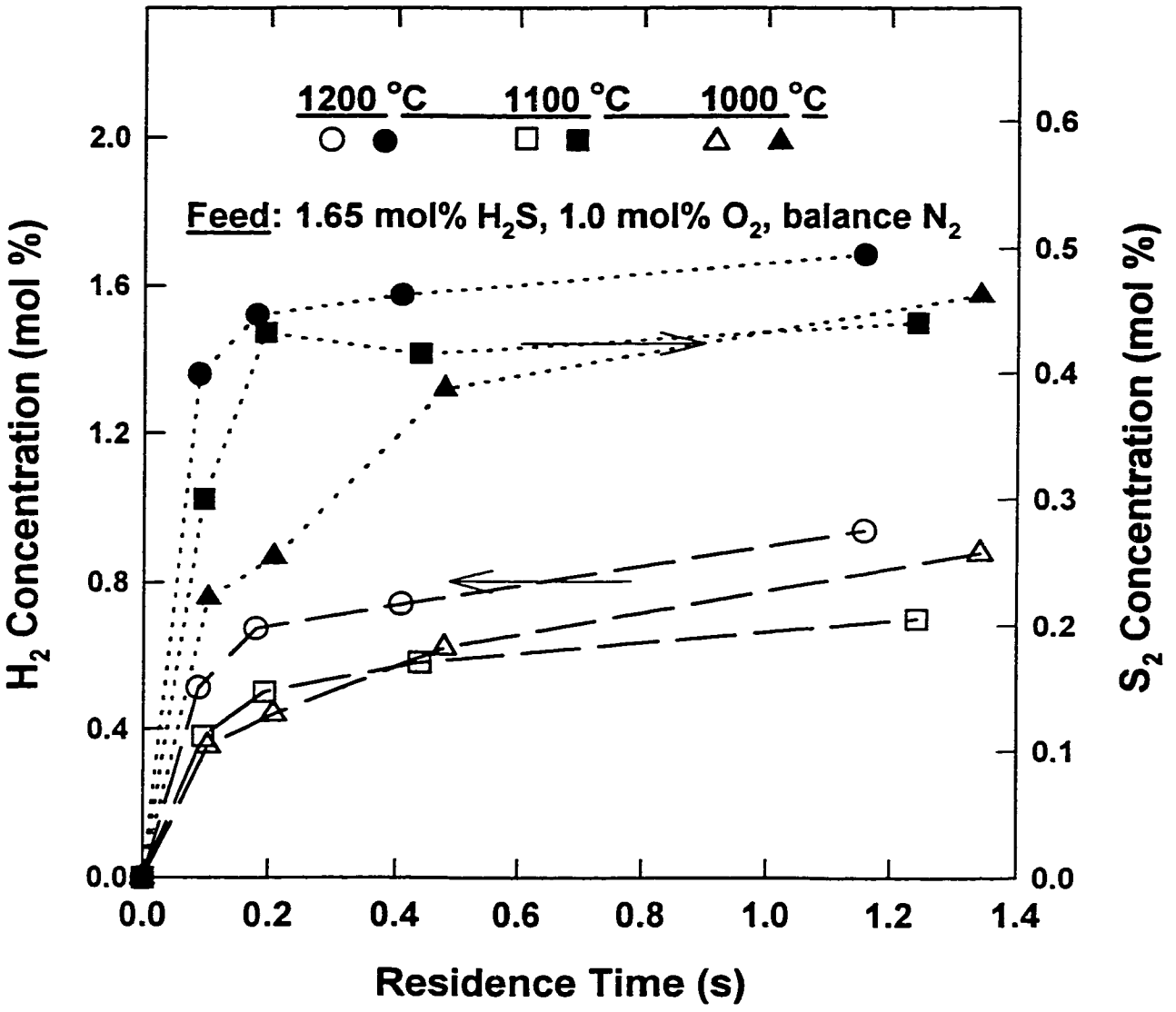

Figure 6.3 S_2 and H_2O concentrations estimated from the element balance equations for feed of 1.65 mol% H_2S, 1.0 mol% O_2 and balance N_2

6.2.3 Kinetic simulation and modeling

A kinetic simulation of the partial oxidation of H_2S, based on the simplified reaction mechanism proposed by Tsuchiya et al. (1997) was first attempted. The reaction mechanism has already been presented in Section 5.3. A computer program was written to calculate the concentration of various species as function of residence time. The details of the program are discussed under section 5.3

Calculations were performed to simulate the experimental conditions. The simulation results showing the temporal profiles of H_2S and SO_2 are presented in Figure 6.4. It can be seen that the trends of decreasing H_2S and SO_2 concentrations with increasing residence time are predicted for the temperatures 1100 °C and 1200 °C. However, for the lower temperature (1000 °C), the H_2S concentrations exhibit decreasing trend while the SO_2 concentrations show a flatter profile. It is easy to attribute the discrepancy between the data and predictions to the inadequacy of the kinetic reaction scheme used for simulation, which does not account for all possible interactions of various species that occur during the experiments. Moreover, the observed data is a factual evidence and cannot be changed, the only change could be done was in the kinetic scheme.

It was thought that the reaction mechanism did not include the HSO_2 reactions that may play an important role. Therefore, to simulate the decreasing SO_2 trends, additional reactions were included in the reaction scheme. These reactions involving HSO_2 species were as follows:

$$H + SO_2 \rightleftharpoons HSO_2 + M \qquad (6.4)$$

$$H + HSO_2 \rightleftharpoons SO_2 + H_2 \qquad (6.5)$$

$$OH + SO + M \rightleftharpoons HSO_2 + M \qquad (6.6)$$

$$OH + HSO_2 \rightleftharpoons SO_2 + H_2O \qquad (6.7)$$

The kinetics for the above reactions was obtained from Zachchariah and Smith (1987). The inclusion of these reactions in kinetic scheme for simulation did not

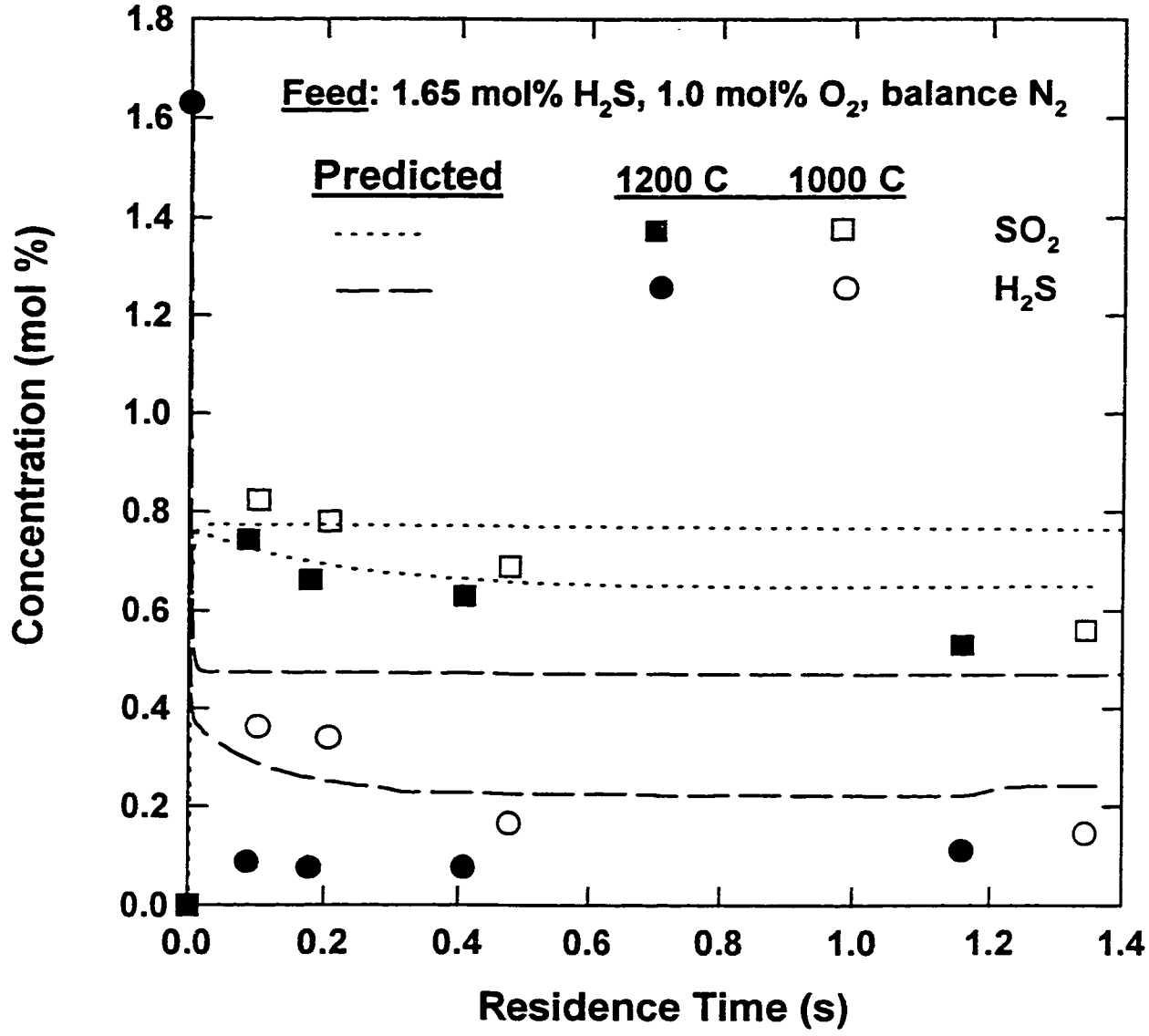

Figure 6.4 A comparison of measured and kinetic model predicted SO_2 and H_2S concentrations for a feed of 1.65 mol% H_2S, 1.0 mol% O_2 and balance N_2.

[Predicted from 30 reaction scheme of Tsuchiya et al. (1997)]

change the predicted trends of SO_2. After further investigation of the literature, the following three reactions on SO_2 reduction proposed by Cambot et al. (1981) were included:

$$H + SO_2 \rightleftharpoons SO + OH \quad (6.8)$$

$$S + SO_2 \rightleftharpoons 2\,SO \quad (6.9)$$

$$H + SO \rightleftharpoons S + OH \quad (6.10)$$

The reaction 6.8 was already included in the 30 reaction mechanism proposed by Tsuchiya et al. (1997). For calculations in this study, the reaction kinetics for reactions 6.9 and 6.10 were obtained from Zachariah and Smith (1987). The predictions of H_2S and SO_2 concentrations, with the inclusion of the two reactions in the kinetic scheme, are shown in Figure 6.5. It can be observed that SO_2 profile at 1200 °C demonstrates the decreasing trend with increasing residence time. However, the predicted SO_2 profile at 1000 °C remained unaffected. A few reasons for this deviation can be proposed. The first reason, obviously is that the reaction mechanism used in the written program does not include other possible key reactions. The second reason may be that the actual gas temperature may be higher than the furnace set point temperature for the experiments. For higher temperatures, the program predicts a decreasing trend for SO_2 concentration with increasing residence time. The higher gas temperatures in the experiments may be attributed to the heat of reaction effects. Although the gas mixtures are highly dilute (> 95 %), the heat released from the complete combustion of H_2S may be high and an increase in temperature of the order of 50-100 °C (estimated from enthalpy balance) may occur. Another reason for the deviation between the data and predictions may de due to the fact that the simulation is not accounting for any reaction occurring during the cooling and in the post-cooling zone. In absence of supporting evidence for any of these hypotheses, the question pertaining to the discrepancy between data and model predictions may need further investigation.

The predicted H_2 profiles are compared with data in Figure 6.6. For 1200 °C, the predicted H_2 profile shows a sharp decrease after a maximum H_2

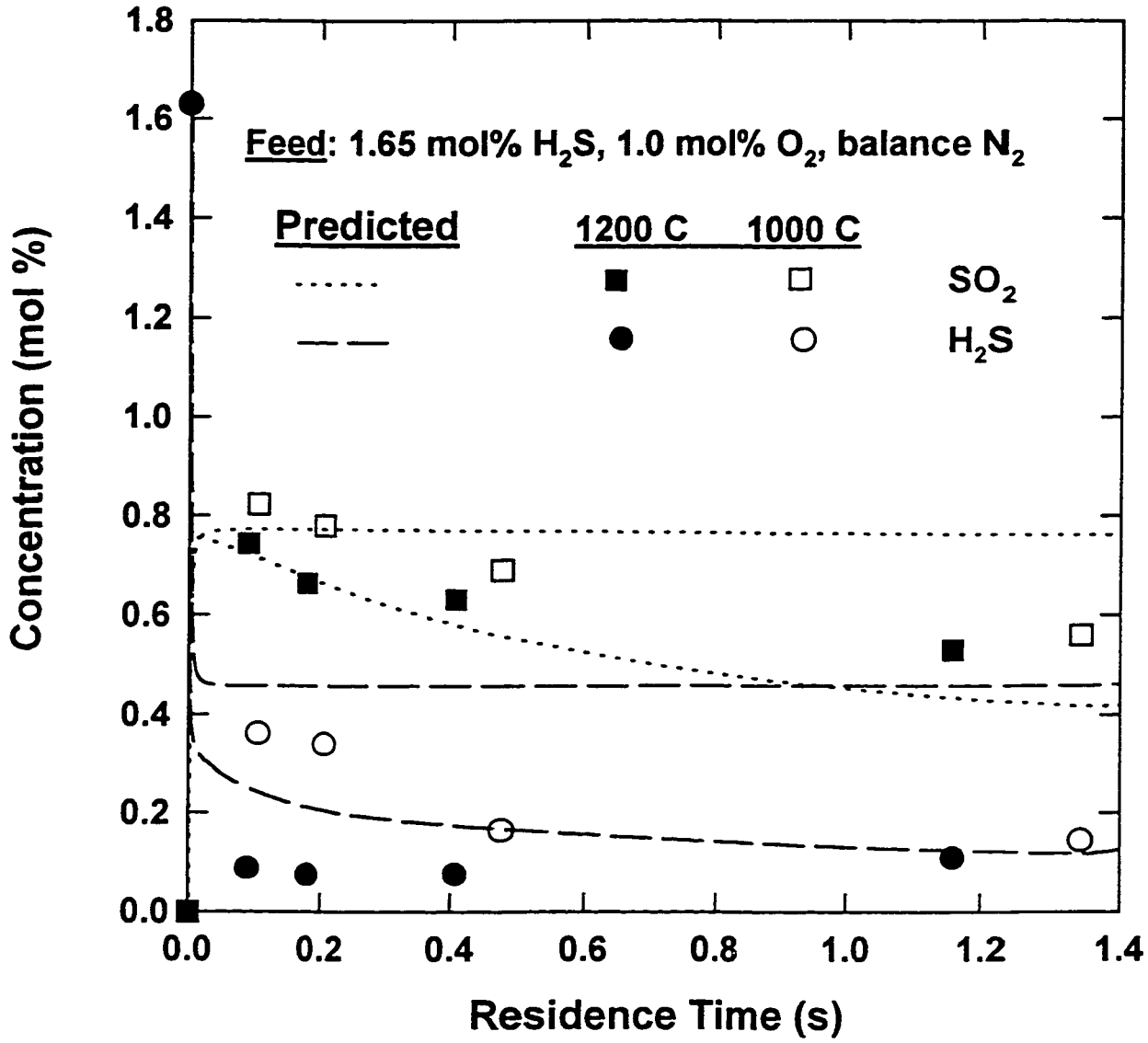

Figure 6.5 A comparison of measured and predicted SO_2 and H_2S concentration profiles for a feed of 1.65 mol%, 1.0 mol% O_2 and balance nitrogen.

[Predicted from 30 reaction scheme of Tsuchiya et al. (1997) + 6 other H-S-O reactions (see text)]

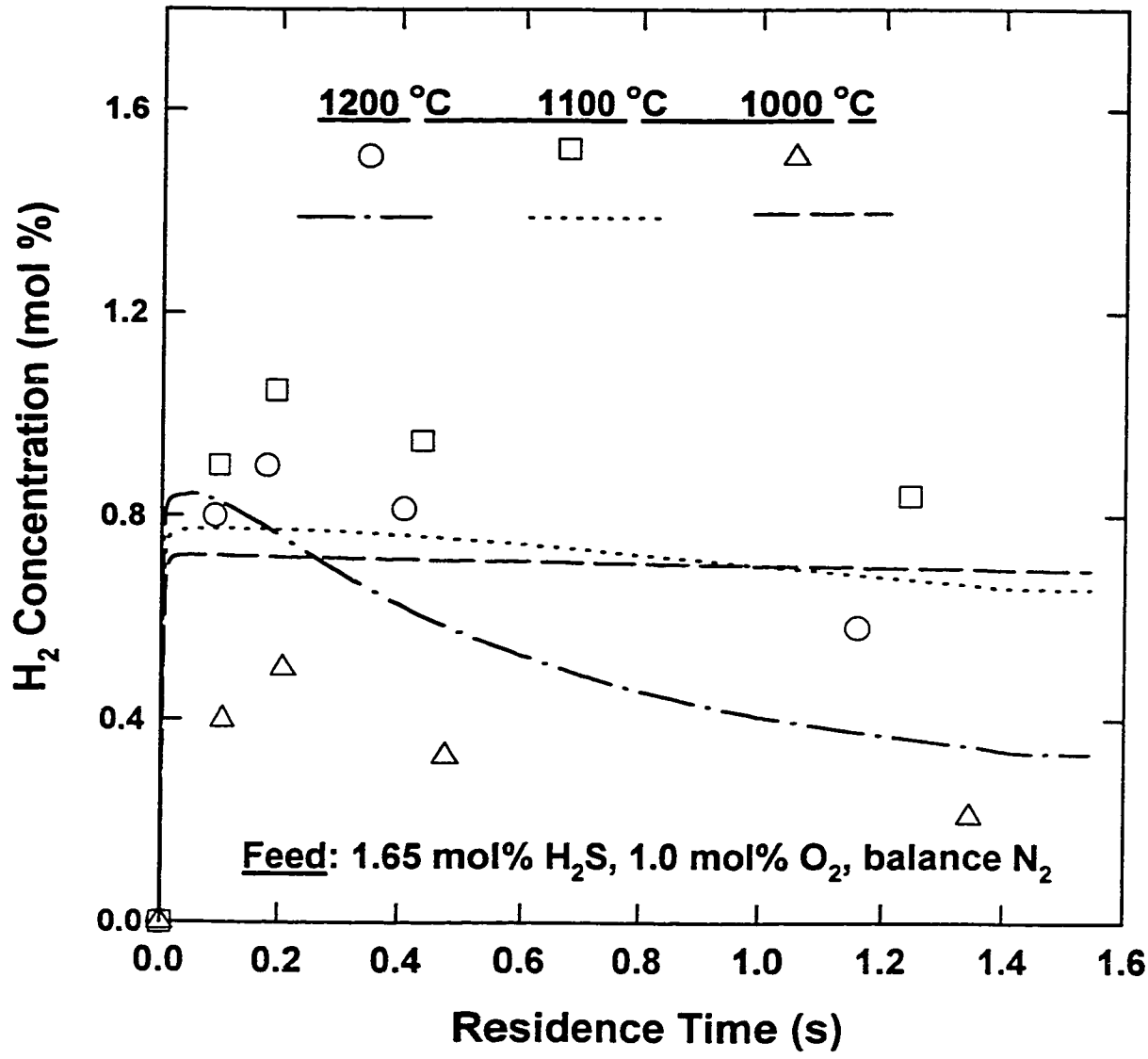

Figure 6.6 A comparison of measured and predicted H_2 concentrations for a feed of 1.65 mol% H_2S, 1.0 mol% O_2 and balance N_2.

[Predicted from 30 reaction scheme of Tsuchiya et al. (1997) + 6 other H-S-O reactions]

concentration is reached at less than 100 ms. For the other temperatures, the H_2 concentration reaches the maxima around the same time but maintains a rather flatter profile. Again, further investigation is necessary to find the actual cause for the deviation between the data and model.

6.3 Partial oxidation of (CO_2+H_2S) mixtures

The major purposes of these experiments were to obtain information on the formation of CO under oxidizing conditions and to find how the H_2S oxidation and the SO_2 formations are affected by the presence of CO_2. While CO_2 may first appear to be inert from an oxidation-reaction point of view, it does participate in the reactions and acts as an oxidizing agent. It must be mentioned here that similar work have been reported by Clark et al. (1997 and 1998). However, they conducted their experiments in alumina tubes. Also, the experiments were not run under dilute conditions. The exothermic oxidation reactions may cause the gas temperatures to be much higher (> 200 °C) than that set by the furnace in which the alumina reactor is placed.

6.3.1 Experimental

6.3.1.1 Experimental conditions

Experiments were conducted in four reactors of lengths 1.6, 3.2, 6.4 and 16.0m at three temperatures of 1000 °C, 1100 °C and, 1200 °C. The total flow rate of gas was maintained at 4.0 L/min. The inlet pressures varied from 98 kPa to 125 kPa. The product gas stream was analyzed for CO_2, CO, CO, H_2S and SO_2. Six different acid gas mixtures were prepared. The gas composition for the six mixtures were as follows:

Acid Gas Mixture	H_2S (mol %)	CO_2 (mol%)	O_2 (mol%)
AG-1	0.42	1.70	0.30
AG-2	1.65	1.70	1.00
AG-3	3.32	1.70	2.00
AG-4	1.65	3.40	1.00
AG-5	0.83	0.88	0.50
AG-6	1.65	0.44	1.00

The gas mixture compositions were selected to study the effect of one component on the formation various species while keeping the other variables constant.

6.3.1.2 Experimental results

6.3.1.2.1 CO formation

The formation of carbon monoxide is expected to be directly influenced by the CO_2 content of the acid gas. Further, if it is assumed that the main CO forming reaction is the water gas shift reaction, the presence of hydrogen will also directly influence the CO formation. Hydrogen is not present in the feed mixture, but is produced from hydrogen sulfide during the oxidation reaction or in the post-oxidation period. The effects of the H_2S and CO_2 content of the acid gas mixtures on CO formation are presented next.

Effect of CO_2 content in acid gas mixture on CO formation

In Figures 6.7 and 6.8, the measured CO concentrations at the reactor exit produced from three acid gas mixtures, have been presented. In Figure 6.7, the data at lower temperature (1000 °C) are presented while in Figure 6.8, the data at 1200 °C are presented. The data in both the Figures exhibit the expected trends of increasing CO concentration with residence time and increasing CO_2 content of the acid gas mixtures.

Effect of H_2S content in acid gas mixtures on CO formation

The effect of H_2S content of acid gas mixtures on CO production was examined and the data of the experiments are presented in Figures 6.9 and 6. 10. In Figure 6.9, the data at 1000 °C are presented while in Figure 6.10, the data at 1200 °C is presented. Again, both Figures exhibit the expected trends of an increasing CO concentration with residence time and with increasing H_2S content of the acid gas mixtures. A higher H_2S content would mean an increased concentration of H_2

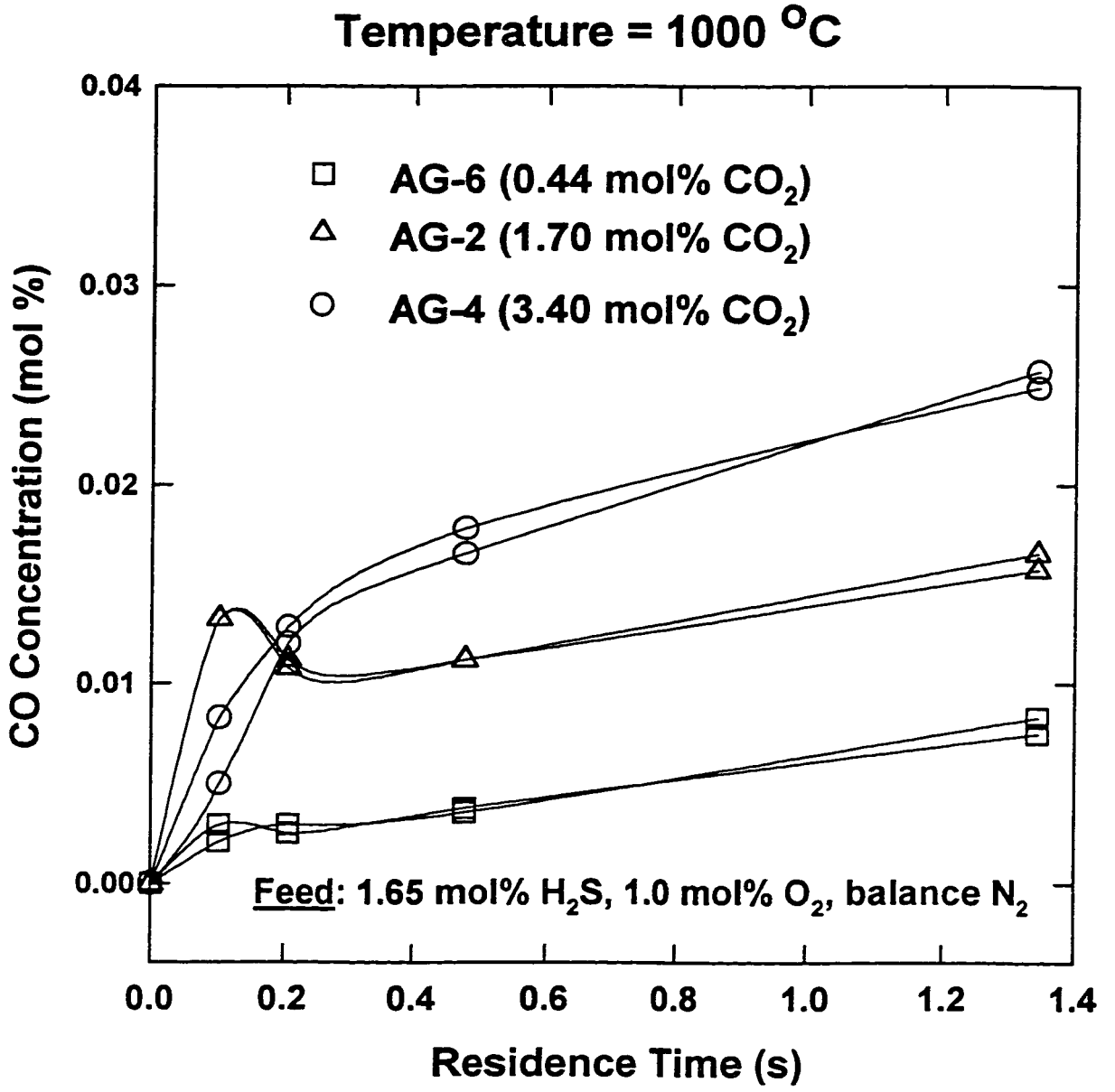

Figure 6.7 Effect of CO_2 content of acid gas mixture on CO formation at 1000 °C for a feed of 1.65 mol% H_2S, 1.0 mol% O_2, varying amount of CO_2 and balance N_2.

(Lines are trendlines only)

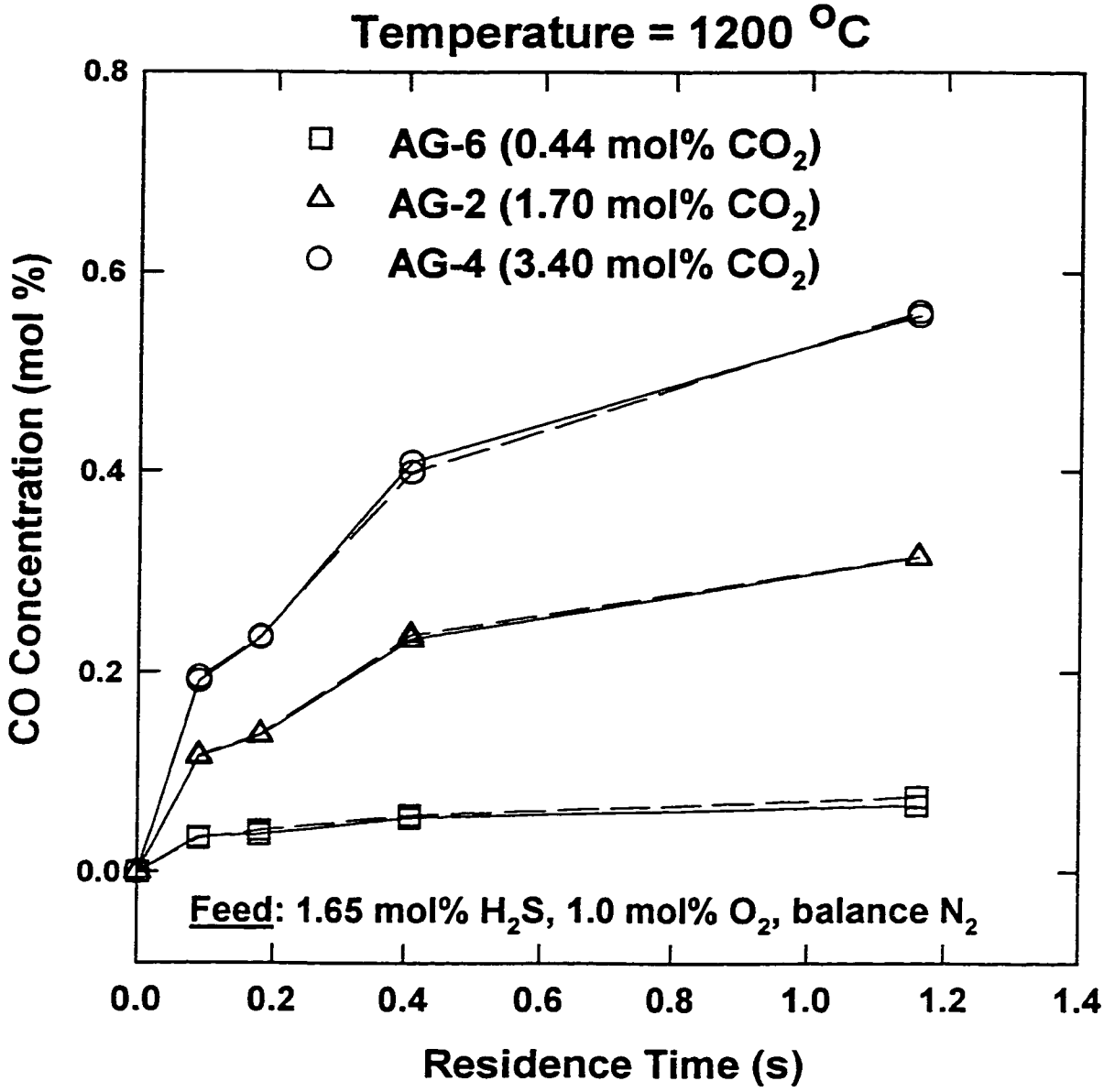

Figure 6.8 Effect of CO_2 content of acid gas mixture on CO formation at 1200 °C for feeds containing 1.65 mol% H_2S, 1.0 mol% O_2, varying amounts of CO_2 and balance N_2

(Lines are trendlines only)

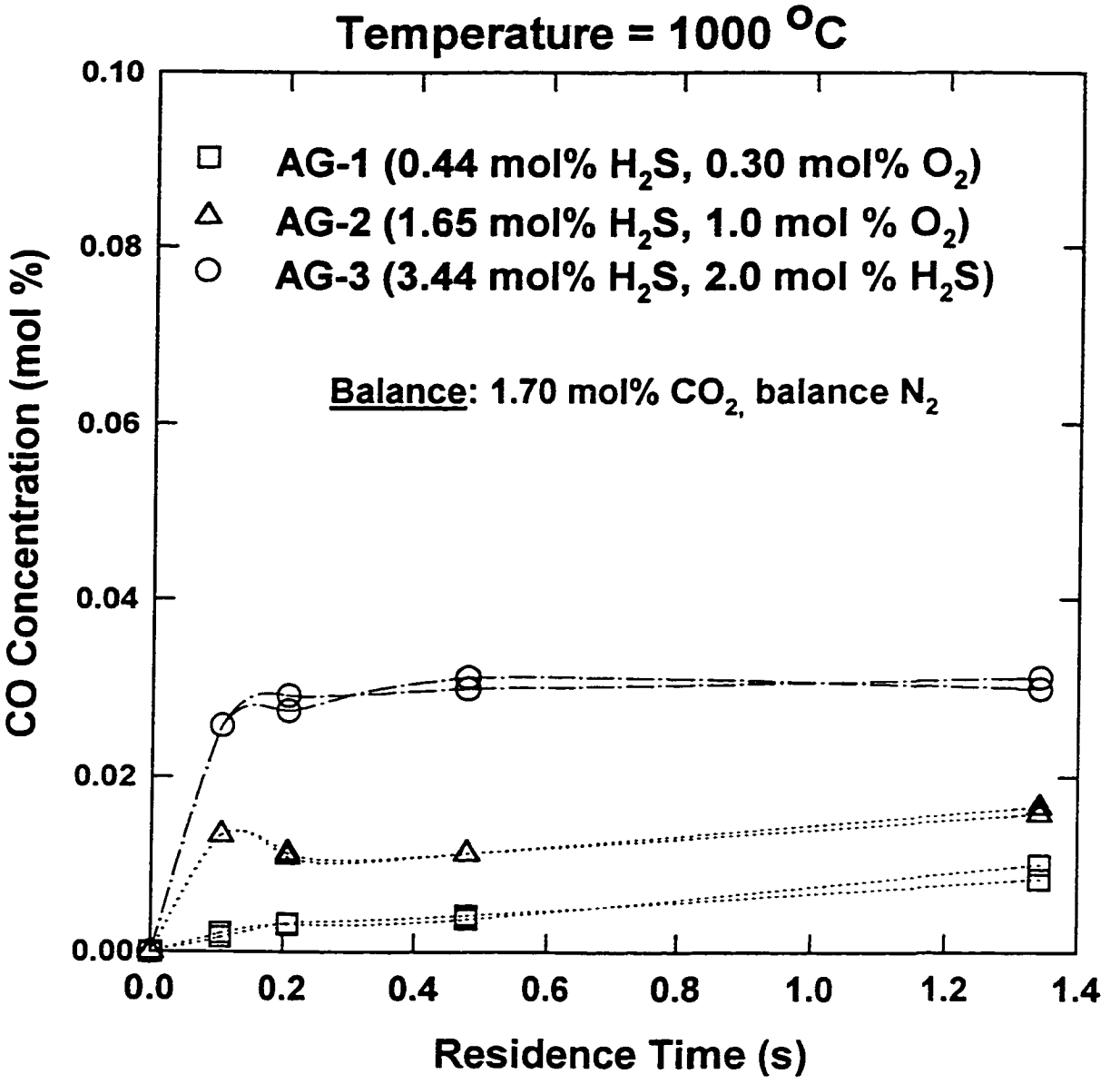

Figure 6.9 Effect of H_2S content of acid gas mixture on CO formation at 1000 °C for feeds of 1.65 mol% H_2S, 1.0 mol% O_2, varying amounts of CO_2, balance N_2.

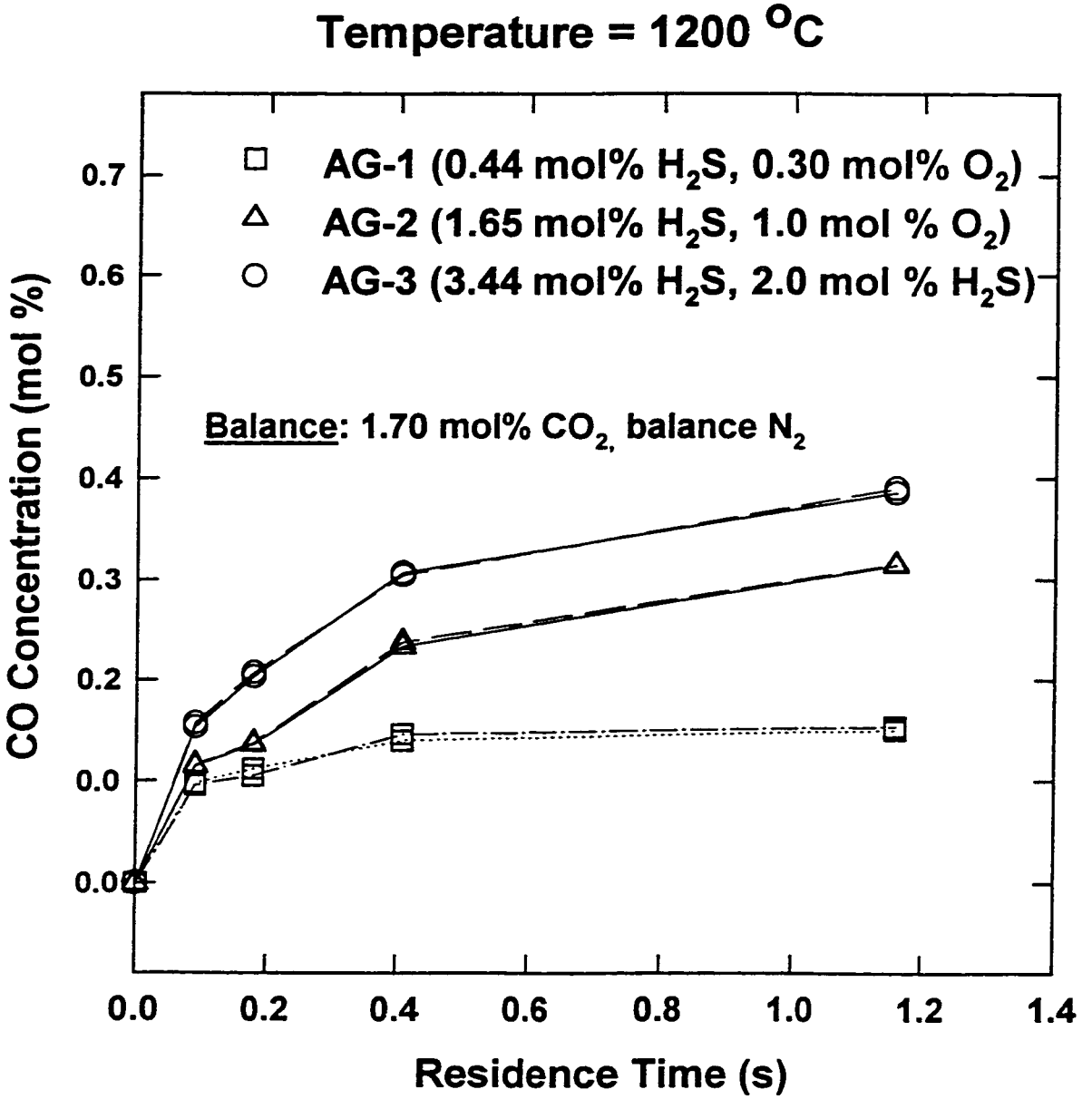

Figure 6.10 Effect of H_2S content of acid gas mixture on CO formation at 1200 °C for feeds of 1.70 mol% CO_2, varying amounts of H_2S + O_2 and balance N_2.

or H species, which are responsible for the CO production via reaction between CO_2 and H atom.

6.3.1.2.2 SO_2 formation

Effect of the CO_2 content in feed gas on SO_2 Formation

The effect of CO_2 content of the acid gas mixtures on SO_2 formation is presented in Figure 6.11. The data at 1000 °C are presented in this Figure. The SO_2 profiles are almost identical for all four gas mixtures indicating no effect of CO_2 content on SO_2 profiles. The data at 1200 °C, presented in Figure 6.12, however show a dependence of SO_2 profiles on the CO_2 concentration in the initial reacting mixture. The SO_2 concentrations show a smaller rate of decline at higher gas residence times with an increase in the CO_2 content of the acid gas mixtures. One possible reaction mechanism that can explain the observation involves the following two reactions:

$$2H_2 + SO_2 \leftrightharpoons 2H_2O + 1/x\ S_x \qquad (6.3)$$

$$H_2 + CO_2 \leftrightharpoons H_2O + CO \qquad (6.12)$$

In the absence of CO_2, the decrease of SO_2 is due to the consumption via reaction 6.3. In acid gas mixtures containing CO_2, the consumption of hydrogen at higher temperatures occurs via reaction 6.12, which may be more rapid than reaction 6.3. Further, the H_2 consumption via reaction 6.12 produces H_2O which, is also one of the products of reaction 6.3. The production of H_2O via reaction 6.12 will also drive the reaction 6.3 to the left resulting in higher SO_2 formation.

6.3.2 Kinetic simulation and modeling

The formation of CO and other species during the oxidation of acid gas mixtures of H_2S and CO_2 were predicted from the computer program written to simulate hydrogen sulfide oxidation. Only one reaction and its associated reverse reaction involving CO_2 was added to the kinetic scheme for H_2S oxidation, to account for CO forming reaction. The formation of CO via the overall water gas shift reaction

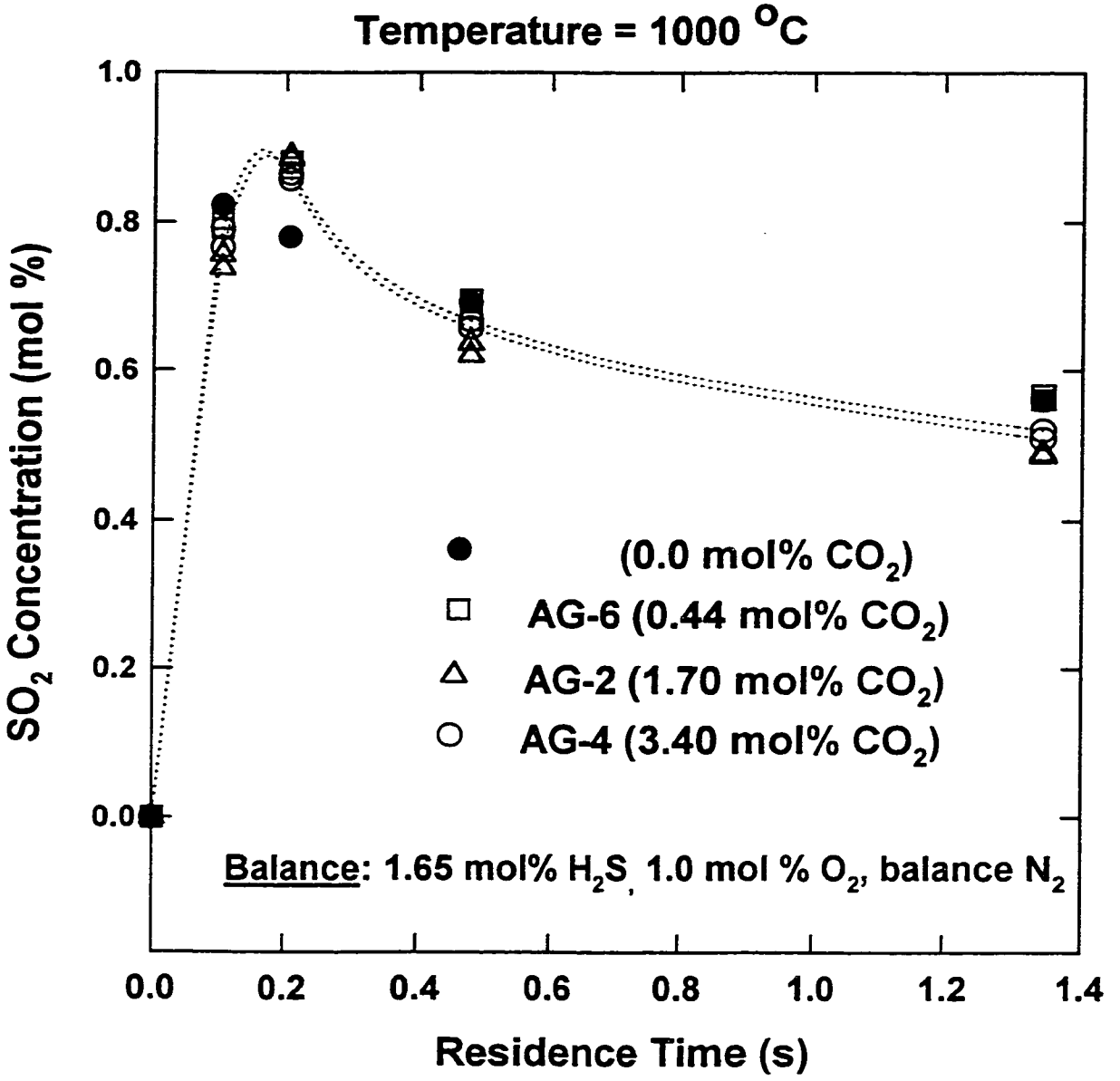

Figure 6.11 Effect of CO_2 content of acid gas mixture on SO_2 formation at 1000 °C for feeds of 1.65 mol% H_2S, 1.0 mol% O_2, varying amounts of CO_2, balance N_2.

(Lines are trendlines)

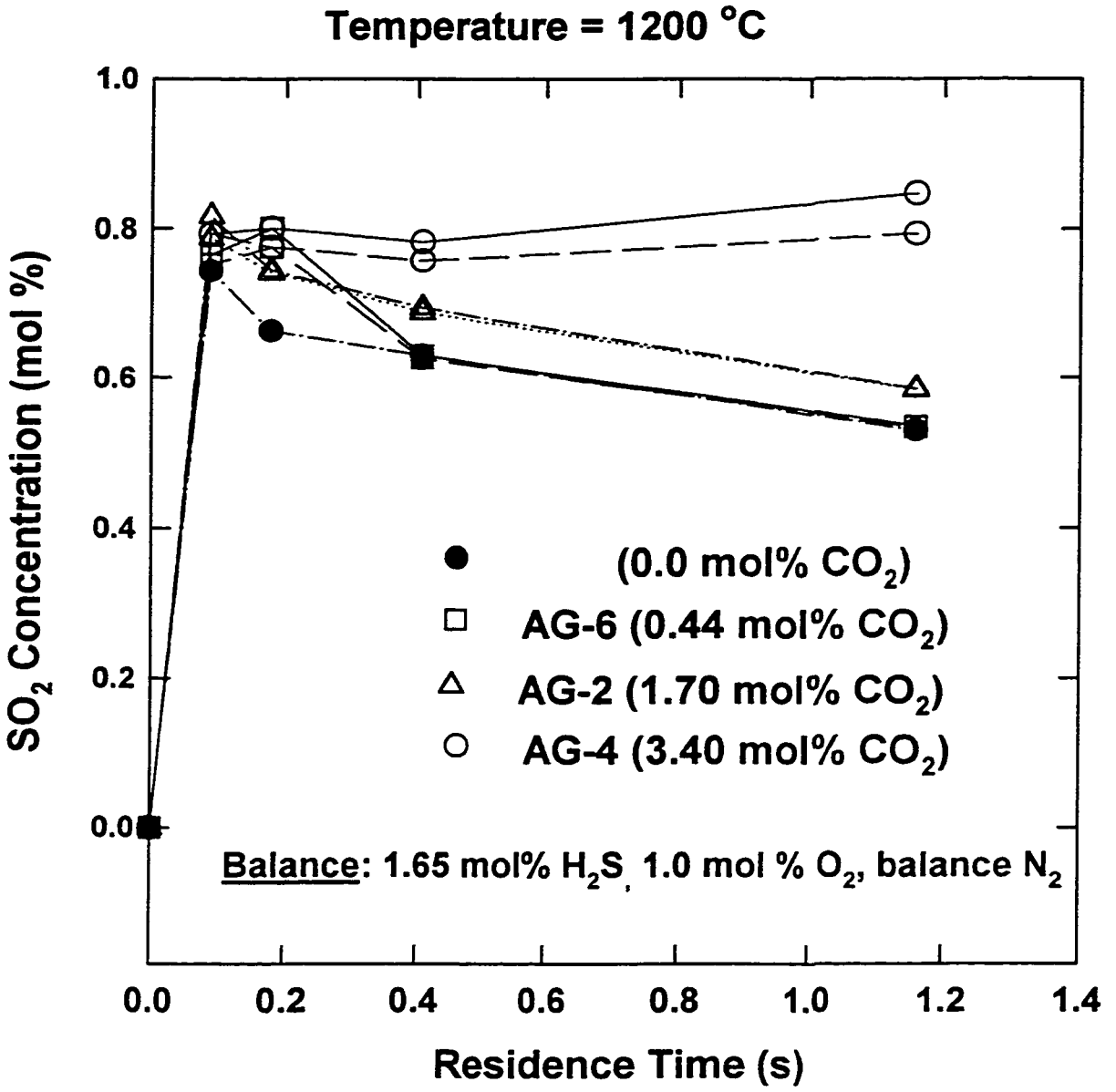

Figure 6.12 Effect of CO_2 content of acid gas mixture on SO_2 formation at 1200 °C for feeds of 1.65 mol% H_2S, 1.0 mol% O_2, varying amounts of CO_2 and balance N_2.

has been discussed in the last Chapter. The main reaction leading to the CO formation is:

$$CO_2 + H \quad \leftrightharpoons \quad CO + OH \qquad (6.13)$$

The key reactions involving the consumption and the formation of the H and OH radicals were already included in the thirty-step reaction mechanism of Tsuchiya et al. (1997). Other reactions for C-H-O systems are also known to occur but were not included in the kinetic scheme for the program for sake of simplicity.

CO Profile

The predicted CO profiles are compared with the data at 1000 °C and 1200 °C in Figures 6.13 and 6.14, respectively. The simulation under-predicts the formation of CO at shorter residence times. However, the agreement between the predictions and the data corresponding to the longest residence attained in the reactor is better.

SO_2 Profile

A comparison between the predicted and experimentally obtained SO_2 profiles is made in Figure 6.15. The comparison is made for a temperature of 1200 °C. The simulation exhibits the trend of reduced SO_2 consumption rates for longer residence times (> 100 ms) with an increase in CO_2 content of acid gas mixture. However, there is a considerable deviation between the predictions and the data for acid gas mixture 4 (AG-4) containing 3.4 mol% CO_2. The maximum deviation is of the order of 35 percent.

6.4 Oxidation of mixture of (CH_4 and H_2S)

Methane and other hydrocarbons are the major source for the formation of carbon disulfide in the Claus reaction furnace. Among the lighter alkanes, methane is relatively more difficult to pyrolyze and to oxidize. However, the oxidation of methane is often assumed to be rapid at temperatures encountered

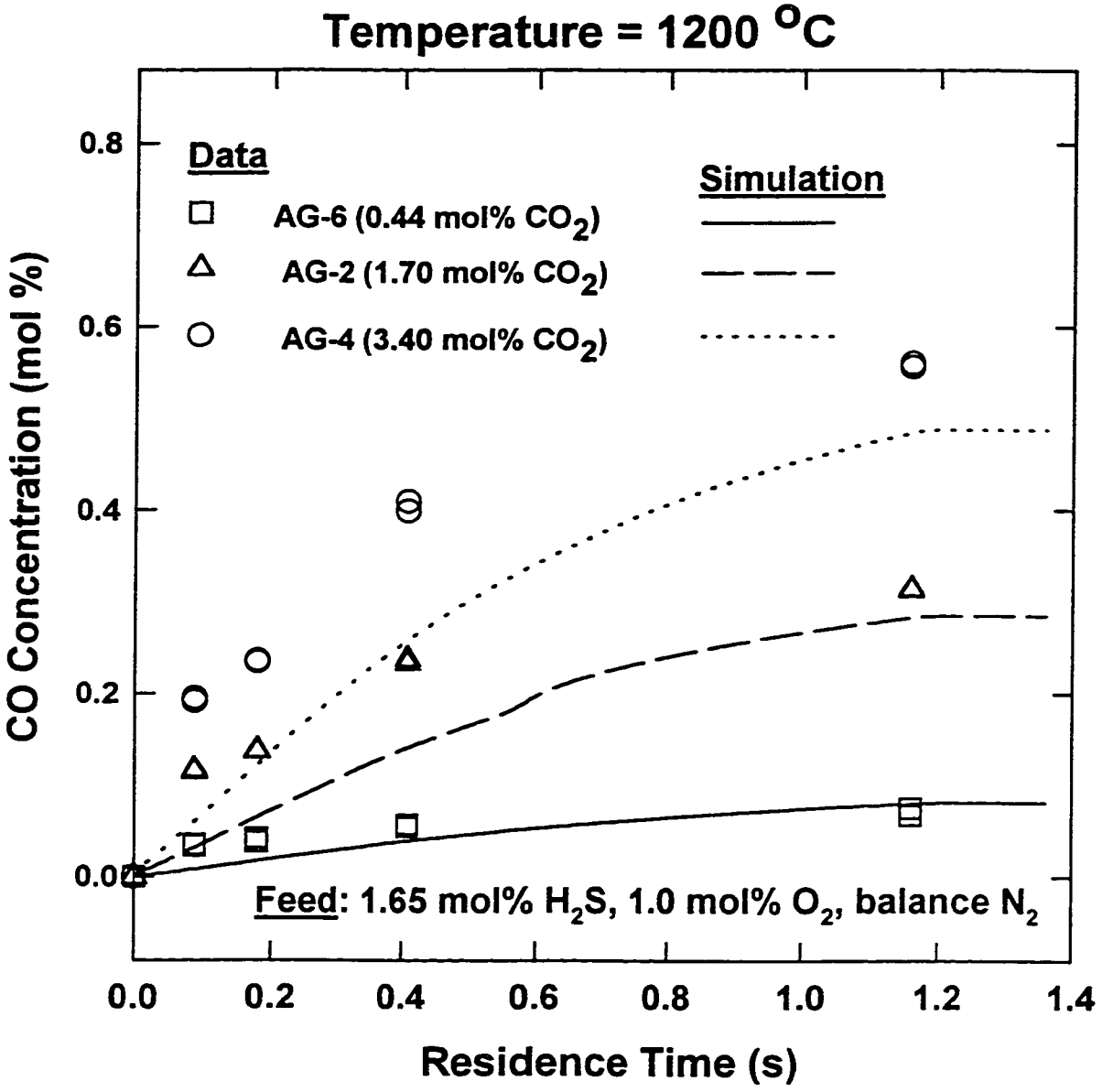

Figure 6.13 A comparison of measured and predicted CO profiles for feeds of 1.65 mol% H_2S, 1.0 mol% O_2varying amounts of CO_2 and balance N_2.

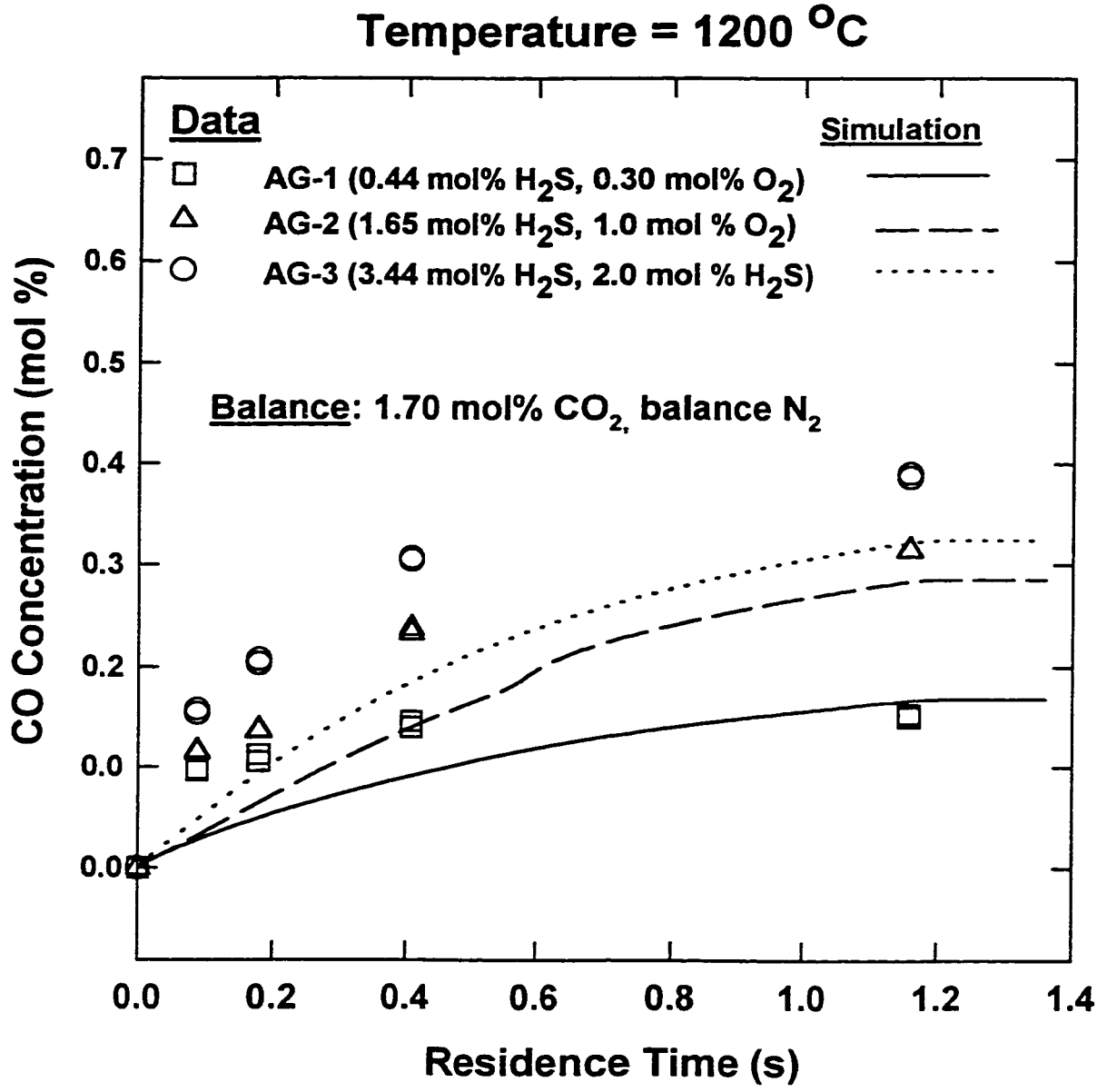

Figure 6.14 A comparison of measured and predicted CO profiles for feeds of 1.70 mol% CO_2, varying amounts of H_2S+O_2 and balance N_2.

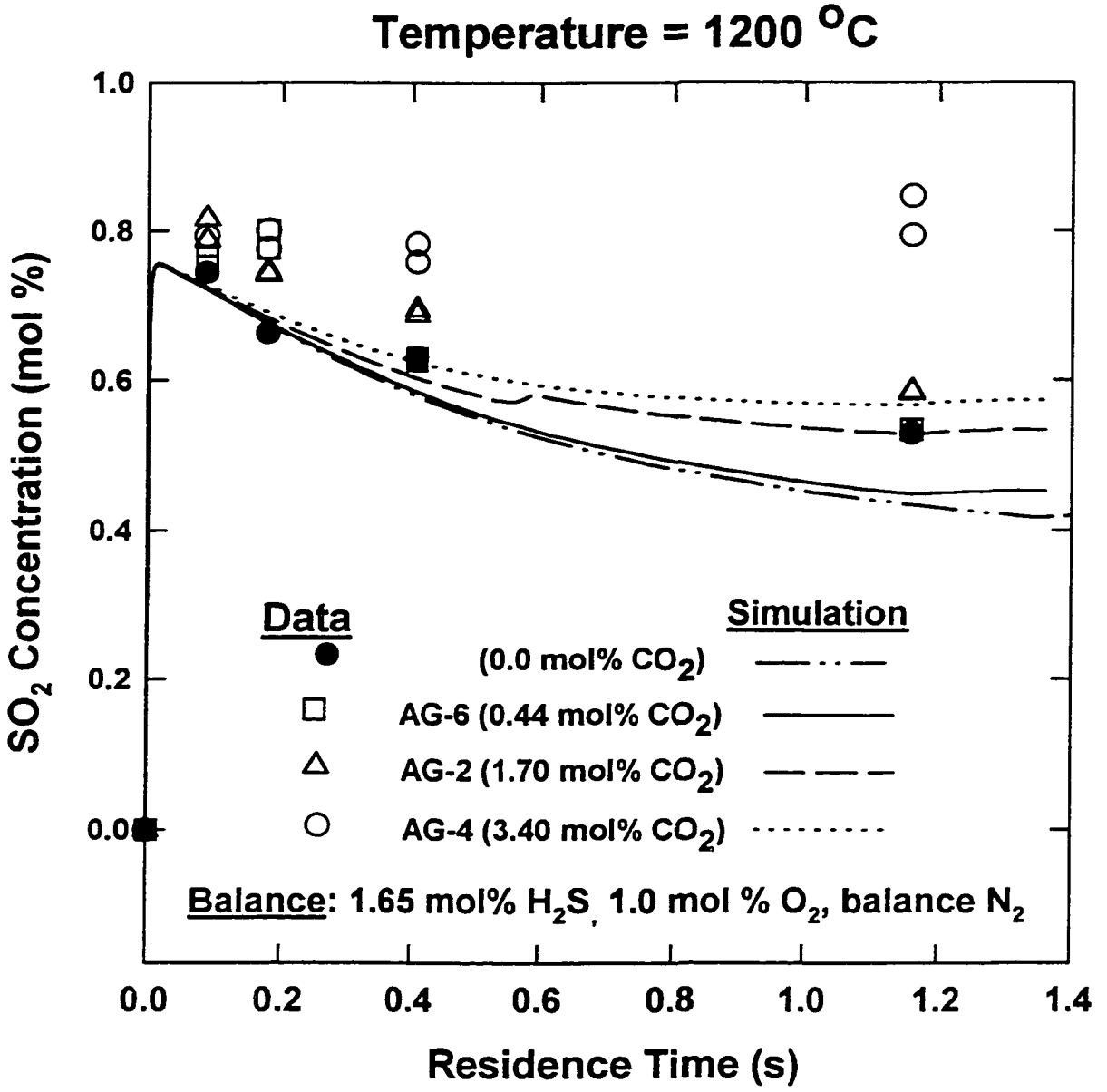

Figure 6.15 A comparison of measured and predicted SO_2 profiles. Effect of CO_2 content of acid gas mixture.

in the Claus furnace, i.e. 975 to 1300 °C. It is anticipated that methane will out-compete the hydrogen sulfide in consuming oxygen. Therefore, the presence of methane in the product stream from the Claus reaction furnace/waste heat boiler is attributed to an incomplete oxidation of methane resulting from the limitation of an incomplete mixing rather than the reaction kinetics. There are limited data on partial combustion of CH_4 and H_2S mixtures at high temperatures such as those encountered in Claus front-end units. Clark et al. (1998) have presented interesting results on the oxidation of methane and hydrogen sulfide separately. They show that hydrogen sulfide oxidizes much faster than methane. Further, their experimental data on oxidation of methane and hydrogen sulfide mixtures at temperatures of 900,1000,1100, 1200 °C indirectly supports their finding from oxidation individual gases, methane and hydrogen sulfide. The residence times in the reactors varied from 1.0-1.14 seconds. Methane profiles at earlier times were not obtained. The product stream from the reactor did not contain any methane but did contain CS_2. The presence of CS_2 was an indirect proof that methane did not combust preferentially and reacted with one of the sulfur containing species to form CS_2.

In another recent paper, Arutyonov et al. (1993) have reported data on methane oxidation in the presence of low concentration hydrogen sulfide. These experiments were conducted in a quartz reactor under static conditions at relatively longer residence times, of the order of tens of minutes. The experiments were conducted at temperatures lower than 727 °C. In their experiments on oxidation of gas mixture, containing 10 % each of methane and hydrogen sulfide, with 5% O_2 at 627 °C and 727 °C, they found that the H_2S is completely converted. At lower temperature incomplete conversion or consumption of H_2S was observed. However, they did not provide quantitative information on methane conversions.

Studies on higher temperature partial oxidation on H_2S and CH_4 are not available in open literature. Therefore, experiments were performed to obtain

information pertaining to the relative kinetic rates of the oxidation of H_2S and CH_4.

6.4.1 Experimental

6.4.1.1 Experimental conditions

Experiments were conducted with two gas mixtures in which the H_2S and O_2 content were fixed at 1.65 mol% and 1.0 mol%, respectively. The methane concentrations in the two mixtures were 0.22 and 0.05 mol%. Methane and H_2S carrying stream were mixed together and flowed through one reactor inlet. To avoid the oxidation in the pre-heat length, the oxygen carrying was flowed through the other inlet. By mixing the H_2S and CH_4 together, it may be expected that the reaction between the two species may occur prior to being mixed with the O_2 stream. Earlier experiments reported in section 5.9, show that little reaction may occur between methane and H_2S at such short reaction times (20-30 ms) and lower than furnace set point temperatures in the pre-heat length.

6.4.1.2 Experimental results

CH_4 consumption profiles

The concentration profiles of methane for the two gas mixtures are presented in Figure 6.16. It can be clearly observed that methane is present at the exit of the longest reactor at temperature of 1000 °C. No trace of oxygen was observed at the reactor exit even for the shortest reactor, indicating complete consumption of oxygen due to oxidation of hydrogen sulfide. The data conclusively demonstrate that the methane oxidation much slower than the hydrogen sulfide oxidation at temperatures below 1100 °C.

The kinetic limitation of methane oxidation in a methane and hydrogen sulfide mixture means that the presence of methane in the Claus reaction furnace exit should not be attributed totally to incomplete mixing.

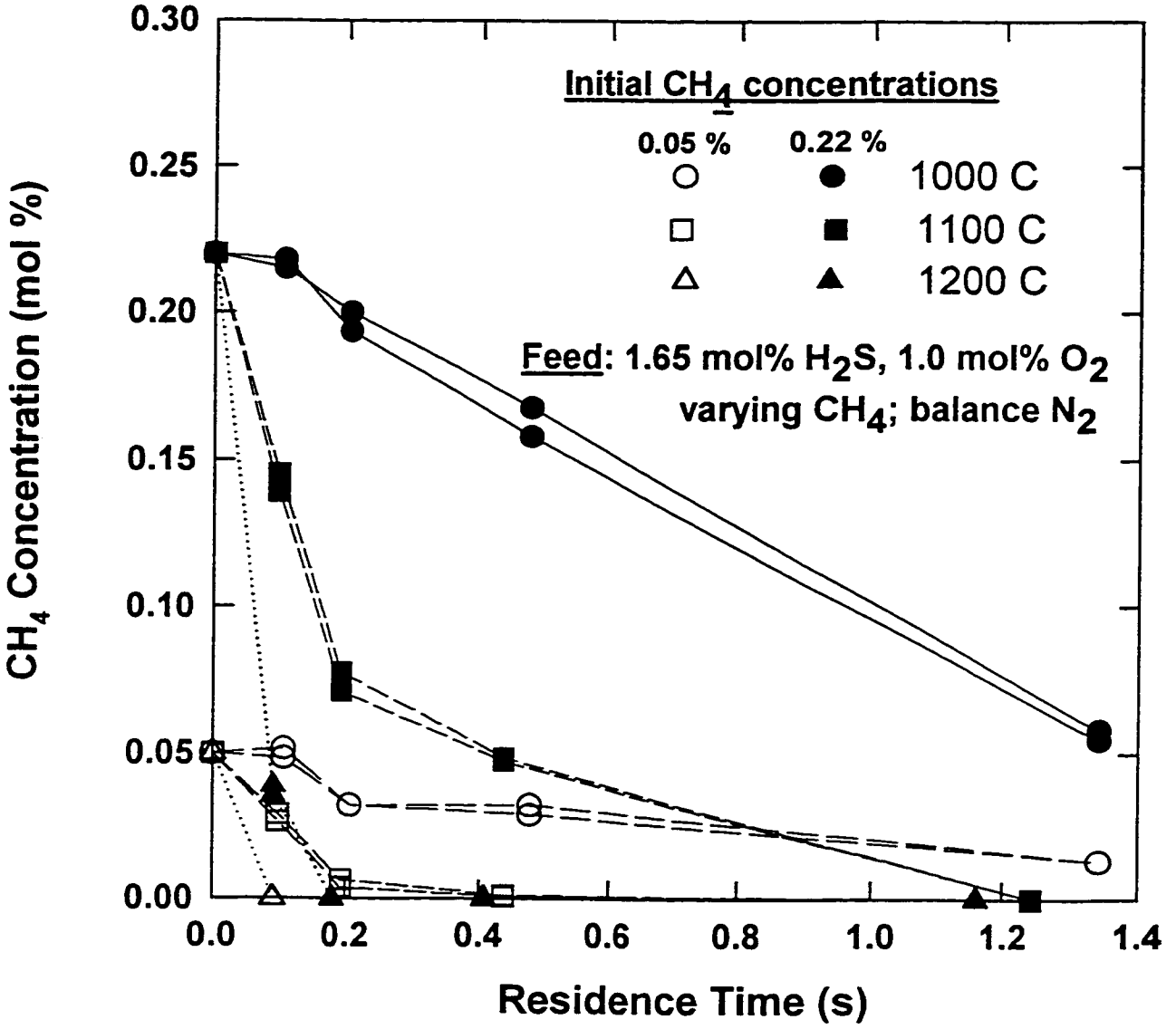

Figure 6.16 Measured CH_4 concentration profiles for gas mixtures with two different initial CH_4 concentration. Effect of temperature.

CO profiles

The CO profiles are presented in Figure 6.17. For gas mixture with the higher methane content, the carbon monoxide concentrations show a sharp increase initially at the temperatures of 1100 °C and 1200 °C. The CO concentration then reduces slightly perhaps due to further oxidation to CO_2.

SO_2 profiles

The measured SO_2 concentration profiles obtained from the experiments with the oxidation of a H_2S and methane mixture are presented in Figure 6.18. The SO_2 demonstrates a similar trend as that observed during the oxidation of hydrogen sulfide only, i.e., a sharp increase in concentration with the maximum value being attained in less than 100 ms. The SO_2 concentration then decreases steadily with an increase in residence time and decreases sharply with an increase in temperature.

From Figure 6.18, it may be noted that the SO_2 concentration measured for the gas mixture containing higher methane content is generally lower than that measured for the lower methane content gas mixture. Whether less SO_2 is produced from hydrogen sulfide oxidation as methane competes with the hydrogen sulfide for oxidation or whether SO_2 is produced and consumed by its reaction with methane or other species cannot be conclusively established. On observing the CO profiles of Figure 6.17 which shows an increasing trend in CO concentration up to 200 ms, it seems more likely that SO_2 is being consumed via its reaction with methane to produce CO.

6.4.2 Kinetic modeling

Detailed kinetic scheme for methane oxidation in flames is available (Smooke, 1991 and Warnatz et al., 1997). The 25 reaction mechanism for methane oxidation reported by Smooke (1991) was employed in this study.

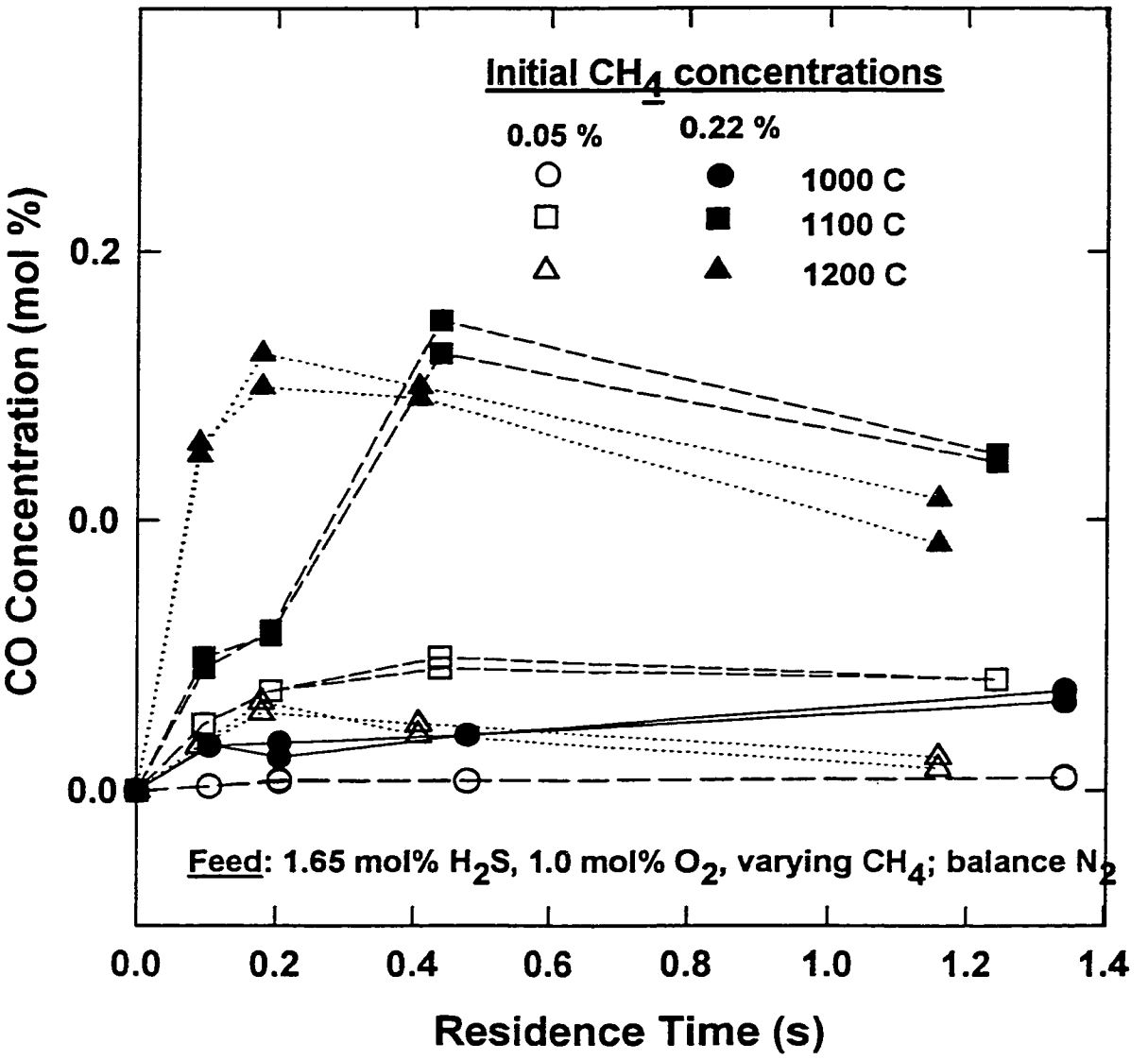

Figure 6.17 Measured CO concentration profiles for gas mixtures with two different initial CH_4 concentration. Effect of temperature.

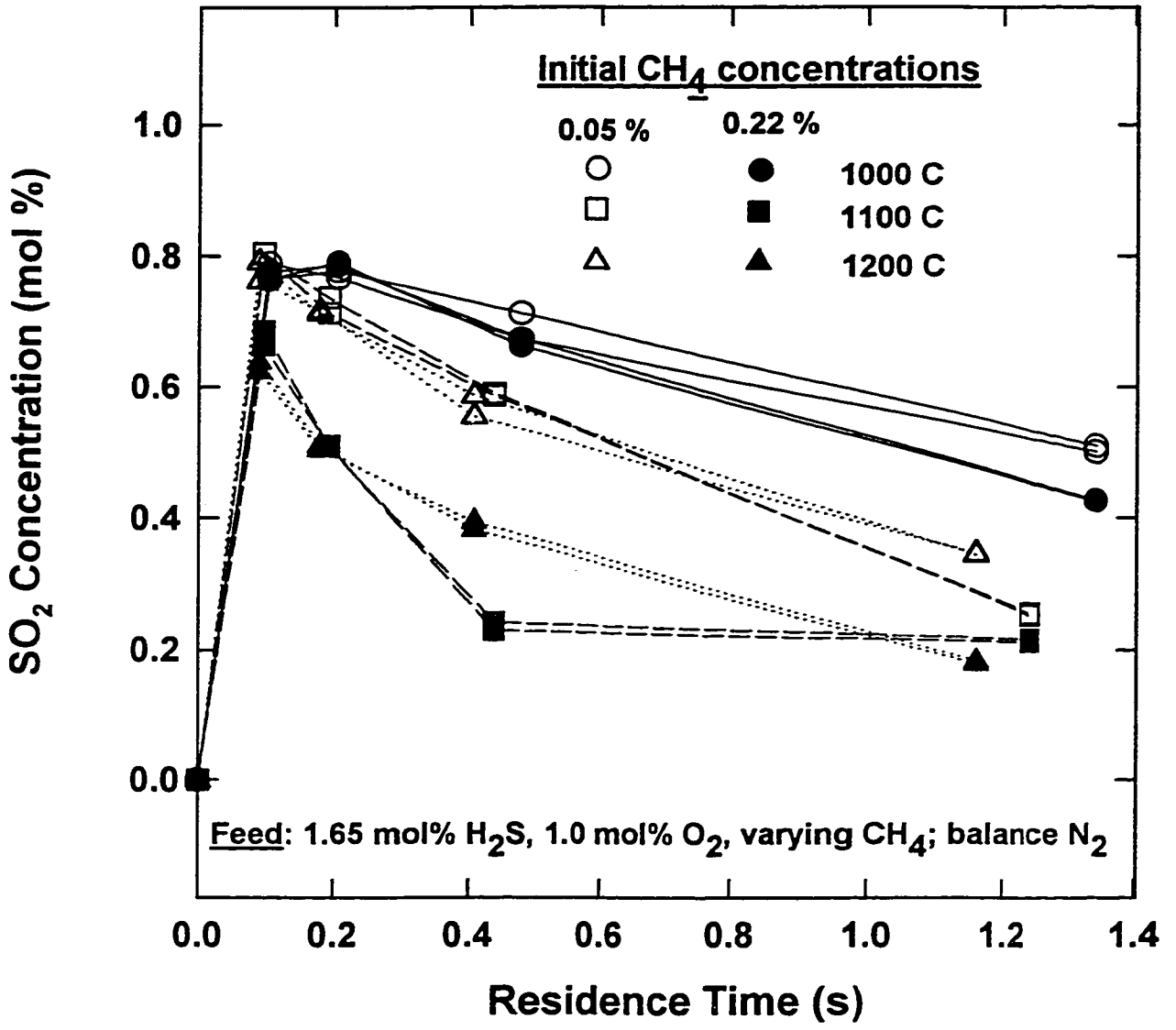

Figure 6.18 Measured SO_2 concentration profiles for mixtures with two different initial CH_4 concentration. Effect of temperature.

Oxidation of CH_4

The result of simulation for the oxidation of methane at 1200 °C is presented in Figure 6.19. The inset provides a zoomed view of the concentration profiles over the time of 65-85 ms, when methane reactions occur very rapidly. The calculations were performed for a fixed temperature and pressure in a constant volume batch reactor. The increase in volume was neglected because dilute system was considered. The initial composition of the reacting mixture was 0.22 mol% CH_4, 0.44 mol% O_2 with the balance made up of nitrogen. From the simulation results shown in the Figure 6.19, the important point to note is that the methane consumption demonstrates an induction period of almost 70 to 80 milliseconds. The hydrogen sulfide consumption during the oxidation does not demonstrate such a long induction period. The inset of Figure 6.19 shows that the rapid reactions occurring in a short period of time when methane concentration decreases sharply to zero. Both hydrogen and carbon monoxide demonstrate an increase in concentrations before complete consumption of methane, after which the concentrations of both hydrogen and CO decrease sharply. The CO_2 and H_2O concentration profiles show a steady increase in concentration prior to complete consumption of methane, after which the concentration of both increases dramatically reaching the final values over a very short period of time. For illustrative purposes the predicted concentration profiles of various species during hydrogen sulfide oxidation at 1200 °C are shown in Figure 6.20. The inset of the Figure shows the concentration profiles of major species over the reaction time of 2 to 5 ms. The results of the simulation show that the oxidation of hydrogen sulfide is over in less than 5 ms. The induction period for H_2S oxidation is approximately one-fifteenth that for methane oxidation. Therefore, for oxidation of methane and hydrogen sulfide mixtures under lean conditions (i.e. oxygen content is lower than that required for by the stoichiometry for complete combustion), hydrogen sulfide will consume all of the oxygen.

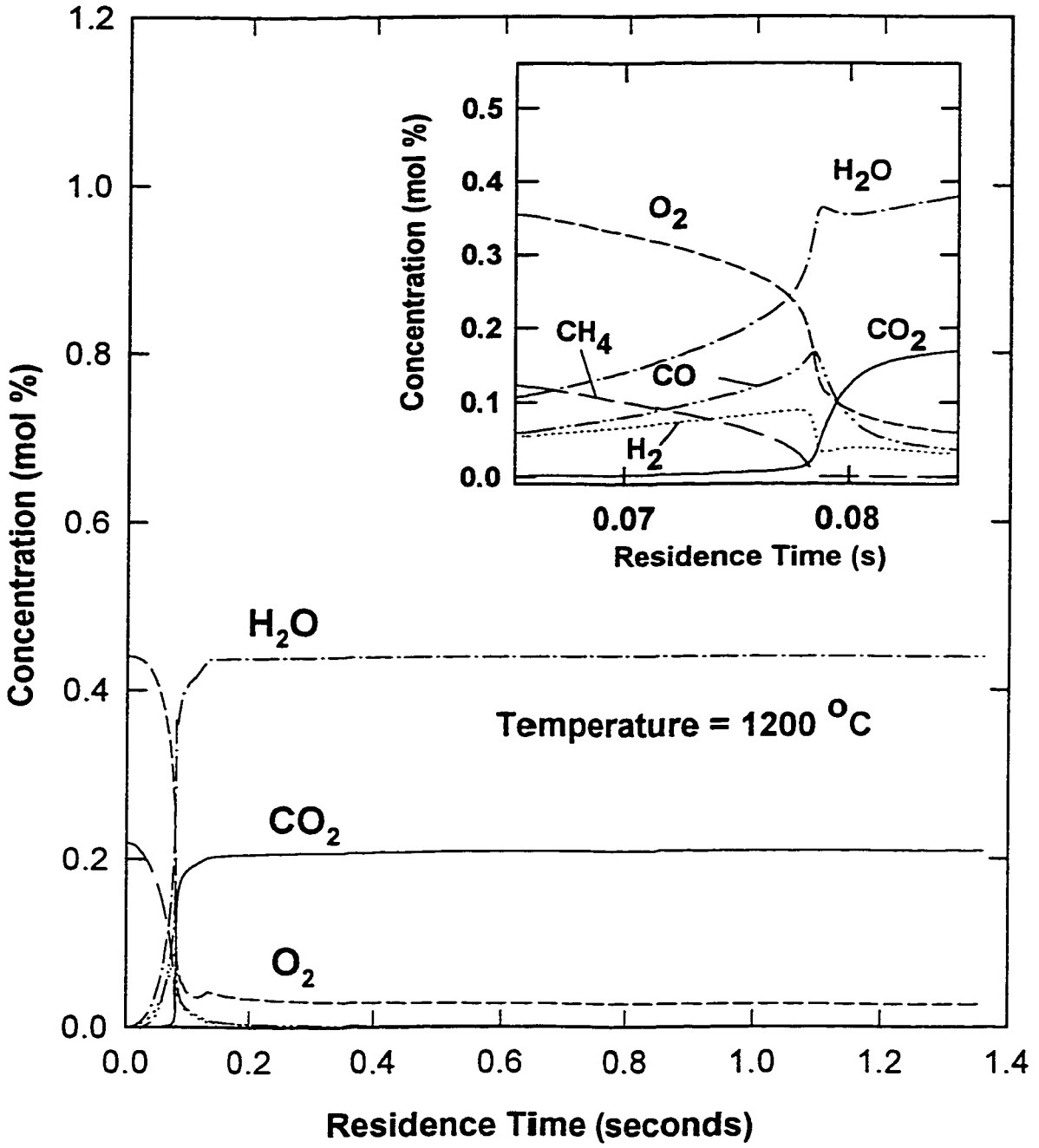

Figure 6.19 Predicted profiles of molecular species during oxidation of methane. [0.22 mol% CH_4, 0.44 mol% O_2, balance N_2]

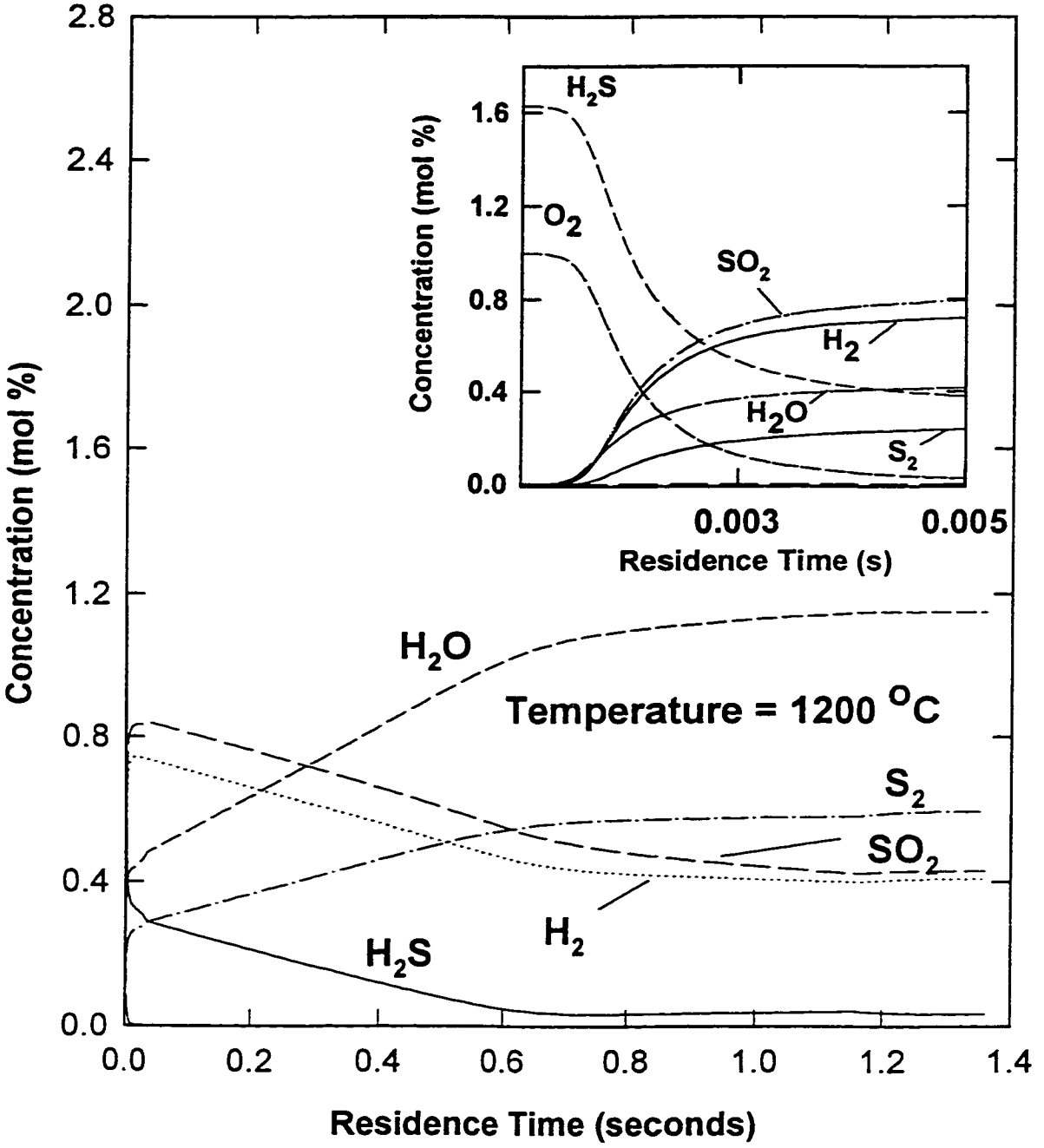

Figure 6.20 Predicted concentrations profiles of molecular species during H_2S oxidation [1.65 mol% H_2S, 1.0 mol% O_2, balance N_2]

Oxidation of CH_4 and H_2S mixture

To simulate the oxidation of methane and hydrogen sulfide mixtures, the kinetic schemes for methane oxidation and hydrogen sulfide were combined. A number of common reactions were present in the reaction schemes for each system. The final reaction scheme involved 58 forward reactions and their associated reverse reactions. The results of simulation for the oxidation of CH_4 and H_2S mixture are shown in Figure 6.21. The predictions show minimal consumption of methane. This was expected, firstly because methane oxidation is much slower than hydrogen sulfide oxidation and secondly because the reactions of methane and sulfur species were not included in the calculations.

It is recommended that similar investigation for the kinetics of the elementary reaction for C-S, C-S-H, C-S-O and C-S-H-O systems should be pursued.

6.5 Oxidation of CO_2, H_2S and CH_4 mixtures

6.5.1 Experimental

6.5.1.1 Experimental conditions

Experiments were conducted with two gas mixtures in which the H_2S, CO_2 and O_2 contents were fixed at 1.65 mol%, 1.70 mol% and 1.0 mol%, respectively. The methane concentrations in the two mixtures were 0.22 and 0.05 mol%. The methane and H_2S carrying stream were mixed together and flowed through one reactor inlet and the oxygen and carbon dioxide streams were mixed together and flowed through the reactor inlet. The total flow rate was maintained at 4.0 L/min and the inlet pressures varied from 98 to 125 kPa.

6.5.1.2 Experimental results

CH_4 Profiles

The measured methane concentration profiles for the oxidation of gas mixtures (1.65 mol % H_2S and 0.22 mol% CH_4) with and without CO_2 are presented in

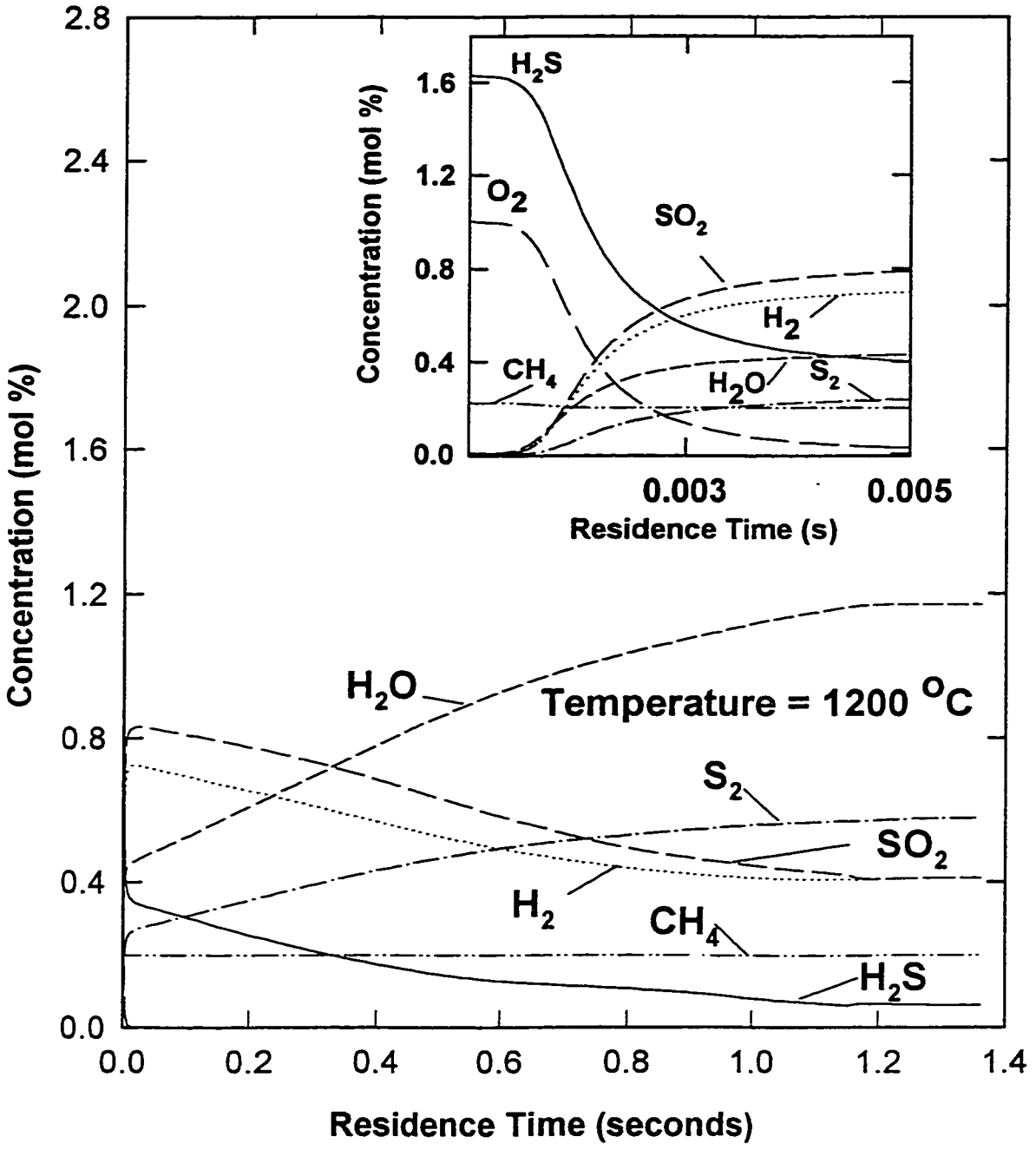

Figure 6.21 Predicted concentration profiles of molecular species during oxidation of (CH_4 + H_2S) mixture.
[1.65 mol% H_2S, 0.22 mol % CH_4, 1.0 mol% O_2, balance N_2]

Figure 6.22. The methane concentration profiles for both the gas mixtures demonstrate similar trend, indicating that the presence of CO_2 does neither inhibit nor promote the methane reactions.

CO Profiles

The measured CO profiles obtained from experiments with the gas mixture containing CO_2, CH_4 and H_2S are presented in Figure 6.23. The data for gas mixtures of (CH_4 and H_2S) and (CO_2 and H_2S) are also shown for comparison. At the lowest temperature investigated experimentally, the CO concentrations are low and do not differ much from each other. However, at 1200 °C the CO concentrations are maximum for gas mixtures containing all three key components, i.e. CH_4, CO_2 and H_2S. At 1200 °C, the CO concentration measured from the oxidation of methane and hydrogen sulfide mixture show a sharp increase initially and, then demonstrate a decreasing trend with increasing residence time. However, the gas mixtures containing CO_2 show an increasing trend for the complete range of residence time.

SO_2 and H_2S

The measured SO_2 and H_2S concentrations for acid gas mixtures containing CH_4, CO_2 and H_2S showed trends similar to that for mixtures of CO_2 and H_2S. Therefore, the results for these components are not presented here.

6.6 Summary

The major findings of the experimental and simulation study on the partial oxidation of acid gas mixtures can be summarized briefly as follows:

On H_2 formation

A majority of the hydrogen production occurs in a very short time during the oxidation process. The simulation of H_2S oxidation, based on the reaction mechanism proposed by Tsuchiya et al (1997), supports this mechanism of hydrogen formation. The combination of experimental finding and simulation

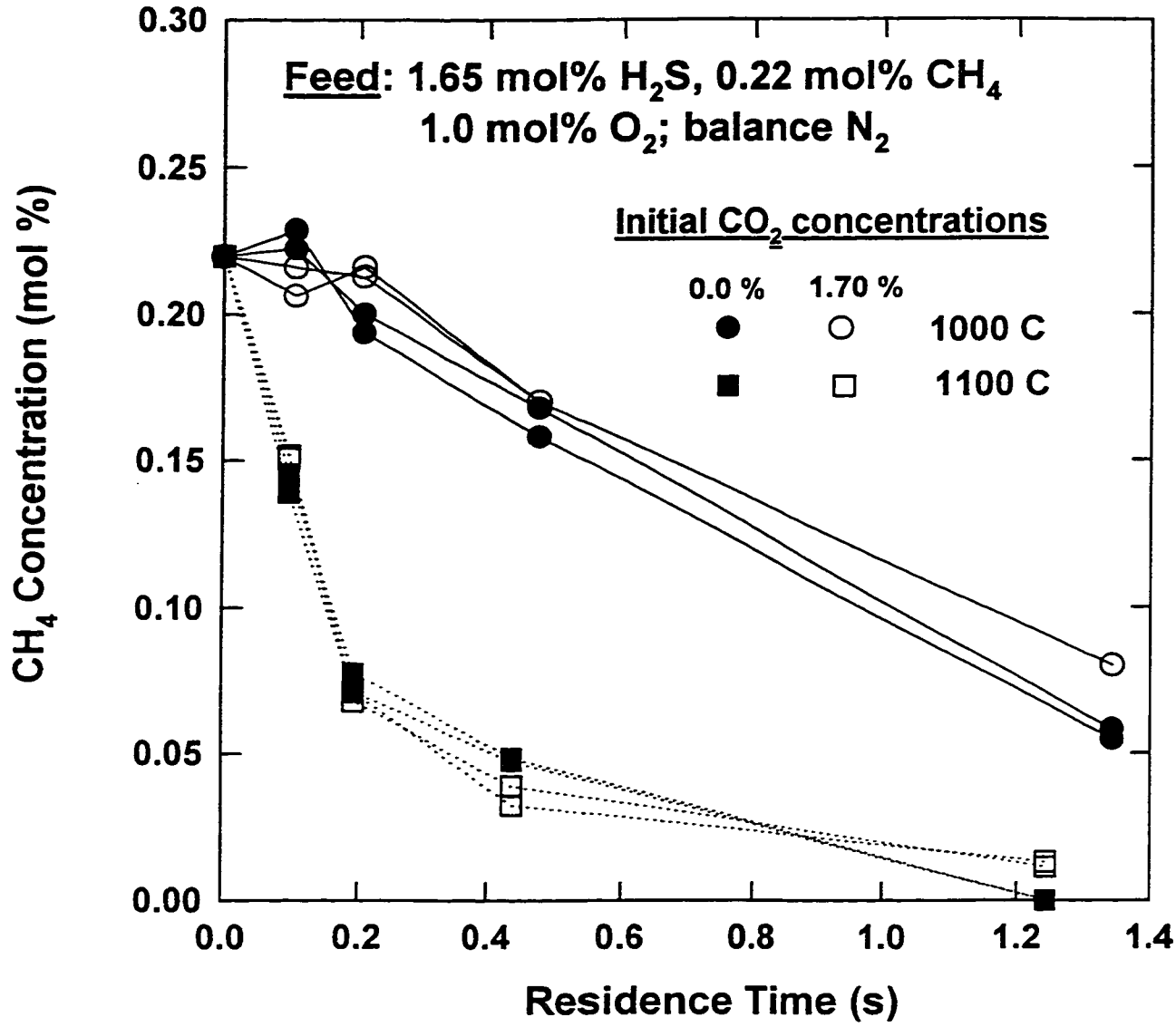

Figure 6.22 Measured CH_4 concentration profiles for oxidation of (CH_4+H_2S) mixtures with and without CO_2.

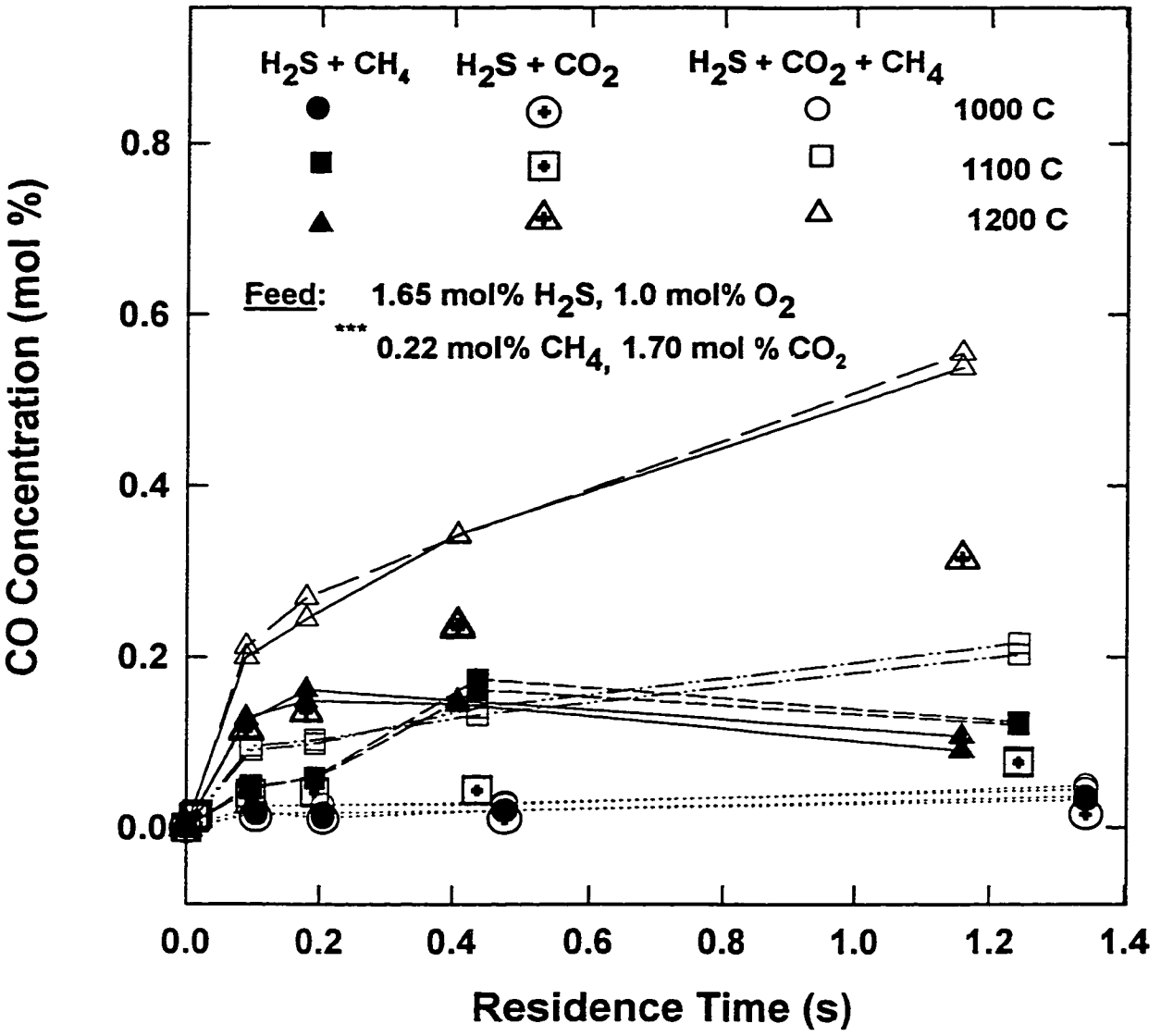

Figure 6.23 Measured CO concentration profiles for mixtures containing varying amounts of initial CO_2 and CH_4. Effect of temperature.

*** concentrations of CH_4 and CO_2, if present in the mixture.

results, therefore, indicate that hydrogen formation from hydrogen sulfide is greatly accelerated in presence of oxygen and that the kinetics for the thermal decomposition of hydrogen sulfide play relatively unimportant role.

On methane oxidation

A major experimental finding from the experimental study was that methane oxidation and its conversion to chemical species is severely kinetically limited at temperatures below 1100 °C. This implies that the observation of methane in the product stream from the Claus reaction furnace is not an absolute proof of incomplete mixing in the furnace; this is contrary to the common belief in the industry.

The simulation results show that oxidation of methane is preceded by an induction period (70-80 ms at 1200 °C) which is significantly larger than that for hydrogen sulfide oxidation (10-15 ms at 1200 °C). For simulation of simultaneous oxidation of methane and hydrogen sulfide, kinetic scheme must include important CH-S and CH-SO reactions. The reliable kinetic information for the elementary reactions in such systems is not available yet.

On CO formation

The experimental results demonstrate that the CO formation is relatively slower than the oxidation reactions and kinetically limited at temperatures up to 1200 °C. The simulation results support this finding.

An important consequence of this finding is that the CO formation from a Claus reaction furnace may be reduced by operating the furnace under conditions that result in a shorter gas residence times. This is possible only if the feed to the furnace does not contain refractory chemical species such as NH_3 and CH_4 that may need longer residence time for consumption. A reduction in CO formation translates directly into a reduction in COS production which, occurs mainly in the waste heat boiler placed immediately after the Claus furnace. The formation of COS is due to the reaction between CO and sulfur.

SO_2 Formation and H_2S Consumption

The experimental results demonstrate that the SO_2 formation occurs in a very short residence time, less than 115 ms. A majority of the hydrogen sulfide is consumed within this short period. These findings are also supported by the simulation results.

Chapter 7

Application of New Kinetics in Claus Plant Modeling

7.1 Introduction

In this chapter, modeling of the front-end units, i.e. the reaction furnace(RF) and the waste heat boiler (WHB) of the Claus plants is presented. One of the major problems in verifying the results of the models is that there is practically no plant data available in the literature, especially those relevant to the front-end units. However, Sames et al. (1990) have conducted a remarkable field study in which they measured gas compositions at the entrance and the exit of the RF and WHB under very difficult situations. The data reported by Sames et al. (1990) are employed in this thesis to compare the predictions for gas compositions at the entrance and exit of the waste heat boiler.

7.2 WHB modeling with new kinetics

Until recently, COS was considered to be formed in the reaction furnace of Claus plants. However, there was one problem with this theory; normally the concentration of COS measured at WHB exits were always greater than that predicted by thermodynamic equilibrium consideration. The difference between predictions and measurements were usually explained by the kinetic limitation of COS consumption reactions.

It is now known that at least one of the COS consumption reaction, the COS decomposition reaction is very rapid at high temperatures such as those encountered in the RF. It is also known that COS is favored thermodynamically to exist at higher concentrations at lower temperatures such as those existing in the WHB. The measured COS concentrations higher than the equilibrium concentration (calculated at furnace temperatures) can thus be explained via its formation at thermodynamically favorable conditions in the waste heat boiler.

As mentioned earlier, Sames et al. (1990) have measured the gas composition across the WHB tube and found an increase in COS and H_2S concentration accompanied by a decrease in concentrations of CO, H_2 and elemental sulfur. Moreover, the amount of COS formed in the WHB was found to be in the range of 62-71 percent of the combined COS formed in the RF and the WHB. This clearly shows that the majority of COS observed at the exit of the RF/WHB unit is formed in the WHB.

Sames et al. (1990) proposed that the following two reactions occurred in the WHB:

$$CO + \tfrac{1}{2} S_2 \rightleftharpoons COS \qquad (7.1)$$

$$H_2 + \tfrac{1}{2} S_2 \rightleftharpoons H_2S \qquad (7.2)$$

In earlier works at the University of Calgary (Karan et al., 1994; Nasato et al., 1994), a computer model was developed to study the reaction quenching capabilities of the WHB. In the absence of reliable and relevant kinetic information on the COS forming reaction, reaction rate constants were extrapolated to higher temperature based on a kinetic study of low temperature flash photolysis reaction between $S(^3P)$ and COS (Klemm and Davis, 1974). The extrapolation of reaction rate constants to conditions beyond the recommended range may have yield significant error, but in absence of relevant kinetic information for this reaction, the kinetics reported by Klemm and Davis were used as a first approximation.

7.2.1 WHB description and design considerations

It is necessary to describe the waste heat boiler of the modified Claus plants before a kinetic model of the same is developed. A detailed schematic of the waste heat boiler is shown in Figure 7.1 It must be mentioned that the WHB has been historically given little important from a process chemistry point of view. Only with the findings of Sames et al. (1990) and the work from our laboratory (Karan et al., 1994; Nasato et al., 1994) has it begun to be treated seriously.

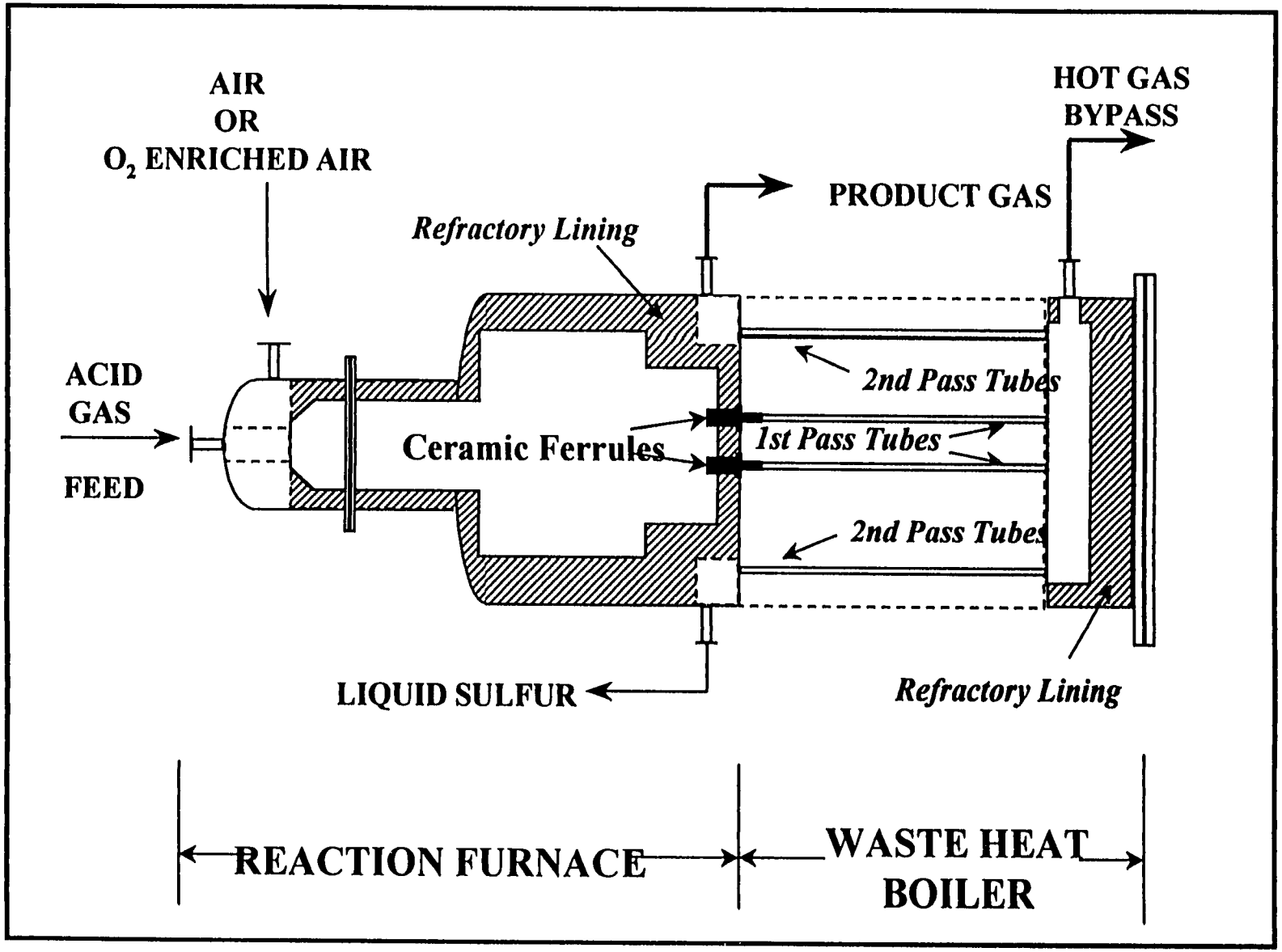

Figure 7.1 Schematic diagram of reaction furnace and waste heat boiler of a Claus plant. (i.e. the front-end of a Claus plant)

In the WHB, the hot gases flow through the tube side while medium to high pressure steam is generated on the shell side. The WHB tubes and tubesheets are exposed directly to the hot furnace product gases, therefore, proper protection is needed. The tubesheets are shielded by use of 3 inches of refractory. The tube inlets have ceramic ferrules that extend 6 inches beyond the inlet tube sheet (as shown in Figure 7.1). The ferrules also protrude about 2-3 inches in front of the inlet tubesheet (Parnell, 1985). A 2 inch sized tube is typically used, however, tubes of diameter up to 6 inches may also be used. The recommended design gas mass velocity in the tubes ranges from 5 to 40 $kg/m^2 \cdot s$ (Parnell, 1985).

Parnell (1985) also recommends that the heat exchange calculations for WHB must include the radiation effects in addition to the convection effects. Ignoring radiative heat transfer may result in overdesign of heat transfer area. An oversized WHB can pose serious operational problems due to premature sulfur condensation, improper reheat, viscous sulfur formation etc.

7.2.2 Mathematical formulation

The model equations for material and heat balances (including radiation from non-transparent gases inside the tube), the details of methods for estimation of thermodynamic and transport properties of gas mixture, and the rate kinetics of the H_2S reaction used in the simulation of WHB have been reported by Nasato et al. (1994) and Karan et al. (1994).

COS kinetics

The kinetics for the direct reaction between CO and S_2 to form COS reaction was obtained from this thesis. The rate of reaction for COS reaction was as follows:

$$(r_{COS}) = k_2 C_{CO} C_{S2} - (k_2/K_{EQ2}) C_{COS} C_{S2}^{0.5} \qquad (7.1)$$

The arrhenius parameters for the rate constant k_2 were obtained from the values reported in Section 5.4 of this thesis.

Solution method.

The material, energy and the momentum balance equations for the WHB represents a set of coupled, stiff, non-linear differential equations. These equations were solved by a program written in Matlab using the Gears algorithm.

Base case condition.

The base case conditions used in the simulation of COS formation in the WHB are those for the Claus plant at the Ultramar Refinery in California and are reported in Table 7.1 Data were reported for the five set of tests that were conducted as a part of the field measurement study by Sames et al. (1990). The molar flow rates of various components of the WHB feed as well as the feed temperature for the five tests has been reported in Table 7.2 The inlet pressures for test numbers 2-5 were back calculated from the molar flow rates, the residence time and furnace temperatures reported by Sames et al (1990). Simulations were performed for the base case conditions for all five tests. To investigate the effect of parameters such as WHB tube diameter and gas mass flux on the reaction quenching in the WHB, the conditions for Test 1 were used in the simulations.

7.2.3 Results

7.2.3.1 Comparison of measured and predicted COS at WHB exit.

The simulation results for COS formation in the waste heat boiler for the five test conducted by Sames et al. (1990) are presented in Figure 7.2. The predictions are compared with the measured COS flow rates at the WHB exit. Excellent agreement is observed for tests 3 and 4, while the predicted COS flow rate for test 5 is about five percent less than the measured value. For tests 1 and 2, the

Table 7.1 Base Case Conditions for the Ultramar Refinery WHB (Sames et al., 1990)

Tube wall temperature, K	487.15
Tube length, m	8.23
Tube inside diameter, mm	43.99
Tube outside diameter, mm	50.80
Number of tubes (single pass)	240

Table 7.2 Inlet Feed Molar Flow Rates to the WHB (Sames et al., 1990)

	molar flow rates, kmol/h				
	Test 1	Test 2	Test 3	Test 4	Test 5
WHB feed temp, °C	1321	1224	1208	1285	1488
WHB feed pres, kPa	162	157	159	159	171
H_2	10.04	7.94	3.86	5.78	11.18
N_2	134.10	146.10	88.67	92.52	113.00
CO	2.74	2.07	1.32	2.07	3.52
CO_2	6.43	5.88	4.80	6.34	6.60
H_2S	10.31	9.66	6.37	9.82	11.52
COS	0.47	0.29	0.24	0.42	0.60
SO_2	5.67	4.30	3.28	4.11	6.17
H_2O	95.30	82.78	45.60	61.47	121.40
S_2	33.86	28.97	20.96	28.91	40.02
Total	298.9	175.1	175.1	211.4	314.0
Oxygen Enrichment	YES	NO	NO	YES	YES

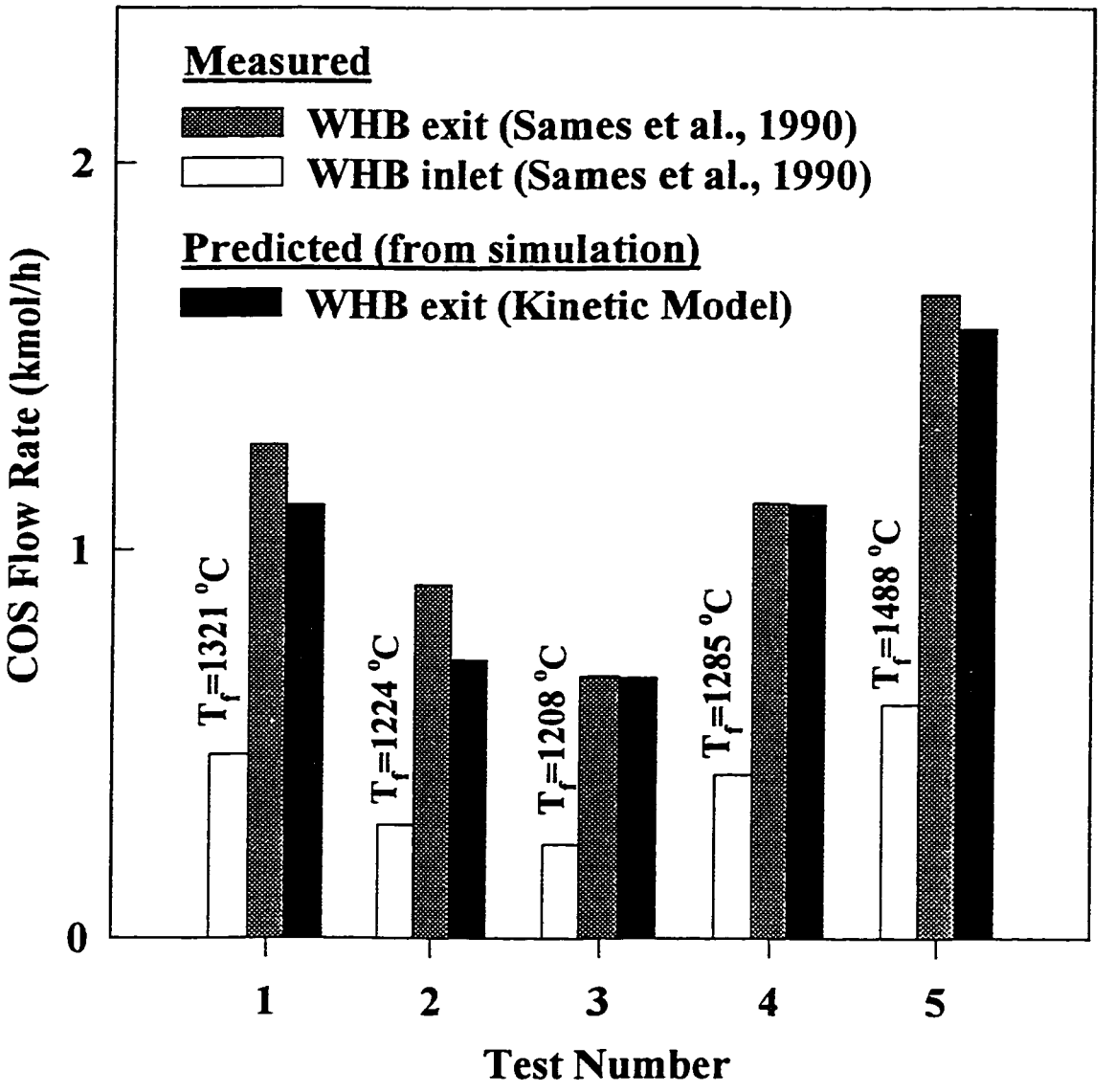

Figure 7.2 Comparison of predicted and measured COS flow rates at exit of an industrial waste heat boiler.

COS flow rates are underpredicted by 13 and 20 percent, respectively. Overall, it can be concluded that the predictions are in good agreement with the measured data. This demonstrates that the developed kinetic model for COS formation is reliable in predicting COS formation in Claus furnace WHB.

Additional information is provided in Figure 7.2 in the form of measured COS flow rates at the WHB inlet. The purpose of this supplementary information is to correlate the amount of COS formed in the RF or WHB with the furnace temperature. In recent years there been a rapid development in technologies for operating Claus reaction furnace in an oxygen-enriched atmosphere which results in higher furnace temperature. The tests 1, 4 and 5 were carried out with oxygen-enriched air while tests 2 and 3 were not. The furnace temperatures reported for tests 1, 4 and 5 as expected are higher than those for tests 2 and 3. It can be observed from Figure 7.2 that the amount of COS formed both in the RF and in the WHB increases with an increase in reaction furnace temperature. Thus, it will become more important from COS formation perspective to quench the product gases, from furnaces operating with oxygen-enrichment, in the WHB more rapidly to reduce the amount of COS formed in the WHB. Hence, the reaction quenching capability of WHB can be investigated with computer simulations, as is done in this thesis. Also, it should be restated here that the problem with COS formation in the WHB is that it contributes very significantly to the total sulfur emissions from a Claus plant.

7.2.3.2 Parametric study

To examine the reaction quenching capability of the WHB, one should be aware of the factors that affect quenching of gases in tubes. The quenching of reactions or gas temperature can be achieved in the WHB by increasing the heat transfer rate from the gas to the tube. This can be achieved by increasing the tube inside heat transfer coefficient or by increasing the heat transfer area. The heat transfer co-efficient for the inside of WHB tube can be increased by increasing the velocity or the gas mass flux. The heat transfer area can be

increased for a given volume of gas contained in WHB tube by decreasing the tube diameter. Thus, calculations were performed to study the effect of tube diameter and gas mass flux on COS reaction quenching.

Effect of WHB tube diameter.

The tube diameter of industrial Claus furnace WHB is, typically, 2 inches or greater. To demonstrate the effect of tube diameter on reaction quenching, calculations were performed for three tube diameters of 1,2 and 3 inches. The gas mass flux was fixed to 6.7 $kg/m^2 \cdot s$ for each case. The molar flow rates of COS along the WHB tube for the three cases are presented in Figure 7.3. It must be mentioned here that the quench times for three cases ranged from over 250 ms for the larger diameter tube to less than 30 ms for the smallest diameter tube (Nasato et al., 1994). As expected, the amount of COS formed increased with increasing tube diameter due to the decreasing quench rates. The predicted COS flow rate at WHB exit is found to increase by approximately 30% on increasing the tube diameter by fifty percent from 2 to 3 inches. The COS flow rates decreases by approximately 30% as the tube diameters are halved from the base case diameter of 2 inches. The important point to note is that the amount of COS formed in WHB alone is halved as the tube diameter is reduced from two inches to one inch. This represents a substantial reduction in COS formation and clearly demonstrates the effectiveness of reaction quenching via the use of smaller diameter tube. However, the actual applicability of small diameter tubes is dependent on overcoming the pressure drop constraint and sulfur misting problems.

Effect of gas mass flux.

To study the effect of gas mass flux on COS reaction quenching, calculation were carried out by varying the gas mass flux from the base case condition of 6.7 $kg/m^2 \cdot s$ up to 105 $kg/m^2 \cdot s$.The results of these simulations are reported in Figure 7.4. It can be observed from Figure 7.4 that the predicted COS formation

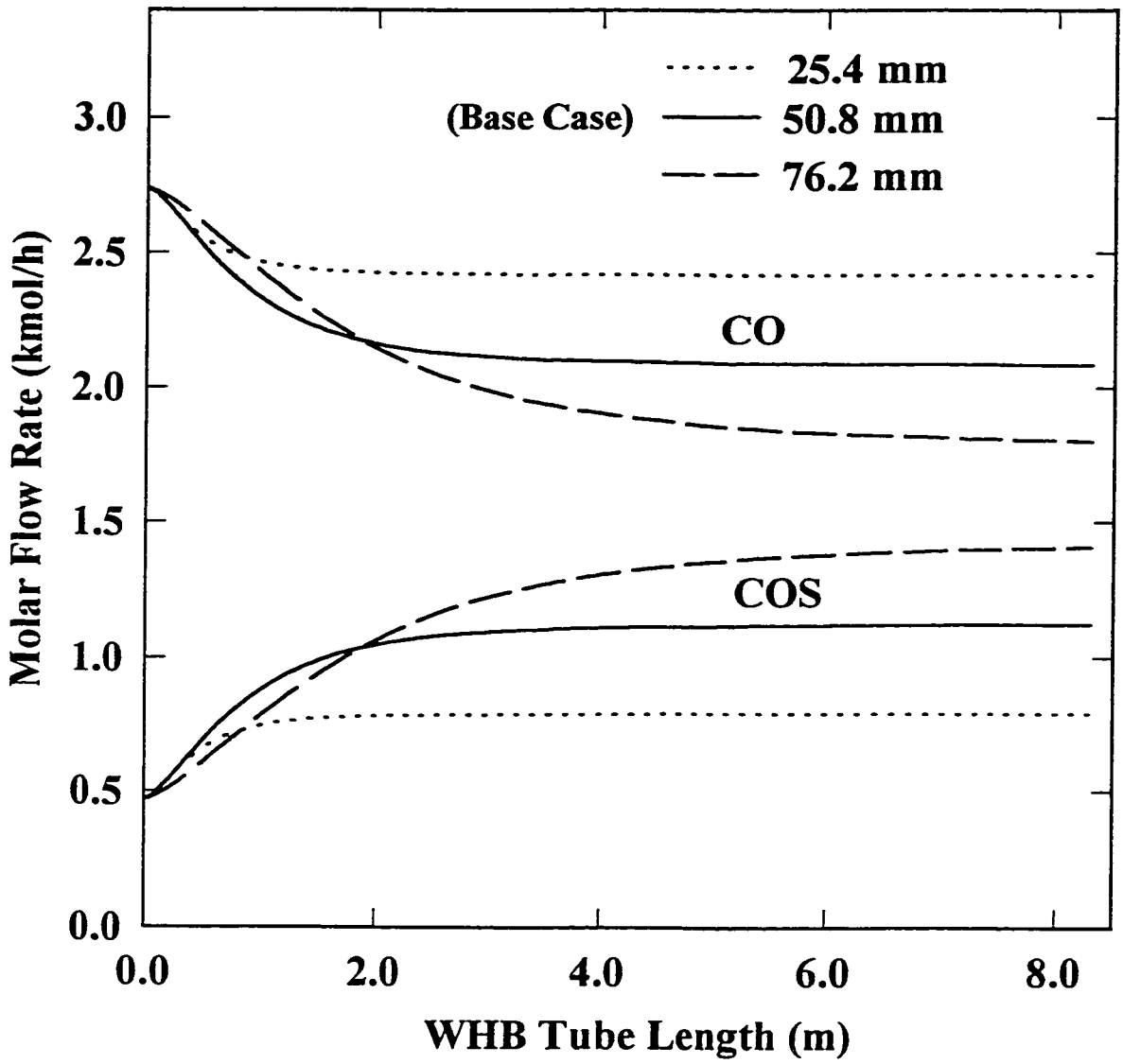

Figure 7.3 Effect of WHB tube diameter on CO and COS flow rates along WHB tube length.
(Gas mass flux = 6.67 kg/m^2.s)

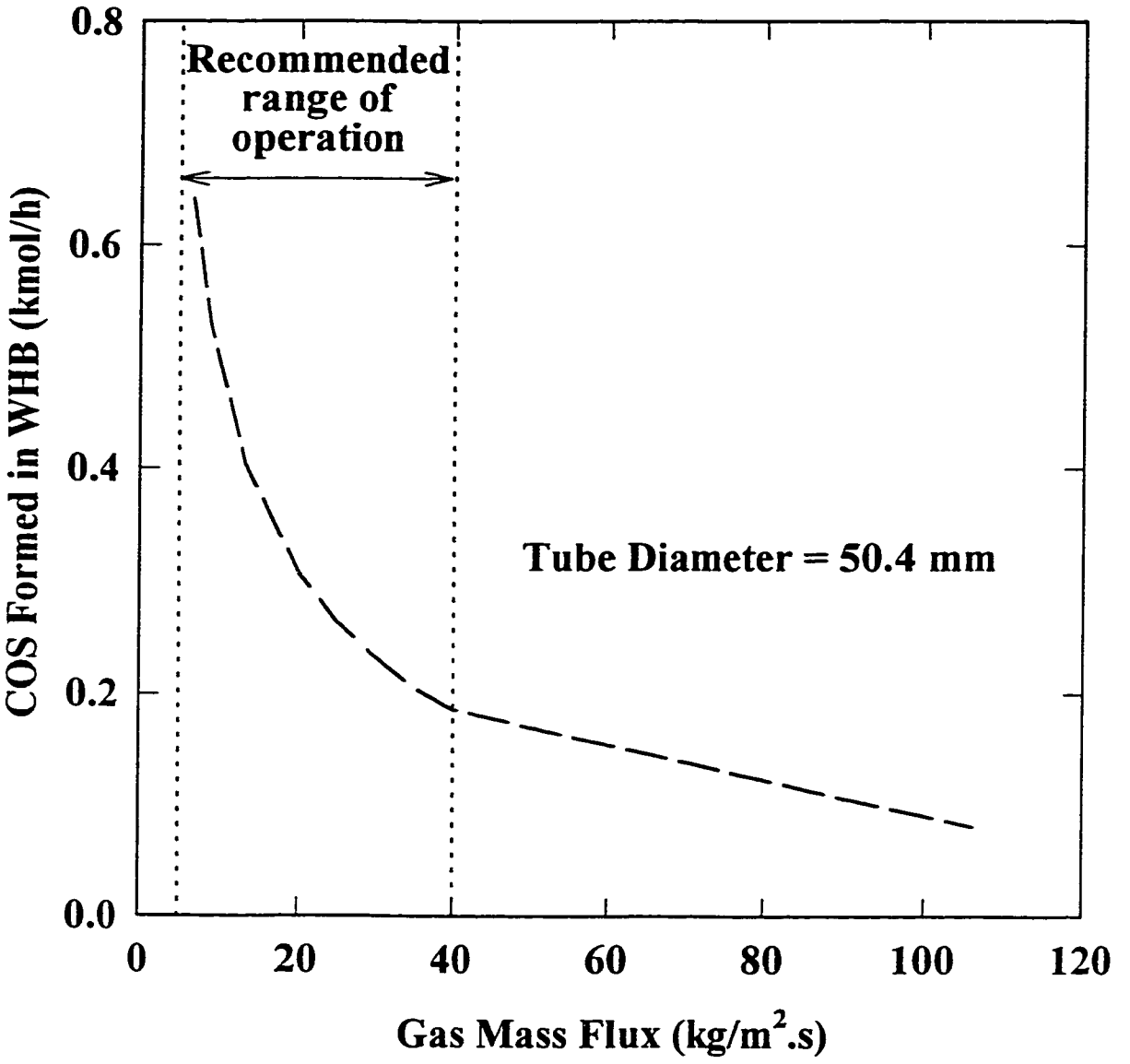

Figure 7.4 Effect of gas mass flux on COS formation in the tubes of an industrial waste heat boiler.

in WHB decreases by a factor of five as the gas mass flux is increased from the base case value of 6.7 to over 100 kg/m^2·s. An increase in operational gas mass flux to 100 kg/m^2·s in an industrial WHB is unrealistic. Moreover, it can be observed from Figure 7.4 that by operating beyond 30-35 kg/m^2·s, the reduction in COS formed reduces by a small amount even with a further increase of over 80 kg/m^2·s. It must also be noted that the recommended range of gas mass flux is 5-40 kg/m^2·s (Parnell, 1985). By operating at the maximum recommended value of 40 kg/m^2·s, a three fold reduction in COS formed in WHB results compared to a base case value of 6.7 kg/m^2·s. Hence, it is recommended that WHB be operated at the maximum possible gas mass flux rate or at conditions resulting in maximum quenching rate.

Operating WHB at Maximum Quench Condition.

Calculations were carried out to predict COS formation at the maximum quench rate that could be attained within the constraints of parameters used in this study, which corresponds to a tube diameter of 1 inch and a gas mass velocity of 40 kg/m^2·s. The results of the calculations are presented in Table 7.3 For all the five test conditions, the predicted COS flow rates reduced to half the value of that measured. This has a huge implication on sulfur recovery from plants. Firstly, contribution of sulfur emissions due to COS reduces to half or less. Secondly, the first catalytic converter could be operated at much lower temperature without being concerned of COS hydrolysis. The low temperature operation of first catalytic converter may result in a considerably higher conversions for main Claus reaction (i.e. the reaction between SO_2 and H_2S) and hence, in a higher sulfur recovery.

7.3 Kinetic modeling of gas composition at reaction furnace exit

A simplified kinetic modeling of the combustion of acid gas mixtures was attempted. It must be mentioned here that a majority of the furnace modeling studies have employed a variation on the equilibrium calculation method to

Table 7.3 Comparison between Predicted COS Formation for WHB Operating at Base Case Condition and at Maximum Quench Condition

	Measured		Predicted COS Formation	
	Sames et al. (1990)	Base Case Condition	Maximum Quench Condition (D=25.4mm, G= 40 kg/m^2·s)	% Reduction
Test 1	1.27	1.115	0.551	50.6
Test 2	0.91	0.715	0.352	50.7
Test 3	0.67	0.670	0.321	52.1
Test 4	1.12	1.116	0.531	52.4
Test 5	1.66	1.570	0.762	51.4

calculation of gas composition from the reaction furnace. This is true for studies reporting kinetic modeling of reaction furnace. In these studies, the kinetically limited species are calculated using empirical correlation, the concentrations of other species are calculated using Gibbs energy minimization with the underlying assumption that thermodynamic equilibrium for the reactions involving these species are attained (Wen et al., 1987, Chou et al., 1991, Monnery et al., 1993).

7.3.1 Modeling gas composition from reaction furnace

Simulations for predicting the product composition from the RF were performed. The detailed reaction kinetic mechanism for oxidation of hydrogen sulfide and carbon dioxide mixtures, as described in Section 6.3.2, was employed. The assumptions of plug flow of gases, isothermal and isobaric conditions were considered. This approach, is of course extremely simplified and hardly represents the actual furnace conditions, except for the assumption of isobaric operations. In the reaction furnace, in the flame region an intense mixing of gases may be occurring. However, in the post flame region as the gases move to the RF exit, the gas flow may be plug flow like. In the absence of relevant hydrodynamics and the mixing characteristics, the assumption of plug flow of gases was applied. There may be large temperature gradients in the furnace. The temperatures in the flame region may well exceed the calculated adiabatic flame temperatures by 200 °C. Again in the absence of information pertaining to the temperature profile, the assumption of isothermal operation may be applied which simplies the calculations.

Solution Method

The material balance equations were solved by a program written in MATLAB using the Gears algorithm. For the calculation purposes, the methane and other hydrocarbons were considered to be inert. This had to be done because the

reaction kinetic scheme for oxidation of methane and hydrogen sulfide mixtures, tested in Chapter 6, showed that negligible conversions of methane was predicted. This, of course is a limitation of the kinetic scheme, which does not account for numerous reactions in a C-H-S-O system.

Plant Data

The data set of Sames et al. (1990) that was used for comparison of WHB model results in the previous section also provides feed gas composition to the reaction furnace. Moreover, the measured furnace temperatures and the calculated adiabatic flame were also reported. Although data for five feed conditions are provided, three of feed gas streams contained ammonia. Therefore, in this study calculations were performed for only two sets of Sames et al. data, Test 3 and Test 4. The feed gas composition, the calculated adiabatic furnace temperature and inlet pressures are reported in Table 7.4

7.3.2 Simulation results

Simulations were performed at the reported adiabatic flame temperature for the two sets of data. A comparison of the measured and predicted gas composition for the two sets of data are presented in Table 7.5 The calculated equilibrium composition as reported by Sames et al. are also shown in the Tables.

The results indicate that the kinetic model overpredicts the hydrogen sulfide and sulfur dioxide concentrations. The equilibrium H_2S concentrations are closer to the measured values than the kinetic values. The equilibrium SO_2 value for Test 3 is slightly worse than the kinetic value and is slightly better than kinetic value for Test 4 in terms of being closer to the measured values. The model predictions for CO are better than the equilibrium values for all sets of data. The sulfur concentrations from the kinetic and equilibrium values are identical for Test 3, both of which underpredict the measured concentration. For Test 4, the equilibrium value is slightly greater than the kinetic value; however,

Table 7.4 Chemical Composition of RF Feed gas, the Flow rates and Adiabatic Flame Temperatures (Sames et al., 1990)

Chemical Species	Molar Gas Composition
N_2	0.0
Ar	0.0
CH_4	0.033
CO	0.0
CO_2	10.567
H_2S	88.799
C2+	0.113
Saturation Condition	
T (C)	32.2
P (kPa)	182.3
Relative Humidity	100

	Test 3 (Set –1)	Test 4 (Set –2)
Acid Gas Flow Rate	59.77 kmol/h	83.22 kmol/h
Air Flow Rate	112.06 kmol/h	123.59 kmol/h
Oxygen Flow Rate	--	6.96 kmol/h
Inlet Pressure	159 kPa	159 kPa
Flame Temperature	1208 C	1285 C

Table 7.5 **A Comparison of the Kinetic Model Predicted and the Measured Mole Fractions of Key Species at the RF Exit.**

Data and Equilibrium Values from Sames et al. (1990)

	Test 3 (Set – 1)			Test 4 (Set –2)		
	Measured	Calculated (Kinetic Model)	Equilibrium	Mesured	Calculated (Kinetic Model)	Equilibrium
H_2	0.0222	0.0245	0.0320	0.0270	0.0282	0.045
CO	0.0076	0.0085	0.0091	0.0098	0.0120	0.0136
H_2S	0.0366	0.0599	0.0480	0.464	0.0698	0.0528
SO_2	0.0188	0.0282	0.0298	0.0195	0.334	0.0328
H_2O	0.2750	0.2289	0.0238	0.2907	0.2566	0.2640
S_2	0.1290	0.1084	0.1086	0.1367	0.1207	0.126
CO_2	0.0273	0.0279	0.271	0.0299	0.287	0.0278

product gas. The predictions from the kinetic model show a significantly better agreement with data than the equilibrium predictions.

The simplified kinetic model used for simulation of furnace product gases may be considered to be a first good approximation and the first step towards development of a true reaction kinetic model for the reaction furnace. Although, the model does not perform well in predicting the SO_2 and H_2S concentration, it performs exceptionally well in predicting H_2 concentrations and reasonably well in predicting carbon monoxide concentrations. A correct concentration of CO at the RF exit or the WHB entrance is required for predicting the correct amounts of COS at the WHB exit. The prediction of correct amount of H_2 concentration is also important for plants employing reduction method in their tail gas clean up units.

7.4 Summary

Based on the simulation studies a few important observation pertaining to the operation and design of the key froont-end units, i..e the RF and the WHB, of Claus plants can be made.

Strategies for minimizing COS formation in WHB and RF

The majority of the COS formation of COS in the front-end of Claus plant is expected to occur via the reaction of CO and sulfur in the WHB. To minimize the COS formation, one has to look at minimizing CO and S_2 formation in the RF. The S_2 formation is rapid, however, the formation of CO is expected to be kinetically limited. Therefore, a reaction furnace with shorter gas residence time should produce lesser CO. However, operational and design consideration under such conditions must to take into account the other important factors, such as the presence of NH_3 and CH_4 in the RF feed. These components are easily destroyed in short reaction times and therefore the RF may be required to operate with larger residence time.

The simulation studies have shown that the COS formed in WHB can be reduced significantly by quenching the hot furnace product gases as rapidly as possible. Enhancement in quenching can be achieved by increasing the gas mass flux through the WHB tube or by using WHB tubes of smaller diameter. In an existing WHB, the tube diameter cannot be changed, however, an increase in gas mass flux can be achieved by plugging some of the tubes. This can be done practically by partially covering the tube sheet with another sheet so that only the required number of tube openings are exposed to the WHB feed gas. As we found from simulation of the Claus furnace WHB of Ultramar Refinery, by operating the WHB at the maximum recommended gas mass flux a 30 percent reduction in COS formed in WHB can be achieved compared to the base case value.

For new WHB units, the smallest possible tube diameter should be chosen to conform to the limitation imposed by pressure drop and fouling consideration. At present, the minimum size of tube diameter is set at 2 inches which is based on conventionally established norm. Field tests are required to provide information on applicability of smaller diameter tubes. The simulation results clearly show the advantage of using smaller sized tubes in quenching the RF product gas. In fact, more than 30% reduction in amount of COS formed in WHB results when the tube diameter is decreased from 2 inches to 1 inch.

Implications of oxygen enrichment furnace operations

With the advent of the reaction furnaces employing new burners for oxygen-enrichment, it is expected that the temperatures in the reaction furnace and that at the WHB will be higher than those in the conventional modified Claus furnace. As mentioned earlier, higher RF temperatures will in general imply higher COS formation in the WHB. Therefore, reliable models for WHB, such as that developed here, will be invaluable in predicting correct COS compositions. Also, the model can be used to study the effect of operational changes such as

oxygen-enrichment or increased/decreased throughputs of Claus feeds on COS formation in WHB.

Chapter 8

Conclusions and Recommendations

8.1 Conclusions

Extensive thermodynamic, experimental and modeling studies on key reactions occurring in the Claus plant front-end units, i.e. the Reaction Furnace and the Waste Heat Boiler, were completed. The rate expressions for key COS forming reactions, CO forming reaction and hydrogen sulfide decomposition reaction were determined. Further, high temperature experimental data for CS_2 forming reactions between methane and sulfur and between methane and hydrogen sulfide were obtained.

Experiments on the oxidation of acid gas mixtures were also conducted. The oxidation of hydrogen sulfide and methane were simulated using detailed reaction kinetic schemes involving elementary reactions. The results of the simulations, in general, verified the major trends; rapid consumption of oxygen by H_2S, formation of majority of hydrogen during oxidation period, and relatively slower consumption of oxygen by methane compared to hydrogen sulfide.

As a final wrap-up, the formation of COS in the waste heat boiler tubes was modeled using the new kinetics obtained in this study. The simulation demonstrated the best elements of a computer simulation by showing that up to a fifty percent reduction in the amounts of COS formed in the WHB could be achieved. This could be possible by operating the WHB at a maximum gas quenching capacity, i.e. at high gas mass flux in the smallest allowable diameter of the WHB tube, in a corresponding reaction quench times of less than 30 ms. Further, the key reactions occurring in the reaction furnace wer simulated using a detailed reaction kinetic scheme. The predictions of the kinetic model for components of interest, CO and H_2, compared well with plant data.

8.2 Recommendations

Following recommendations are made for future work:

- Experiment should be designed and performed to evaluate the residence time distribution in the coiled reactor.
- Further investigation into the kinetics of COS decomposition reaction is needed.
- Experiments should be performed to determine the kinetics of COS formation via reaction between CH_4 and SO_2.
- Experimental studies should be conducted to determine the reaction rate kinetics of CS_2 formation via reaction between cyclic hydrocarbons and sulfur species (mainly, S_2 and H_2S).
- Experimental studies on consumption reaction of COS and CS_2 needs to conducted. Specifically, the homogeneous gas phase hydrolysis reactions should be studied.
- Further effort is required to develop a kinetic model is needed to correctly describe the behavior during the partial oxidation of methane and hydrogen sulfide mixtures.
- Refinement in kinetic model for reaction furnace is needed.

References

Adesina, A.A., Meeyoo, V., Foulds, G., (1995) Thermolysis of Hydrogen Sulfide in an Open Tubular Reactor, *Int J Hydrogen Energy*, **20**(10), 777.

Arutyyunov, A.V., Vedeneev, V.I., Nikisha, L.V., Polyak, S.S. Romanovich, L.B., Sokolov, O.V., (1993) Kinetic Studies of Methane and Hydrogen Sulfide Cooxidation *Kinetics and Catalysis*, **34 (2)**, 194-197.

Anderson, J.R., Chang, Y.F., Pratt, K.C., Foger, K. (1993) *React Kinet Catal Lett*, **49 (2)**, 261-263.

Baulch, D.L., Cobos, C.J., Cox, R.A. (1992) Evaluated Kinetic Data for Combustion Modeling. *Journal of Physical and Chemical Reference Data.*

Benson, S. W. (1960) *The Foundations of Chemical Kinetics*; McGraw-Hill Book Company Inc.: New York.

Bennett, H.A. and Meisen, A. (1973) Hydrogen Sulphide-Air Equilibria under Claus Furnace Conditions, *Can J. Chem Eng*, **51**, 721-724.

Berk, D., Heidemann, R.A., Svrcek, W.Y., Behie, L. (1991) Thermodynamic Analysis of the Thermochemical Decomposition of H_2S in the Presence of Iron Sulphide", *Can J. Chem Eng,* **69,** 944.

Berger, S.A., Talbot, L., Yao, L.S. (1983) Flow in Curved Pipes. *Ann. Rev. Fluid. Mech*, **15**, 461-512.

Boas, A.H. and Andrade, R.C. (1971) Simulate Sulfur Recovery Plants, *Hydrocarbon Processing*,**3**, 81-84.

Bowman, C.T. and Dodge, L.G. (1976) Kinetics of the Thermal Decomposition of Hydrogen Sulfide Behind Shock Waves, *16th Symposium (Int) on Combustion*, Combustion Institute: Pittsburgh, 971.

Bradley, J.N. and Dobson, D.C. (1967) Oxidation of Hydrogen Sulfide in Shock Waves, *J Phys Chem*, **46**, 2865.

Buekens, A G. and Froment, G.F. (1968) Thermal Cracking of Propane *Ind Eng Chem Proc Des Dev* **7 (3)**, 435-447.

Cambot, J.B., Vovelle, C., Delbourgo, R. (1981) Flame Structures of H_2S-Air Diffusion Flames", *18th Symposium (Int)* on Combustion, Combustion Institute: Pittsburgh, 777.

Chase, M.W. Jr., Davies, C.A., Dawney, J.R. Jr., Frurip, D.J., McDonald, R.A., Syverud, A.N. (1985). *JANAF Thermochemical Tables*, National Bureau of Standards, Washington DC, Vol. 4, Third Ed.

Chenery, J.A., Fakhr, A., Wood, M.I., Simpson, C.J.S.M. (1983) Vibrational Analysis of the Products from Thermal Decomposition of OCS and CO_2. *Chem. Phys. Lett, 96*(2), 143.

Chiari, M., Grottoli, M.G., Villa, S. and Pierucci, S. (1997) Refinery Sulphur Plant Optimization. *Sulphur*, **250**, 53-59.

Chivers, T., J.B. Hyne, C. Lau (1980) The Thermal Decomposition of Hydrogen Sulfide over Transition Metal Sulfides, *Int J Hydrogen Energy*, **5**, 499.

Chou, J.S., Chen, D.H., Walker, R.E., Maddox, R.N. (1991) Mercaptans affect Claus units, *Hydrocarbon Processing*, **4**, 39-42.

Clark, P.D., Dowling, N.I., Huang, M. (1997) Mechanism of CS_2 Formation in the Claus Front-End Reaction Furnace. *Proceedings of the 47th Annual Laurance Reid Gas Conditioning Conference, March 2-5, 1997, Oklahoma Center for Continuing Education, The University of Oklahoma*, 321-337.

Clark, P.D., Dowling, N.I., Huang, M. (1998) Understanding Claus Furnace Chemistry: Development of a 'modified' Claus for low H_2S-Content Acid Gases. *Proceedings of the 48th Annual Laurance Reid Gas Conditioning Conference, March 1-4, 1998, Oklahoma Center for Continuing Education, The University of Oklahoma*, 241-263.

Cutler, A.H., Antal Jr., M.J., Jones Jr., Maitland, (1988) A Critical Evaluation of the Plug-Flow Idealization of Tubular-Flow Reactor Data. *Ind Eng Chem Res,* **24 (4)**, 691-697.

Dalla Lana, I.G. and Truong, T. (1979) Equilibrium Performance for Claus Processing Plants, *Energy Processing Canada*, **2**, 37-44.

Darwent, B. de B. and Roberts, R. (1953) The Photochemical and Thermal Decompositions of Hydrogen Sulphide, *Proc Royal Soc, A*, **216**, 344.

Dokiya, M., Fukuda, K., Yokokava, H. and Kameyama, T. (1978) The Study of Thermochemical Hydrogen preparation. VI. A Hydrogen Evolving Step through the H_2S-CO Cycle. *Bulletin of the Chemical Society of Japan* **50**, 150-153.

EPS Report 2/PN/2 (1993) Evaluation of Options to Reduce Sulphur Dioxide Emissions from Natural Gas Processing and Tar Sands Industries.

Faraji, F., Safarik, I., Strausz, O.P., Torres, M.E., Yildrim, E. (1996) CO-Catalyzed Conversion of H_2S to H_2 + S. 1. Reaction between CO and H_2S. *Industrial and Engineering Chemistry Research* **35**, 3854-3860.

Fisher, H., (1974) Burner/fire box design improves sulfur recovery *Hydrocarbon Processing*, **10,** 125-130.

Folkins, H.O., Miller, E., Hennig, H. (1956) Carbon Disulfide from Natural Gas and Sulfur *Ind Eng Chem*, **42(11)** 2202-2207.

Fookes, R.A. (1996) High Temperature Reactor Development, *MSc Thesis, University of Calgary, Calgary, Alberta, Canada.*

Frenkenlach, M., J.H. Lee, J.N. White, W.C. Gradiner Jr. (1981) Oxidation of Hydrogen Sulfide", *Combust Flame*, **41**, 1.

Fukuda, K., Dokiya, M., Kameyama, T., Kotera, Y. (1977) Catalytic Activity of Metal Sulfides for the Reaction, H_2S + CO = H_2 + COS. *Journal of Catalysis* **49**, 379-382.

Gamson, B.W. and Elkins, R.H. (1953) Sulfur from Hydrogen Sulfide. *Chem. Eng Prog*, **49**, 203-215.

Gas Processors Suppliers Association (GPSA) Engineering Data Book (1987). Chap. 22, Published by GPSA, Tulsa, Oklahoma .

Glasstone, S., Laidler, K. J., Eyring, H. (1941) *The Theory of Rate Processes*; McGraw-Hill Book Company Inc.: New York.

Grancher, P. (1978) Advances in Claus Technology, *Hydrocarbon Processing* **9**, 25-262.

Graven, W. M. and Long, F. J. (1954) Kinetics and Mechanisms of the Two Opposing Reactions of the Equilibrium CO + H_2O = CO_2 + H_2. *Journal of the American Chemical Society* **76**, 2602-2607.

Hatcher, N.A., Johnson, J.A., Halka, L.E. (1998) Integrate Cansolv® System Technology into Your Sour Gas Treating/Sulphur Recovery Plant, *Proceedings of the 48th Annual Laurance Reid Gas Conditioning Conference, March 1-4, 1998, Oklahoma Center for Continuing Education, The University of Oklahoma*, 381-402.

Hay, A.J. and Belford, R.L. (1967) High-Temperature Gas-Kinetic Study of Carbonyl Sulfide Pyrolysis Performed with a Shock Tube and Quadrupole Mass Filter, *J Chem. Phys.* **41**, 3944.

Haas, L.A. and Khalafalla, S.E. (1973) Catalytic Thermal Decomposition of Carbonyl Sulfide and Its Reaction with Sulfur Dioxide", J Catalysis, **30**, 451-459.

Higashihara,T., Saito, K., Yamamura, H. (1976) S_2 Formation during the Pyrolysis of H_2S in Shock Waves, *Bull Chem Soc Japan*, **49**(4), 965.

Hyne, J.B. and Goar, B.G. (1996 a) The Claus Revisted – Part 1, *Sulphur*, **245**, 39-44.

Hyne, J.B. and Goar, B.G. (1996 b) The Claus Revisted – Part 2, *Sulphur*, **246**, 73-80.

Hyne, J.B. and Goar, B.G. (1996 c) The Claus Revisted – Part 3, *Sulphur*, **247**, 40-45.

Hyne, J.B. and Goar, B.G. (1997) The Claus Revisted – Part 4, *Sulphur*, **248**, 43-48.

Kaloidas, V.E., Papayannakos, N.G. (1987). Hydrogen Production from the Decomposition of Hydrogen Sulphide. Equilibrium Studies on the System $H_2S/H_2/S_i$ (i=1,...,8) in the Gas Phase. *Hydrogen Energy*. Vol. 12, No. 6, 403-409.

Kaloidas, V., and Papayannakos, N. (1989) Kinetics of Thermal, Non-Catalytic Decomposition of Hydrogen Sulphide", *Chem Eng Sci*, **44**, 1983.

Karan, K.; Mehrotra, A.K; Behie, L.A. (1994). Including Radiative Heat Transfer and Reaction Quenching in Modeling a Claus Plant Waste Heat Boiler. *Ind. Eng. Chem. Res.* **33**, 2651-2655.

Kay, W.M. and Crawford, M.E. (1980) *Convective Heat and Mass Transfer* McGraw Hill Book Company, USA.

Kerr, R.K., Paskall, H.G., Ballash, N. (1976) Claus Process: Catalytic Kinetics: Part 1-Modified Claus Reaction. *Energy Processing Canada,* **5**, 66-72.

Kerr, R.K. and Paskall, H.G. (1976) Claus Process: Catalytic Kinetics: Part 2-COS and CS_2 Hydrolysis. *Energy Processing Canada,* **6**, 38-44.

Kerr, R.K., Paskall, H.G., Ballash, N. (1977) Claus Process: Catalytic Kinetics: Part 3-Deactivation and Mechanisms Evaluations and Catalyst. *Energy Processing Canada,* **1**, 40-51.

Kerr, R.K., Paskall, H.G., Biswanger, L.C. (1976) Sulphur Plant Waste Gases-Incineration Kinetics and Fuel Consumption. *Energy Processing Canada,* **2**, 32-40.

Khudenko, B.M., Gitman, G.M., Wechsler, N. (1993) Oxygen Based Claus Process for Recovery of Sulfur from H_2S Gases. *J Env Eng* **119 (6)**, 1233-1251.

Klemm, R.B. and Davis, D.D.(1974) A Flash Photolysis-Resonance Fluorescence Kinetic Study of the Reaction $S(^3P)$ + OCS. *J. Phys. Chem.* **78**, 1137.

Kondrat'ev, V. N. *Chemical Kinetics of Gas Reactions*; Permagon: Oxford, 1964.

Kurbanov, M.A. and Mamedov, Kh. F. (1995) The Role of CO + $SH^{\cdot} \rightarrow$ COS + $H^{\cdot}$ in Hydrogen Formation in the Course of Interaction between CO and H_2S. *Kinetics and Catalysis* **36** (4), 455-457.

Kwong, V. and Meissener, R.E. (1995). Rounding Up Sulfur. *Chemical Engineering* Vol. 102, No. 2, 74-83.

Levy, A. and Merryman, E.L. (1965) The Microstructure of Hydrogen Sulphide Flames, *Combust Flame*, **9**, 229.

Luinstra, E.A. and d'Haene, P.E. (1989). Catalyst Added to Claus Furnace Reduces Sulfur Losses. *Hydrocarbon Process.* Vol. 68, No. 7, 53-57.

Marsh, K.N.; Gammon, B.E.; Wilhoit, R.C.; Aljoe, K.L.; Bailey, D.; Boyd, B.; Chao, J.; Das, A.; Ferguson, A.M.; Gadall, A.; Rodgers, A.S.; Somayajulu, G.R. (1985). *TRC Thermodynamic Tables, Hydrocarbons."* Texas Engineering Experimental Station, Texas A & M University System, Texas.

Mehrotra, A.K., Karan, K., Behie, L.A. (1995) Estimate Gas Emmisivities for Equipment and Process Design, *Chem Eng Prog*, September, 70-77.

Meisen, A. and Bennet, H.A. (1974) Consider all Claus Reactions, *Hydrocarb Process.* **11**, 171-174.

Merryman, E.L. and Levy, A. (1967) Kinetics of Sulfur-Oxide Formation in Flames: II. Low Pressure H_2S Flames", *J Air Pollution Control Ass*, **17**, 800.

Moore, B.G. (1993) Simulation of Claus Sulphur Plants, *M. Eng Thesis, University of Calgary, Calgary, Alberta Canada.*

Monnery, W.D.; Svrcek, W.Y.; Behie, L.A. (1993) Modelling of the Modified Claus Process Reaction Furnace and the Implications on Plant Design and Recovery. *Can. J. Chem. Eng.* **71**, 711.

Muller III, C.H., Schofield, K., Steinberg, M., Broida, H.P. (1979) Sulfur Chemistry in Flames, *17th Symposium (Int) on Combustion*, Combustion Institute: Pittsburgh, 867.

Nabor, G.W., and Smith, J.M. (1953) Kinetics of the Sulfur-Methane Reaction *Ind Eng Chem* **45 (6)**, 1272-1281.

Nasato, L.V., Karan, K., Mehrotra, A. K., Behie, L. A. (1994) Modeling Quench Times in the Waste Heat Boiler of a Claus Plant. *Ind. Eng. Chem. Res.* **33**, 7.

Olschewski, H.A., Troe, J., Wagner, H. Hg. (1994) UV Absorption Study of the Thermal Decomposition Reaction $H_2S \rightarrow H_2 + S(^3P)$, *J Phys Chem*, **98**, 12964.

Oya, M., Shiina, H., Tsuchiya, K., Matsui, H. (1994) Thermal Decomposition of COS, *Bull. Chem. Soc. Jpn.* **67**, 2311.

Partington, J.R. and Neville, H.H. (1951) "The Thermal Decomposition of Carbonyl Sulphide, *J. Chem Soc., London* **23**,1230-1237.

Paskall, H.G. (1979). Capability of the Modified-Claus Process. A Final Report to the Department of Energy and Natural Resource of the Province of Alberta, Chap. IV.

Pearson, M.J. (1981) Special Catalyst Improves C-S Compounds Conversion. *Hydrocarbon Processing* **60**, 131-134.

Raymont, M. E.D. (1975) Make Hydrogen from Hydrogen Sulphide, *Hydrocarb Process,* **54**(7), 139.

Rebick, C. (1980) Hydrogen Transfer Catalysis in Hydrocarbon Pyrolysis, in . *Frontiers of Fee Radical Chemistry*, Ed.William A. Pryor. Academic Press Inc., New York.

Roth, P., Lohr, R., Braner, U. (1982) Thermal Decomposition of Hydrogen Sulfide at Low Concentrations, *Combust Flame*, **45,** 273.

Shiina, H., Oya, M., Yamashita, K., Miyoshi, A., Matsui, H. (1996) Kinetic Studies on the Pyrolysis of H_2S, *J Phys Chem*, **100**, 2136.

Sames, J. A. and Paskall, H.G. (1984). So You Don't Have a COS/CS_2 Problem, eh?. *Sulphur;* **172**, 47-50.

Sames, J.A., Paskall, H.G., Brown, D.M., Chen, M. S. K., Sulkowski, D. (1990). Field Measurements of Hydrogen Production in an Oxygen-Enriched

Claus Furnace. *Proceedings Sulfur 1990 International Conference,* Cancun, Mexico; British Sulphur Corp. Ltd; 89-105.

Saxena, A. K. and Nigam, K.D.P. (1979) On RTD for Laminar Flow in Helical Coils *Chem Eng Sci* **34**, 425-426.

Schecker, H.G. and Wagner, H. Gg. (1969) On the Thermal Decomposition of $COS^{\bullet}$. *Int. J. Chem Kin.* ***1***, 541.

Shiina, H., Oya, M., Yamashita, K., Miyoshi, A., Matsui, H. (1996) Kinetic Studies on the Pyrolysis of H_2S. *The Journal of Physical Chemistry* **100**, 2136-2140.

Smith, W.R. and Missen, R.W. (1991). *Chemical Reaction Equilibrium Analysis: Theory and Algorithm.* Chap 2, Krieger Publishing Company, Malabar, Florida.

Smooke, M.D. (1991) *Reduced Kinetic Mechanisms and Asymptotic Approximations for Methane-Air Flames* Topical Volume 384, Springer Verlag; Berlin-Heidelberg.

Sundaram, K.M. and Froment, G.F. (1977a) G.F. Modeling of Thermal Cracking Kinetics–I. Thermal Cracking of Ethane, Propane and their Mixtures. *Chem. Eng. Sci.* **32,** 601-608

Sundaram, K.M. and Froment, G.F. (1977b) Modeling of Thermal Cracking Kinetics–II Thermal Cracking of Ethane, Propane and their Mixtures. *Chem. Eng. Sci.* **32**, 609-617

Sundaram, K.M. and Froment, G.F. (1979) Kinetics of Coke Deposition in the Thermal Cracking Propane *Chem. Eng. Sci.* **34**, 635-644.

Stull, D.R. (1949) Thermodynamics of Carbon Disulfide Production *Ind Eng Chem* **41(9)**, 1968-1973.

Tesner, P.A., Nemirovskii, M.N., Motyl, D.N. (1990) Kinetics of the Thermal Decomposition of Hydrogen Sulfide at 600-1200 °C" *Kinet Katal*, **31**, 1232.

Towler, G. P. and Lynn, S. (1993). Development of a Zero-Emissions Sulfur-Recovery Process. 1. Thermochemistry and Reaction Kinetics of Mixtures of H_2S and CO_2 at High Temperature. *Ind. Eng. Chem. Res.* **32**, 2800-2811.

True, W. R., (1995) US Gas Processing Consolidates while World Tempo Increases *Oil and Gas J,* **7**, 49-54

Tsuchiya, K., Kamiya, K., Matsui, H. (1997) Studies on the Oxidation Mechanism of H_2S Based on Direct Examination of the Key Reaction. *Int J Chem Kinet*, **29**, 57.

Thacker, C.M. and Miller, E. (1944) Carbon Disulfide Production *Ind Eng Chem* **36(2)**, 182-184.

Van Andel, E., Kramers, H., Voogd, A.E., (1964) The Residence Time Distribution of Laminar Flow in Curved Tubes. *Chem Eng Sci*, **19**, 77-79.

Van Damme, P.S., Narayanan S., Froment G.F. (1975) Thermal Cracking of Propane and Propane-Propylene Mixtures: Pilot Plant versus Industrial Data *AIChE J* **21 (6)**, 1065-1073.

Walas, S. M. (1985). *Phase Equilibria in Chemical Engineering*, Butterworth-Heinemann, Boston, MA.

Wan, C.G. and Ziegler, E.M. (1970) On the Axial Dispersion Approximation for Lmainar Flow Reactors. *Chemi Eng Sci*, **25**, 723-777.

Wen, T.C., Chen. D.H., Hopper J.R., Maddox, R.N. (1987) Claus Simulation with kinetics, *Energy Processing Canada*, **4**, 25-31.

White, W.B., Johnson, S.M., Dantzig, G.B. (1958) Chemical Equilibrium in Complex Mixtures, *J Chem Phys*, **28**, 751-755.

Woiki, D and Roth, P. (1992) Shock Tube Measurements on the Thermal Decomposition of COS. *Ber. Bunsengens. Phys. Chem.* ***96*****(1),** 1347.

Woiki, D., Markus, M. W., Roth P. (1993) A Shock Tube-Laser Flash Photolysis Study of $COS + S \leftrightharpoons CO + S_2$. *J. Phys. Chem.* ***97***, 9682.

Woiki, D. and Roth, P. (1994) Kinetics of the High-Temperature H_2S Decomposition", *J Phys Chem*, **98**, 12958.

Yetter, R.A., Dryer, F.L., Rabitz, H. (1991) A Comprehensive Reaction Mechanism for Carbon Monoxide/Hydrogen/Oxygen Kinetics *Combust Sci and Tech* **79,** 97-128.

Zachariah, M.R. and O.I. Smith (1987) Smith Experimental and Numerical Studies of Sulfur Chemistry in $H_2/O_2/SO_2$ Flames, *Combust and Flame*, **69**, 125-139.